Contract FP6-IST 508009

ACE

Antenna Centre of Excellence

Instrument: Network of Excellence
Thematic Priority: IST - Information Society Technologies
Mobile and wireless systems beyond 3G

Deliverable A1.2D2
First Facility Comparison Campaign

Due date of deliverable: 31/12/2005
Actual submission date: 23/12/2005

Start date of project: 1/1/2004 Duration: 24 months

Organisation name of lead contractor for this deliverable: Technical University of Denmark

Revision: 1.0

Document Number: FP6-IST-508009-A1.2D2
Workpackage: 1.2-2
Estimated Person Months: TBD
Dissemination level (PU,PP,RE,CO): PU (Public)
Nature (R, P, D, O): R (Report)
Version: 1
Total Number of Pages: 164
File name: WP1.2D2.pdf
Editors: Janus E. Pallesen (DTU), Sergey Pivnenko (DTU), Olav Breinbjerg (DTU).
Participants: Manuel Sierra Castañer (UPM), Pablo Caballero Almena (UPM), Cristian Martínez Portas (UPM), José Luis Besada Sanmartín (UPM), Jordi Romeu (UPC), Sebastian Blanch (UPC), Christian Sabatier (FTRD), Alain Calderone (FTRD), Gérard Portier (FTRD), Håkan Eriksson (EMW), Jan Zackrisson (SES).

Abstract

This report documents the results of the *First Facility Comparison Campaign* (ACE WP1.2-2) with the 12 GHz DTU-ESA Validation Standard Antenna (VAST12). The campaign included 7 partners and 9 facilities. The partners consisted of both public research institutions and commercial companies and the included facility types were spherical near-field, planar near-field, compact range, and far-field facilities.

Keyword List

Antenna Measurements, Facility Comparison, Validation, Benchmarking.

Document Evolution

Revision	Date	Reason of change
1.0	23/12/2005	First Edition

Contents

The information contained in this document should be used only for the scope of the contract for which this document is prepared.

The information contained in this document should be used only for the scope of the contract for which this document is prepared.

Chapter 1

Introduction

1.1 Organizational Background

Within the European Union (EU) 6th framework research program, the *Antenna Centre of Excellence* (ACE) has conducted the activity A1.2 *Antenna Measurement Techniques and Facilities sharing*. As a part of this, the work package *First Facility Comparison Campaign*, which is formally denoted ACE WP1.2-2, has been carried out.

In order to facilitate the comparisons between the participating measurement facilities, the European Space Agency (ESA) has permitted the use of the 12 GHz Validation Standard Antenna (VAST12). The VAST12 antenna has been measured at the participating facilities and the measurement results have been collected and compared by the Technical University of Denmark (DTU).

1.2 Technical Background

Preceding the work done within the First Facility Comparison Campaign results from other antenna measurement comparisons have been published by different authors.

The Technical University of Denmark has over the past 25 years been involved in several facility comparison projects. The major part of the facility comparison projects have been conducted with the purpose of verifying the performance of particular facilities and/or to qualify these facilities for specific tasks. In 1983 an inter-comparison of the DTU-ESA Spherical Near-Field Test Facility, a compact range at the Technical University of Eindhoven, and a cylindrical near-field range at the Space Division of Messerschmitt-Bölkow-Blohm was conducted using a 12 GHz elliptical offset fed reflector antenna [1]. A similar inter-comparison [2], [3], using the same antenna, was conducted in 1986. In this comparison campaign the participants were the DTU-ESA Spherical Near-Field Test Facility, a cylindrical near-field range at Marconi Space Systems, and a spherical near-field facility at British Aerospace PLC. Aside from the inter-comparisons [1], [2], [3], other facility comparisons have also been conducted with the aim of verifying the accuracy of particular facilities or qualifying facilities for specific measurement tasks. In [4] the ESTEC Compact Antenna Test Range was compared to the DTU-ESA Spherical Near-Field Test Facility using the elliptical offset fed reflector antenna that was also used in [1]. In [5] a spherical near-field range at CASA was compared to the DTU-ESA Spherical Near-Field Test Facility using the ERS-1 Breadboard Antenna Panel. In [6] a plane polar near-field scanner at Alcatel Espace was compared to

The information contained in this document should be used only for the scope of the contract for which this document is prepared.

the DTU-ESA Spherical Near-Field Test Facility using the ERS-1 Breadboard Antenna Panel.

Results from a large inter-comparison campaign were published in 1996 [7]. This inter-comparison campaign, which was focused on comparisons of gain and polarization measurements of an X-band horn antenna, was initiated in 1978 and had 7 participating facilities. This comparison campaign stands out particularly due to the large number of participants. The results of a comparison between two facilities have recently been published [8]. This comparison was a part of the qualification of a spherical near-field facility at Alenia-Marconi Space (AMS), where measurements at that facility were compared to measurements at a cylindrical near-field facility, also at AMS.

It is clear that a substantial amount of material has been published on inter-comparisons of different measurement facilities. However, the number of facilities included in each of the inter-comparisons is generally low, and only in the X-band horn inter-comparison [7], a large number of facilities are included. This comparison is however limited to only considering gain and polarization characteristics. Hence, it is of great interest to consider a campaign which includes comparisons of a large number of facilities, and which includes comparisons of pattern, gain and polarization characteristics. Furthermore, if different measurement techniques are used at the individual facilities this will offer a great possibility to compare differences in the results obtained through these different techniques.

1.3 Purpose and Objectives

The objective for the WP1.2-2 "First Facility Comparison Campaign" was stated in the Technical Annex of the ACE project [9, p. 75] as

> *The objective of this work package is to conduct a comparison of several antenna measurement facilities employing the existing and available DTU-ESA 12GHz Validation Standard Antenna as a reference antenna. At least 5 facilities should enter this first campaign. The work includes a measurement plan - the specification of the characteristics of the reference antenna that are to be determined, and the procedure for comparing and reporting the measurement results of the different facilities. Next, the participating facilities must be identified and agreements must be reached with each. Following the measurements themselves, the results are collected, compared and analysed. Finally, the campaign must be evaluated as an input to subsequent campaigns.*

As it is seen from the statement above, a few particular issues must be addressed. For example, in order to fulfill the objective of the comparison campaign a measurement plan allowing for a large number of participating facilities must be developed. Furthermore, comparison techniques, which are suitable for comparisons of large amounts of data must be identified and/or developed in order to facilitate an analysis of the results.

The purpose of the "First Facility Comparison Campaign" falls under the general purpose of activity A1.2 "Antenna Measurement Techniques and Facilities sharing", which was stated in the Technical Annex of the ACE project [9, p. 32] as

The information contained in this document should be used only for the scope of the contract for which this document is prepared.

The purpose of the integrating activity on antenna measurement techniques is to facilitate the consolidation and expansion of European expertise in research and development of antenna measurements. This will help antenna developers meet, more efficiently and more effectively, the challenges resulting from the increasing use of wireless communication and sensing technologies in the modern information society.

Aside from the general purpose stated above, the "First Facility Comparison Campaign" also has some specific purposes. Development of new and improvements on the currently used comparison techniques, which are involved in such a project, is one specific purpose. This will be accomplished by applying proposed techniques on the available data from the campaign, and through this investigating how to extract the most information from the comparisons.

Another specific purpose is that the facility comparison campaign will provide a mean for validation, benchmarking, and analysis of the facilities as detailed below.

1.3.1 Validation

The validation of a measurement facility is understood as a documentation or a proof that the facility performs according to an acceptable standard. This is obviously of strong interest to the individual participating facility.

1.3.2 Benchmarking

The benchmarking of a measurement facility is understood as the ranking of the facility compared to other facilities on basis of its performance. If this is based on comparisons between individual facilities, the benchmarking will obviously be relative. However, if a reference result exists, the benchmarking will be absolute. Hence, this facility comparison campaign will address the issue of establishing a reference result for the VAST12 antenna.

1.3.3 Analysis

The analysis of measurement and comparison results is understood as the process of extracting information about the individual facilities from these results. This will allow determining advantages and disadvantages of different measurement techniques and/or the manner these are implemented. Furthermore, it will help to identify specific errors or inaccuracies of the facility.

1.4 Report Structure

The report is structured in the following way. In Chapter 2 a description of the VAST12 antenna are given and definitions of the coordinate systems that are used in this report is presented. Following this a presentation of each of the participating measurement facilities is given in Chapter 3. An overview of the measurement campaign presenting the execution of the campaign and listing the acquired measurements is given in Chapter 4. In Chapter 5 a detailed discussion on how to compare the available measurement data is given. This discussion covers comparisons of patterns, gain/directivity, and polarization characteristics. From this discussion a specific comparison strategy is chosen in Chapter 6, and using this,

The information contained in this document should be used only for the scope of the contract for which this document is prepared.

comparisons of the measurement data are presented. Finally, conclusions for the campaign and suggestions for further work are presented in Chapter 7.

The information contained in this document should be used only for the scope of the contract for which this document is prepared.

Chapter 2

The VAST12 Antenna and Measurement Coordinate Systems

The 12 GHz Validation Standard (VAST12) Antenna was designed and manufactured at the Technical University of Denmark in 1992 under the European Space Research and Technology Centre (ESTEC) contract No. 7407/87/NL/PB "Technical assistance for the design and development of antenna test range validation standardization" [10]. The VAST12 antenna is shown in Figure 2.1. The purpose of the VAST12 antenna is to facilitate antenna test range inter-comparisons for the European Space Agency (ESA) with the DTU-ESA Spherical Near-Field Antenna Test Facility being the coordinating organization.

Figure 2.1 The 12 GHz Validation Standard Antenna.

The information contained in this document should be used only for the scope of the contract for which this document is prepared.

2.1 Description of the VAST12 Antenna

A complete description of the VAST12 antenna is given in [10]. The description of the mechanical and electrical interfaces are given below.

The mechanical interface of the VAST12 antenna is a circular mounting flange of 206 mm diameter with 6 mounting holes having M12 thread arranged on a circle of 140 mm diameter with 60° separation in between. There are also 3 holes having M6 thread arranged on a circle of 140 mm diameter with 120° separation in between, reserved for special purposes. In the center of the mounting flange there is a hole of 90 mm diameter, which can be used for centering purposes.

The electrical interface of the VAST12 antenna is a SMA female connector on a waveguide-to-coax transition. The SMA connector represents a reference port for the gain and the reflection coefficient.

2.2 Coordinate System Definition

The contents of this chapter is based on chapter II in [11], but modified for the purpose of the present application.

For purposes of inter-comparison of measurements of the antenna on different antenna test ranges, it is important that the results are reported in a clearly defined coordinate system. The coordinate system should be capable of being implemented by any measurement facility.

The VAST12 coordinate system, which is denoted the optical coordinate system, is defined by an optical mirror cube mounted at a convenient location of the antenna structure. A test facility has the choice of aligning the antenna with respect to the cube directly in the facility. Likewise, the antenna can be measured in an arbitrary measurement coordinate system. Thereafter, the antenna patterns can be transformed into the optical coordinate system once the Euler angles defining the optical coordinate system with respect to the measurement coordinate system are determined. The former requires proper alignment tools in the form of theodolite or tracking laser and a test antenna mounting head, which can be adjusted in θ and ϕ. The latter is a complex mathematical exercise; in a spherical near-field measurement, as carried out in the DTU-ESA Facility, this entails rotation of the spherical mode coefficients.

As this presents a set of requirements for measurement facilities, which may not always be available, it has been decided to define two supplementary coordinate systems so as to not exclude them from inter-comparisons. These two alternatives are a mechanical coordinate system definition and an electrical coordinate system definition. All three coordinate systems are as defined below.

2.2.1 Optical Coordinate System

The preferred coordinate system for inter-comparison purposes is that defined by the optical mirror cube mounted atop the antenna reflector as depicted in Figure 2.2. The coordinate system is a normal right hand coordinate system with $\hat{x}$, $\hat{y}$, and $\hat{z}$ unit vectors coinciding

The information contained in this document should be used only for the scope of the contract for which this document is prepared.

with the normal unit vectors of 3 faces of the mirror cube as shown in Figure 2.2. Due to the mounting of the mirror cube, the positive x axis is not available. Thus the $-x$ axis is to be used instead for alignment purposes, however, $\phi = 0°$ is still to be defined with respect to the positive x axis.

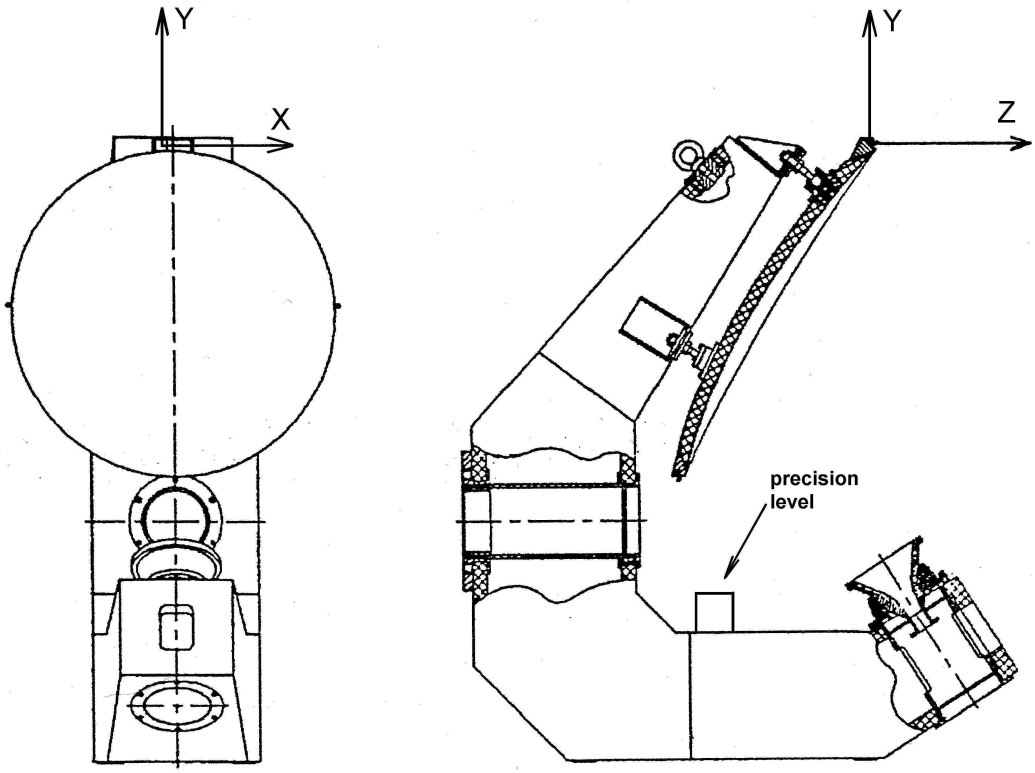

Figure 2.2 Front view (left) and side view (right) of the VAST12 antenna showing its coordinate system defined by the optical mirror cube located on the top rim of the reflector.

2.2.2 Mechanical Coordinate System

The mounting flange of the VAST12 defines the xy plane and thus the z axis of the mechanical coordinate system. The orientation of the x axis ($\phi = 0°$) is then defined with a precision level placed in the specified place on the feed support arm, as shown in Figure 2.2, and setting the ϕ axis to 0° when this indicates a levelled situation.

2.2.3 Electrical Coordinate System

Conventional far field ranges in many instances do not have the ability to define a coordinate system with regard to one of the above two definitions. Thus an electrical coordinate system is defined here that will allow reporting of results irrespective of the type of far field range used, e.g. roll over azimuth or azimuth over elevation.

The z axis is defined by the direction of absolute maximum of total directivity. In order to find the absolute maximum, the direction perpendicular to the mounting flange can be

The information contained in this document should be used only for the scope of the contract for which this document is prepared.

taken as starting point as the maximum is very close to it. In this process, the antenna can be assumed primarily vertically-polarized, i.e. the electric field vector is primarily in the zy plane, as referred to Figure 2.2. Care should be exercised here as the VAST12 has a rather flat top in the main beam. Once the absolute peak is detected, the corresponding angular indicators are zeroed.

A minimum signal is then obtained from the orthogonal port of the range probe by rotating the range probe around its symmetry axis or by rotating the antenna around the above defined z axis. Once the minimum is obtained, the corresponding angular indicator is zeroed and the x axis is thus defined. This procedure assumes a very good linearly polarized probe. Alternatively, the probe polarization properties should be determined and taken into account during the definition of the x axis.

The information contained in this document should be used only for the scope of the contract for which this document is prepared.

Chapter 3

Participating Facilities

A brief description of the participants and the participating measurement facilities is given in this chapter. Where provided, this includes a description of the physical layout of each measurement facility, a description of the equipment, and a description of the measurement procedure. Further, accuracy estimates or error budgets are presented for the facilities, which have provided such.

Aside from the measurement facilities, which are presented here, the VAST12 antenna has also been measured at Ericsson Microwave Systems (EMW) and the University of Liverpool (LIVUNI). The measurement at the EMW facility is documented in their measurement report which is included as Appendix B. It has however not been possible to include the EMW data in the comparisons presented in this report. For different reasons it has also not been possible to include the measurement data from LIVUNI in the comparisons.

3.1 Technical University of Denmark

3.1.1 DTU-ESA Spherical Near-Field Antenna Test Facility

The VAST12 antenna was measured at the DTU-ESA facility two times. First, it was measured in May 2004 before the outset of the campaign. For the second time, it was measured in April 2005 as the final step of the measurement phase of the campaign. The two measurements were slightly different in their procedures, since some modifications of the procedure were made during the second measurement as result of experience gained in the first measurement. Particularly, the alignment of the mechanical setup before the second measurement has been improved making use of electrical measurements and information extracted from the phase patterns.

In this section, a description is given of the technique, the setup, the procedure, and the parameters of the measurements carried out at the DTU-ESA Spherical Near-Field Antenna Test Facility. It includes the general aspects as well as specific descriptions of the measurements of the VAST12 antenna. The description in this section is an extract from [12].

The information contained in this document should be used only for the scope of the contract for which this document is prepared.

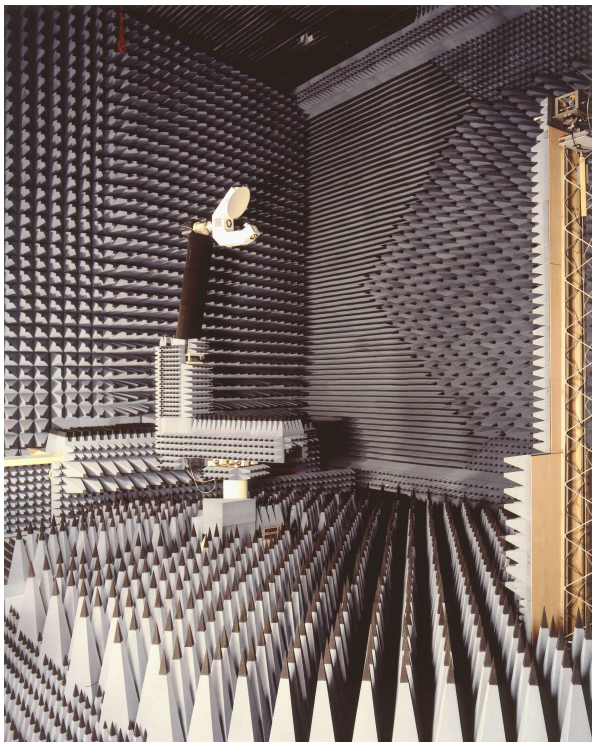

Figure 3.1 The VAST12 Antenna during measurements at the DTU-ESA Spherical Near-Field Test Facility.

3.1.1.1 Measurement Technique

The radiation measurement is carried out in two steps: first, the near-field of the Antenna Under Test (AUT) is measured in a number of points on a full sphere. Next, the near-field is transformed to the corresponding far-field using a mathematical algorithm based on a spherical wave expansion of the near-field. During the transformation, a value for the total radiated power is also found. The directivity in any direction can then be found as the ratio between the power density in that direction and the average radiated power density. For a detailed treatment of the spherical near-field measurement technique, the reader is referred to [13].

The gain measurement is performed using a substitution technique, where the amplitude of the AUT near-field is compared with the amplitude of the near-field of a Standard Gain Horn (SGH). Combined with the knowledge of the near- and far-fields of the two antennas, obtained from full-sphere measurements of both, the ratio between the gains of the AUT and the SGH can be determined. The gain of the SGH is found by subtracting the loss from the directivity. The directivity is found from a full sphere measurement, while the loss in the waveguide and in the pyramidal section is estimated using well known formulas for the ohmic losses in a rectangular waveguide (see e.g. [14, p. 423]). The loss in the coax-to-waveguide transition is measured. A detailed treatment of the gain determination technique can be found in [13, pp. 210-214].

The input reflection coefficients of the AUT, the signal source, and the SGH are also measured and accounted for to accurately determine the gain of the AUT.

The information contained in this document should be used only for the scope of the contract for which this document is prepared.

3.1.1.2 Measurement Setup

The measurement setup is shown in Figure 3.2. In the first measurement the VAST12 antenna was mounted through the extension flange to the mounting flange of the antenna tower. In the second measurement the VAST12 antenna was mounted directly to the antenna tower.

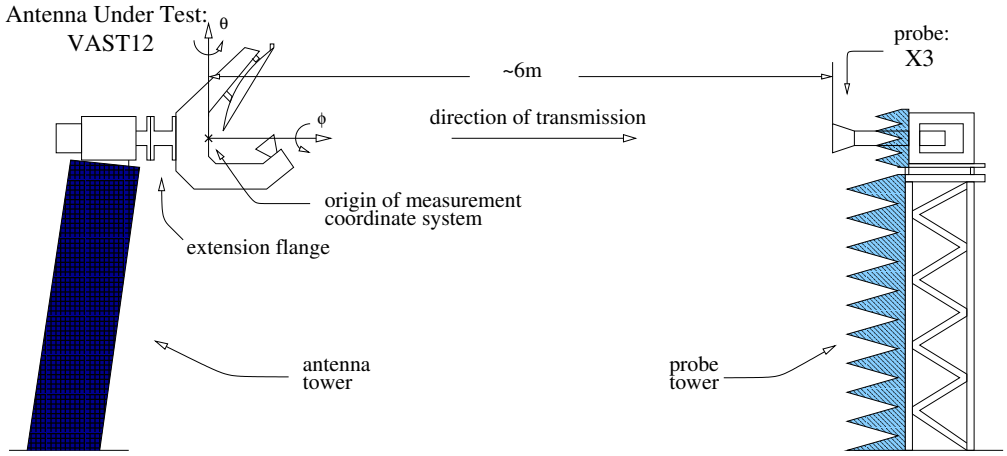

Figure 3.2 Measurement setup.

The antenna tower provides two axes of rotation: a vertical axis (θ-axis) and a horizontal axis (ϕ-axis). The near-field of the AUT can hereby be measured in any (θ, ϕ)-direction at a constant distance, i.e. a full sphere measurement, using the probe mounted on the probe tower. Two orthogonal components of the near-field are measured.

The RF system comprises a Scientific Atlanta SA2180 signal source and a Scientific Atlanta SA1795 vector measurement receiver. To ensure that the signal source is well matched, the cable connecting the signal source and the AUT is fitted with an isolator. The measurement is automated and controlled by a computer program developed at the facility. The near-field to far-field transformation is performed by the SNIFTD software [15]. The rotation of the spherical coefficients to transform the far-field from the measurement coordinate system into the optical coordinate system is performed by the ROSCOE software [15]. The S-parameters of the AUT and the SGH are measured using a calibrated HP8510 vector network analyzer.

3.1.1.3 Measurement Procedure

Prior to making any measurements of the AUT, pattern and polarization calibrations of the probe are performed. Before the last step of the polarization calibration is performed, the probe is placed in its final position on the probe tower. The probe is then not removed before the measurements of the AUT and the SGH are completed. The measurement procedure is outlined below and it is the same for both measurements.

1. Mechanical alignment of the antenna tower and the probe tower.
2. Pattern and polarization calibration of the probe.
3. Mounting and alignment of the SGH on the antenna tower.

The information contained in this document should be used only for the scope of the contract for which this document is prepared.

4. Full sphere measurement of the SGH.
5. Near-field point measurement of the SGH for gain determination by substitution.
6. Dismounting of the SGH and mounting and mechanical alignment of the AUT on the antenna tower.
7. Near-field point measurement of the AUT for gain determination by substitution.
8. Optical measurements of the mirror cube on the AUT.
9. Full sphere measurement of the AUT.
10. S-parameters measurements for the AUT and the SGH and loss measurements in the coax-to-waveguide transition of the SGH.

The procedure for the data processing is as follows:

1. Probe correction coefficients are calculated.
2. Spherical coefficients of the AUT are found, including probe correction, in the measurement coordinate system. Total radiated power, directivity and the radiation pattern are calculated.
3. The spherical coefficients of the AUT are transformed from the measurement coordinate system to the optical coordinate system and the radiation pattern is again calculated.
4. Plots of co- and cross-polar radiation patterns are made. The far-field data are converted from the binary file format to the ASCII file format.
5. The SGH raw measurement data are transformed to the corresponding far-field including probe correction. The SGH directivity is calculated. Losses in the SGH including coax-to-waveguide transition are determined and the gain of the SGH thus obtained.
6. The gain of the AUT is calculated using near-field and far-field data for the AUT and SGH. Losses in the AUT are calculated.

The measurement coordinate system coincides with the mechanical coordinate system of the VAST12 antenna (see Figure 3.2). The three Euler angles determined in the first measurement and used for transformation from the measurement coordinate system to the mirror cube (optical) coordinate system were: $(\phi, \theta, \chi) = (228.418,\ 0.621,\ 131.401)$. The definition of the Euler angles and the description of the corresponding rotations are given in Appendix A. The three Euler angles determined in the second measurement and used for transformation from the measurement coordinate system to the mirror cube (optical) coordinate system were: $(\phi, \theta, \chi) = (228.189,\ 0.620,\ 131.634)$. In order to transform from the measurement coordinate system to the electrical coordinate system, the location of the maximum value of the co-polar field component in the measurement coordinate system was found with the resolution 0.02° in θ and 1° in ϕ. The Euler angles were then defined as follows: In the first measurement these were: $(\phi, \theta, \chi) = (228.300,\ 0.180,\ 132.000)$. In the second measurement these were: $(\phi, \theta, \chi) = (269.080,\ 0.140,\ 91.000)$.

The information contained in this document should be used only for the scope of the contract for which this document is prepared.

3.1.1.4 Measurement Accuracy

Table 3.1 provides a list of electrical and mechanical sources of inaccuracy in the spherical near-field antenna measurement and their influence on the on-axis directivity. Table 3.2 provides a similar list of inaccuracy sources in the gain determination by the substitution method.

Source	Accuracy	Influence on directivity [dB]
Reflectivity level	< -50 dB	–
Multiple reflections	$\pm 0.2\%$	± 0.018
Antenna tower pointing	$\pm 0.05°$	± 0.058
Measurement distance	± 2 mm	–
Axes intersection	± 0.1 mm	± 0.001
Probe position	± 0.3 mm	± 0.008
Amplitude drift	$\pm 0.17\%$	± 0.015
Amplitude noise	$\pm 0.06\%$	± 0.005
Amplitude non-linearity	$\pm 0.5\%$	± 0.043
Phase drift	$\pm 0.2°$	–
Phase noise	$\pm 0.1°$	–
Phase shift in rotary joints	$\pm 0.1°$	–
Channel balance amplitude	$\pm 0.14\%$	± 0.003
Channel balance phase	$\pm 0.1°$	± 0.005
Probe polarization amplitude	$\pm 0.1\%$	± 0.001
Probe polarization phase	$\pm 0.02°$	–
Mode truncation	± 0.001 dB	± 0.001
Worst case sum		± 0.158
Root Sum Square (RSS)		± 0.077
Standard deviation (σ)		± 0.044
3σ		± 0.132

Table 3.1 Accuracy estimate for on-axis directivity of the VAST12 antenna.

The reflectivity level is the experimentally verified specification of the anechoic chamber [16]. The accuracies of the following sources are found from measurements during this project: multiple reflections, antenna tower pointing, measurement distance, axes intersection, probe position, amplitude drift and noise, phase drift and noise, channel balance amplitude and phase, probe polarization amplitude and phase, mode truncation, SGH gain, mismatch correction, cable variations. The accuracies related to the Scientific Atlanta SA1795 measurement receiver (amplitude non-linearity) and to the rotary joints (phase shift) are taken from the manufacturer's specification.

The influence of the individual sources of inaccuracy has been found by either analytic estimation or by introducing changes in the measured near-field data and observing the corresponding changes in the calculated far-fields.

The information contained in this document should be used only for the scope of the contract for which this document is prepared.

Source	Accuracy	Influence on gain [dB]
AUT directivity	±0.08 dB	±0.08
SGH gain	±0.07 dB	±0.07
Amplitude non-linearity	0.05 dB/10 dB	±0.05
Signal-to-noise ratio	80 dB	–
Multiple reflections	±0.2%	±0.02
Mismatch correction	±0.05 dB	±0.05
Cable variations	±0.05 dB	±0.05
Worst case sum		±0.32
Root Sum Square (RSS)		±0.14
Standard deviation (σ)		±0.08
3σ		±0.24

Table 3.2 Accuracy estimate for on-axis gain of the VAST12 antenna.

All the contributions in Table 3.1 and Table 3.2 can be considered to have a rectangular distribution between the lower and the upper bound values. Therefore, the corresponding standard deviation is $1/\sqrt{3}$ times the upper bound value. Similarly, the total standard deviation, σ, will be $1/\sqrt{3}$ times the RSS value. The total influence on the gain value therefore corresponds to a standard deviation σ of 0.08 dB and a 3σ-value of 0.24 dB.

The information contained in this document should be used only for the scope of the contract for which this document is prepared.

3.2 Polytechnic University of Madrid

Measurements have been done in three different facilities at the Polytechnic University of Madrid. The facilities consist of a spherical near-field system (UPM1), a planar near-field system (UPM2), and a compact range system (UPM3). The results from the measurements and a description of each facility have been presented in [17]. The facility descriptions given below are an extract of what is given in that work.

3.2.1 UPM Spherical Near-Field System

This part describes the test procedure for the VAST12 carried out at the LEHA-UPM Spherical Near-Field System (UPM1). It describes the general aspects of the test procedure: measurement instrumentation, measurement environmental conditions, measurement techniques, measurement setups and measurement procedures.

3.2.1.1 Measurements

In the spherical near-field system the measured parameters were at 12 GHz: radiation pattern (co-polar and cross-polar), directivity, gain and polarization characteristics.

Measurement frequencies:	12 GHz
Measurement type:	Full sphere measurement
Measurement distance:	530 cm
Scan axis:	ϕ
Scan angle range:	$0^\circ \leq \phi \leq 359^\circ$
Scan angle increment:	1°
Step axis:	θ
Step angle range:	$0^\circ \leq \theta \leq 180^\circ$
Step angle increment:	1°
Probe:	Single channel. Corrugated conical horn
Probe pattern correction:	Included
Probe polarization correction:	Included

3.2.1.2 Measurement instrumentation

- Chamber dimensions (L,W,H): 7.3 x 4.3 x 4.3 meters
- Frequency range: 1 - 20 GHz
- Positioner System: ORBIT 3 axis system for polarization, roll and azimuth, equipped with synchronous (Positioner programmer Orbit AL-4706-3A and Power unit: Orbit AL-4146-2)
- Rotary joints: precision rotary joints up to 18 GHz, built by SIVERS Ltd.
- RF equipment: based on the Agilent 8530A system, equipped with test set 8511B and a synthesizer (HP8341A)
- The system is controlled with a PC equipped with IEEE488 bus.

The information contained in this document should be used only for the scope of the contract for which this document is prepared.

- Transformation Software: TICRA-TUD SNIFTD [15] to convert from spherical near field to far field

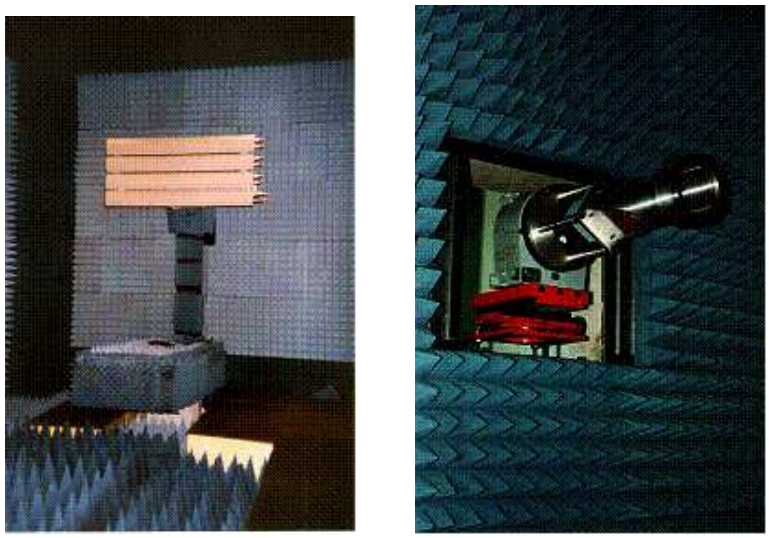

(a) (b)

Figure 3.3 LEHA-UPM Spherical near-field system. (a) AUT Positioner. Roll over Azimuth on longitudinal table. (b) Polarization Positioner.

3.2.1.3 Measurement environmental conditions

- Temperature: 21°C ± 2°C
- Relative humidity: 35% to 50%
- Pressure: 702 ± 25 mm Hg

3.2.1.4 Measurement technique

The radiation pattern is carried out in two steps: first, the near field of the Antenna Under Test (AUT) is measured in a number of points in a full sphere. Next, the near field is transformed to the corresponding far field using a mathematical algorithm based on a spherical wave expansion of the near field (SNIFTD). During this transformation, a value for the total radiated power is also found.

The directivity in any direction can be found as the ratio between the power density in that direction and the average radiated power density.

The gain measurement is performed using a substitution technique, where the amplitude of the AUT near field is compared with the amplitude of the field of a Standard Gain Horn at the same distance (rectangular horn). Combined with the knowledge of the near and far

The information contained in this document should be used only for the scope of the contract for which this document is prepared.

fields of two antennas, obtained from full-sphere measurement of both, the ratio between the gains of the AUT and Standard Gain Horn (SGH) can be determined. The gain of the SGH is found by subtracting the loss from its directivity. The directivity is found from a full sphere measurement, while the loss (very low value) in the waveguide and in the pyramidal section is estimated using well known formulas for the ohmic losses in a rectangular waveguide. The loss of the transitions are included in the calculation.

The polarization is measured with the three antenna technique [18], measuring the VAST12 antenna, the standard gain horn and the corrugated conical horn used as probe.

3.2.1.5 Measurement Setup

The measurement setup is shown in Figure 3.4. The AUT, in this case the VAST12 antenna, is mounted through an extension flange to the roll turntable. This positioner is on the tower over the azimuth positioner of the spherical near field system. The near field of the AUT can hereby be measured in any direction at a constant distance −530 cm, distance between AUT and probe-, that is a full sphere measurement.

The probe (corrugated conical horn) is mounted on a plate provided of one axis of rotation (polarization) to acquire two orthogonal polarizations (theta and phi).

The measurement is automated and controlled by a computer software developed at LEHA-UPM (PROCENCA), including transformation to far field with SNIFTD software.

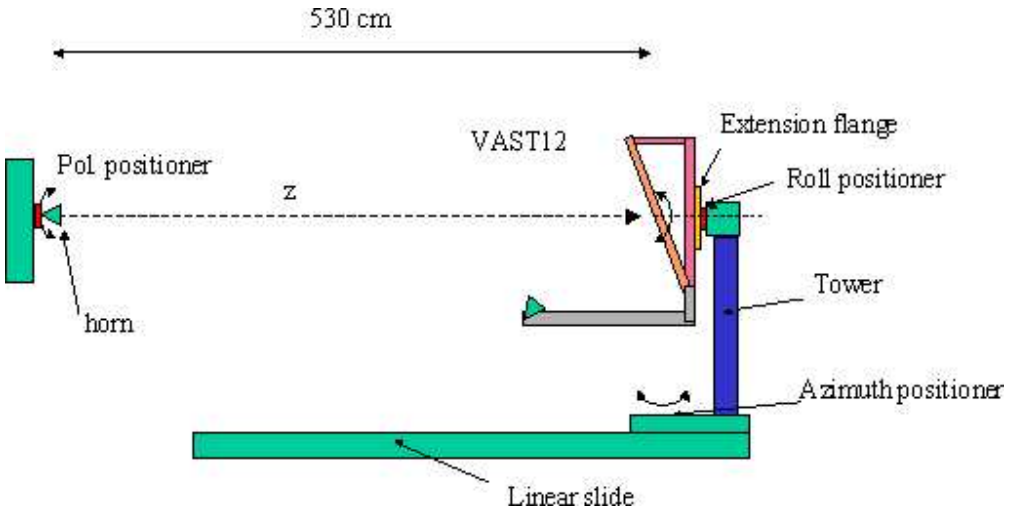

Figure 3.4 Spherical near-field system measurement setup.

3.2.1.6 Measurement procedure

Probe Calibration:

The used Ku probe is a corrugated conical horn with a maximum cross-polar radiation level equal to −35 dB. In the axis, the cross-polar level is −60.21 dB. This probe has a

The information contained in this document should be used only for the scope of the contract for which this document is prepared.

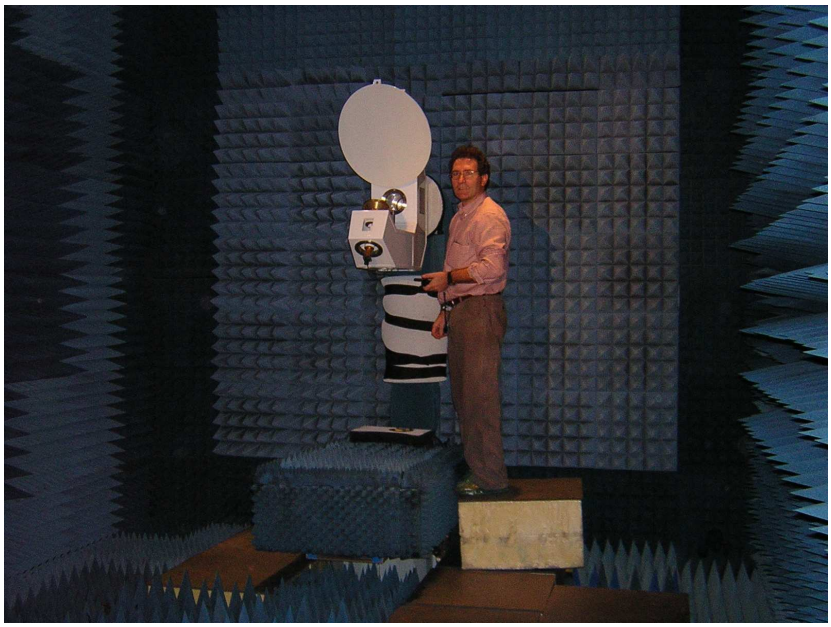

Figure 3.5 VAST12 in LEHA-UPM Spherical near-field system.

mechanized plane on its flange normal to the E-plane, that allows to move the antenna from one system to another one keeping the position. The error of the orthogonality between the plane and the electric field is 0.2°. This error was obtained using the three antennas polarization method. The process is:

1. Mechanical alignment of the antenna tower and the probe tower in the spherical system. This alignment was realized with a theodolite [13].

2. Mounting and alignment of the Ku probe in spherical system. The probe is placed with the level, adjusting the roll value to 90°. For this calibration, a NARDA rectangular horn (cross-polar level in the axis lower than −60 dB) is used as probe. This horn is also placed with a level, and it was also measured with the three antennas polarization method.

3. Pattern and polarization calibration of the probe in spherical system for the measurements in spherical and planar near field system, according to the method explained in SNIFTD software. For the Ku probe, these measurements are realized directly in far field.

4. Full sphere measurement of the Ku probe in spherical system to obtain the values of the directivity.

5. Measurement with a VNA (Vector Network Analyzer) the losses of the coax to waveguide transition to estimate the total losses and calculate the gain of the probe.

Near field acquisition:

1. Mounting and alignment of the VAST12 in the spherical near field system.

The information contained in this document should be used only for the scope of the contract for which this document is prepared.

2. Mounting and alignment of the probe in the spherical near field system.
3. Full sphere near field acquisition of the VAST12 antenna in the spherical near field system.
4. Near field measurement of the VAST12 in $\theta = 0°$ direction for gain determination by substitution.
5. Dismounting of the VAST12 of the spherical near field system.
6. Mounting and alignment of the SGH in the spherical near field system.
7. Near field measurement of the SGH in $\theta = 0°$ direction for gain determination by substitution.
8. Standard Gain Horn (SGH) calibration (same procedure as probe calibration).

Near field to far field transformation process:

1. The VAST12 antenna acquisition in spherical near field system is transformed to far field values, including probe correction. Total radiated power and directivity are calculated, using SNIFTD.
2. Plots of co- and cross-polar radiation pattern for the VAST12 are made.
3. VAST12 gain is calculated using spherical near field data, far field data, directivities, total radiated power and reflection coefficients for VAST12 and SGH. Losses of the VAST12 antenna are calculated from directivity and gain.

3.2.1.7 Measurement Errors

Error budget for directivity measurement:

Concept	Distribution	Main beam error (dB)
Mechanical setup inaccuracies	Normal (3σ)	0.020
Multiple reflections	Uniform (ε)	0.015
Receiver non linearity	Normal (3σ)	0.030
Noise standard deviation	Normal (3σ)	0.003
Thermal drift	Uniform (ε)	0.020
Scattering and absorption by the antenna tower	Uniform (ε)	0.020
VNA Sampling errors	Uniform (ε)	0.001
Rotary joints errors	Uniform (ε)	0.005
TOTAL RSS ERROR (3σ)		$\pm$0.089 dB

Table 3.3 Error budget for directivity measurement.

Error budget for gain measurement:

The information contained in this document should be used only for the scope of the contract for which this document is prepared.

Concept	Distribution	Main beam error (dB)
Mechanical setup inaccuracies	Normal (3σ)	0.020
Multiple reflections	Uniform (ε)	0.015
Receiver non linearity	Normal (3σ)	0.030
Noise standard deviation	Normal (3σ)	0.003
Thermal drift	Uniform (ε)	0.020
Scattering and absorption by the antenna tower	Uniform (ε)	0.020
VNA Sampling errors	Uniform (ε)	0.001
Rotary joints errors	Uniform (ε)	0.005
SGH gain error	Normal (3σ)	0.12
Comparison Measurements error	Normal (3σ)	0.05
TOTAL RSS ERROR (3σ)		$\pm$0.158 dB

Table 3.4 Error budget for gain measurement.

Where

$$3\sigma = \sqrt{\sum_{\text{normal}} (3\sigma_i)^2 + \sum_{\text{uniform}} (1.73\varepsilon_i)^2}. \tag{3.1}$$

Error for loss measurement:

$$3\sigma_{loss} = \sqrt{(3\sigma_{directivity})^2 + (3\sigma_{gain})^2} = \pm 0.181 \text{ dB} \tag{3.2}$$

3.2.2 UPM Planar Near-Field System

This part describes the test procedure for the VAST12 carried out at the LEHA-UPM Planar Near Field System (UPM2). It describes the general aspects of the test procedure: measurement instrumentation, measurement environmental conditions, measurement techniques, measurement setups and measurement procedures.

3.2.2.1 Measurements

In the planar near field system the measurements were: co-polar and cross-polar radiation pattern ($-30^\circ \leq \theta \leq 30^\circ$) and gain.

The information contained in this document should be used only for the scope of the contract for which this document is prepared.

Measurement frequencies:	12 GHz
Measurement type:	Planar scanning
Measurement distance:	80 cm
Scan axis:	y
Scan range (cm):	$80 \leq y \leq 328.5$
Scan increment (cm):	1.75
Step axis:	x
Step range (cm):	$125 \leq x \leq 373.5$
Step increment (cm):	1.75
Probe:	Single channel. Corrugated conical horn
Probe pattern correction:	Included
Probe polarization correction:	Not Included (due to the polarization purity of the probe)

3.2.2.2 Measurement Instrumentation

- Chamber dimensions (L,W,H): 15 x 8 x 7.3 meters.
- Frequency range: 0.9 - 40 GHz.
- Maximum Scan area: 4.75 x 4.75 meters.
- Positioner System: 5 axis for probe polarization, x-axes, y-axes, roll and azimuth, equipped with optical encoders. This measure has been carried out with x, y and polarization axes. Roll over azimuth is used in the antenna alignment.
- Rotary joints: precision rotary joints up to 40 GHz, built by SIVERS Ltd.
- RF equipment: based on the Agilent 8530A system, equipped with test set 8511B for planar acquisition.
- The system is controlled with a PC equipped with IEEE488 bus.
- Software: PNIFT [19] to convert from planar near field to far field.

The z-accuracy in planar scanner has been checked with a laser tracker obtaining results shown in Figure 3.7. The errors are lower than ±0.16 mm in the measured plane (4000 mm x 4500 mm). This means a phase error at 12 GHz lower than ±2.3 deg (peak value). The x and y position accuracy is ±0.2 mm. This value has been also obtained with the laser tracker. The cables used in this system are Gore™ Phaseflex® with a high phase stability (change in phase specification, with flexure, equal to ±3.4° at 12 GHz).

3.2.2.3 Measurement Environmental conditions

- Temperature: 21°C ± 2°C
- Relative humidity: 35% to 50%
- Pressure: 702 ± 25 mm Hg

The information contained in this document should be used only for the scope of the contract for which this document is prepared.

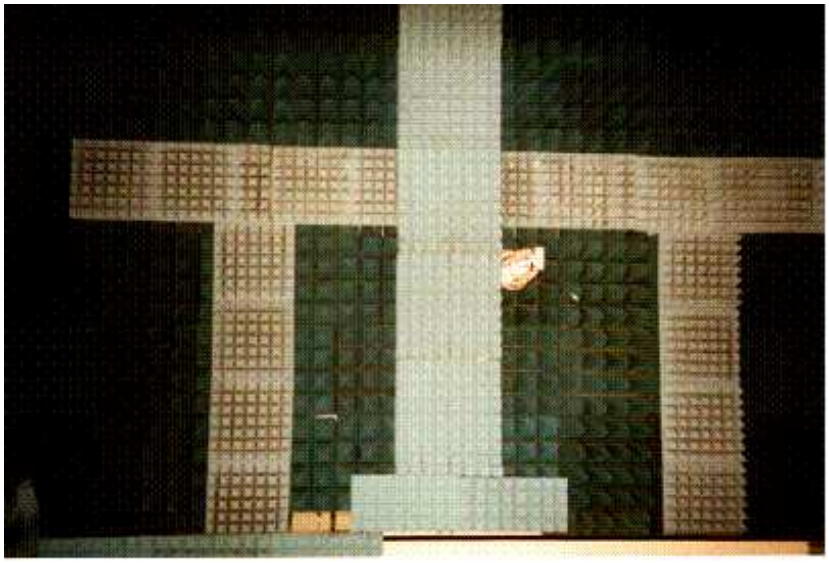

Figure 3.6 LEHA-UPM Planar Scanner.

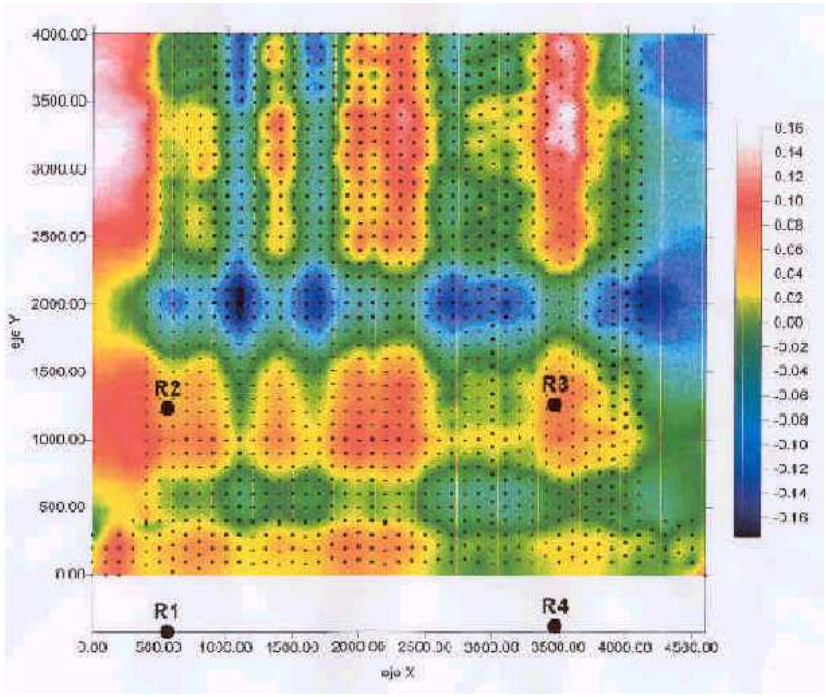

Figure 3.7 z-accuracy of the scanner.

3.2.2.4 Measurement Technique

The radiation measurement is carried out in two steps: first, the near field of the Antenna under Test (AUT) is measured in a number of points on the plane. The second step is the post-process to transform the acquired measurements in far field pattern. This transformation is realized with a mathematical algorithm based on a planar wave transformation of the near field, including pattern and polarization probe correction. The valid angular range of the

The information contained in this document should be used only for the scope of the contract for which this document is prepared.

radiation pattern (Figure 3.8) depends on the antenna dimensions, planar scanner surface and distance from the antenna to the scanner. For this antenna the dimension of the measured plane was adjusted to 248.5 x 248.5 cm, to reduce the measured time. The scanning zone was adjusted to the limits where acquired near field level were −45 dB (respect the maximum value). The distance from the antenna to the scanner was adjusted to 80 cm and the antenna aperture diameter is 50.8 cm In this case the valid angular range for the measurement is ±51° in both planes. The step between points was adjusted to 1.75 cm. This value limits the valid angular range, without aliasing, to ±45.6°.

$$A_x = A_y = 1.75 \text{ cm} \leq \frac{\lambda}{2\sin\theta} \Rightarrow \theta = 45.6^\circ \tag{3.3}$$

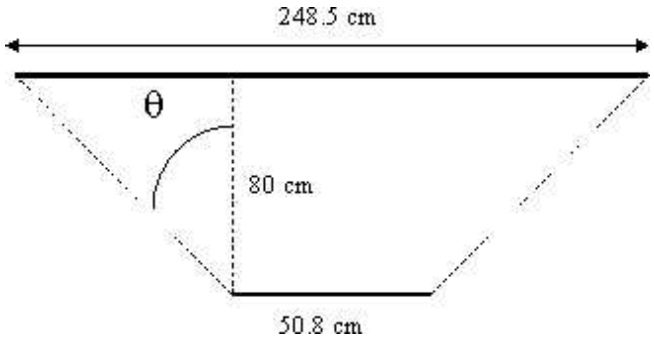

Figure 3.8 Valid angular range in the planar scanner.

The gain measurement is performed using the direct technique [20]. This technique requires the knowledge of the gain of the probe and the insertion losses of the system. The probe gain is obtained through measurement of the probe directivity in a spherical system and the measurement of the losses of the coax to waveguide transition. The insertion losses of the system are obtained joining (thru) the probe and AUT cables (reflection coefficients are accounted).

3.2.2.5 Measurement Setup

Figure 3.9 shows the VAST12 antenna in the Planar near field system. The measurement setup is shown in Figure 3.10. The AUT is mounted on the turntable of the roll over azimuth positioner of the system, at the top of the tower placed on the linear slide. The AUT is fixed on that position.

The probe (corrugated conical horn) is mounted on the turntable of the polarization positioner to acquire two orthogonal polarizations (horizontal and vertical).This positioner is mounted on the vertical table of the xy acquisition system.

The RF system comprises an Agilent 8530A system: signal source (synthesizer HP83620A) and test set (HP8511B). The S-parameters of the AUT and probe are measured using a calibrated Agilent PNA Vector Network Analyzer. The measurement is automated and controlled

The information contained in this document should be used only for the scope of the contract for which this document is prepared.

by a computer software developed at LEHA-UPM, and transformed to far field with PNIFT software (also developed at LEHA-UPM).

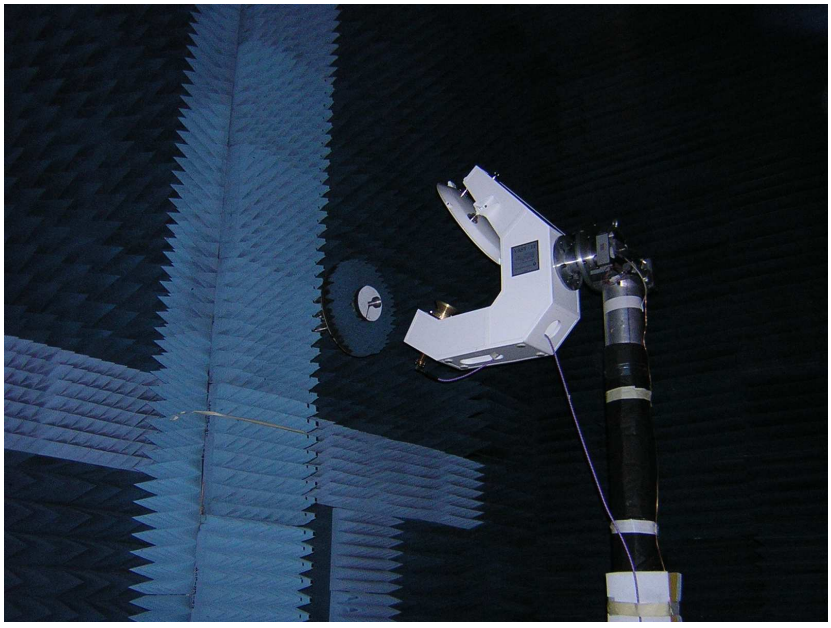

Figure 3.9 VAST12 in LEHA-UPM Planar near-field system.

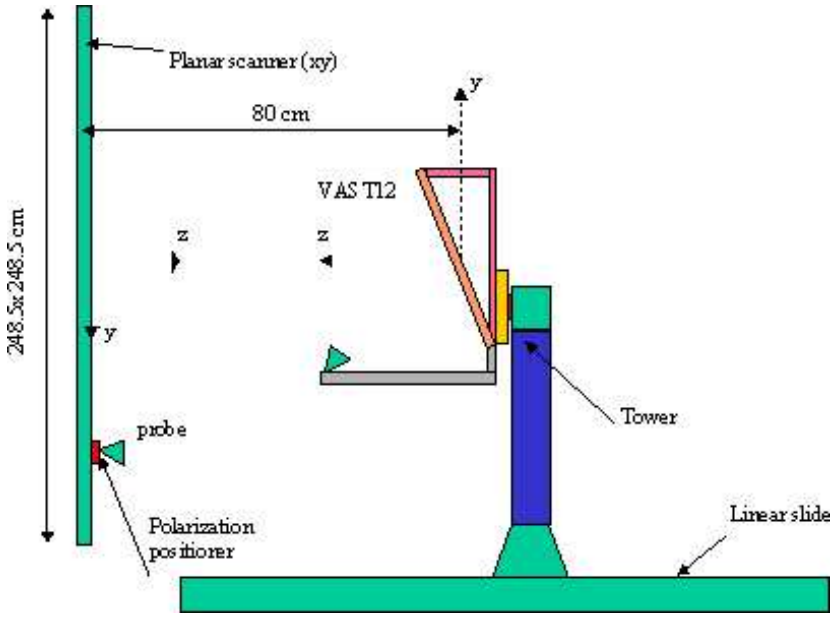

Figure 3.10 Planar near-field system setup.

The information contained in this document should be used only for the scope of the contract for which this document is prepared.

3.2.2.6 Antenna and system alignment

The antenna axis are defined according with the mechanical coordinate system in this way: z-axes is normal to the interface plate of the VAST12, and pointing out of the antenna and x-axis is in the plane of the interface plate, and horizontal.

Prior to the installation of the AUT on the positioner, an alignment process of the antenna tower was realized, with a laser placed on the roll turntable and a mirror placed on the probe polarization positioner. Azimuth positioner is rotated until the laser reflection coincides with its transmission iris. If there were used a precision laser and a good parallelism between scanner and polarization turntable existed, this alignment would assure the coincidence of the scanner z-axis with the antenna z-axis.

3.2.2.7 Measurement Procedure

1. Probe calibration (as explained for Spherical Near Field System).
2. Mechanical alignment of the antenna tower (as explained in Section 3.2.2.6).
3. Mechanical alignment of the Ku probe on the polarization positioner of the planar scanner with a precision level.
4. Mounting of the VAST12 antenna on the antenna tower of the planar system.
5. Planar acquisition of the near field (both polarizations) of the VAST12.
6. Direct connection between the probe cable and VAST12 cable, to measure the insertion loss of the system (direct method of gain measurement).
7. Dismounting of the VAST12 and probe of the planar near field system.

The process is as follows:

1. Probe correction coefficients for planar and spherical measurement systems are calculated with SNIFTD
2. The Ku probe acquisition in spherical near field system is transformed to far field values with SNIFTD, that also calculates total radiated power and directivity. Losses in the probe including coax-to-waveguide transition are determined and the gain of the probe is obtained.
3. The VAST12 antenna acquisition in planar near field system is transformed to far field values (in the valid angular range), including probe correction with PNIFT, that also calculates radiated power through the plane
4. Plots of co- and cross-polar radiation pattern for the VAST12 are made.
5. VAST12 gain is calculated using planar far field data, near field data, gain of the probe, reflection coefficients, directivities and losses of the cable. Gain is referenced to the coaxial input.

The information contained in this document should be used only for the scope of the contract for which this document is prepared.

3.2.2.8 Measurement Errors

AUT Radiation pattern Error budget:

The VAST12 gain pattern is calculated by far field transformation (PNIFT). The error of the parameter is obtained from the following error budget:

NF/FF	Concept	Distribution	Main beam error (dB)
NF	Probe position error (xy plane)	Normal (3σ)	0.013
	Probe position error (z axis)	Normal (3σ)	0.003
	Probe scatter and multipath	Uniform	0.009
	Room reflections	Uniform	0.006
	Cable flexions	Normal (3σ)	0.003
	Thermal drift	Uniform	0.035
	Receiver noise	Normal (3σ)	0.002
	Receiver non linearities	Normal (3σ)	0.045
	Test port mismatch	Normal (3σ)	0.050
FF	Transformed Phase errors	Normal (3σ)	0.012
	Scan truncation	Normal (3σ)	0.080
	Aliasing	Normal (3σ)	0.030
	Probe gain calibration	Normal (3σ)	0.120
	Thru repetitively	Normal (3σ)	0.030
	Total (RS 3σ)		0.177

Table 3.5 Error budget for gain measurement.

3.2.3 UPM Compact Range System

This part describes the test procedure for the VAST12 carried out at the LEHA-UPM Compact Range System (UPM3). It describes the general aspects of the test procedure: measurement instrumentation, measurement environmental conditions, measurement techniques, measurement setups and measurement procedures.

3.2.3.1 Measurements

The measurements carried out in the Compact Range are the co-polar and cross-polar radiation patterns at 12 GHz and the gain.

The information contained in this document should be used only for the scope of the contract for which this document is prepared.

Measurement frequencies:	12 GHz
Measurement type:	Far field (Gregorian Compact Range)
Scan axis:	θ
Scan range:	$-179^\circ \leq \theta \leq 179^\circ$
Scan increment:	0.075° for $-30^\circ \leq \theta \leq 30^\circ$
	0.5° for $-179^\circ \leq \theta \leq 179^\circ$
Step axis:	ϕ
Step range (cm):	0°, 45°, 90°, 135°
Probe:	Single channel. Corrugated conical horn

VSWR was also measured.

3.2.3.2 Measurement instrumentation

- Chamber dimensions (L,W,H): 15 x 8 x 7.3 meters.
- Subreflector Chamber dimensions: 6 x 3 x 2.4 m.
- Frequency range: 6 - 40 GHz
- Positioner System: 4 axis for feed polarization, elevation, roll and azimuth, equipped with synchronous.
- Quiet zone at X band: 2.5 m. diameter (± 0.25 dB, $\pm 3^\circ$).
- Rotary joints: precision rotary joints up to 40 GHz.
- RF equipment: based on the Agilent 8530A system, equipped with test set 8511B for planar acquisition.
- This antenna range consists in a Gregorian Compact Range. It two chambers, one smaller where it is placed the feed and the subreflector. The main reflector and the tower for the antenna under test is placed in the main chamber. Some photographs of the measurement system are in Figure 3.11.

3.2.3.3 Measurement Environmental conditions

- Temperature: 21°C $\pm$ 2°C
- Relative humidity: 35% to 50%
- Pressure: 702 $\pm$ 25 mm Hg

3.2.3.4 Measurement Technique

The first step is the system alignment: this is done measuring the Radar Cross Section of a metallic plate, plane and parallel to the turntable, fabricated in aluminum, that is a 50 cm radius circle. The system will be aligned in the angle where the maximum RCS is located.

The information contained in this document should be used only for the scope of the contract for which this document is prepared.

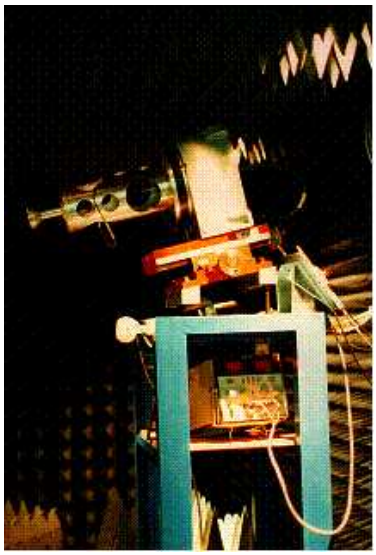

Feeder

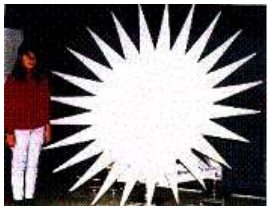

Subreflector

Main reflector

Figure 3.11 Compact Range System.

After aligning the system, the radiation patterns are measured rotating in azimuth the antenna tower. The phi values are obtained rotating the roll positioner.

The antenna gain is obtained by substitution with a SGH (previously calibrated at the spherical system).

The input reflection coefficients of the AUT and SGH are also measured and accounted for to accurately determine the gain of the AUT.

3.2.3.5 Measurement Setup

VAST12 antenna in the LEHA-UPM Gregorian Compact Range System is shown in Figure 3.12. The measurement setup is shown in Figure 3.13. The AUT, in this case the VAST12 antenna, is mounted through a extension flange to the roll turntable. This positioner is on the tower over the elevation over azimuth positioner of the compact range system. The far field from the Ku-probe (obtained through the two reflectors Gregorian System) can hereby be measured in any angular direction rotating the AUT over roll or azimuth axis of the antenna positioning system.

The probe (corrugated conical horn) is mounted on a plate provided of one axis of rotation (polarization) to acquire two orthogonal polarizations (theta and phi).

3.2.3.6 Measurement procedure

The SGH measurement follows the same procedure than shown in Section 3.2.2.7.

The information contained in this document should be used only for the scope of the contract for which this document is prepared.

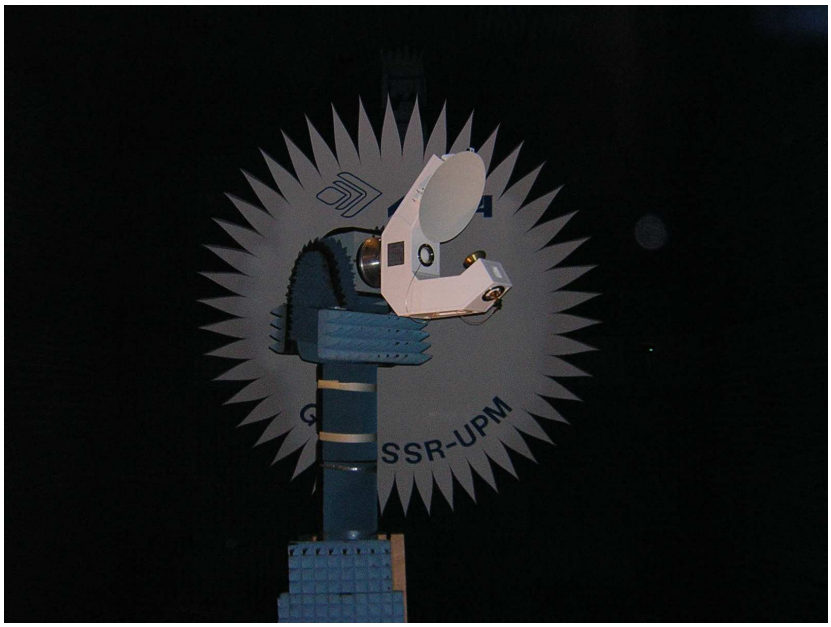

Figure 3.12 VAST12 in LEHA-UPM Compact Range System.

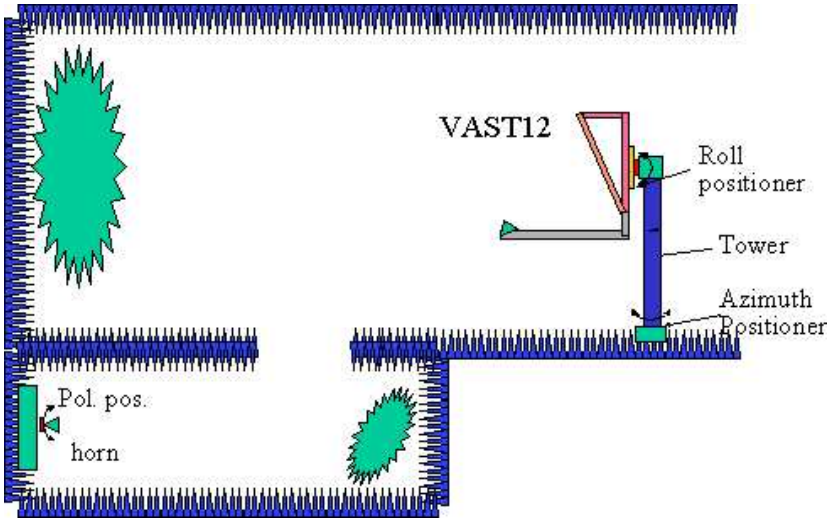

Figure 3.13 Compact Range Measurement Setup.

1. Mounting and alignment of the probe in the compact range system.
2. Antenna tower alignment.
3. Mounting and alignment of the VAST12 in the compact range system.
4. Measurement of radiation patterns of the VAST12 antenna for different phi angles.
5. Measurement of VSWR of the VAST12.
6. Mounting and alignment of the SGH in the compact range system.

The information contained in this document should be used only for the scope of the contract for which this document is prepared.

7. Measurement of the SGH radiation in broadside direction.

After the data acquisition, the process continue with these steps:

1. Plots of co- and cross-polar radiation pattern for the VAST12 are made.
2. Calculation of the gain by comparison between measurements of SGH and VAST12 in theta=0 deg values.

3.2.3.7 Measurement Errors

The error budget is considered for gain pattern measurement.

Concept	Distribution	Main beam error (dB)
Mechanical setup inaccuracies	Normal (3σ)	0.020
Multiple reflections	Uniform (ε)	0.015
Receiver non linearity	Normal (3σ)	0.030
Noise standard deviation	Normal (3σ)	0.003
Thermal drift	Uniform (ε)	0.020
Scattering and absorption by the antenna tower	Uniform (ε)	0.020
VNA Sampling errors	Uniform (ε)	0.001
Rotary joints errors	Uniform (ε)	0.005
SGH internal losses estimation error	Normal (3σ)	0.005
Phase and amplitude errors in quiet zone	Normal (3σ)	0.250
SGH Gain error	Normal (3σ)	0.120
TOTAL RSS ERROR		$\pm$0.29 dB

Table 3.6 Error budget for gain measurement.

3.3 France Telecom Research & Development

France Telecom Research & Development (FTRD) have provided measurement results for the comparisons from their far-field measurement facility. The description of the facility which is provided here is taken from [21].

3.3.1 FTRD Far-Field Range

Based at La Tête de Chien, on top of a rocky promontory above Monaco, the La Turbie site is an ideal location for the measurement of electromagnetic radiation. It offers:

- An optimal topography: a 300 meters deep valley between the transmitter station, located 1450 meters away, and the antenna under test, and a steep cliff behind the measurement area overlooking the sea, providing a pure environment free of parasitic reflection.

The information contained in this document should be used only for the scope of the contract for which this document is prepared.

- Good weather conditions throughout the year.
- Protection from radio interference due to the establishment of a "quiet zone" around the site.

The quality of the radiated electromagnetic field leads to exceptional precision in antenna measurements, and a dynamic range attaining 80 dB, making La Turbie a unique site throughout the world.

Figure 3.14 Photo of the radome.

3.3.1.1 General characteristics

The radome, comprised of a resin dome with a fabric "window" which is transparent at microwave frequencies, is a sheltered environment for the measurement of satellite antennas. The air within the radome can be filtered, to provide clean room conditions with strictly controlled temperature, humidity, and air purity.

Main characteristics are:

- Diameter of base 15 m, useful internal height 8.5 m, useful volume 1150 m^3.
- 3 axis-positioner, with X, Y offset table, elevation over azimuth positioner and polarization positioner. The whole is set on a mounting lift (4-th axis) with the possibility of movement on a precision rail.
- Maximum AUT size 3.50 m, maximum load 800 kg function of the assembly.

3.3.1.2 Radio-electric characteristics and used material

- Frequency band 0.5 to 50 GHz
- Reflectivity: -40 dB for $F > 4$ GHz

The information contained in this document should be used only for the scope of the contract for which this document is prepared.

- Transmitted power: 30 dBm
- Angular accuracy: azimuth, site 1/100° (encoder 16 bits), polarization 2/100° (selsyns 1/1 and 36/1).
- Angular range ±30° elevation and ±60° azimuth
- Equipment: microwave receiver HP 8530, LAVAUR Positioners, controls ACC, workstation B1000 model.

Figure 3.15 shows the synopsis of the far-field range

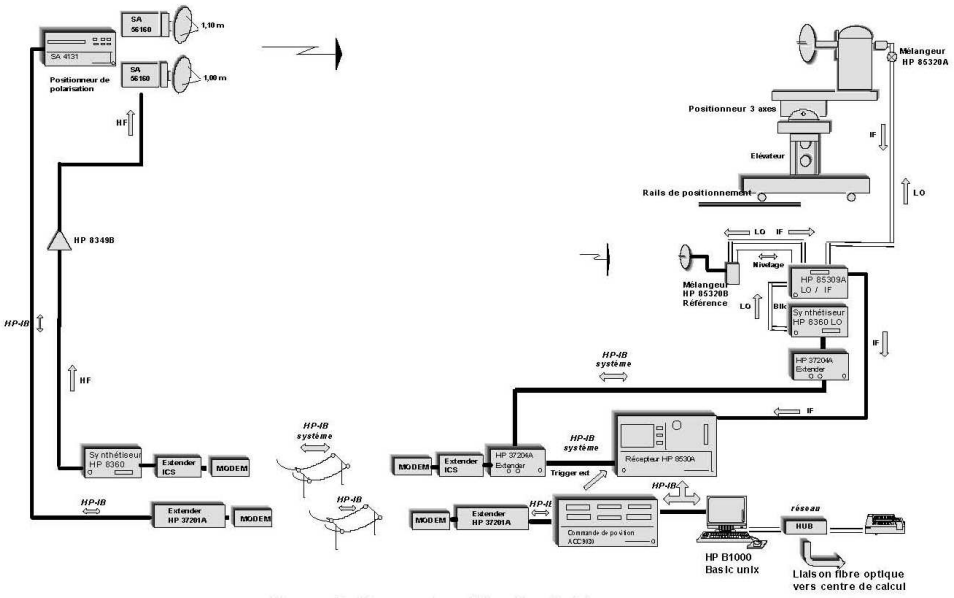

Figure 3.15 Synopsis of the far-field range.

3.3.1.3 Mount of the VAST12 Antenna and Axis

The best way to describe the axis used for the characterization of the VAST12 antenna is to give a picture. Figure 3.16 shows the antenna and the two axis.

3.3.1.4 Transmit Antenna

Figure 3.17 shows the transmit antenna used during the characterization of the VAST12 antenna.

The information contained in this document should be used only for the scope of the contract for which this document is prepared.

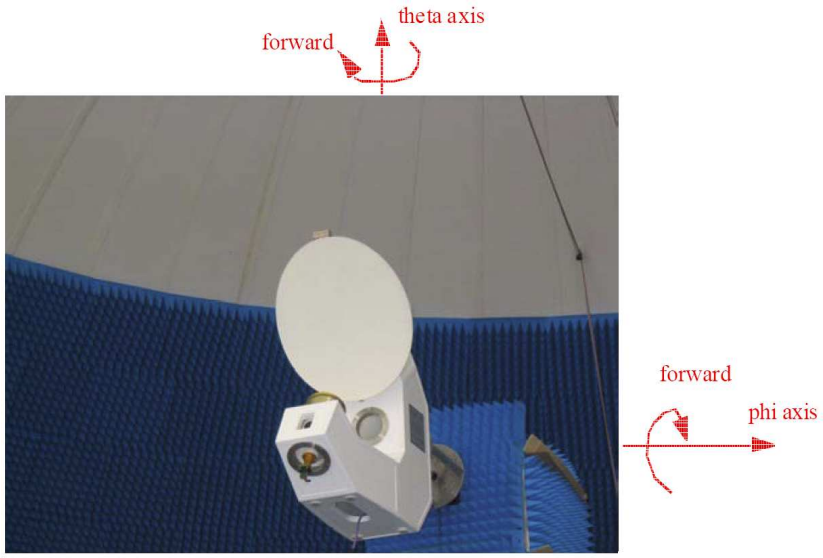

Figure 3.16 VAST12 Antenna and the two axis (front view).

Figure 3.17 Transmit antenna.

The information contained in this document should be used only for the scope of the contract for which this document is prepared.

3.4 Saab Ericsson Space

Saab Ericsson Space (SES) have provided measurement results for the comparisons from their A6 test range. The description of the facility which is provided here is taken from [22].

3.4.1 SES A6 Spherical Near-Field Test Range

The A6 test range is a dual mode facility where the AUT can be either a passive antenna or an active antenna and measured in either receive or transmit mode. It is used for applications that range from far-field measurements of small antennas to near-field testing of directive reflector and array antennas.

The anechoic chamber is a 5 (width) x 5 (height) x 9 (length) m^3 rectangular chamber lined with pyramidal absorbers. To protect the measurements from external disturbances, or to protect the outer environment when active antennas are tested, the facility is RF shielded. The level of shielding is better than 90 dB. Access to the test object is via a drawbridge, see figure. The frequency range covered is 0.8 - 40 GHz and the measurement distance is 6 m. The quiet zone diameter is 0.5 m for far-field measurements and more than 1.2 m for near-field measurements.

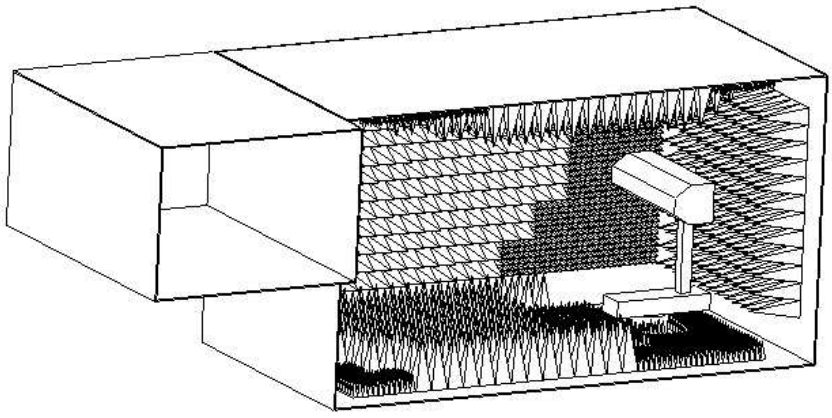

Figure 3.18 Outline of facility.

The RF subsystem is based on an HP8530 microwave receiver with distributed mixers. The signal and LO sources are of the HP8360 family. The range antennas used are two dual linearly polarized wide band horns for 0.8 - 4.5 GHz and 2 - 18 GHz and two standard gain horn antennas for 18 - 26 GHz and 26 - 40 GHz. It is possible to measure four ports on the AUT and two polarizations on the range antenna.

The positioner system features a high precision roll over slide over azimuth system with a tower between the slide and roll positioner. The roll axis is interchangeable between a high precision high load positioner (100 kg load) and an extremely low profile positioner (10 kg load) for measurement of small antennas. The positioner control is accomplished by an

The information contained in this document should be used only for the scope of the contract for which this document is prepared.

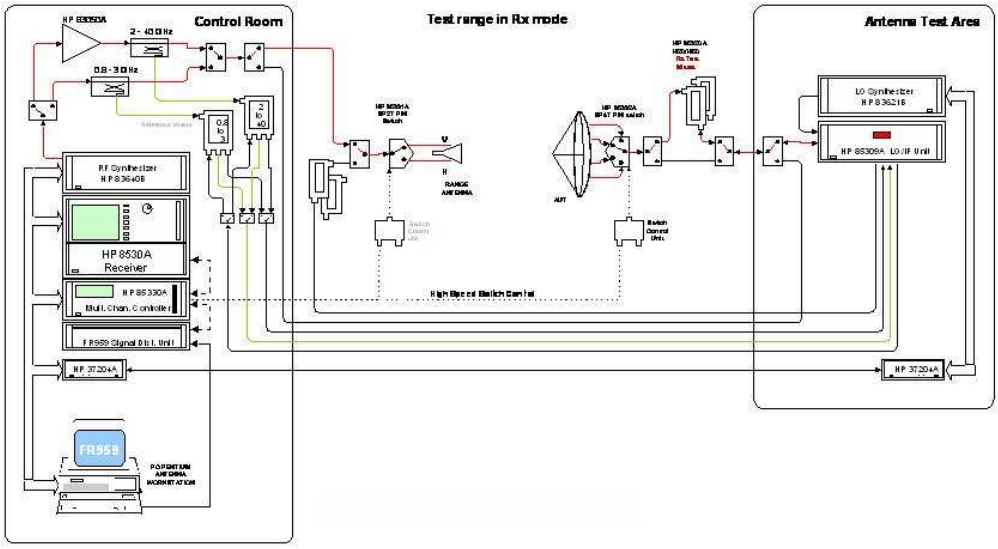

Figure 3.19 RF System.

Orbit/FR AL-4146-2 power amplifier and a DSP card in the range computer.

The data acquisition system is a standard FR959 Antenna measurement workstation. It consists of modified antenna measurement software and a control PC (range computer). The software is enhanced with utilities for call of NetCDF conversion software and a real time angular display option.

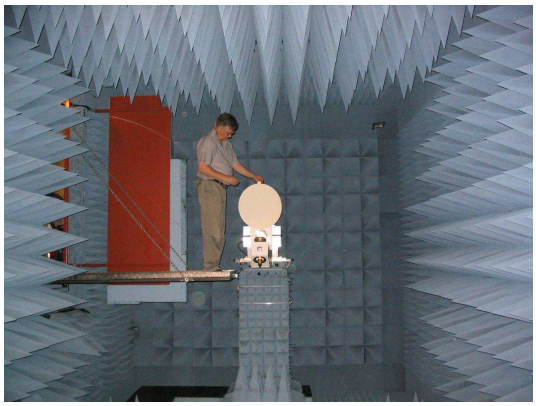

(a)

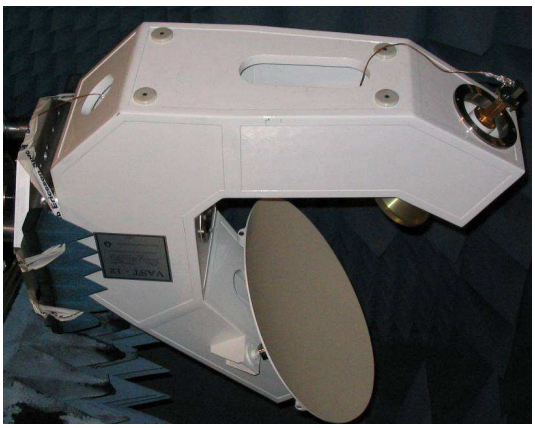

(b)

Figure 3.20 (a) VAST12 Antenna at the test range. (b) VAST12 Antenna mounted on the positioner.

The information contained in this document should be used only for the scope of the contract for which this document is prepared.

3.5 Polytechnic University of Catalonia

The Polytechnic University of Catalonia (UPC) has provided measurement results for the comparisons from their spherical near-field range. An important note on the measurement that was conducted at the UPC facility is that the data from this measurement has not been probe corrected.

3.5.1 Spherical Near-Field Range at UPC

The UPC anechoic chamber has dimensions of (LxWxH) 10 x 7.5 x 7.2 m, and is covered by absorbent panels. The reflectivity of the panels at L band is estimated to be −30dB. For the antenna pattern measurement the Antenna Under Test (AUT) is placed in a positioner system *roll over azimuth* (Figure 3.21) that constitute an spherical measurement system. A probe antenna (usually a horn antenna) is placed in front of the AUT. The distance from the antenna to the probe is constant (about 5.5m) and the combined movement of both positioners allows the rotation of the AUT in all directions respect the probe. The movements of the azimuth positioner are movements along the *theta* angle of the spherical coordinate system and the movements of the roll positioner are movements along the *phi* angle. The center of the spherical coordinate system is placed in the intersection of the rotation axis of both positioners and z axis is the rotation axis of the roll positioner.

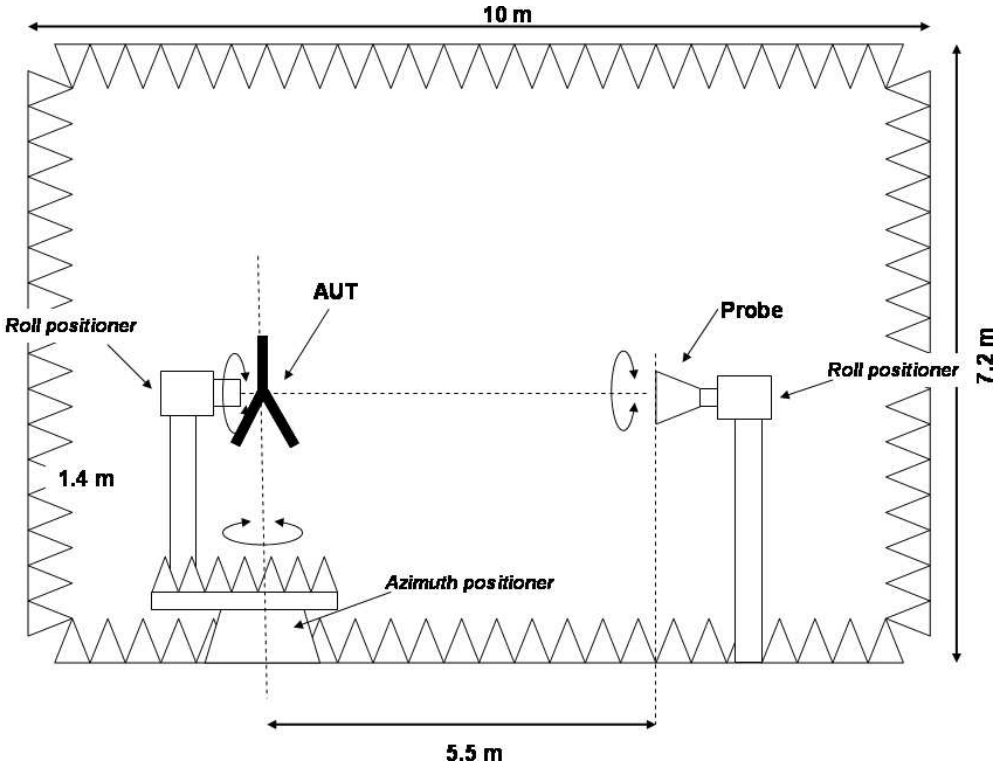

Figure 3.21 Anechoic chamber geometry.

The RF measurement system is based on the HP8530 network analyzer, with a specific *test-set* for antenna measurements (Figure 3.22). The signal generated by a synthesizer feeds the probe antenna. A sample of the signal is sent to the test-set as reference signal. The

The information contained in this document should be used only for the scope of the contract for which this document is prepared.

signal received by the antenna is also sent to the test-set and compared with the reference signal for to compensate the fluctuations in the synthesizer. A rotary joint allows a complete freedom of movements in the positioners, and also the position of cables is totally fixed, and his stability is guaranteed.

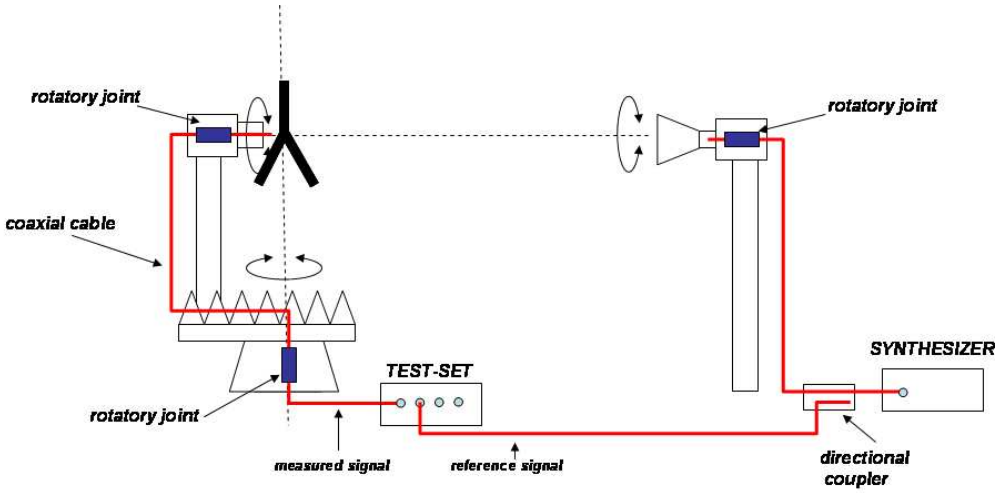

Figure 3.22 RF set-up.

The information contained in this document should be used only for the scope of the contract for which this document is prepared.

Chapter 4

Measurement Campaign

A brief description of preparation and development of the campaign, the actual time-line as well as an overview of the conducted measurements are given in this chapter.

4.1 Campaign Preparation and Planning

There is a series of questions to be answered and issues to be discussed in the process of preparation of any facility comparison campaign. Particularly, a candidate antenna should be found, a list of antenna parameters to be measured and compared, the format for the data provided for the comparison and contents of the reports, a schedule of the antenna measurements as well as the data comparison strategy.

The VAST12 antenna has been chosen as the candidate antenna for the planned campaign, since it satisfies most of the requirements set for such an antenna [10]. The concepts of the Verification Test Plan (VTP) and the User Data Package (UDP) were adopted from the previous campaigns carried out at DTU for the European Space Agency [23], but modified for the purpose of the present campaign.

The VTP accepted for the present campaign includes the following parts: a short description of the measurement, the name and affiliation of the measurement facility, its technical details, a list of the antenna parameters to be measured, and a description of the data format. The VTP was prepared by DTU as an Excel sheet to be filled in by the participants. All the VTPs received from the participants can be found in Appendix C

The UDP includes the following documents:

1. VAST12 antenna Storage and Handling Manual;
2. VAST12 antenna Visual Inspection and Damage Status Report;
3. Description of the VAST12 antenna mechanical and electrical interface;
4. Time schedule of the campaign.

Most of the issues for discussion mentioned above were discussed and agreed between the participants of the planned campaign at several progress meetings of the Activity 1.2 of the ACE network. The actual time-line of the campaign is given in the next section.

The information contained in this document should be used only for the scope of the contract for which this document is prepared.

4.2 Campaign Time-line

1. The VAST12 antenna was briefly introduced at the ACE kick-off meeting in Noordwijk, the Netherlands on January 30, 2004 and the participants of the Activity 1.2 meeting were invited to join the First Facility Comparison Campaign.

2. The campaign started by measurement of the VAST12 antenna at the DTU-ESA Spherical Near-Field Antenna Test Facility in May 2004.

3. The major part of the campaign planning has taken place at the second progress meeting at Gothenburg, Sweden on June 10, 2004. First, the VAST12 antenna has been introduced to the participants: its mechanical and electrical characteristics together with the three available coordinate systems have been presented. Next, the concepts of the VTP and the UDP have been presented and their contents have been discussed between the potential participants of the campaign. Then, a tentative plan for the campaign has been discussed and agreed.

4. A template of the VTP has been prepared by DTU and sent around.

5. Participants have signed up for the campaign, delivered their filled-in VTPs, and indicated the most suitable period for the antenna measurement.

6. DTU has established the optimum time schedule and sent the VAST12 together with the UDP to the participants according to the schedule. The final schedule of the campaign is shown in Table 4.1.

7. Participants have carried out the measurements and delivered measurement reports and the data to DTU.

8. The data have been presented to the participants at the progress meetings in Paris, France on April 1, 2005 and in Noordwijk, the Netherlands on May 30, 2005.

9. Different comparison strategies and first processed results have been discussed at the progress meeting in Copenhagen, Denmark on September 23, 2005.

10. A first draft of the final report has then been prepared and sent to the participants by the end of November 2005. The contents of the report has been discussed at the progress meeting in Noordwijk, the Netherlands on December 2, 2005 and actions have been agreed for finalizing the report.

The information contained in this document should be used only for the scope of the contract for which this document is prepared.

Dates	Participant
May 18 – May 31, 2004	Measurement at DTU
Sep. 13 – Oct. 1, 2004	University of Liverpool
Oct. 4 – Oct. 22, 2004	France Telecom R&D La Turbie
Oct. 25 – Oct. 29, 2004	DTU
Nov. 1 – Nov. 19, 2004	University of Madrid
Nov. 22 – Dec. 10, 2004	Athens, "Demokritos"
Dec. 13, 2004 – Jan. 7, 2005	DTU
Jan. 10 – Jan. 28, 2005	University of Catalonia
Jan. 31, 2005	DTU
Apr. 18 – May 2, 2005	Measurement at DTU

Table 4.1 Time schedule of the First Facility Comparison Campaign.

4.3 Measurement Overview

During the initial stage of the campaign it has been realized by a couple of the participating facilities that the measurement of the VAST12 antenna, for technical reasons, is too complex to be conducted at those facilities. Hence, one facility has conducted only a minor part of the planned measurement and another facility has withdrawn.

On the other hand, in addition to the measurements described above, the VAST12 antenna has also been measured in two other measurement facilities, at the Saab Ericsson Space (SES) and at Ericsson Microwave Systems (EMW), both in Sweden, during the summer 2004. Both of these facilities decided to join the campaign at a later stage, in the spring 2005. It has however only been possible to include the measurement data from SES in the present comparisons. The report documenting the measurement at EMW can be found in Appendix B. An overview of the collected data is shown below in Table 4.2.

DTU1 and DTU2 correspond to the measurements carried out at DTU in 2004 and 2005, respectively. UPM1, UPM2, and UPM3 correspond to the measurements carried out at UPM on the spherical near-field setup, the planar near-field setup and the compact range.

The information contained in this document should be used only for the scope of the contract for which this document is prepared.

	DTU1	DTU2	SES	FTRD	UPM1	UPM2	UPM3	UPC
Setup	SNF	SNF	SNF	FF	SNF	PNF	CR	SNF
Mechanical CS	x	x	x		x	x	x	
Pattern	x	x	x		x	x	x	
Polarization	x	x	(x)		x			
On-axis directivity	x	x	x		x			
Peak directivity	x	x			x			
On-axis gain	x	x	x		x	x	x	
Peak gain	x	x			x	x		
Electrical CS	x	x		x	x	x		
Pattern	x	x		x	x	x		
Polarization	x	x			x			
On-axis directivity	x	x		x	x			
Peak directivity	x	x		x	x			
On-axis gain	x	x		x	x	x		
Peak gain	x	x		x	x	x		
Optical CS	x	x	x		x	x		x
Pattern	x	x	x		x	x		x
Polarization	x	x	(x)		x			x
On-axis directivity	x	x	x		x			
Peak directivity	x	x	x		x			x
On-axis gain	x	x	x		x	x		
Peak gain	x	x	x		x	x		
Loss	x	x	x		x			
Accuracy budget	x	x			x	x	x	

Table 4.2 An overview of the data collected in the First Facility Comparison Campaign.

The information contained in this document should be used only for the scope of the contract for which this document is prepared.

Chapter 5

Comparison Strategy

The measurement data-sets available for the comparisons contain a large amount of information about the performance of the participating measurement facilities. As comparisons of this data can be approached in different ways this chapter is dedicated to presenting and discussing strategies for such. This includes discussions on comparisons of pattern shapes, comparisons of gain and directivity, and comparisons of polarization characteristics.

5.1 Pattern

As the terms radiation pattern, pattern shape, and pattern can be taken to refer to any of the common electromagnetic field quantities it is expedient for the discussions in the following sections that the meaning of these terms as used in this report is defined. The patterns are considered in the far-field region and, when suppressing a time dependence of $e^{j\omega t}$, it is thus possible to express the radiated electric field $\mathbf{E}(r, \theta, \phi)$ as

$$\mathbf{E}(r, \theta, \phi) = V_0 \frac{e^{-jkr}}{r} \mathbf{F}(\theta, \phi), \tag{5.1}$$

where $\mathbf{F}(\theta, \phi)$ will be denoted the far-field pattern function and V_0 is an amplitude constant. (r, θ, ϕ) are the spherical coordinates to the observation point. The amplitude constant V_0 is defined such that the co-polar component of $\mathbf{F}(\theta, \phi)$ will have a magnitude in the interval [0,1] when using Ludwig's third definition for the co- and cross-polar components

$$\mathbf{F}(\theta, \phi) = \hat{e}_{co} F_{co}(\theta, \phi) + \hat{e}_{cx} F_{cx}(\theta, \phi), \tag{5.2}$$

where $\hat{e}_{co}$ is a unit vector in the co-polarization direction and $\hat{e}_{cx}$ is a unit vector in the cross-polarization direction. $F_{co}(\theta, \phi)$ and $F_{cx}(\theta, \phi)$ are the co- and cross-polarized components of the pattern function respectively. It is seen that V_0 can thus be expressed as

$$V_0 = \max\{r|E_{co}(r, \theta, \phi)|\} \tag{5.3}$$

The information contained in this document should be used only for the scope of the contract for which this document is prepared.

Hence, when discussing how to compare the patterns in the following sections basis is taken in the far-field pattern function as defined here. As this definition effectively corresponds to a normalization of the magnitude of the co-polar component of the far-field pattern function $\mathbf{F}(\theta, \phi)$ this will also be referred to as the normalized pattern. As the magnitude of this complex far-field pattern function will be considered often in the following this will be denoted $f(\theta, \phi)$ such that

$$f(\theta, \phi) = |F(\theta, \phi)| \tag{5.4}$$

where $f(\theta, \phi)$ and $F(\theta, \phi)$ refer to either the co- or the cross-polar component of the pattern function.

5.1.1 Types of Comparisons

In order to extract the most information from the measurement data-sets that are available in the project it is important to consider how to perform comparisons of this data in the most efficient way. It is important to consider how to best illuminate particular properties of the measurement data-sets and how to, through these properties, compare the different measurement facilities.

A direct inter-comparison between all the measurement data-sets gives a large amount of results. Such an investigation allows for considering both statistical deviations between measurement data-sets and an identification of measurements, which deviates in specific ways from others. From these results it may be possible to both assess the general accuracy and noise level of the measurements relative to each other and to identify measurement data that are deviating from the other data, and through an analysis of these deviations suggest reasons for this behavior.

Comparisons of each measurement data-set to a common reference pattern essentially reduces the number of comparisons relative to a full inter-comparison, and further allows a benchmarking of the measurement data-sets. However, as the true error-free reference pattern for the test antenna is not known it is required that a reference pattern is defined in some way. This can be done in several ways from the available measurement data-sets. One measurement data-set with the best accuracy estimate could be chosen as the reference or an average of all or some of the available data-sets could be compiled and used as the reference. Regardless of how the reference pattern is defined from the available measurement data-sets, it will contain some degree of error which will influence the comparisons.

5.1.1.1 Reference Pattern

Ideally comparisons against a reference pattern should be based on a reference pattern which can be considered error free. However, as such a reference is not available for the present comparisons it is of interest to define a reference pattern based on the measured radiation patterns to which a high degree of confidence can be attributed.

A good way to do this would be to base the reference pattern on all the available measurements by computing a weighted average of these, with weights based on the accuracy estimates of each facility. This way the accuracy of the reference pattern is improved by each

The information contained in this document should be used only for the scope of the contract for which this document is prepared.

measurement that is included in it. As accuracy estimates are only available from few of the participating facilities in the present comparison, this definition of the reference pattern is unfortunately not practical here.

One possible definition of a reference pattern would be to simply take the arithmetic mean of all available patterns. As any information regarding the accuracy of each measurement is disregarded in this definition it is difficult to assess the accuracy of the resulting reference pattern. However, it can be considered the most fair definition based on the available data, as each participating facility is attributed equal significance.

A second possible definition of a reference which will be considered here is based on the use of only measurements from spherical near-field facilities. As an accuracy estimate is not available from all facilities of this type either, the reference pattern is again found as the arithmetic mean of the available patterns.

5.1.2 Definitions of Differences

5.1.2.1 Logarithmic Difference

When presenting radiation patterns graphically the magnitude of the pattern is usually given in a logarithmic scale. Hence, when comparing patterns for the same antenna from two separate sources a natural and often used investigation is to present these logarithmically in a single plot and subsequently compare them through visual inspection. An example of such a plot is given in Figure 5.1. This practice is reflected in the definition of the Logarithmic difference, which is given as the simple difference of the magnitudes of two patterns in logarithmic scale

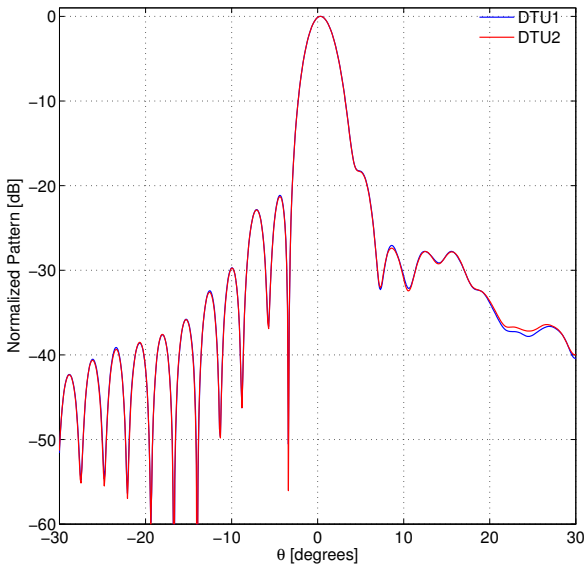

Figure 5.1 Normalized pattern at $\phi = 90^\circ$ for the co-polar component of the DTU1 and DTU2 patterns in the optical coordinate system.

$$\Delta_{log}(\theta, \phi) = 20 \log_{10} f_1(\theta, \phi) - 20 \log_{10} f_2(\theta, \phi), \tag{5.5}$$

The information contained in this document should be used only for the scope of the contract for which this document is prepared.

where $f_1(\theta, \phi)$ and $f_2(\theta, \phi)$ are the magnitudes of the considered component of the two pattern functions. Considering Figure 5.1 it is very clear that this difference simply represents the visual difference between the curves. Hence, the Logarithmic difference has a strength in the fact that it provides an intuitively clear measure for the difference between the patterns. However, due to the difference being calculated from patterns in a logarithmic scale, it will be characterized by becoming low in directions with high pattern levels while becoming large close to nulls and in directions with low pattern levels, as illustrated in Figure 5.2. This behavior is undesirable for investigations of differences over a full pattern. The Logarithmic difference is thus not well suited for investigations, where e.g. the standard deviation of the difference is calculated.

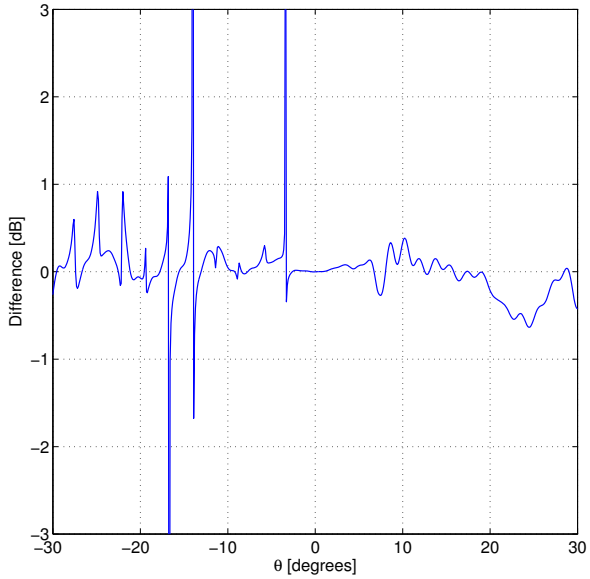

Figure 5.2 The Logarithmic difference at $\phi = 90°$ for the co-polar component of the DTU1 and DTU2 patterns in the optical coordinate system.

5.1.2.2 Weighted Logarithmic Difference

The Weighted logarithmic difference is introduced in order to facilitate a weighting of the Logarithmic difference according to some predefined criteria. One such criterion could be to de-emphasize the large spikes of the Logarithmic difference, which are present near the sharp nulls in the patterns. These spikes are clearly visible in Figure 5.2. Other criteria can be set, and further discussion of these and the associated weighting functions is deferred to Section 5.1.4.1. The Weighted logarithmic difference will here simply be defined as

$$\begin{aligned} \Delta_{w,log}(\theta, \phi) &= W_{log} \cdot \Delta_{log}(\theta, \phi) \\ &= W_{log} \cdot (20 \log_{10} f_1(\theta, \phi) - 20 \log_{10} f_2(\theta, \phi)) \end{aligned} \tag{5.6}$$

where W_{log} is a weighting function, which should generally be considered to be given as $W_{log} = W_{log}(\mathbf{F}_1(\theta, \phi), \mathbf{F}_2(\theta, \phi))$ as many definitions are possible depending on the particular

The information contained in this document should be used only for the scope of the contract for which this document is prepared.

purpose of the present investigation. Such definitions will be considered in more detail in Section 5.1.4.1. A particular weighting function that will de-emphasize the difference at low pattern levels is $W_{log} = (f_1(\theta, \phi))^{\beta}$ where the value of β can be chosen according to the desired behavior of the weighting function. Using this definition of the weighting function with $\beta = 0.5$ the Weighted logarithmic difference will behave as shown in Figure 5.3. As it is clearly seen from a comparison of this figure to the behavior of the Logarithmic difference given in Figure 5.2 the large spikes of the Logarithmic difference, which are present where nulls occur in the radiation patterns, have been greatly reduced. Hence, it is clear that the Weighted logarithmic difference is well suited for investigations that require certain characteristics of the Logarithmic difference to be emphasized or de-emphasized. Specifically weighting can be used for (de)-emphasizing characteristics in the Logarithmic difference so that the Weighted logarithmic difference can be used for investigations where statistical data such as the standard deviation is calculated. A tradeoff for introducing a weighting in the difference is an added complexity in the direct interpretation of what the difference expresses as this requires an understanding of the weighting function and what this expresses. This in particular becomes an issue if a more complex definition of the weighting function is chosen.

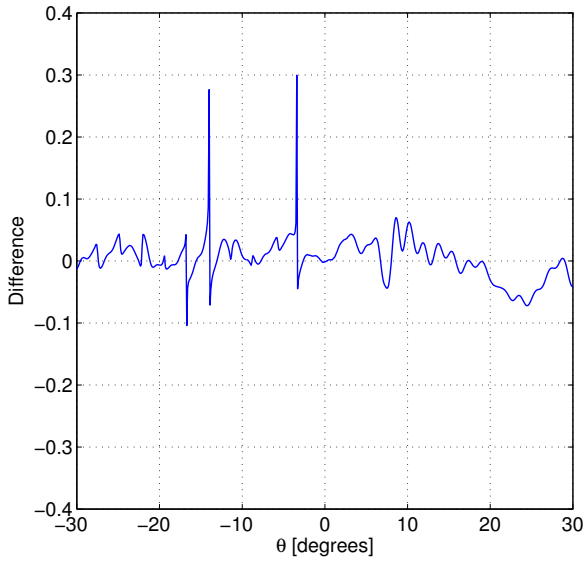

Figure 5.3 The Weighted logarithmic difference at $\phi = 90^{\circ}$ using $W_{log} = (f_1(\theta, \phi))^{\beta}$ with $\beta = 0.5$ for the co-polar component of the DTU1 and DTU2 patterns in the optical coordinate system.

5.1.2.3 Linear Difference

The Linear difference is calculated as the simple difference between the patterns on a linear scale. This difference will generally be large where the level of the pattern is large and low where the pattern is low. Hence, this difference has an opposite behavior compared to the Logarithmic difference. An expression for the Linear difference becomes

$$\Delta_{lin}(\theta, \phi) = f_1(\theta, \phi) - f_2(\theta, \phi) \tag{5.7}$$

The information contained in this document should be used only for the scope of the contract for which this document is prepared.

In Figure 5.4 it is seen that the Linear difference does indeed become relatively large at high pattern levels and very low at low pattern levels. Thus, this difference is also not well suited for general investigations over the full pattern and for examining mean and standard deviation over the full pattern.

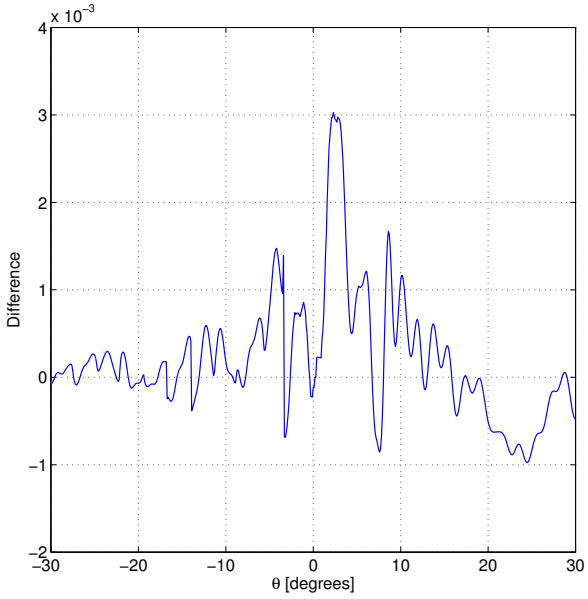

Figure 5.4 The Linear difference at $\phi = 90°$ for the co-polar component of the DTU1 and DTU2 patterns in the optical coordinate system.

From the definition of the Linear difference it is seen that it is the difference in amplitude of two electric fields. Hence, the difference can be considered as a noise signal that should be added to $f_1(\theta, \phi)$ in order to get $f_2(\theta, \phi)$. For this reason the Equivalent Noise difference[1] is defined by representing the Linear difference in a logarithmic scale

$$\Delta_{noise} = 20 \log_{10}(|f_1(\theta, \phi) - f_2(\theta, \phi)|) \tag{5.8}$$

A graphical representation of this difference is given in Figure 5.5.

5.1.2.4 Weighted Linear Difference

As was the case when introducing the Weighted logarithmic difference in relation to the Logarithmic difference it may also be of interest to emphasize or de-emphasize particular characteristics of the Linear difference. Based on the Linear difference the Weighted linear difference will be defined as

$$\begin{aligned} \Delta_{w,lin} &= W_{lin} \cdot \Delta_{lin}(\theta, \phi) \\ &= W_{lin} \cdot (f_1(\theta, \phi) - f_2(\theta, \phi)), \end{aligned} \tag{5.9}$$

[1]The Equivalent Noise difference was suggested for the investigations by Håkan Eriksson, Ericsson Microwave Systems AB.

The information contained in this document should be used only for the scope of the contract for which this document is prepared.

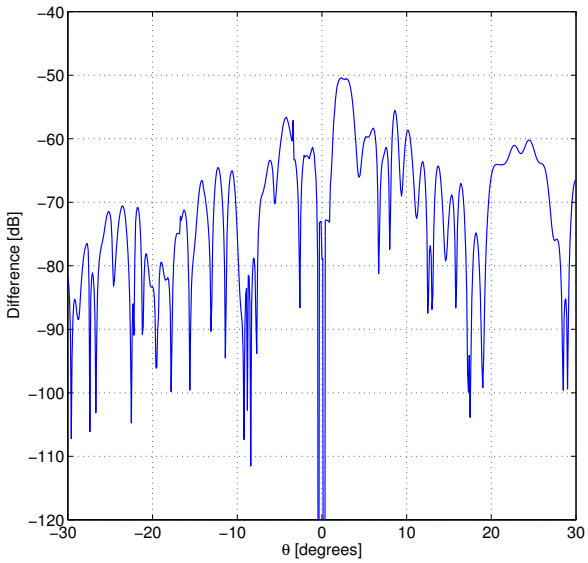

Figure 5.5 The Equivalent noise difference at $\phi = 90°$ for the co-polar component of the DTU1 and DTU2 patterns in the optical coordinate system.

where W_{lin} is a weighting function that can be defined in different ways. As was the case for the weighting function for the Weighted logarithmic difference W_{lin} should generally be considered to be given as $W_{lin} = W_{lin}(\mathbf{F}_1(\theta,\phi), \mathbf{F}_2(\theta,\phi))$, as many definitions are possible. Such definitions will be considered in more detail in Section 5.1.4.1. If the weighting function is chosen as $W_{lin} = (f_1(\theta,\phi))^{-1}$ the Weighted linear difference can be understood as representing the relative difference between the patterns. For this choice of the weighting function the Weighted linear difference is presented in Figure 5.6.

While the Weighted linear difference with the weighting function $W_{lin} = (f_1(\theta,\phi))^{-1}$, gives a good representation of the difference between two patterns it generally suffers from very large spikes when the denominator becomes close to zero. These makes visual comparisons problematic and can give large contributions when a quantification of the difference is over the full pattern attempted through computation of e.g. the standard deviation and the mean.

The information contained in this document should be used only for the scope of the contract for which this document is prepared.

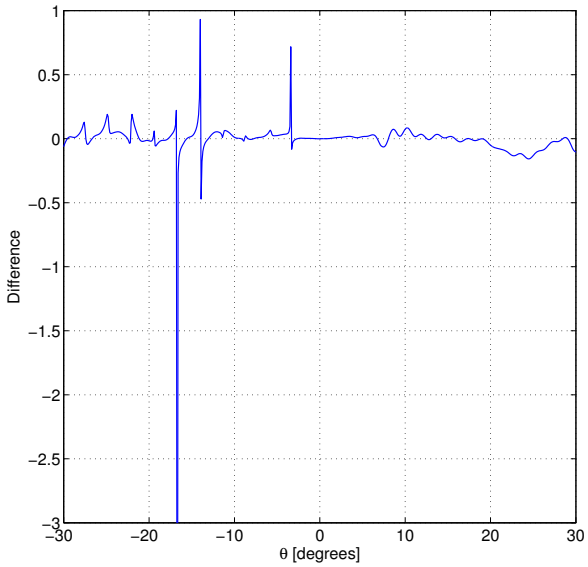

Figure 5.6 The Weighted linear difference at $\phi = 90^\circ$ with $W_{lin} = (f_1(\theta, \phi))^{-1}$ for the co-polar component of the DTU1 and DTU2 patterns in the optical coordinate system.

The information contained in this document should be used only for the scope of the contract for which this document is prepared.

5.1.2.5 Summary of Difference Definitions

A brief summary of the differences, which have been defined and will be used for the later comparisons, is given in Figure 5.7.

Given $f_1(\theta,\phi)$ and $f_2(\theta,\phi)$ which are the magnitudes of either the co- or cross-polar components of two pattern functions, the following differences have been defined in order to facilitate a comparison of the patterns.

Logarithmic Difference

$$\Delta_{log}(\theta,\phi) = 20\log_{10} f_1(\theta,\phi) - 20\log_{10} f_2(\theta,\phi)$$

Weighted Logarithmic Difference

$$\Delta_{w,log}(\theta,\phi) = W_{log} \cdot (20\log_{10} f_1(\theta,\phi) - 20\log_{10} f_2(\theta,\phi))$$

Linear Difference

$$\Delta_{lin}(\theta,\phi) = f_1(\theta,\phi) - f_2(\theta,\phi)$$

Weighted Linear Difference

$$\Delta_{w,lin}(\theta,\phi) = W_{lin} \cdot (f_1(\theta,\phi) - f_2(\theta,\phi))$$

Figure 5.7 List of the definitions of the differences.

As seen in Figure 5.7 a total number of 4 difference definitions have been proposed. It is possible to introduce other definitions, which are not covered by the proposed differences, but through the inclusion of particularly the two weighted differences many special cases are actually covered by the current definitions. For instance it would be natural to consider the relative linear difference. However, this difference is covered by the Weighted linear difference by choosing the weight appropriately. As an example, the weighting function $W_{lin} = (f_1(\theta,\phi))^{-1}$ used for Figure 5.6 in Section 5.1.2.4 corresponds to computing the Linear difference relative to $f_1(\theta,\phi)$. Likewise for the Weighted logarithmic difference the weighting function can be chosen appropriately so that the difference reflects interesting special cases. As an example, the weighting function can be chosen such that the Logarithmic difference is weighted proportionally to the pattern level. This is reflected in the weighting function $W_{log} = (f_1(\theta,\phi))^{\beta}$, used for Figure 5.3 in Section 5.1.2.2, which weights the difference according to the pattern level in linear scale.

The information contained in this document should be used only for the scope of the contract for which this document is prepared.

5.1.3 Measures of Merit

In order to achieve a quantitative figure, which describes the difference between two patterns in general or a particular characteristic of the difference, different measures of merit are considered here.

In the definitions of the differences in Section 5.1.2 it was mentioned that some of the differences were suited for use in computing the mean and standard deviation of the difference between two patterns. These statistical quantities are well known and understood and can for this reason be considered as useful measures of merit when comparing the general differences between all the patterns. Other statistical measures can be of value for examining the behavior of the differences and a list of the statistically based quantities that is used in this work along with their mathematical formulations is given here

$$\text{Mean value (Mean) :} \qquad \mu = \frac{1}{N}\sum_{i=1}^{N}\Delta_i. \tag{5.10}$$

$$\text{Standard deviation (STD) :} \qquad \sigma = \left(\frac{1}{N}\sum_{i=1}^{N}(\Delta_i - \mu)^2\right)^{1/2}. \tag{5.11}$$

$$\text{Root Mean Square (RMS) :} \qquad \psi = \left(\frac{1}{N}\sum_{i=1}^{N}(\Delta_i)^2\right)^{1/2}. \tag{5.12}$$

$$\text{Cumulative Distribution Function (CDF) :} \qquad F(|\Delta_i| \leq D) = \frac{N(\Delta_i \leq D)}{N}. \tag{5.13}$$

In the above given relations Δ_i represents the difference in each of the discrete points considered. N is the total number of points in which the difference is computed and $N(|\Delta_i| \leq D)$ is the number of points in which the condition that the absolute value of the difference Δ_i is less than or equal to a given value D, is fulfilled.

Aside from the statistical measures, other measures of merit can be defined for expressing different specific characteristics of the differences between the examined patterns. One such measure is defined in the Feature Selective Validation (FSV)[2] method [24, 25] which aims to give a measure of the degree of identity of patterns. This method is not based on the differences defined in Section 5.1.2, and is instead computed in a relatively complicated way using Fourier transforms of the patterns and derivatives of these. While the only information that can be attributed to the value, which is found through this method, is a measure of how alike the two patterns are considered to be, the FSV may provide a good measure for comparisons of measured radiation patterns.

[2]This measure has been suggested for the present investigations by Philippe Besnier, Institut National des Sciences Appliquees de Rennes.

The information contained in this document should be used only for the scope of the contract for which this document is prepared.

Another useful measure of merit for the present purposes[3] has been proposed in [26]. This measure is based on the use of a piecewise linear tolerance curve for the Logarithmic difference at different pattern levels. Based on the tolerance and the Logarithmic difference, at a given pattern level, a measure is then defined such that when integrated over a closed unit sphere a measure of merit of 1 is found if the difference is inside the tolerances at all points, and 0 if the difference is outside the tolerances at all points. Formulated mathematically the measure of merit S can be expressed as

$$S = \frac{1}{4\pi} \int_0^{2\pi} \int_0^{\pi} H(\theta, \phi) \sin\theta \, d\theta d\phi, \tag{5.14}$$

where the function $H(\theta, \phi)$ is given as

$$H(\theta, \phi) = \begin{cases} 1, & \text{if } \alpha(\theta, \phi) < 1 \\ 0, & \text{otherwise,} \end{cases} \tag{5.15}$$

with

$$\alpha(\theta, \phi) = \left| \frac{\Delta_{log}(\theta, \phi)}{\text{tol}(\max(f_1(\theta, \phi), f_2(\theta, \phi)))} \right|. \tag{5.16}$$

Here $\text{tol}(\max(f_1(\theta, \phi), f_2(\theta, \phi)))$ refers to the tolerance at the pattern level of the pattern with the highest level in the considered observation point. An example, presented in [26][4], of a set of tolerances that defines the tolerance curve, which could be used for the measure of merit is given in Table 5.1.

Normalized pattern level [dB]	-50	-40	-30	-20	-10	-5	0
Tolerance [dB]	50	30	10	5	3	2	1

Table 5.1 Example of a set of tolerances for calculating the measure of merit S taken from [26].

Another definition of the function $H(\theta, \phi)$, which provides a more sensitive figure of merit when considering patters that are close to identical, is also presented in the paper as

$$H(\theta, \phi) = \begin{cases} 1 - \alpha(\theta, \phi), & \text{if } \alpha(\theta, \phi) < 1 \\ 0, & \text{otherwise,} \end{cases} \tag{5.17}$$

By rewriting the tolerances and the definition of the function $H(\theta, \phi)$ in a different way, this measure of merit can also be adapted for use with the Linear difference. A particular feature of the measure of merit given in [26] is that due to its relatively simple definition some interpretation and understanding relating to the behavior of the difference can be derived from it.

[3] This investigation has been suggested by Jordi Romeu, Universitat Politecnica de Catalunya.

[4] The tolerances specified in the paper [26] have been converted to positive numbers here.

The information contained in this document should be used only for the scope of the contract for which this document is prepared.

5.1.4 Methods for Comparisons

In the definitions of the differences in Section 5.1.2 a weighting of both the Logarithmic and the Linear differences was introduced. The weighting functions are chosen in a specific way in order to achieve certain properties of the differences, for example to emphasize or de-emphasize the difference in particular parts of the pattern. Hence, the functions used for this purpose are chosen according to certain criteria in order to illustrate particular effects or properties in the difference in the best way.

Another method for comparing the patterns and analyzing the differences is to separate the data into discrete intervals corresponding to intervals in the pattern level. This would allow for investigations of the performance of the different facilities at specific pattern levels. However, by splitting the data into multiple intervals the extend of the comparisons also increases dramatically.

5.1.4.1 Continuous Weighting

As it was mentioned in Section 5.1.2, when discussing the weighted differences, one particular motivation for applying a continuous weighting to the patterns can be to emphasize or de-emphasize the difference in parts of the pattern. As an example of this a continuous weighting function can be used to de-emphasize the influence on the difference from a noise floor in the measurement data. Based upon a known noise floor n three possible noise weighting functions[5], $W_{n,1}$, $W_{n,2}$, and $W_{n,3}$, which will de-emphasize the influence on the difference from a noise floor in the measurement data are illustrated in Figure 5.8 for a noise floor of $n = -60$ dB.

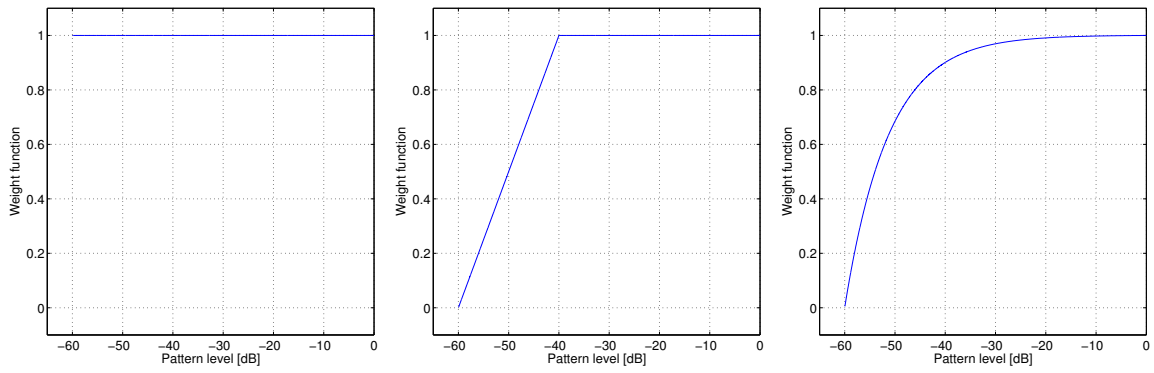

Figure 5.8 Examples of choices for weighting functions which can de-emphasize the influence on the difference from a noise floor in the measurement data.

The noise weighting functions in Figure 5.8 all attribute no confidence to a difference if the pattern level is below the noise floor $n = -60$ dB, but differ in the confidence attributed to the difference as the pattern level approaches n. Using the pattern $f_1(\theta, \phi)$ for the pattern level and expressing this in a logarithmic scale

$$D_1(\theta, \phi) = 20 \log_{10}(f_1(\theta, \phi)) \tag{5.18}$$

[5]This concept for the weighting functions has been suggested by Philippe Besnier, Institut National des Sciences Appliquees de Rennes.

The information contained in this document should be used only for the scope of the contract for which this document is prepared.

expressions for the noise weighting functions $W_{n,1}$, $W_{n,2}$, and $W_{n,3}$ can be given as

$$W_{n,1} = \begin{cases} 1, & -60 \text{ dB } \leq D_1(\theta,\phi) \leq 0 \text{ dB} \\ \text{Discard}, & D_1(\theta,\phi) < -60 \text{ dB} \end{cases} \tag{5.19}$$

$$W_{n,2} = \begin{cases} 1, & -40 \text{ dB } \leq D_1(\theta,\phi) \leq 0 \text{ dB} \\ \frac{D_1(\theta,\phi)}{20} + 3, & -60 \text{ dB } \leq D_1(\theta,\phi) < -40 \text{ dB} \\ \text{Discard}, & D_1(\theta,\phi) < -60 \text{ dB} \end{cases} \tag{5.20}$$

$$W_{n,3} = \begin{cases} 1 + 10^{\frac{n}{20}} - \frac{10^{\frac{n}{20}}}{f_1(\theta,\phi)}, & \text{if } 1 + 10^{\frac{n}{20}} - \frac{10^{\frac{n}{20}}}{f_1(\theta,\phi)} \geq 0 \\ \text{Discard}, & \text{Otherwise} \end{cases} \tag{5.21}$$

The noise weighting functions $W_{n,1}$ and $W_{n,2}$ are particularly simple examples of how the weighting of the difference can be chosen. $W_{n,1}$ represents an immediate drop to zero confidence in in the difference when the noise floor at -60 dB is reached. In $W_{n,2}$ a linear drop in the interval -40 dB to -60 dB is introduced in order to model a gradual drop in the confidence at low pattern levels when approaching the noise floor. The final weighting function $W_{n,3}$ models a drop in confidence, which is inversely proportional to the signal-to-noise ratio such that full confidence is attributed to the difference at the peak pattern level, and then dropping to zero when approaching the noise floor. The weighting function becomes zero at a pattern level which is slightly below the noise floor. This can be corrected in the definition, however the effect of this is clearly negligible. In the weighting functions all differences at pattern levels below the threshold at, or very close to, the noise floor are discarded as no confidence is attributed to these.

In order to illustrate the effect of these noise weighting functions for the Weighted logarithmic difference this has been computed using the same patterns, which were used in Section 5.1.2, and are illustrated in Figure 5.9. Note the discontinuity of these weighted differences where the pattern level is below the noise floor and the difference is hence discarded in accordance with the definition of the noise weighting functions.

An additional weighting of the difference can be introduced if the significance attributed to the measured patterns at low levels is smaller than at higher levels due to effects other than a noise floor. Such a pattern weighting can be achieved by a weighting function expressed as

$$W_p = \big(f(\theta,\phi)\big)^{\beta}, \tag{5.22}$$

where the parameter β will determine the specific behavior of W_p. This pattern weighting function is illustrated in Figure 5.10 for different choices of β.

As an example, a choice of $\beta = -\log_{10}(1/2) = 0.301$ reflects that the significance attributed to the difference is halved for every 20 dB drop in the pattern level. By introducing a second weighting function like this, the combined weighting function will be

The information contained in this document should be used only for the scope of the contract for which this document is prepared.

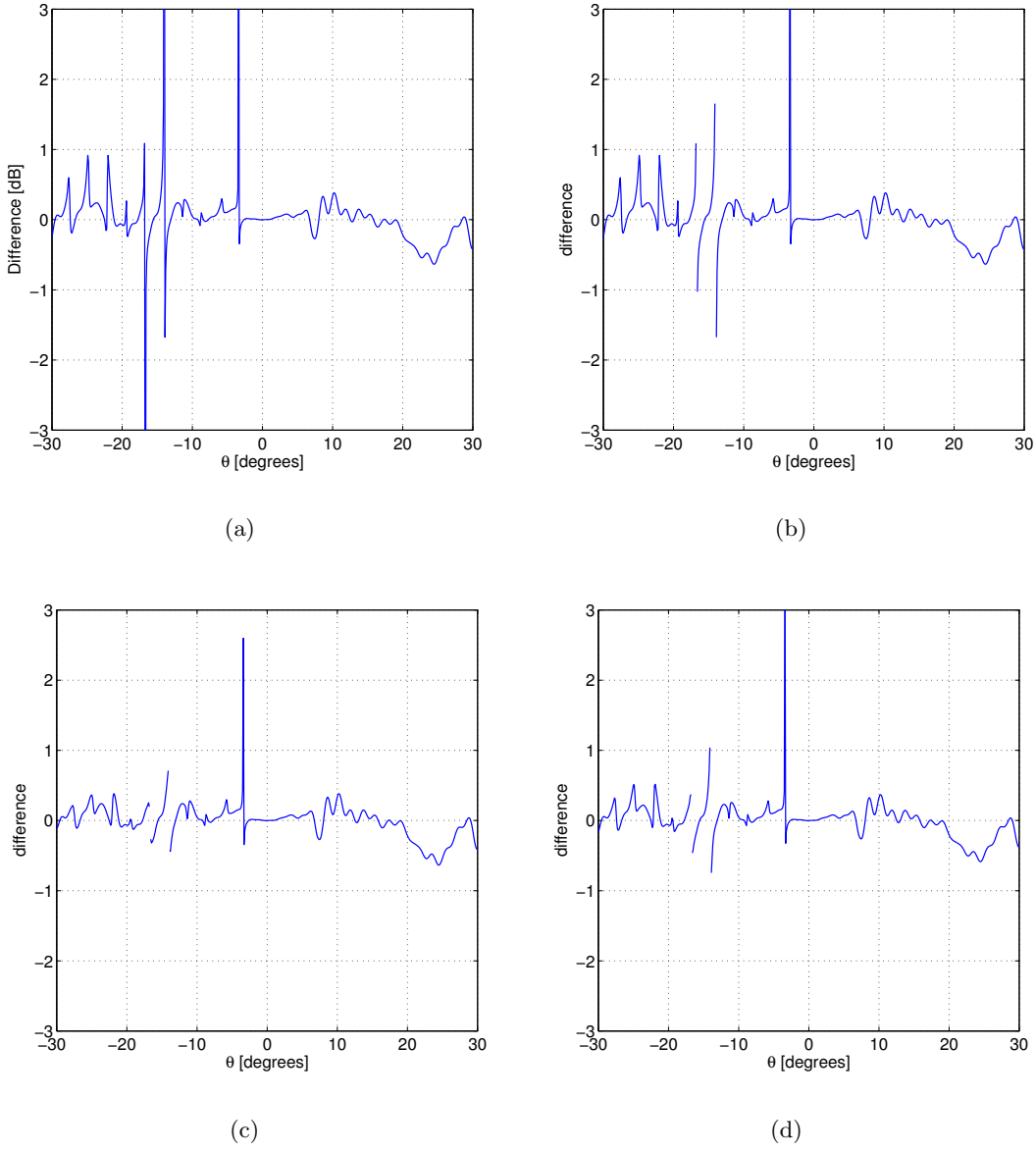

Figure 5.9 The Weighted logarithmic difference using the 3 noise weighting functions illustrated in Figure 5.8. The co-polar component of the DTU1 and DTU2 patterns at $\phi = 90°$ in the optical coordinate system have been used in this example. In (a) the Logarithmic difference with no weighting is shown, in (b) the $W_{n,1}$ weighting function is used, in (c) $W_{n,2}$ is used, and in (d) $W_{n,3}$ is used.

$$W = W_p W_n, \tag{5.23}$$

and when using $\beta = 0.301$ an example of the Weighted logarithmic difference using the combined weighting function is given in Figure 5.11.

The weighting functions listed so far depend only on the pattern level of one of the

The information contained in this document should be used only for the scope of the contract for which this document is prepared.

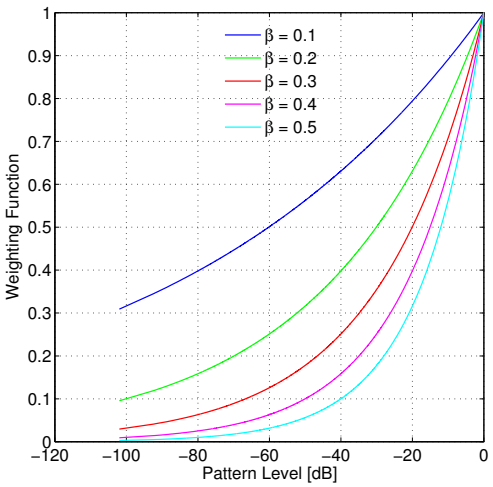

Figure 5.10 Examples of the pattern weighting function W_p for different choices of β.

patterns. However, as the weighting functions can be chosen arbitrarily these could just as well be chosen to depend on a combination of the two patterns such as the average. This choice would then also reflect that no single pattern can be said to be a true reference in the present investigation.

The information contained in this document should be used only for the scope of the contract for which this document is prepared.

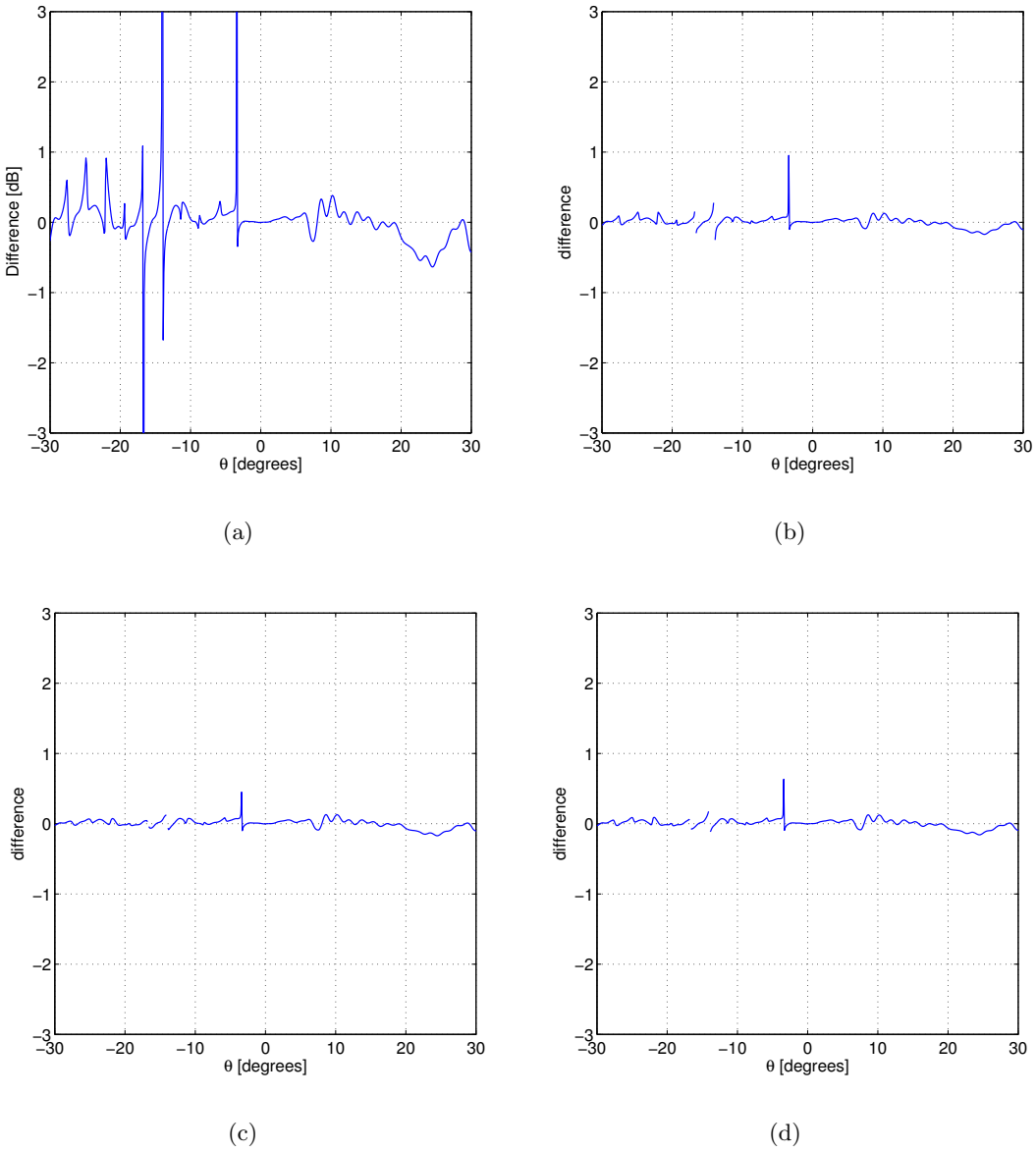

Figure 5.11 The Weighted logarithmic difference using the combined weighting function $W = W_p W_n$ with $\beta = 0.301$ for the pattern weighting function W_p. The co-polar component of the DTU1 and DTU2 patterns at $\phi = 90^\circ$ in the optical coordinate system have been used in this example. In (a) the Logarithmic difference with no weighting is shown, in (b) $W = W_p W_{n,1}$ is used, in (c) $W = W_p W_{n,2}$ is used, and in (d) $W = W_p W_{n,3}$ is used.

The information contained in this document should be used only for the scope of the contract for which this document is prepared.

5.1.4.2 Separation into Discrete Intervals

A separation of the patterns into discrete intervals depending on pattern level allows for comparisons of different parameters such as mean and standard deviation at different pattern levels. Another example of this method of comparison is an investigation of the cumulative distribution function (CDF) using behavior for the difference between two patterns depending on pattern level[6]. Based upon the definition (5.13) in Section 5.1.3 the CDF in each interval can be expressed as

$$F(|\Delta_i| \leq x_s) = \frac{N_s(|\Delta_i| \leq x_s)}{N_s}, \tag{5.24}$$

where Δ_i represents the difference in each of the discrete points considered, N_s is the total number of points in the interval, and $N_s(|\Delta_i| \leq x_s)$ is the number of points in the interval for which the condition that the absolute value of the difference Δ_i is less than or equal to a given value x_s is fulfilled. The subscript s denotes the considered interval. Based upon the Logarithmic difference this investigation would then for chosen discrete pattern levels find a limit value x_s, such that the difference is below this limit with a pre-specified probability. In practice this involves defining an interval around the considered discrete pattern levels, e.g. ± 1 dB or ± 3 dB intervals, and then determine the limit value in these intervals according to the specified probability for the CDF. An example of a CDF calculated in ± 3 dB intervals for $F(|\Delta_i| \leq x_s) = 0.9$ is presented in Figure 5.12, where also the standard deviation and mean are presented.

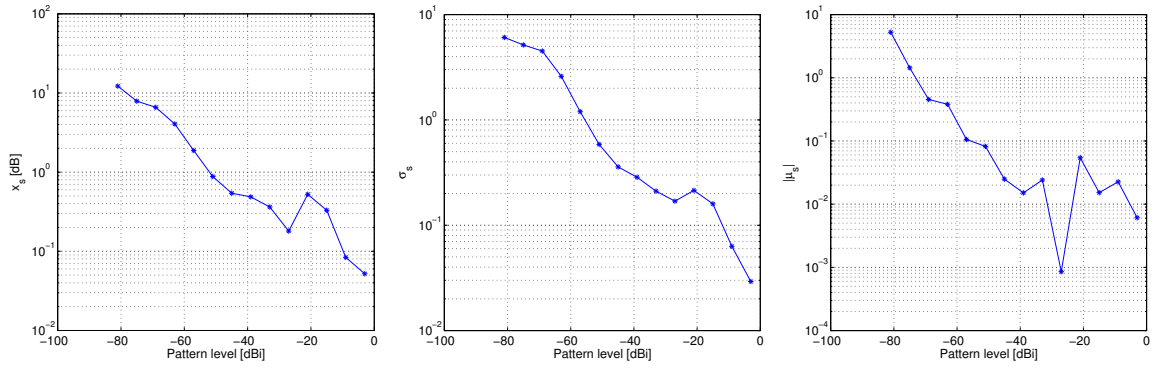

Figure 5.12 Statistical measures for the Logarithmic difference calculated for discrete intervals in the pattern level. The intervals used here are ± 3 dB around the considered level. (a) illustrates the limit value x_s of the difference for the cumulative distribution function $F(|\Delta_i| \leq x_s) = 0.9$, (b) is the standard deviation for the difference in the same intervals, and (c) is the mean. The co-polar component of the DTU1 and DTU2 patterns at $\phi = 90^\circ$ in the optical coordinate system have been used in this example.

If the interval in pattern level is chosen to be just ± 1 dB around the considered level the curves can be represented by more points as is illustrated in Figure 5.13. However, if the

[6]This investigation has been suggested by Jordi Romeu, Universitat Politecnica de Catalunya.

The information contained in this document should be used only for the scope of the contract for which this document is prepared.

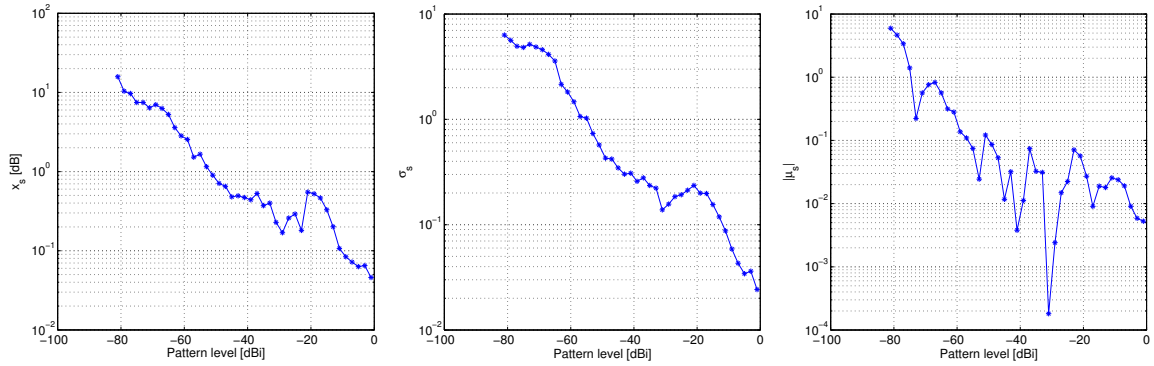

Figure 5.13 Statistical measures for the Logarithmic difference calculated for discrete intervals in the pattern level. The intervals used here are ±1 dB around the considered level. (a) illustrates the limit value x_s of the difference for the cumulative distribution function $F(|\Delta_i| \leq x_s) = 0.9$, (b) is the standard deviation for the difference in the same intervals, and (c) is the mean. The co-polar component of the DTU1 and DTU2 patterns at $\phi = 90^\circ$ in the optical coordinate system have been used in this example.

intervals are chosen to be too narrow it is possible that the number of sample points that fall into each of the intervals is not enough to form a statistically significant basis for the calculation of the statistical measures. In Figure 5.14 the number of sample points in each of the intervals of the pattern level is presented for both the ±3 dB or ±1 dB intervals. From this figure it is seen that for the ±3 dB intervals a significant number of samples are present at all levels, but for the ±1 dB intervals the number of samples present at some pattern levels is relatively low. From a closer inspection it has been found that the lowest number of samples present in a ±1 dB interval is 31, which is sufficient to consider the calculated statistical measures correct. Hence, when performing this investigation for different patterns, it is important to verify that the calculated measures are based on statistically significant amounts of samples.

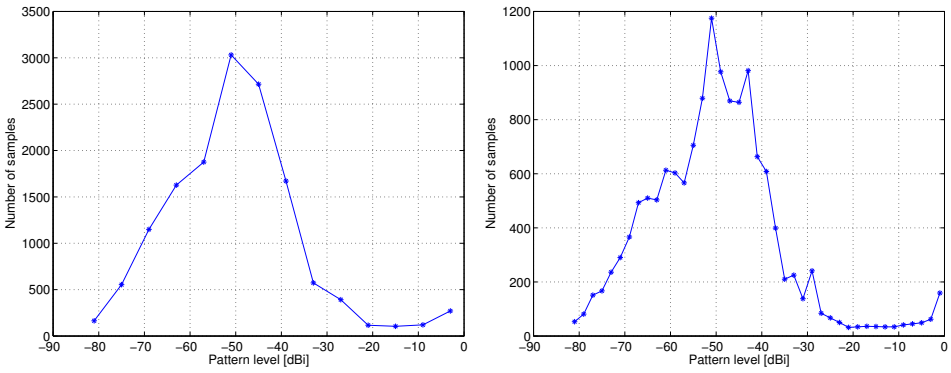

Figure 5.14 The number of samples which fall into each interval in pattern level when using the DTU1 pattern for defining the pattern level. (a) corresponds to the intervals of ±3 dB used in Figure 5.12 and (b) corresponds to the ±1 dB intervals used in Figure 5.13.

The information contained in this document should be used only for the scope of the contract for which this document is prepared.

5.2 Gain/Directivity

When discussing gain and directivity in this report basis will be taken in the IEEE definitions of these quantities as given in [27]. This is particularly important to note for the specification of gain, as the IEEE definition of the gain in a specific direction is referred to as "4π times the ratio of the power radiated per unit solid angle in that direction to the net power accepted by the antenna" [28], whereas the gain in other sources is often presented as related to the power available at the antenna. This latter definition is referred to as the realized gain and is not the same as the gain as it will include losses due to mismatch at the antenna input terminals. The directivity in a specific direction is defined by the IEEE as "4π times the ratio of the power radiated per unit solid angle in that direction to the total power radiated by the antenna" [28]. Hence, when using the IEEE definitions for gain and directivity the difference between these quantities represent purely internal losses of the antenna.

The directivity of an antenna can be determined from antenna measurements when the full field pattern has been found, while a determination of the gain will require additional measurements. Hence, when comparing the measurements of directivity and gain from the different facilities in this project it should be expected that the determined directivities will correspond better than the determined gains due to additional inaccuracies introduced in the gain measurements. The expected increase in the gain difference over the directivity difference can then be attributed to differences in how the gain is determined between the facilities or possible differences in the gain definition.

In the measurements at the participating facilities the gain and the directivity has generally been determined in two observation points. This is due to the particular feature of the VAST12 antenna in which the main beam is steered slightly off axis and consequently makes the peak gain and the on-axis gain slightly different.

5.3 Polarization Characteristics

The polarization of the electric field, or the corresponding pattern function in the far-field region, in each observation point, is usually described through the polarization ellipse. For this ellipse characteristics such as the axial ratio, the tilt angle, and the sense of rotation can then be expressed if the full complex representation of the electric field or pattern function is known. A convenient quantity for relating these characteristics is the complex polarization ratio [13, p. 53] which, when using the time dependence $e^{j\omega t}$, can be expressed as

$$Q(\theta,\phi) = \frac{F_{RC}(\theta,\phi)}{F_{LC}(\theta,\phi)} = \frac{F_{co}(\theta,\phi) - jF_{cx}(\theta,\phi)}{F_{co}(\theta,\phi) + jF_{cx}(\theta,\phi)} = e^{-2j\phi}\frac{F_{\theta}(\theta,\phi) + jF_{\phi}(\theta,\phi)}{F_{\theta}(\theta,\phi) - jF_{\phi}(\theta,\phi)}. \tag{5.25}$$

Here $F_{RC}(\theta,\phi)$ and $F_{LC}(\theta,\phi)$ denote the right- and left-hand components of the pattern function, $F_{co}(\theta,\phi)$ and $F_{cx}(\theta,\phi)$ denote the co- and cross-polar components of the pattern function, and $F_{\theta}(\theta,\phi)$ and $F_{\phi}(\theta,\phi)$ denote the components of the pattern function along the spherical unit vectors. Relations between the components of the pattern function are as given in [13], where $F_{co}(\theta,\phi)$ and $F_{cx}(\theta,\phi)$ are defined with $\phi_0 = 0^\circ$ from Ludwig's third definition. With the complex polarization ratio established the axial ratio can then be found as

The information contained in this document should be used only for the scope of the contract for which this document is prepared.

$$AR(\theta,\phi) = \frac{|Q(\theta,\phi)|+1}{|Q(\theta,\phi)|-1}, \tag{5.26}$$

and the tilt angle can be found as

$$\tau(\theta,\phi) = -\frac{1}{2}\arg(Q(\theta,\phi)). \tag{5.27}$$

The full complex representation of the electric field at the observation points is only available from a few of the participating facilities. However, for some of the facilities the axial ratio, tilt angle, and sense of rotation have been specified in particular points. As the magnitude of the co- and cross-polar components are available in the patterns from all facilities one figure for describing the polarization characteristics, which can be used for the present comparisons, is the cross polarization ratio

$$R(\theta,\phi) = \frac{f_{cx}(\theta,\phi)}{f_{co}(\theta,\phi)}, \tag{5.28}$$

where $f_{co}(\theta,\phi)$ and $f_{cx}(\theta,\phi)$ are the magnitude of the co- and cross-polar components of the pattern function as was presented in Section 5.1.

The information contained in this document should be used only for the scope of the contract for which this document is prepared.

Chapter 6

Comparison Results

6.1 Re-formatting of Measurement Data

The measurement data sets which have been received from the participating facilities are formatted in different ways. In particular the supplied patterns may or may not be normalized according to the pattern definition given in Section 5.1 and they may have different angular resolutions in theta. Hence, in order to perform a comparison of the patterns from all the participating facilities, these should be converted to a common format. The normalization of the patterns is readily achievable by using the relations given in Section 5.1. In order to perform a comparison of the patterns on a point by point basis it is necessary that the pattern levels are given in the same angular points for all the patterns. This requirement is met by performing an interpolation of the patterns. The interpolation is made such that all patterns have an 0.1° resolution in theta and has a point in $\theta = 0^\circ$. Most of the patterns have been supplied with a resolution in theta of 0.1° and do thus not require interpolation. The patterns requiring interpolation are from the FTRD, UPM2, and UPM3 measurements. An overview of the angular dependency of all the supplied patterns is given in Table 6.1.

Facility	Range in θ	Step-size in θ
DTU1	$\theta \leq 180^\circ$	0.1°
DTU2	$\theta \leq 180^\circ$	0.1°
SES	$\theta \leq 180^\circ$	0.1°
FTRD	$\theta \leq 90^\circ$	0.25°
UPM1	$\theta \leq 180^\circ$	0.1°
UPM2	$\theta \leq 30^\circ$	non-uniform
UPM3	$\theta \leq 179^\circ$	0.5°
UPC	$\theta \leq 30^\circ$	0.1°

Table 6.1 Properties of the patterns that have been provided by the participating facilities.

When interpolating the patterns it of course important that as little error as possible is introduced as a result. A piecewise cubic interpolation is used for interpolating the patterns in these investigations. This interpolation method has been found to provide accurate results from the available data. An investigation has been done by re-sampling the co- polar com-

The information contained in this document should be used only for the scope of the contract for which this document is prepared.

ponent of the DTU2 measurement data with a step size in θ of 0.5° and then interpolating this data to a step size of 0.1°. The interpolated data can then be compared to the the original and re-sampled data, and the accuracy of the interpolation can be assessed. The original and interpolated patterns are presented in Figure 6.1. From this figure it is seen that the interpolated pattern generally fits well with the original pattern, but that nulls are not reproduced properly when no samples fall in these. However, as the information about these is not contained in the re-sampled data this should be expected.

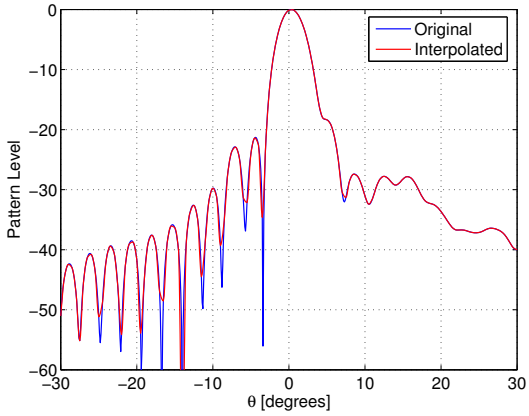

Figure 6.1 Comparison of original pattern and a pattern which has been interpolated from the original one using a reduced number of samples.

6.2 Chosen Comparison Strategy

Based upon the discussions in Chapter 5 a strategy for the comparisons, which are presented in this chapter, is chosen here. The choices involved in the definition of this strategy are concerned mainly with how to compare the available patterns as the possibilities of how to perform this are many.

A presentation of the patterns in each cut is given for direct visual comparison as this method is widely used and can give a good qualitative impression of the difference between patterns. Following this the Weighted logarithmic difference, which was defined in Section 5.1.2.2, is calculated in each cut using a combined weighting function $W = W_n W_p$ as discussed in Section 5.1.4.1. The noise weighting function W_n is computed using the $W_{n,3}$ definition with a noise floor of $n = -55$ dB such that

$$W_n = \begin{cases} 1 + 10^{\frac{-55}{20}} - \frac{10^{\frac{-55}{20}}}{f_1(\theta,\phi)}, & \text{if } 1 + 10^{\frac{-55}{20}} - \frac{10^{\frac{-55}{20}}}{f_1(\theta,\phi)} \geq 0 \\ \text{Discard}, & \text{Otherwise.} \end{cases} \tag{6.1}$$

The noise floor of $n = -55$ dB is chosen to be representative of the different noise floors in the measurements from the participating facilities as these individual noise floors are not known. The pattern weighting function is chosen to reflect that the significance of the difference is

The information contained in this document should be used only for the scope of the contract for which this document is prepared.

halved for each 10 dB drop in the pattern level. This corresponds to $\beta = -\log_{10}(1/4) = 0.602$, and the pattern weighting function thus becomes

$$W_p = \big(f(\theta, \phi)\big)^{0.602}. \tag{6.2}$$

Based on the Weighted logarithmic difference, which has been found, the mean and standard deviation are found and tabulated following the definitions given in Section 5.1.3. This is done using the difference in all cuts, and is found for both the largest interval in θ where the comparison has been possible and for the $\theta \leq 30^\circ$ interval.

As a final investigation a comparison of the patterns at different pattern levels is made, following the principles discussed in Section 5.1.4.2. The investigation is made for ± 3 dB intervals in the pattern level for the CDF, mean, and standard deviation.

6.2.1 Reference Patterns

Based upon the discussion in Section 5.1.1.1 two reference patterns are chosen for use in the comparisons. In order to make it possible to compare most of the available measurement data to a reference pattern one reference patterns is defined in the optical coordinate system and the other is defined in the electrical coordinate system.

Reference pattern 1 (REF1) is defined in the optical coordinate system and is constructed from the DTU2, SES, and UPM1 patterns. This pattern is constructed from the arithmetic average of selected patterns which are expected to be of good accuracy as they are all found from spherical near-field measurements. The DTU1 pattern which is also a spherical near-field measurement has been omitted from the constructed reference as it is not independent of the DTU2 pattern.

Reference pattern 2 (REF2) is defined in the electrical coordinate system and is constructed as the arithmetic average of the DTU2, UPM1, UPM2, and FTRD patterns. In this definition all available patterns are used to construct the reference pattern. Again the DTU1 pattern is omitted when constructing the reference as it is not independent of the DTU2 pattern.

The information contained in this document should be used only for the scope of the contract for which this document is prepared.

6.3 Pattern Comparisons

6.3.1 Repeatability Comparison

As measurement data is available from two separate measurements of the VAST12 antenna at the DTU-ESA Spherical Near-Field Test Facility it is possible to investigate the ability of this facility to reproduce its own measurement results. This investigation can give an insight into the possible deviations between repeated measurements at a single facility and a possibility to identify sources of these errors.

The comparison between DTU1 and DTU2 is done in the optical coordinate system.

The information contained in this document should be used only for the scope of the contract for which this document is prepared.

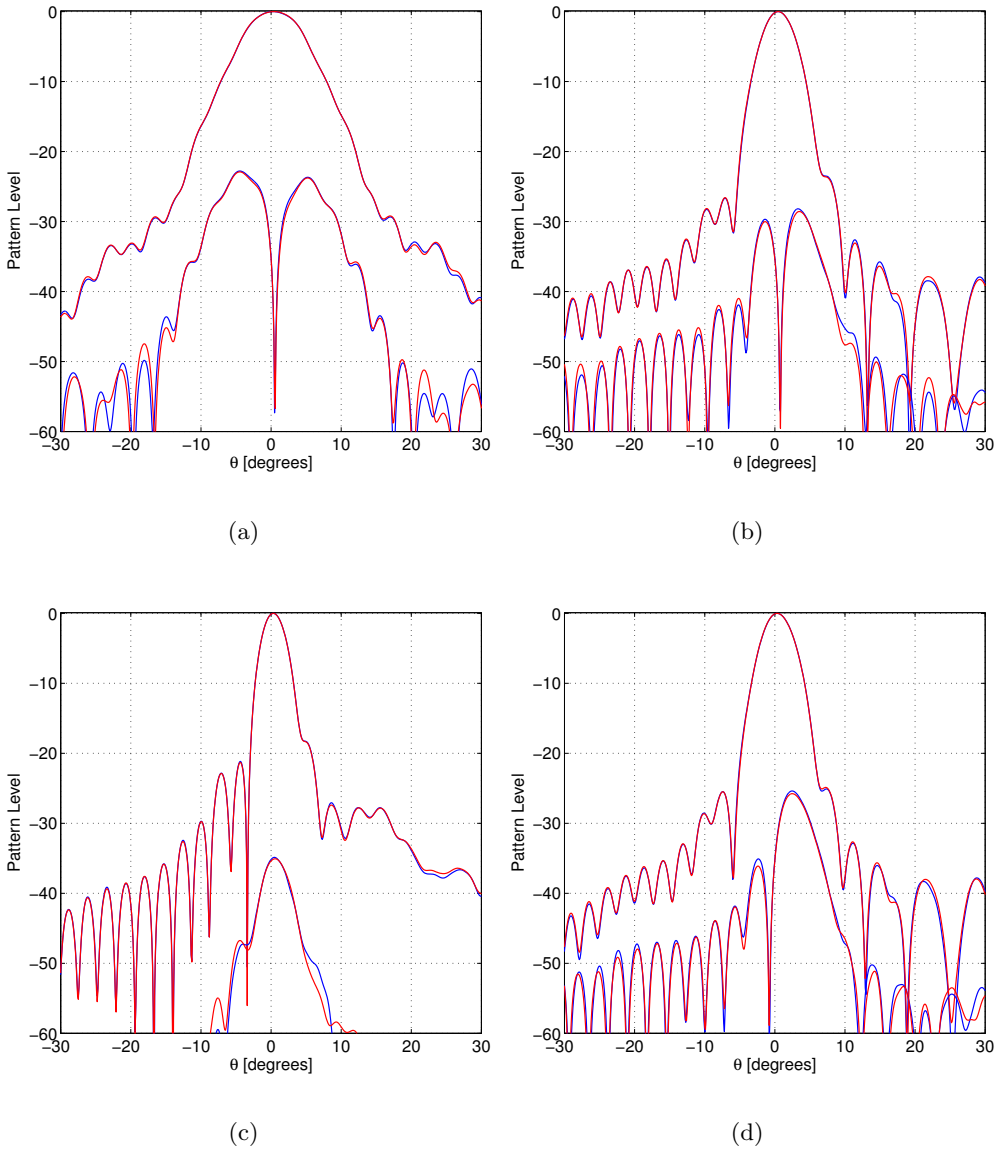

Figure 6.2 The co- and cross-polar patterns for the DTU1 and DTU2 measurements. In (a), (b), (c), and (d) the $\phi = 0°$, $\phi = 45°$, $\phi = 90°$, and $\phi = 135°$ cuts are shown, respectively. The blue graph shows the DTU1 measurement and the red graph shows the DTU2 measurement.

The information contained in this document should be used only for the scope of the contract for which this document is prepared.

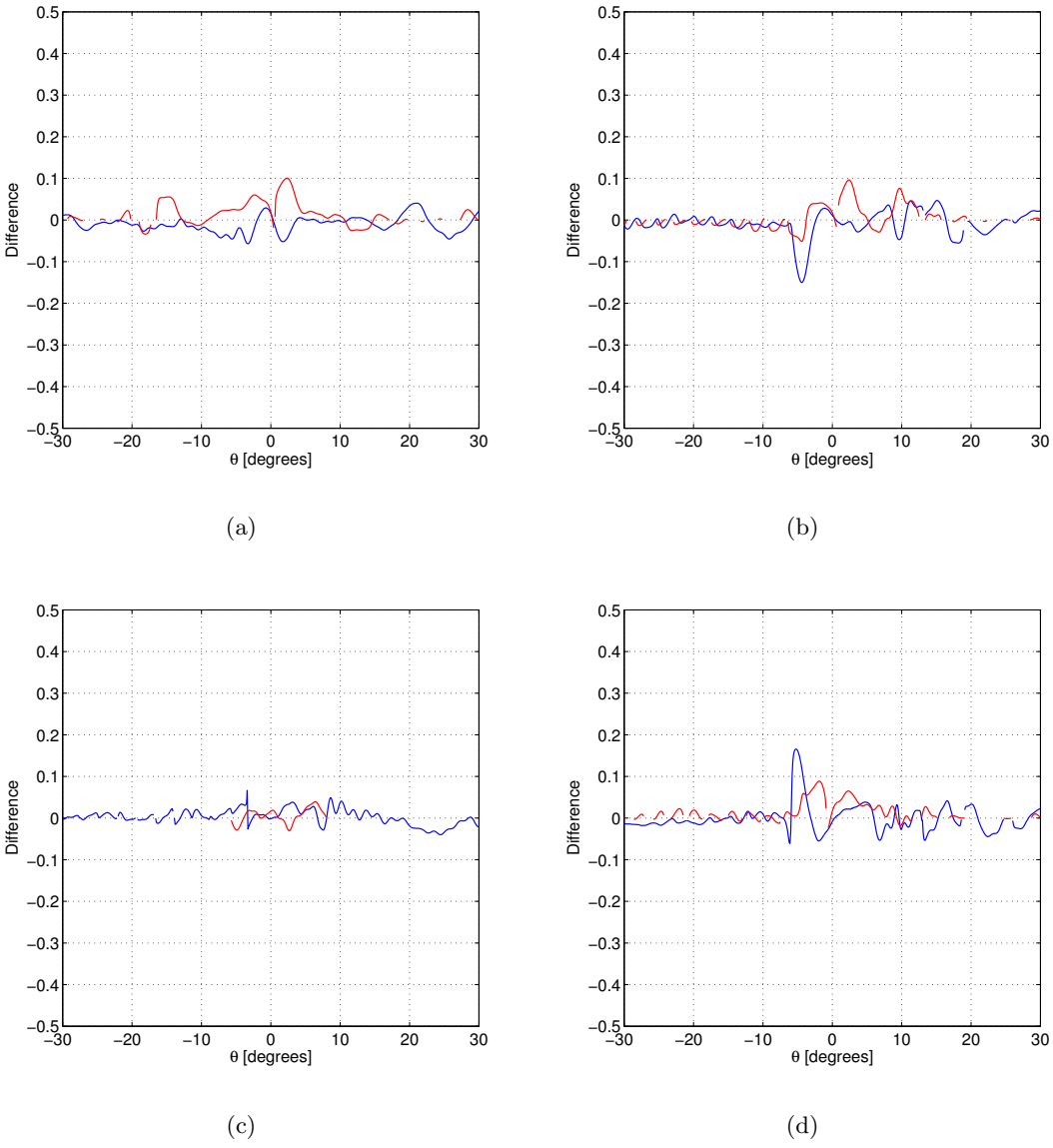

Figure 6.3 The Weighted logarithmic difference for the DTU1 and DTU2 measurements. In (a), (b), (c), and (d) the difference in the $\phi = 0°$, $\phi = 45°$, $\phi = 90°$, and $\phi = 135°$ cuts are shown, respectively. The blue graph shows the difference for the co-polar component and the red graph shows the difference for the cross-polar component.

From the comparisons the following observations can be made

- From the patterns in Figure 6.2 very good agreement is observed for both the co- and cross-polar patterns. However, in all cuts a difference in the co-polar component around $\theta = 25°$ is visible at levels above -40 dB.
- From the CDF in Figure 6.4 it seen that the value of x_s for the co-polar component is not increasing monotonously with a decrease in the pattern level in the -10 to -25 dB interval. This observation is true for the STD in Figure 6.6 as well.

The information contained in this document should be used only for the scope of the contract for which this document is prepared.

- From the CDF in Figure 6.4 and the STD in 6.6 it is seen that a good correspondence exists between the values calculated for the co-polar and the cross-polar components.

	Mean	STD
co-polar ($\theta \leq 30°$)	-0.004	0.027
cross-polar ($\theta \leq 30°$)	0.012	0.027
co-polar ($\theta \leq 180°$)	0.000	0.015
cross-polar ($\theta \leq 180°$)	0.004	0.015

Table 6.2 Statistical data for the Weighted logarithmic difference between DTU1 and DTU2.

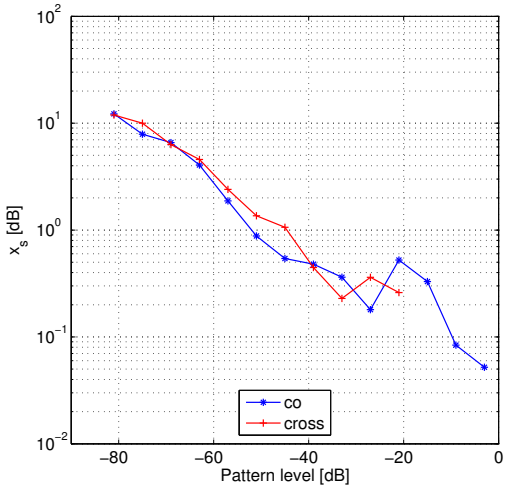

Figure 6.4 Limit value x_s of the Logarithmic difference for the CDF $F(\Delta_i \leq x_s) = 0.9$ in each ±3 dB interval.

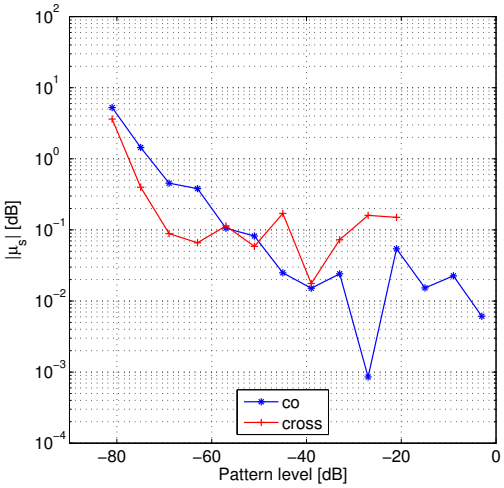

Figure 6.5 Absolute value of the mean $|\mu_s|$ of the Logarithmic difference in each ±3 dB interval.

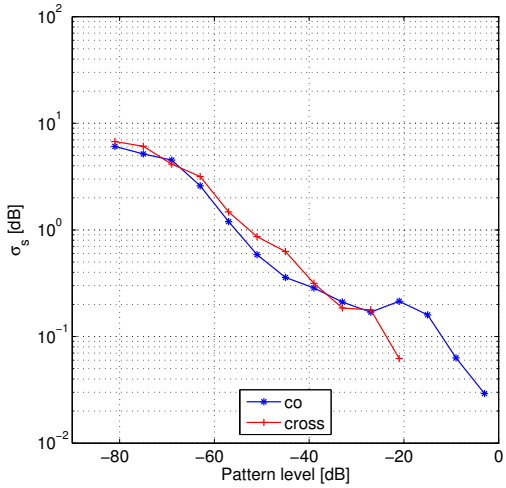

Figure 6.6 Standard deviation σ_s of the Logarithmic difference in each ±3 dB interval.

The information contained in this document should be used only for the scope of the contract for which this document is prepared.

6.3.2 Comparison of Measurement Techniques

The VAST12 antenna has been measured in four different types of facilities during the measurement campaign; Spherical near-field facility, planar near-field facility, compact range facility, and far-field range facility. This offers an opportunity to compare results obtained through different measurement techniques. In this investigation the far-field measurement technique is left out and will be considered specifically at a later point.

The UPM1 spherical near-field, UPM2 planar near-field, and UPM3 compact range measurements, given in the mechanical coordinate system, are used for this comparison.

The information contained in this document should be used only for the scope of the contract for which this document is prepared.

6.3.2.1 Spherical Near-Field and Compact Range Measurements

A spherical near-field measurement (UPM1) and a compact range measurement (UPM3) are compared.

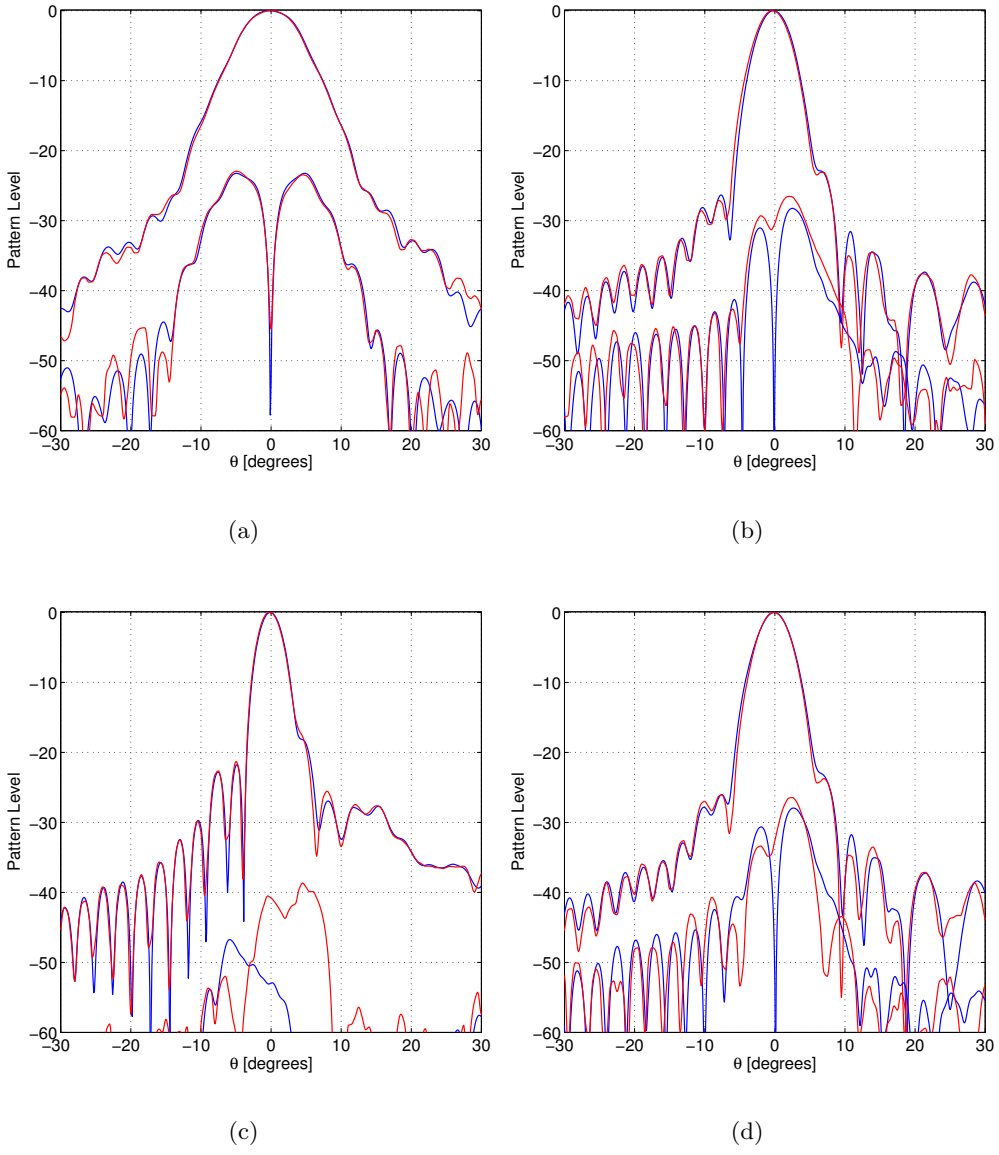

Figure 6.7 The co- and cross-polar patterns for the UPM1 and UPM3 measurements. In (a), (b), (c), and (d) the $\phi = 0°$, $\phi = 45°$, $\phi = 90°$, and $\phi = 135°$ cuts are shown, respectively. The blue graph shows the UPM1 measurement and the red graph shows the UPM3 measurement.

From the comparisons the following observations can be made

- From Figure 6.7 it is seen that a generally good agreement between the patterns can be observed, but that noticeable differences can be observed in some areas for both the co- and cross-polar components in all cuts. The differences are particularly clear in the main lobe region, which is also evident from the differences shown in Figure 6.8.

The information contained in this document should be used only for the scope of the contract for which this document is prepared.

- From the results presented in Table 6.3 it can be observed that the STD in the $\theta \leq 30°$ region is 0.201 and 0.142 for the co- and cross-polar component, respectively.
- From the CDF in Figure 6.9 a non monotonic behavior of x_s for the co-polar component can be observed and likewise for the STD in Figure 6.11.
- From both the CDF in Figure 6.9 and the STD in Figure 6.11 a difference between the values for the co- and cross-polar components at high pattern levels can be observed.

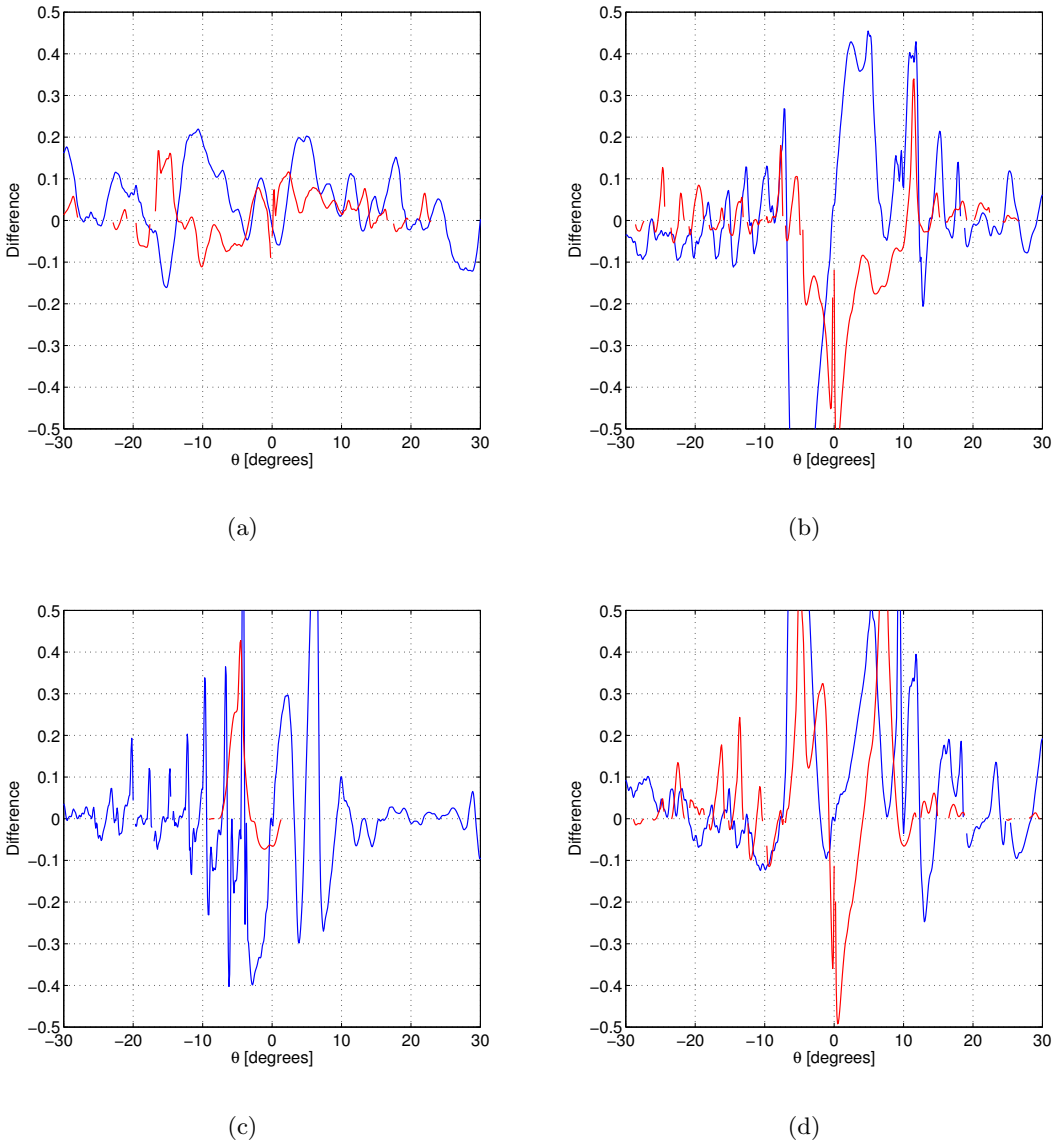

Figure 6.8 The Weighted logarithmic difference for the UPM1 and UPM3 measurements. In (a), (b), (c), and (d) the difference in the $\phi = 0°$, $\phi = 45°$, $\phi = 90°$, and $\phi = 135°$ cuts are shown, respectively. The blue graph shows the difference for the co-polar component and the red graph shows the difference for the cross-polar component.

The information contained in this document should be used only for the scope of the contract for which this document is prepared.

	Mean	STD
co-polar ($\theta \leq 30°$)	0.031	0.201
cross-polar ($\theta \leq 30°$)	0.009	0.142
co-polar ($\theta \leq 179°$)	0.025	0.111
cross-polar ($\theta \leq 179°$)	0.035	0.122

Table 6.3 Statistical data for the Weighted logarithmic difference between UPM1 and UPM3.

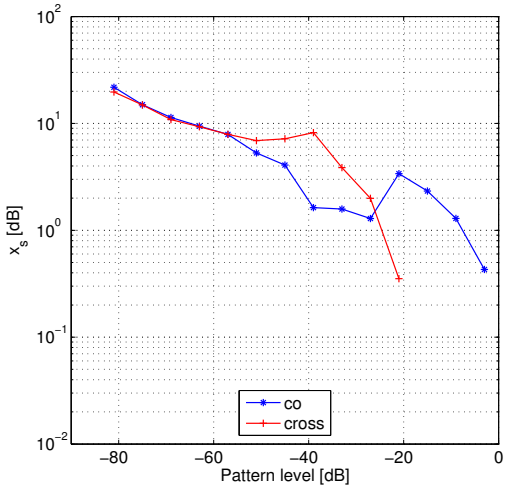

Figure 6.9 Limit value x_s of the Logarithmic difference for the CDF $F(\Delta_i \leq x_s) = 0.9$ in each ±3 dB interval.

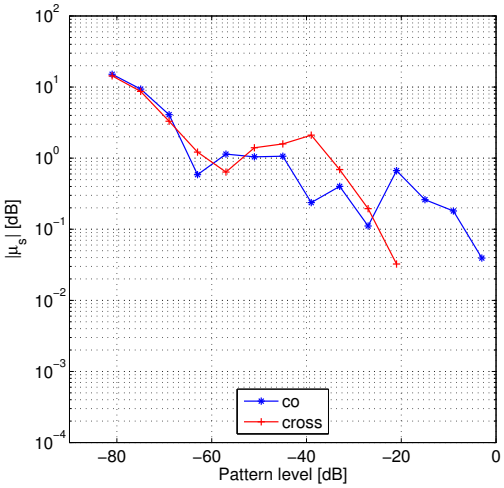

Figure 6.10 Absolute value of the mean $|\mu_s|$ of the Logarithmic difference in each ±3 dB interval.

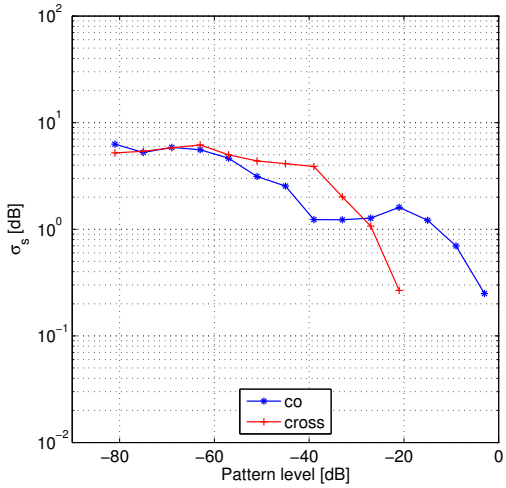

Figure 6.11 Standard deviation σ_s of the Logarithmic difference in each ±3 dB interval.

The information contained in this document should be used only for the scope of the contract for which this document is prepared.

6.3.2.2 Spherical Near-Field and Planar Near-Field Measurements

A spherical near-field measurement (UPM1) and a planar near-field measurement (UPM2) are compared.

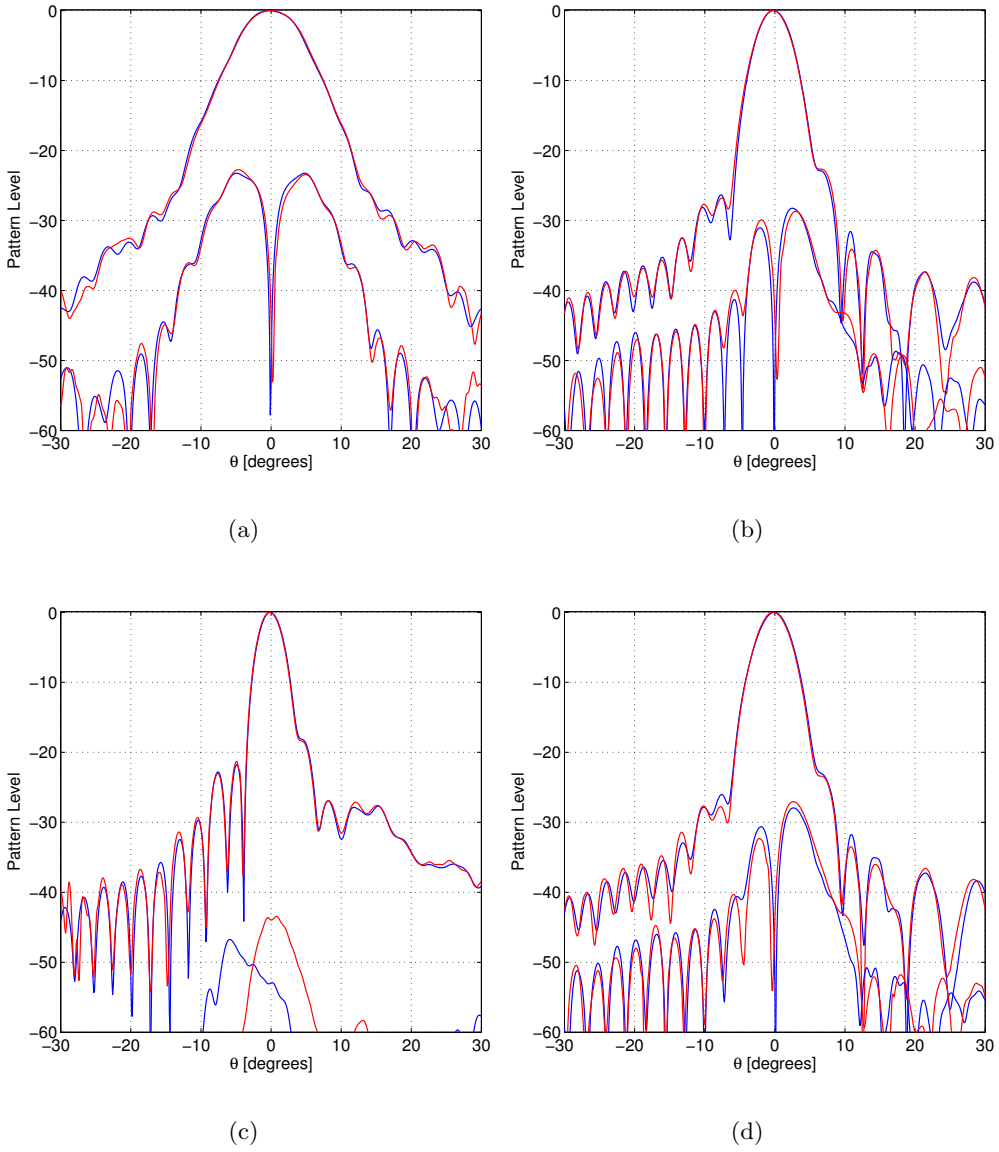

Figure 6.12 The co- and cross-polar patterns for the UPM1 and UPM2 measurements. In (a), (b), (c), and (d) the $\phi = 0^\circ$, $\phi = 45^\circ$, $\phi = 90^\circ$, and $\phi = 135^\circ$ cuts are shown, respectively. The blue graph shows the UPM1 measurement and the red graph shows the UPM2 measurement.

From the comparisons the following observations can be made

- From the patterns in Figure 6.12 it is seen that a good agreement between the patterns can be observed in all cuts.
- From the differences in Figure 6.13 a sharp spike/edge can be observed for the cross-

The information contained in this document should be used only for the scope of the contract for which this document is prepared.

polar component close to $\theta = 0°$ in the $\phi = 45°$, $\phi = 0°$, and $\phi = 135°$ cuts.

- From the results presented in Table 6.4 it can be observed that the STD in the $\theta \leq 30°$ region is 0.124 and 0.130 for the co- and cross-polar component, respectively.
- From the CDF in Figure 6.14 and the STD in Figure 6.16 a generally monotonic behavior of the values is observed.

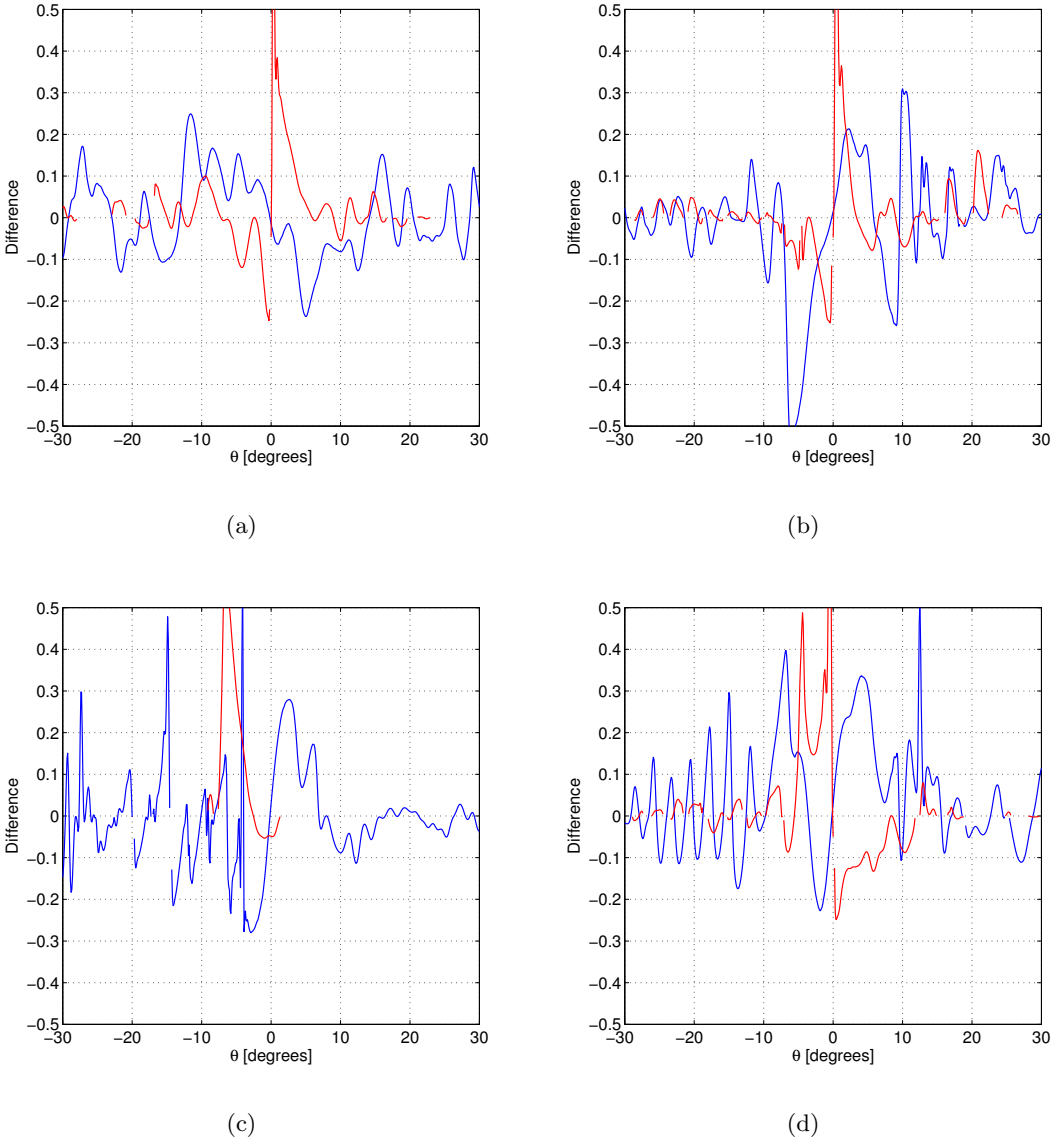

Figure 6.13 The Weighted logarithmic difference for the UPM1 and UPM2 measurements. In (a), (b), (c), and (d) the difference in the $\phi = 0°$, $\phi = 45°$, $\phi = 90°$, and $\phi = 135°$ cuts are shown, respectively. The blue graph shows the difference for the co-polar component and the red graph shows the difference for the cross-polar component.

The information contained in this document should be used only for the scope of the contract for which this document is prepared.

- From both the CDF in Figure 6.14 and the STD in Figure 6.16 a difference between the values for the co- and cross-polar components at high pattern levels can be observed.

	Mean	STD
co-polar ($\theta \leq 30°$)	0.008	0.124
cross-polar ($\theta \leq 30°$)	0.024	0.130

Table 6.4 Statistical data for the Weighted logarithmic difference between UPM1 and UPM2.

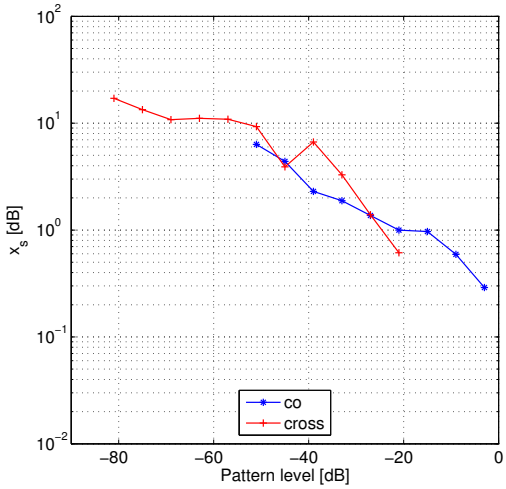

Figure 6.14 Limit value x_s of the Logarithmic difference for the CDF $F(\Delta_i \leq x_s) = 0.9$ in each ±3 dB interval.

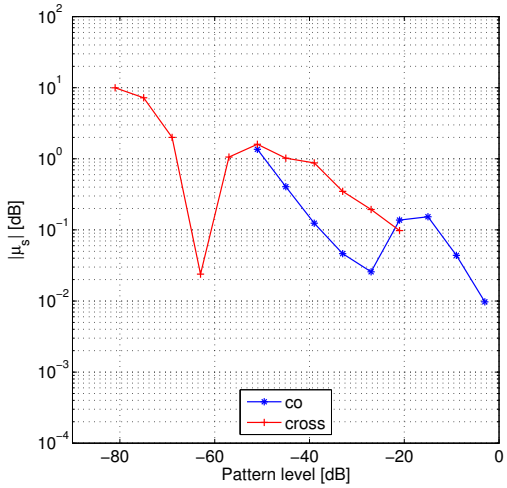

Figure 6.15 Absolute value of the mean $|\mu_s|$ of the Logarithmic difference in each ±3 dB interval.

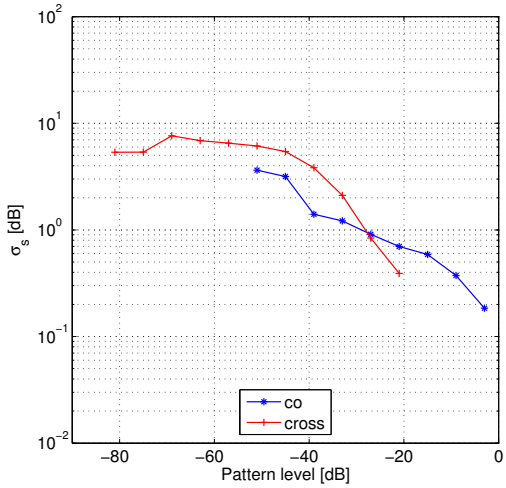

Figure 6.16 Standard deviation σ_s of the Logarithmic difference in each ±3 dB interval.

The information contained in this document should be used only for the scope of the contract for which this document is prepared.

6.3.2.3 Compact Range and Planar Near-Field Measurements

A compact range measurement (UPM3) and a planar near-field measurement (UPM2) are compared.

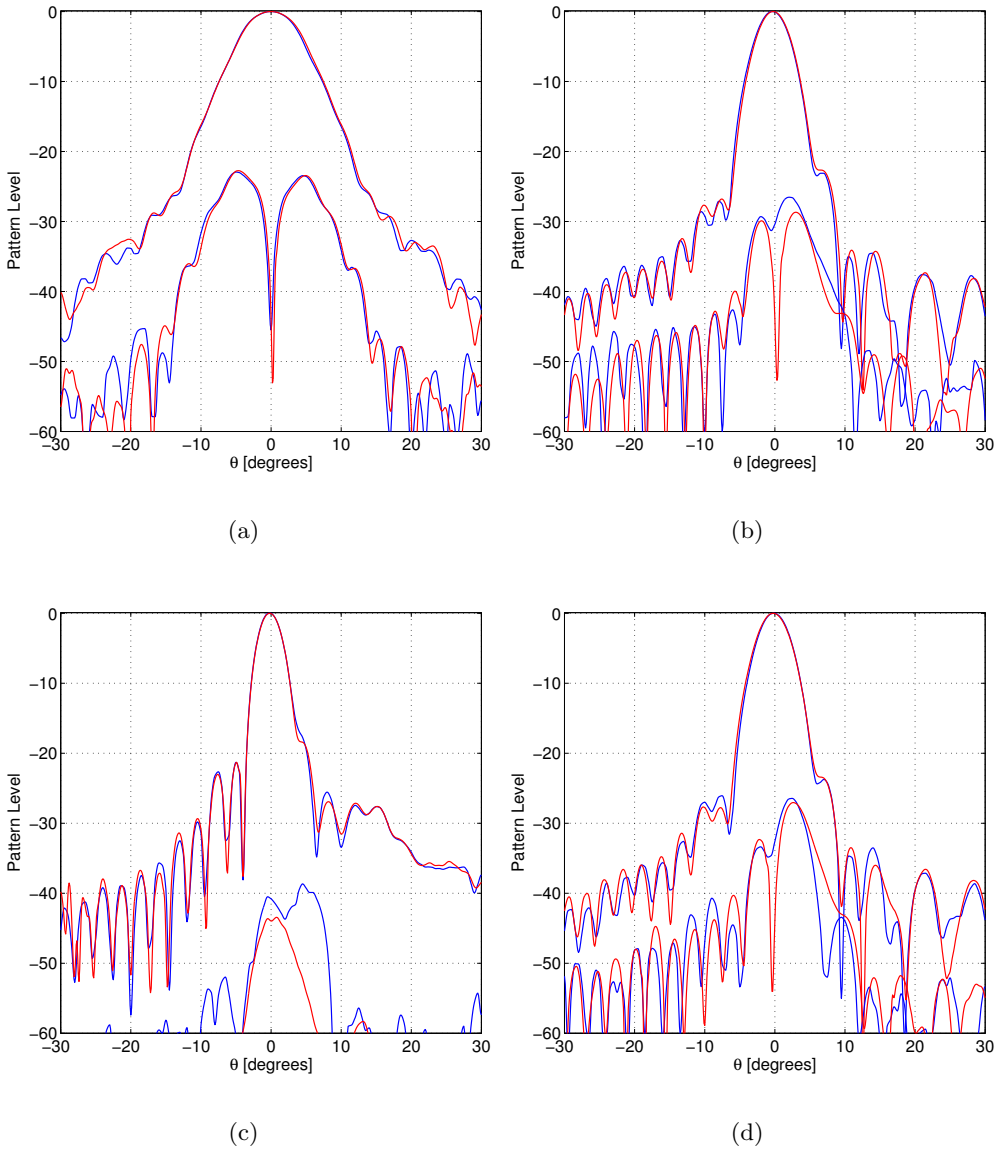

Figure 6.17 The co- and cross-polar patterns for the UPM3 and UPM2 measurements. In (a), (b), (c), and (d) the $\phi = 0°$, $\phi = 45°$, $\phi = 90°$, and $\phi = 135°$ cuts are shown, respectively. The blue graph shows the UPM3 measurement and the red graph shows the UPM2 measurement.

From the comparisons the following observations can be made

- From the patterns in Figure 6.17 a good agreement between the co-polar patterns can generally be observed, while the agreement of the cross-polar patterns, particularly in the $\phi = 45°$ and $\phi = 135°$ cuts, is poor.

The information contained in this document should be used only for the scope of the contract for which this document is prepared.

- From the results presented in Table 6.5 it can be observed that the STD in the $\theta \leq 30°$ region is 0.168 and 0.269 for the co- and cross-polar component, respectively.
- From the CDF in Figure 6.19 and the STD in Figure 6.21 a generally monotonic behavior of the values is observed.
- From both the CDF in Figure 6.19 and the STD in Figure 6.21 a difference between the values for the co- and cross-polar components at high pattern levels can be observed.

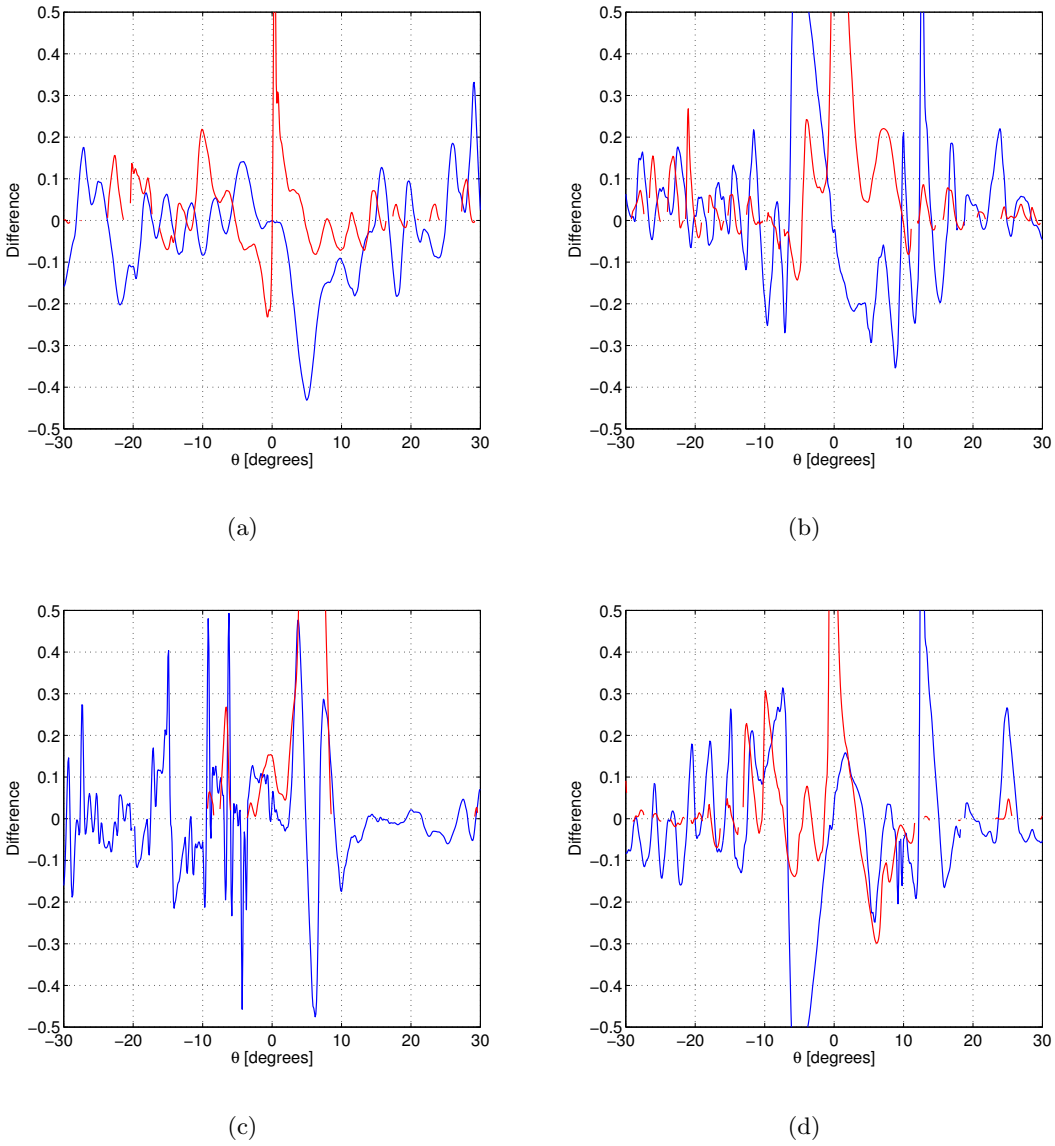

Figure 6.18 The Weighted logarithmic difference for the UPM3 and UPM2 measurements. In (a), (b), (c), and (d) the difference in the $\phi = 0°$, $\phi = 45°$, $\phi = 90°$, and $\phi = 135°$ cuts are shown, respectively. The blue graph shows the difference for the co-polar component and the red graph shows the difference for the cross-polar component.

The information contained in this document should be used only for the scope of the contract for which this document is prepared.

	Mean	STD
co-polar ($\theta \leq 30°$)	-0.006	0.168
cross-polar ($\theta \leq 30°$)	0.083	0.269

Table 6.5 Statistical data for the Weighted logarithmic difference between UPM3 and UPM2.

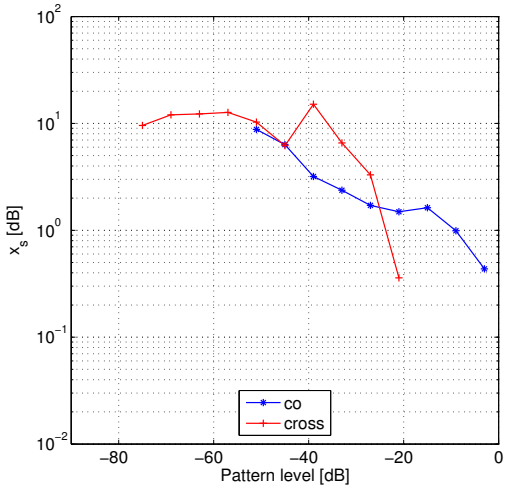

Figure 6.19 Limit value x_s of the Logarithmic difference for the CDF $F(\Delta_i \leq x_s) = 0.9$ in each ±3 dB interval.

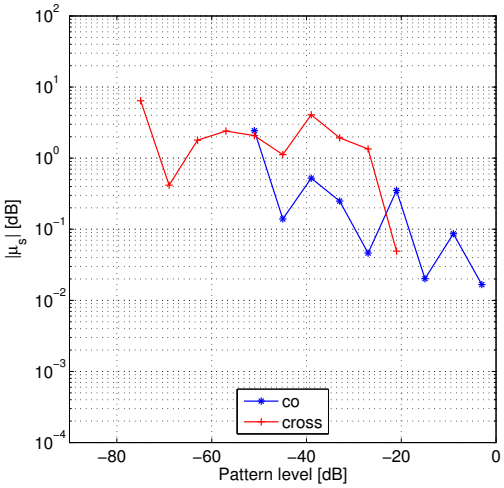

Figure 6.20 Absolute value of the mean $|\mu_s|$ of the Logarithmic difference in each ±3 dB interval.

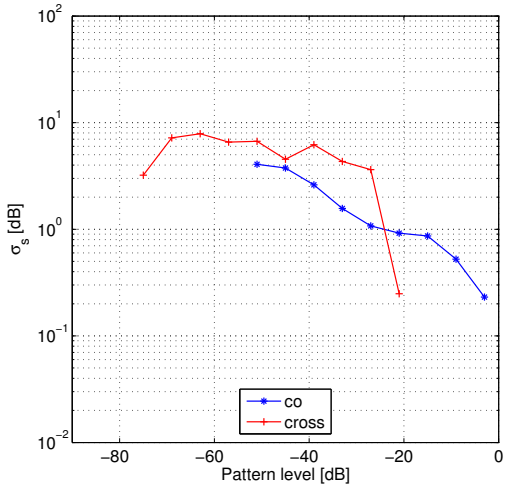

Figure 6.21 Standard deviation σ_s of the Logarithmic difference in each ±3 dB interval.

The information contained in this document should be used only for the scope of the contract for which this document is prepared.

6.3.3 Comparison of Different Spherical Near-Field Measurements

It can be argued that the spherical near-field measurement technique is the most accurate method for experimentally determining the radiation pattern of an antenna. As several of the participating facilities employ this method it is of interest to investigate how well the measurements from two of these facilities correspond.

For this investigation the DTU2 and SES data given in the optical coordinate system is used.

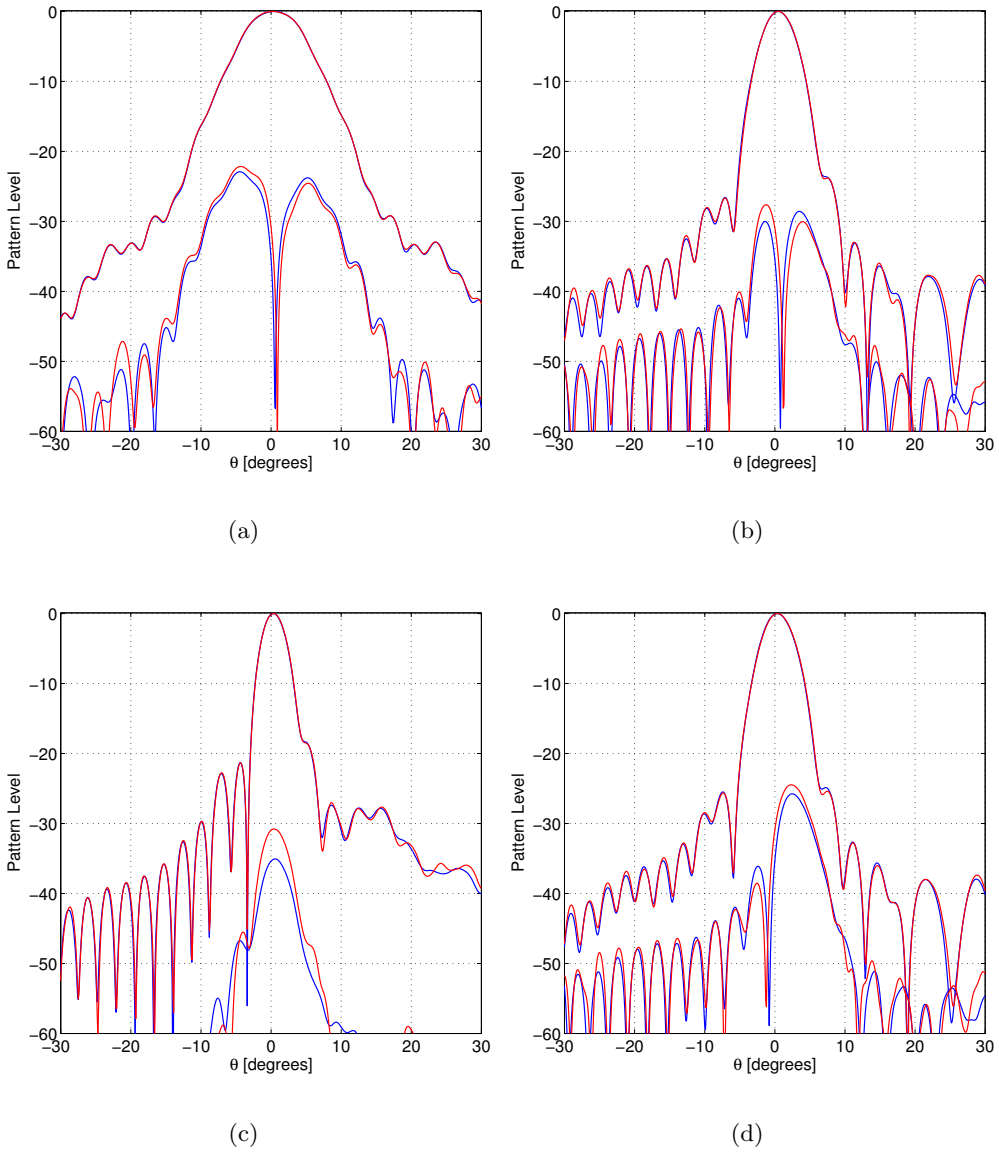

Figure 6.22 The co- and cross-polar patterns for the DTU2 and SES measurements. In (a), (b), (c), and (d) the $\phi = 0°$, $\phi = 45°$, $\phi = 90°$, and $\phi = 135°$ cuts are shown, respectively. The blue graph shows the DTU2 measurement and the red graph shows the SES measurement.

The information contained in this document should be used only for the scope of the contract for which this document is prepared.

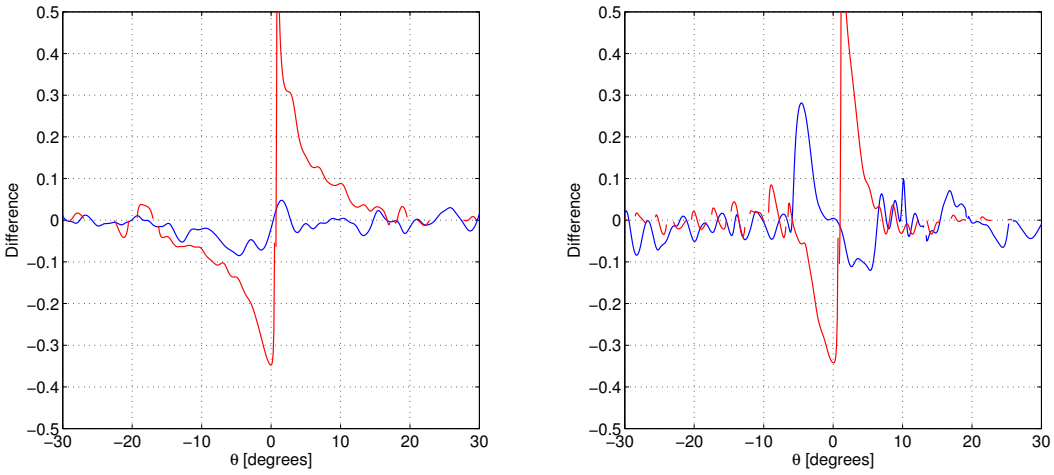

(a) (b)

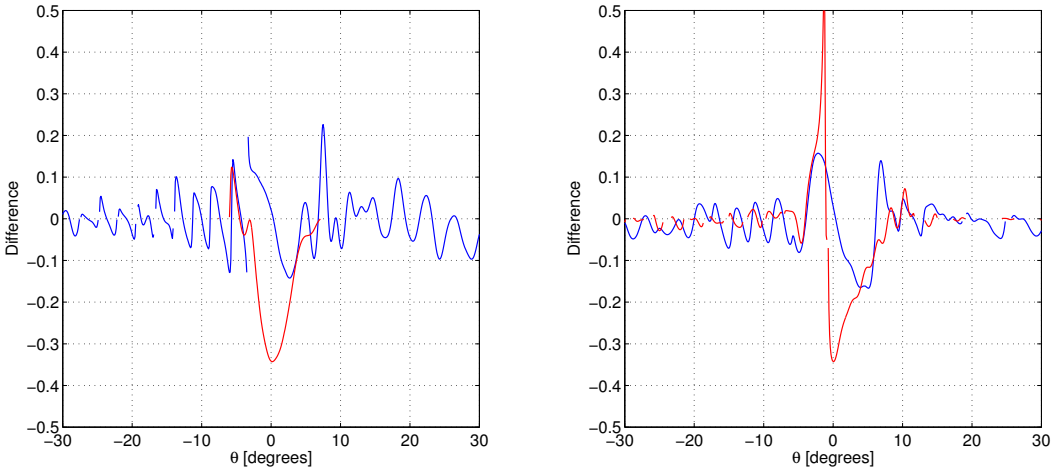

(c) (d)

Figure 6.23 The Weighted logarithmic difference for the DTU2 and SES measurements. In (a), (b), (c), and (d) the difference in the $\phi = 0°$, $\phi = 45°$, $\phi = 90°$, and $\phi = 135°$ cuts are shown, respectively. The blue graph shows the difference for the co-polar component and the red graph shows the difference for the cross-polar component.

From the comparisons the following observations can be made

- From the patterns in Figure 6.22 very good agreement is observed for both the co- and cross-polar patterns. However, in all cuts a difference in the co-polar component around $\theta = 25°$ is visible at levels above -40 dB.
- From Figure the differences in 6.23 a sharp spike/edge can be observed for the cross-polar component close to $\theta = 0°$ in the $\phi = 45°$, $\phi = 0°$, and $\phi = 135°$ cuts.

The information contained in this document should be used only for the scope of the contract for which this document is prepared.

- From the CDF in Figure 6.24 and the STD in Figure 6.26 a generally monotonic behavior of the values is observed.
- From both the CDF in Figure 6.24 and the STD in Figure 6.26 a difference between the values for the co- and cross-polar components at high pattern levels can be observed.

	Mean	STD
co-polar ($\theta \leq 30°$)	-0.008	0.055
cross-polar ($\theta \leq 30°$)	-0.016	0.144
co-polar ($\theta \leq 180°$)	-0.001	0.034
cross-polar ($\theta \leq 180°$)	-0.003	0.074

Table 6.6 Statistical data for the Weighted logarithmic difference between DTU2 and SES.

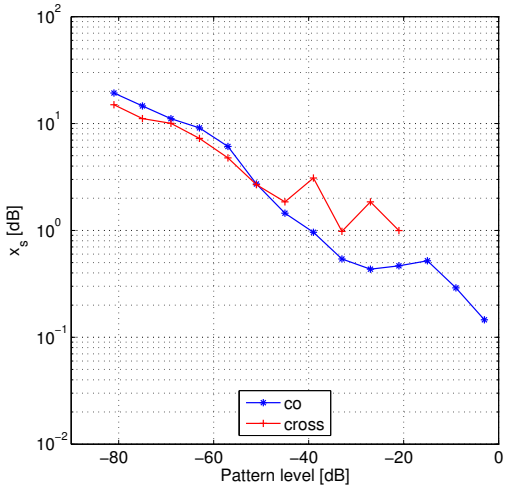

Figure 6.24 Limit value x_s of the Logarithmic difference for the CDF $F(\Delta_i \leq x_s) = 0.9$ in each ±3 dB interval.

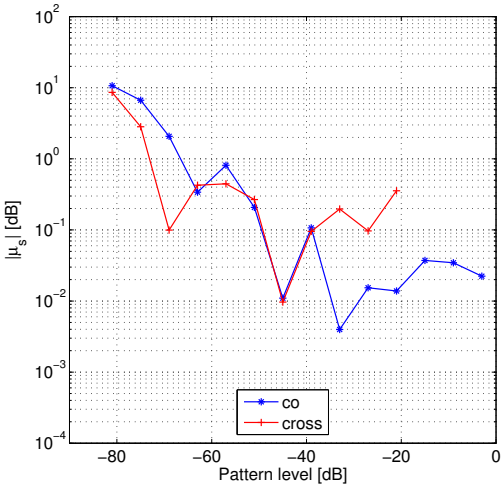

Figure 6.25 Absolute value of the mean $|\mu_s|$ of the Logarithmic difference in each ±3 dB interval.

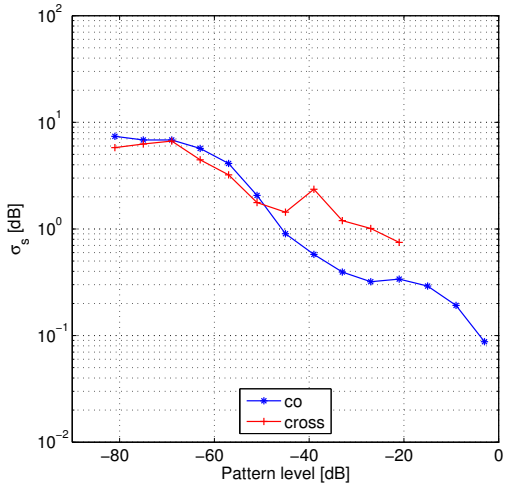

Figure 6.26 Standard deviation σ_s of the Logarithmic difference in each ±3 dB interval.

The information contained in this document should be used only for the scope of the contract for which this document is prepared.

6.3.4 Comparison of Spherical Near-Field Measurements and Far-Field Measurements

As the far-field measurement technique is fundamentally different from the near-field techniques it is of interest to investigate how well the results from these techniques correspond. The spherical near-field technique is expected to be the most accurate of the near-field techniques and is for this reason used in this comparison.

For this investigation the DTU2 and FTRD data in the electrical coordinate system is used.

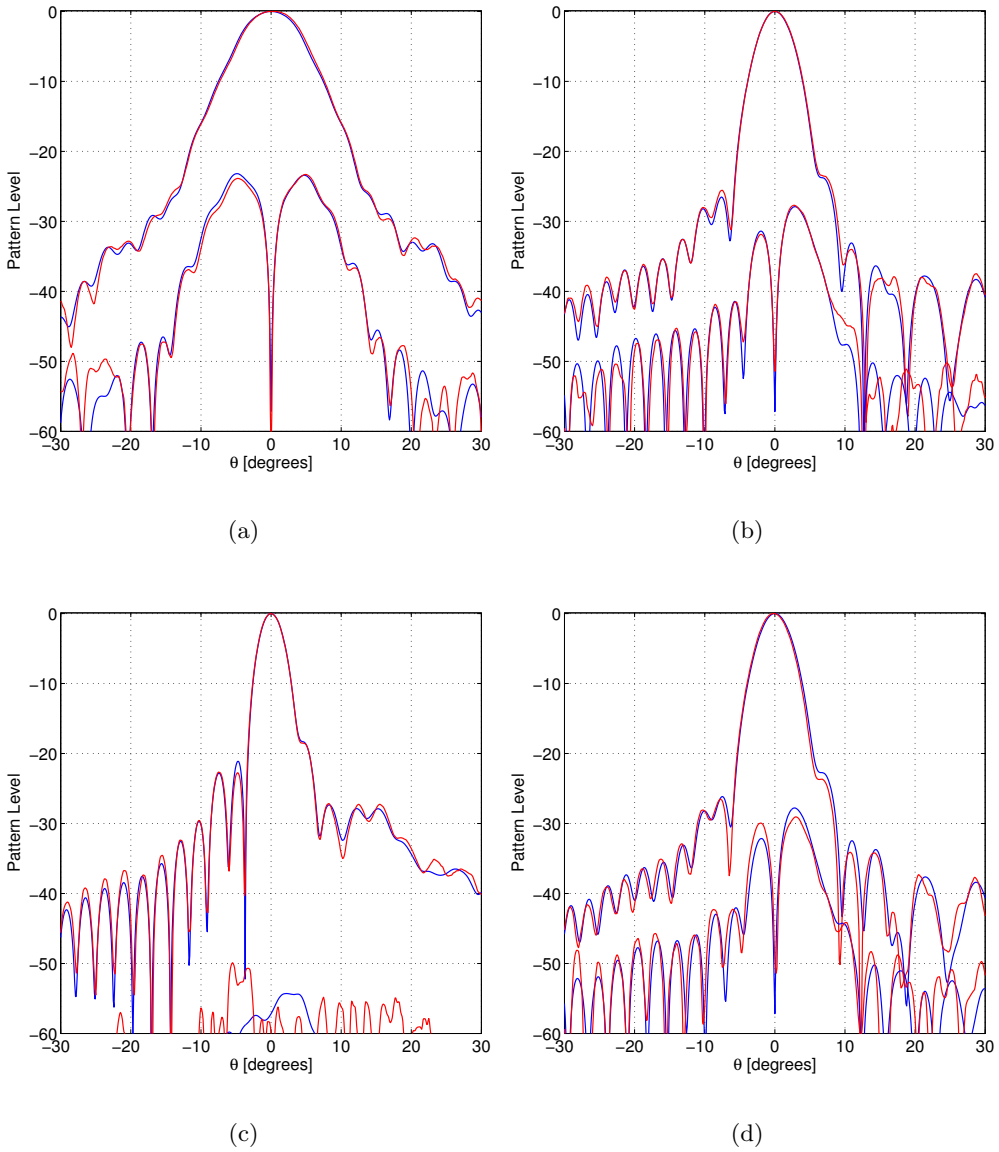

Figure 6.27 The co- and cross-polar patterns for the DTU2 and FTRD measurements. In (a), (b), (c), and (d) the $\phi = 0°$, $\phi = 45°$, $\phi = 90°$, and $\phi = 135°$ cuts are shown, respectively. The blue graph shows the DTU2 measurement and the red graph shows the FTRD measurement.

The information contained in this document should be used only for the scope of the contract for which this document is prepared.

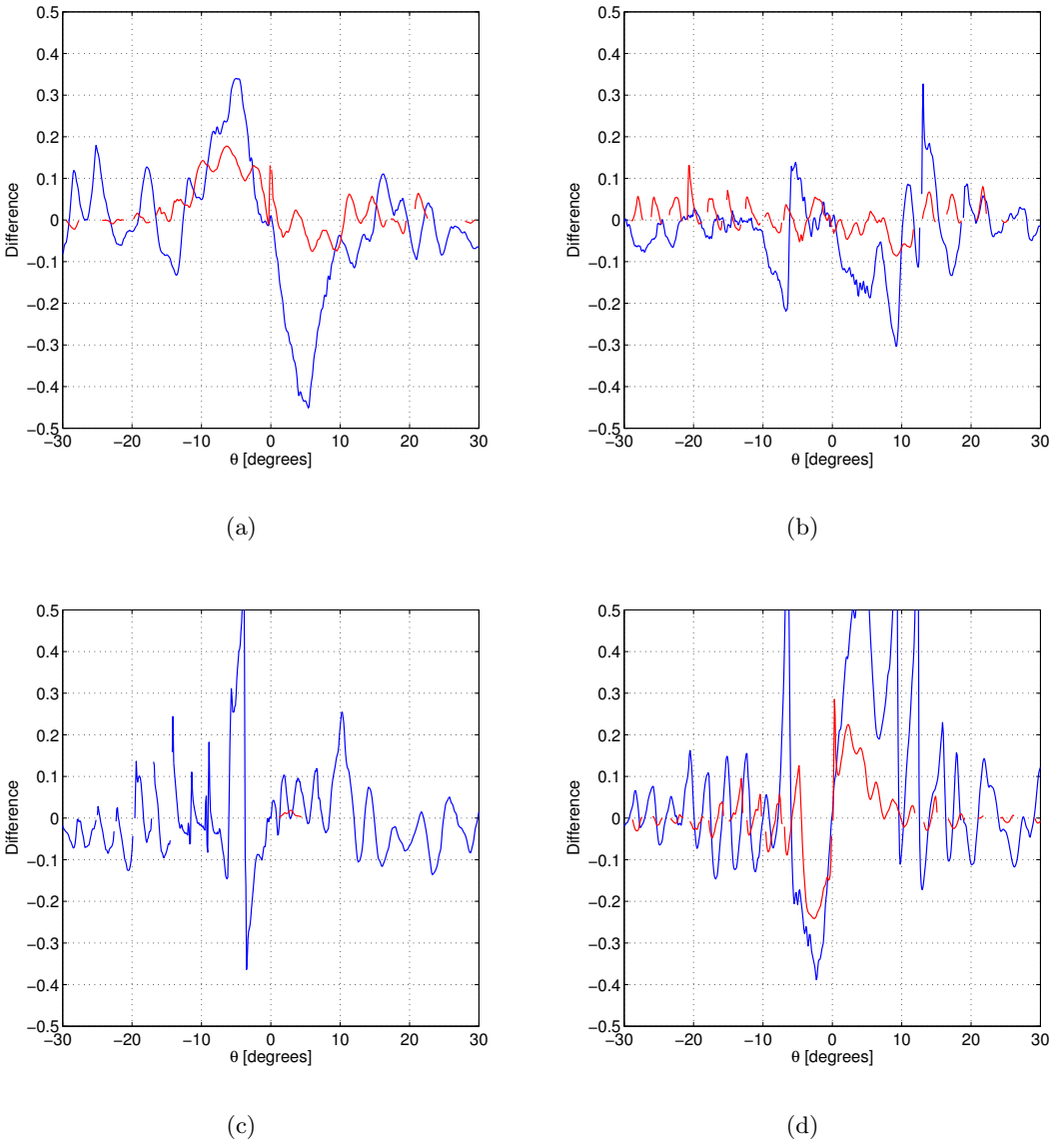

Figure 6.28 The Weighted logarithmic difference for the DTU2 and FTRD measurements. In (a), (b), (c), and (d) the difference in the $\phi = 0°$, $\phi = 45°$, $\phi = 90°$, and $\phi = 135°$ cuts are shown, respectively. The blue graph shows the difference for the co-polar component and the red graph shows the difference for the cross-polar component.

From the comparisons the following observations can be made

- Considering Figure 6.27 it is found that the patterns generally correspond well. However, some differences are noticeable even in the co-polar component at high pattern levels.
- The curves of Figure 6.29 and 6.31 are seen to be generally monotonic and the curves for the co- and cross-polar components correspond well.
- From the CDF in Figure 6.29 and the STD in Figure 6.31 a generally monotonic behavior of the values is observed.

The information contained in this document should be used only for the scope of the contract for which this document is prepared.

- From the CDF in Figure 6.29 and the STD in 6.31 it is seen that a good correspondence exists between the values calculated for the co-polar and the cross-polar components.

	Mean	STD
co-polar ($\theta \leq 30°$)	0.004	0.158
cross-polar ($\theta \leq 30°$)	0.013	0.066
co-polar ($\theta \leq 90°$)	0.004	0.108
cross-polar ($\theta \leq 90°$)	0.010	0.055

Table 6.7 Statistical data for the Weighted logarithmic difference between DTU2 and FTRD.

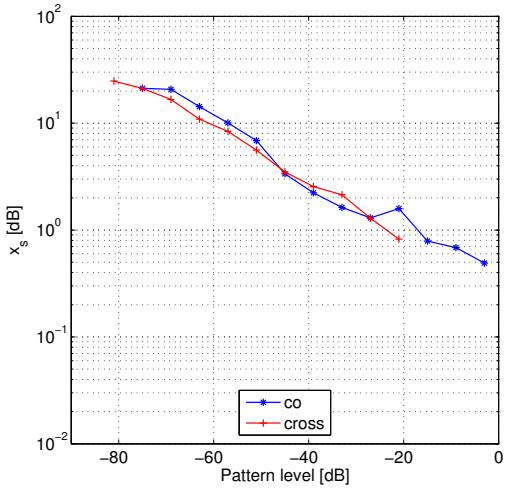

Figure 6.29 Limit value x_s of the Logarithmic difference for the CDF $F(\Delta_i \leq x_s) = 0.9$ in each ±3 dB interval.

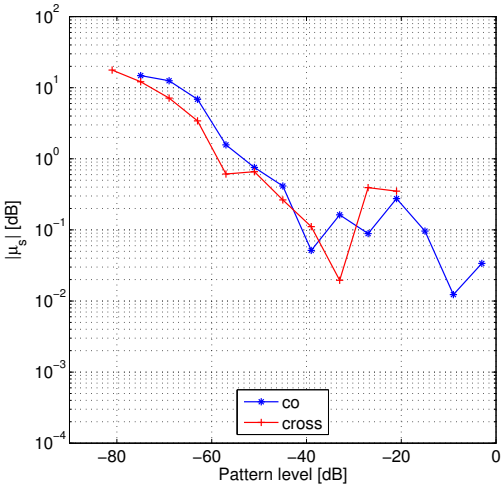

Figure 6.30 Absolute value of the mean $|\mu_s|$ of the Logarithmic difference in each ±3 dB interval.

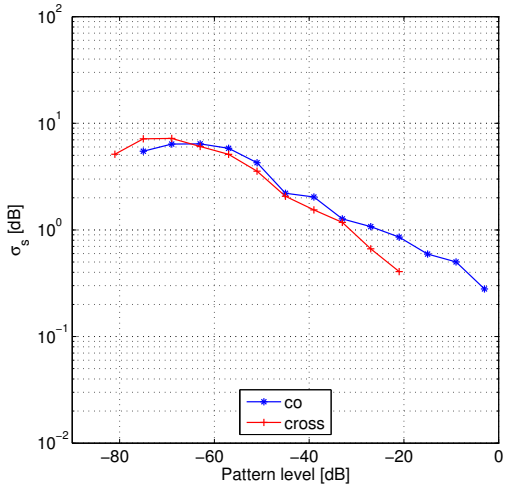

Figure 6.31 Standard deviation σ_s of the Logarithmic difference in each ±3 dB interval.

The information contained in this document should be used only for the scope of the contract for which this document is prepared.

6.3.5 Comparison of Measurements to Common Reference Pattern 1

In order to evaluate the performance of the participating facilities the measured patterns from these are compared to a reference pattern. Reference pattern 1 (REF1), which was defined in Section 6.2.1, is constructed in the optical coordinate system from the DTU2, UPM1, and SES patterns.

In this investigation the reference pattern is compared to: DTU1, DTU2, UPM1, UPM2, SES, and UPC.

The information contained in this document should be used only for the scope of the contract for which this document is prepared.

6.3.5.1 Comparison of DTU1 Measurement to Reference Pattern 1

The results from a comparison of the DTU1 spherical near-field measurement and Reference Pattern 1 are presented here. The results are presented without comments and observations. However, the results of all comparisons with Reference pattern 1 are summarized in Section 6.3.5.7.

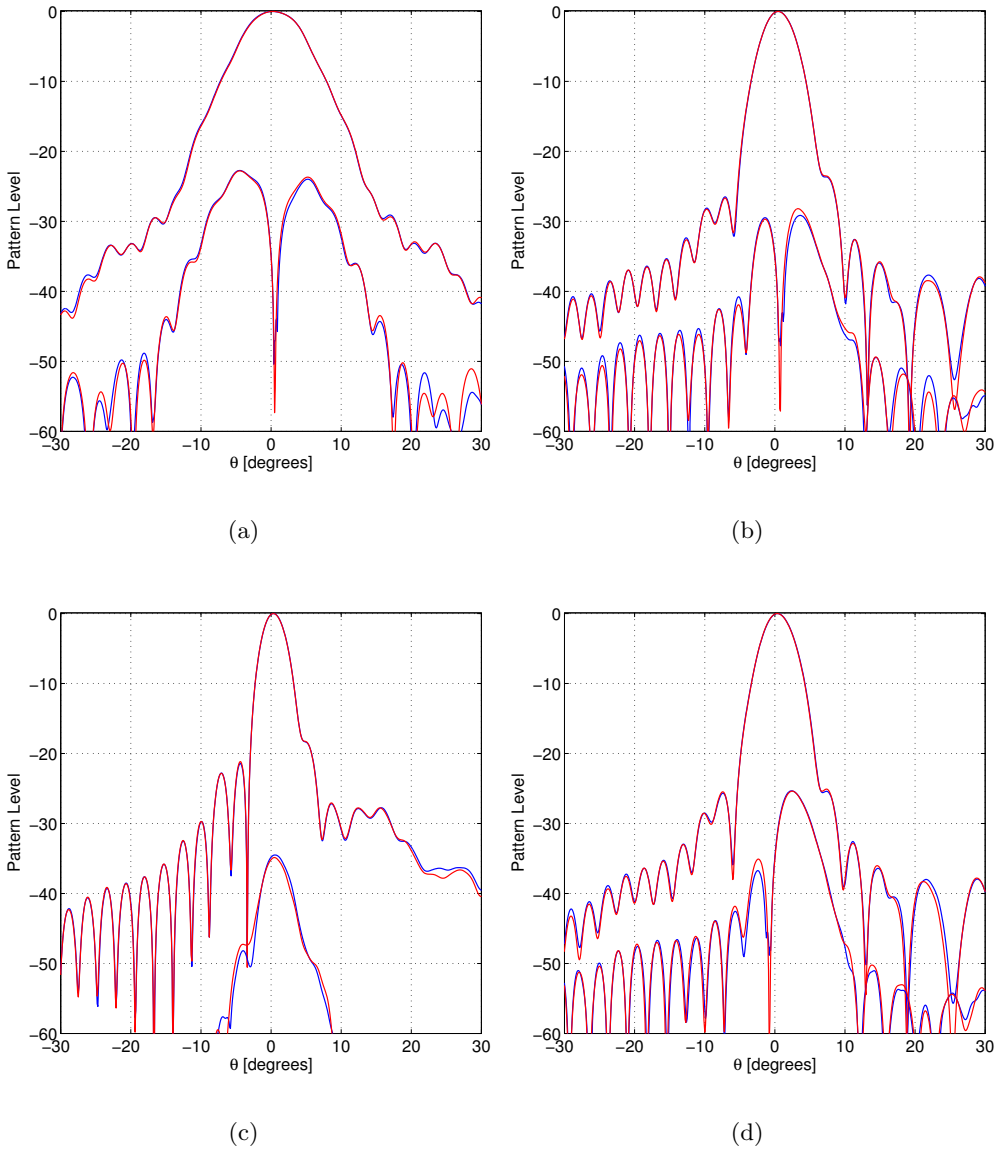

(a) (b)

(c) (d)

Figure 6.32 The co- and cross-polar patterns for the REF1 and DTU1 patterns. In (a), (b), (c), and (d) the $\phi = 0°$, $\phi = 45°$, $\phi = 90°$, and $\phi = 135°$ cuts are shown, respectively. The blue graph shows the REF1 pattern and the red graph shows the DTU1 pattern.

The information contained in this document should be used only for the scope of the contract for which this document is prepared.

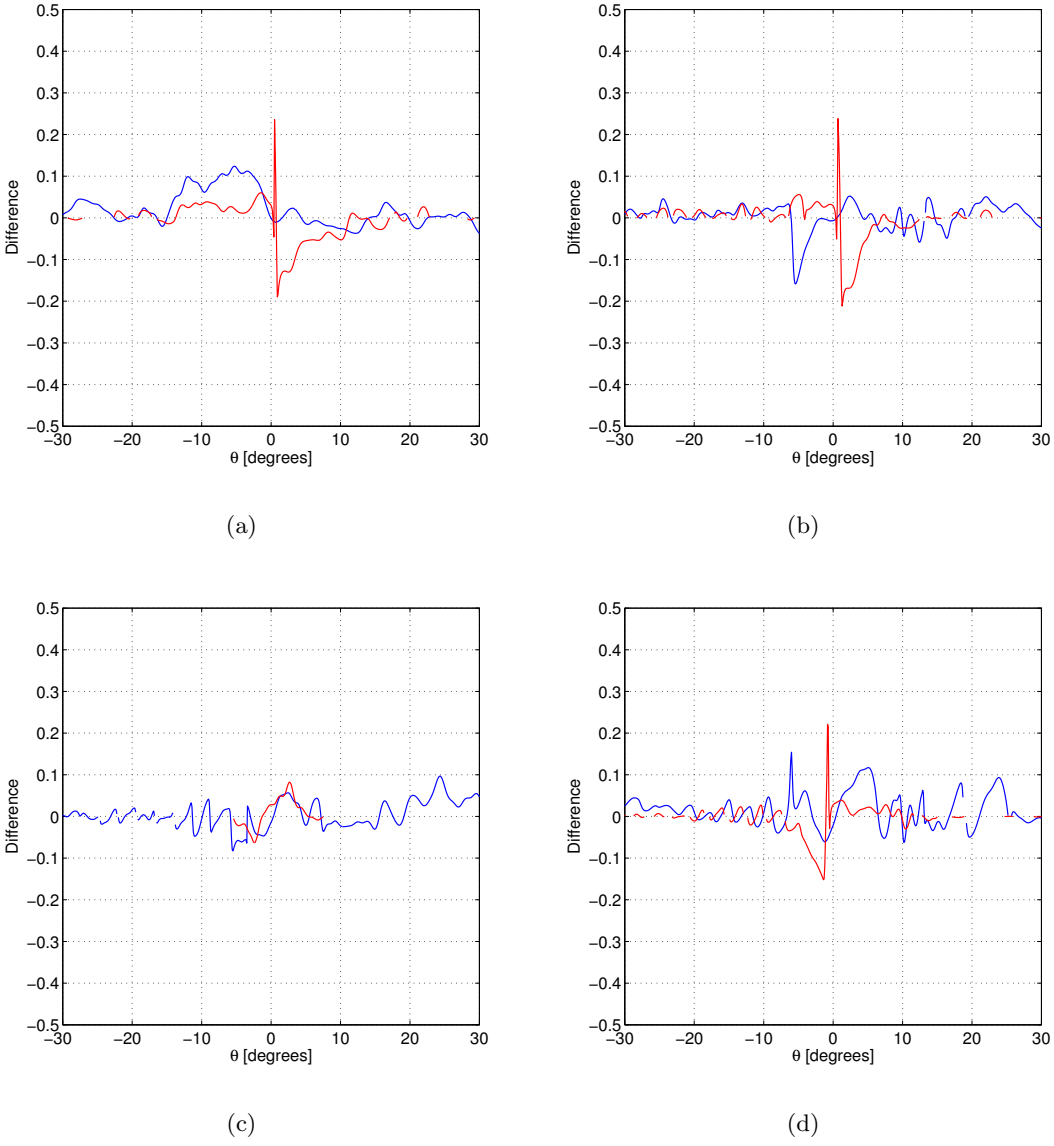

Figure 6.33 The Weighted logarithmic difference for the REF1 and DTU1 patterns. In (a), (b), (c), and (d) the difference in the $\phi = 0°$, $\phi = 45°$, $\phi = 90°$, and $\phi = 135°$ cuts are shown, respectively. The blue graph shows the difference for the co-polar component and the red graph shows the difference for the cross-polar component.

The information contained in this document should be used only for the scope of the contract for which this document is prepared.

	Mean	STD
co-polar ($\theta \leq 30°$)	0.011	0.037
cross-polar ($\theta \leq 30°$)	-0.004	0.043
co-polar ($\theta \leq 180°$)	0.004	0.022
cross-polar ($\theta \leq 180°$)	-0.001	0.026

Table 6.8 Statistical data for the Weighted logarithmic difference between REF1 and DTU1.

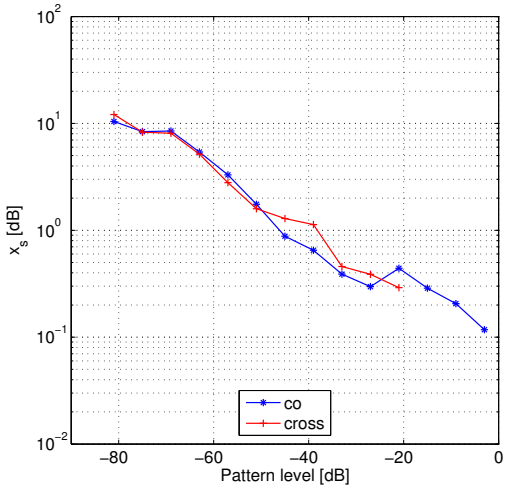

Figure 6.34 Limit value x_s of the Logarithmic difference for the CDF $F(\Delta_i \leq x_s) = 0.9$ in each ±3 dB interval.

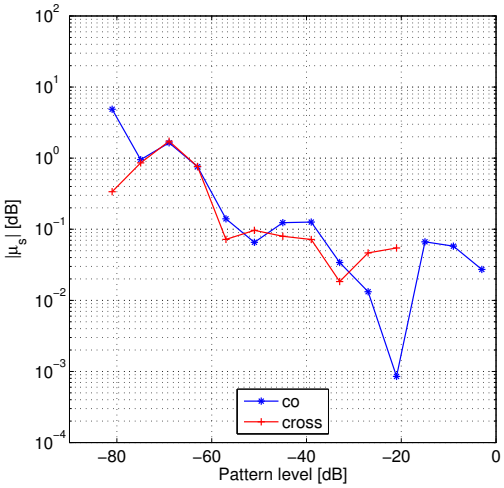

Figure 6.35 Absolute value of the mean $|\mu_s|$ of the Logarithmic difference in each ±3 dB interval.

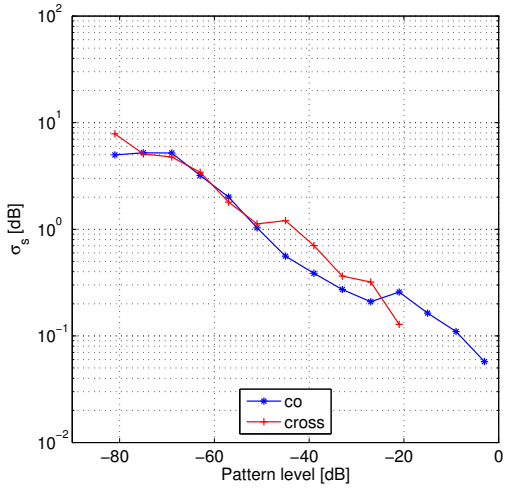

Figure 6.36 Standard deviation σ_s of the Logarithmic difference in each ±3 dB interval.

The information contained in this document should be used only for the scope of the contract for which this document is prepared.

6.3.5.2 Comparison of DTU2 Measurement to Reference Pattern 1

The results from a comparison of the DTU2 spherical near-field measurement and Reference Pattern 1 are presented here. DTU2 is one of the patterns that were used in the definition of Reference Pattern 1. The results are presented without comments and observations. However, the results of all comparisons with Reference pattern 1 are summarized in Section 6.3.5.7.

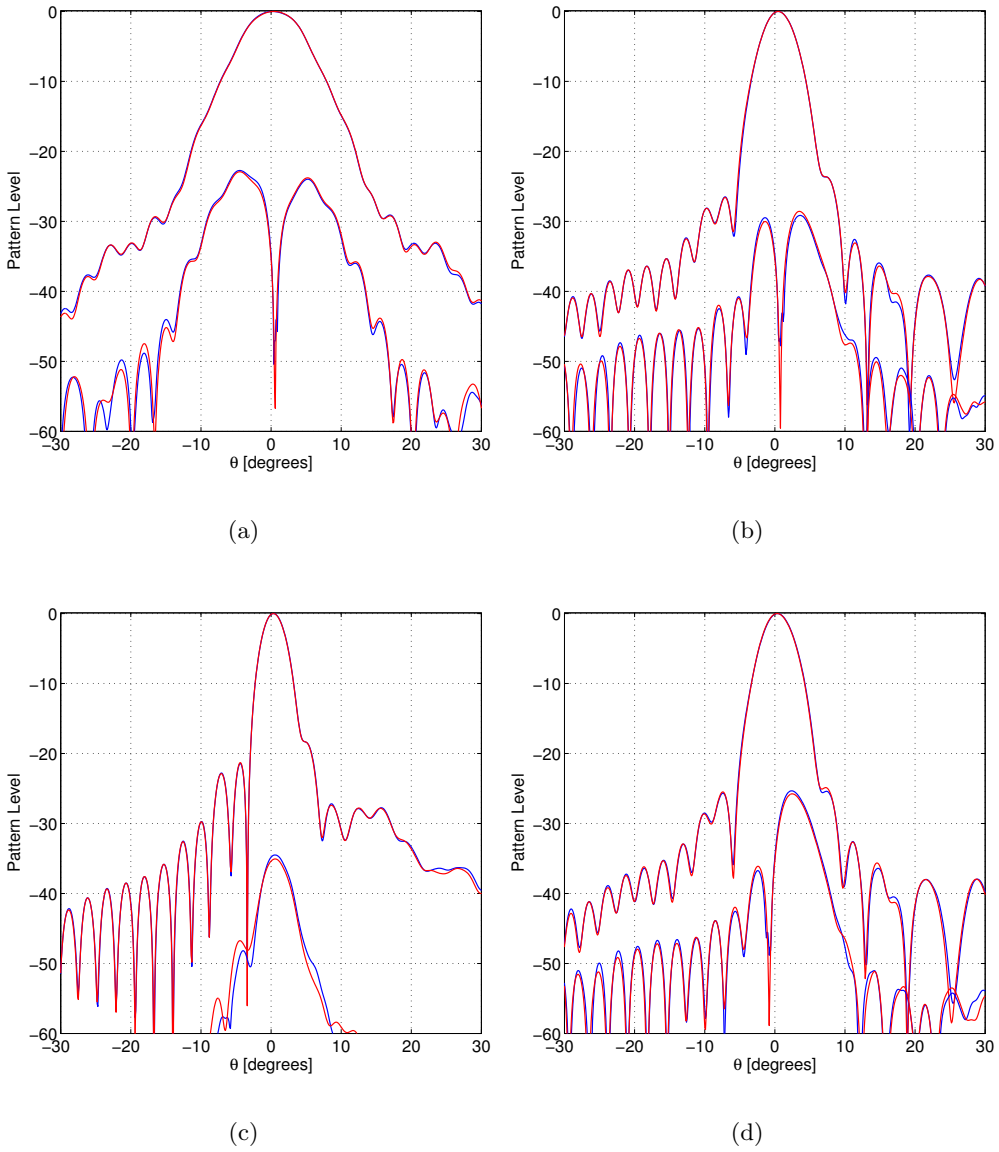

Figure 6.37 The co- and cross-polar patterns for the REF1 and DTU2 patterns. In (a), (b), (c), and (d) the $\phi = 0°$, $\phi = 45°$, $\phi = 90°$, and $\phi = 135°$ cuts are shown, respectively. The blue graph shows the REF1 pattern and the red graph shows the DTU2 pattern.

The information contained in this document should be used only for the scope of the contract for which this document is prepared.

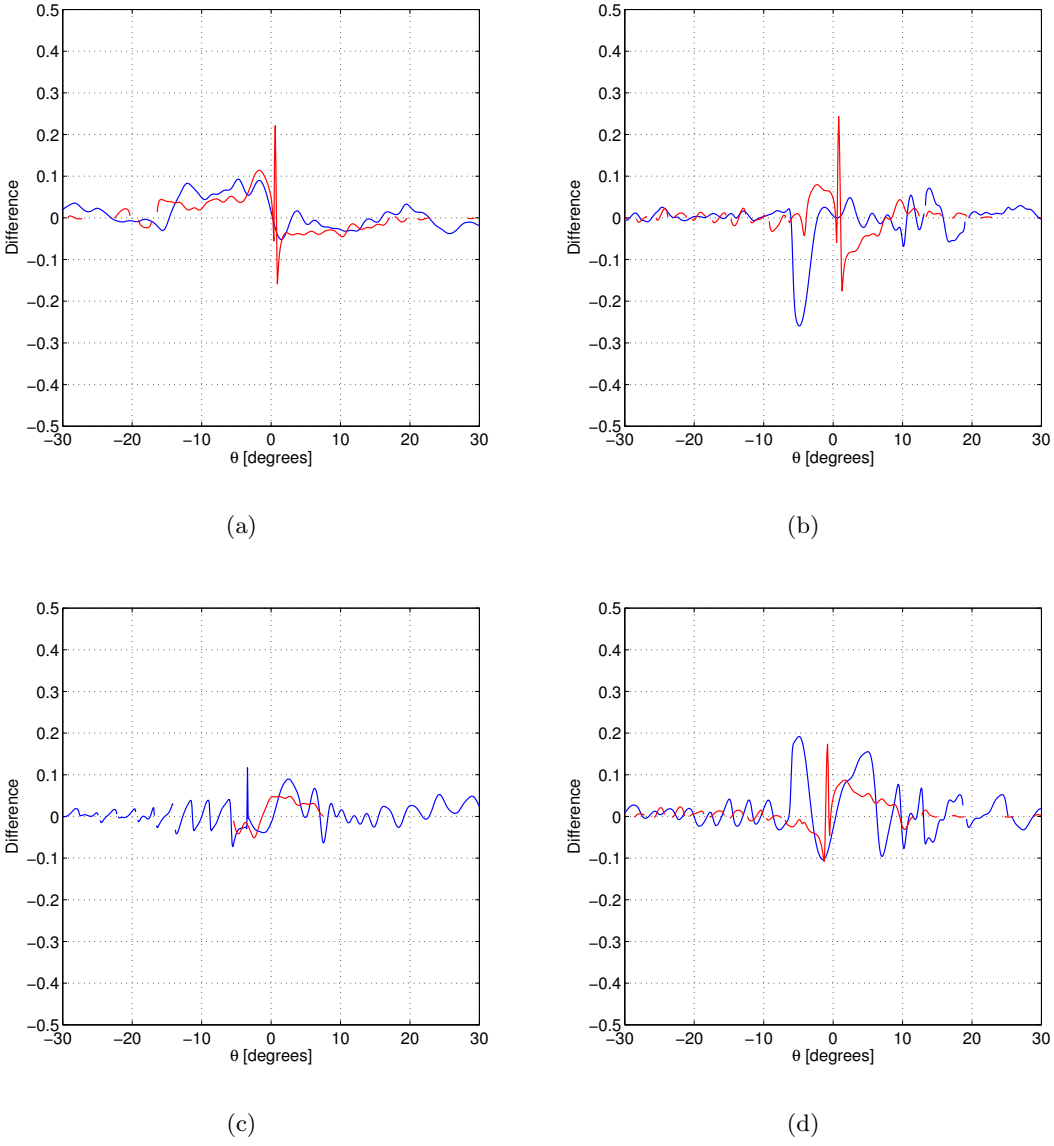

Figure 6.38 The Weighted logarithmic difference for the REF1 and DTU2 patterns. In (a), (b), (c), and (d) the difference in the $\phi = 0°$, $\phi = 45°$, $\phi = 90°$, and $\phi = 135°$ cuts are shown, respectively. The blue graph shows the difference for the co-polar component and the red graph shows the difference for the cross-polar component.

The information contained in this document should be used only for the scope of the contract for which this document is prepared.

	Mean	STD
co-polar ($\theta \leq 30°$)	0.007	0.045
cross-polar ($\theta \leq 30°$)	0.006	0.038
co-polar ($\theta \leq 180°$)	0.004	0.025
cross-polar ($\theta \leq 180°$)	0.002	0.024

Table 6.9 Statistical data for the Weighted logarithmic difference between REF1 and DTU2.

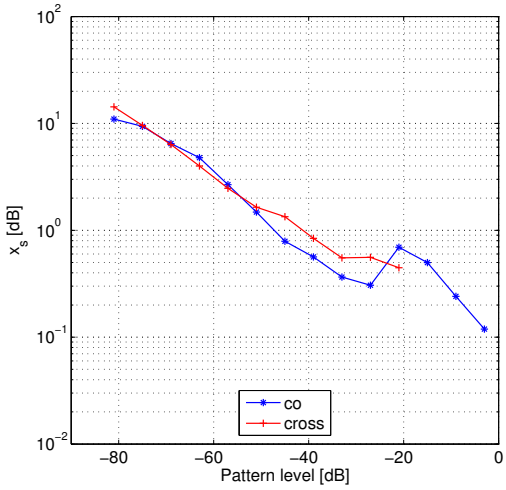

Figure 6.39 Limit value x_s of the Logarithmic difference for the CDF $F(\Delta_i \leq x_s) = 0.9$ in each ±3 dB interval.

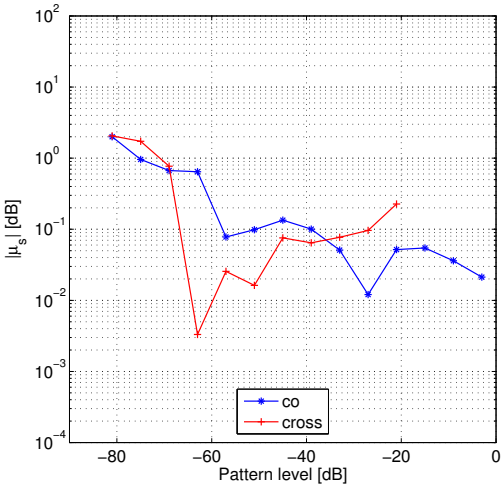

Figure 6.40 Absolute value of the mean $|\mu_s|$ of the Logarithmic difference in each ±3 dB interval.

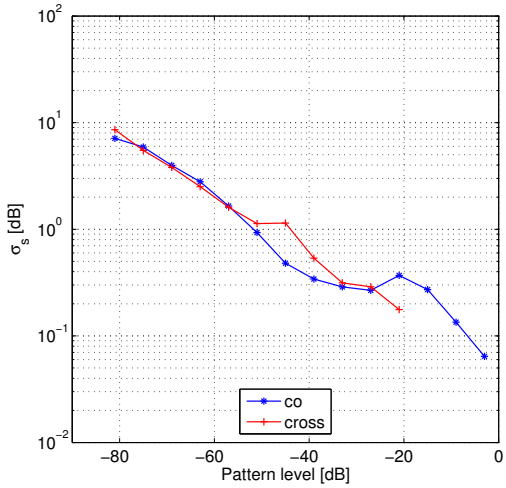

Figure 6.41 Standard deviation σ_s of the Logarithmic difference in each ±3 dB interval.

The information contained in this document should be used only for the scope of the contract for which this document is prepared.

6.3.5.3 Comparison of UPM1 Measurement to Reference Pattern 1

The results from a comparison of the UPM1 spherical near-field measurement and Reference Pattern 1 are presented here. UPM1 is one of the patterns that were used in the definition of Reference Pattern 1. The results are presented without comments and observations. However, the results of all comparisons with Reference pattern 1 are summarized in Section 6.3.5.7.

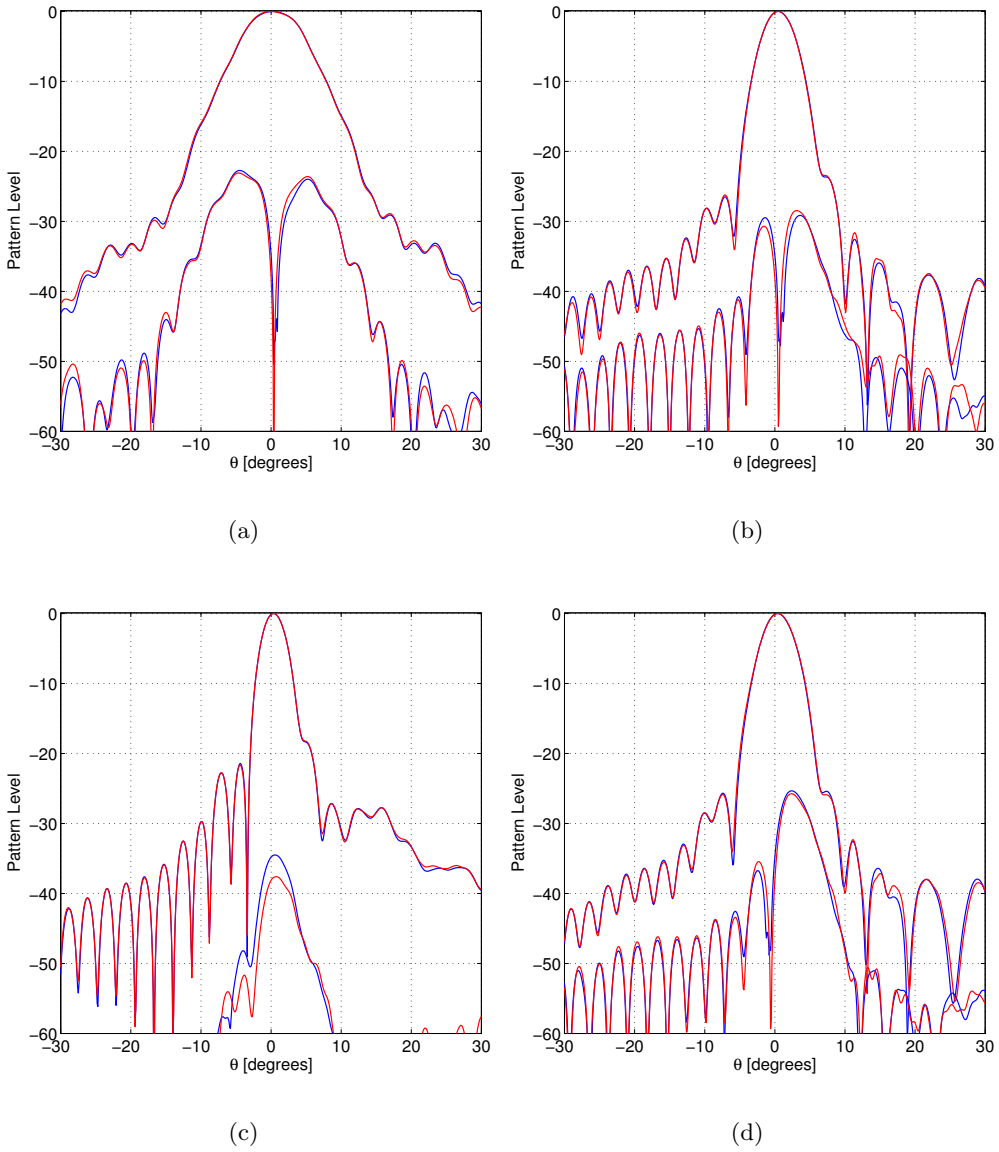

(a) (b)

(c) (d)

Figure 6.42 The co- and cross-polar patterns for the REF1 and UPM1 patterns. In (a), (b), (c), and (d) the $\phi = 0°$, $\phi = 45°$, $\phi = 90°$, and $\phi = 135°$ cuts are shown, respectively. The blue graph shows the REF1 pattern and the red graph shows the UPM1 pattern.

The information contained in this document should be used only for the scope of the contract for which this document is prepared.

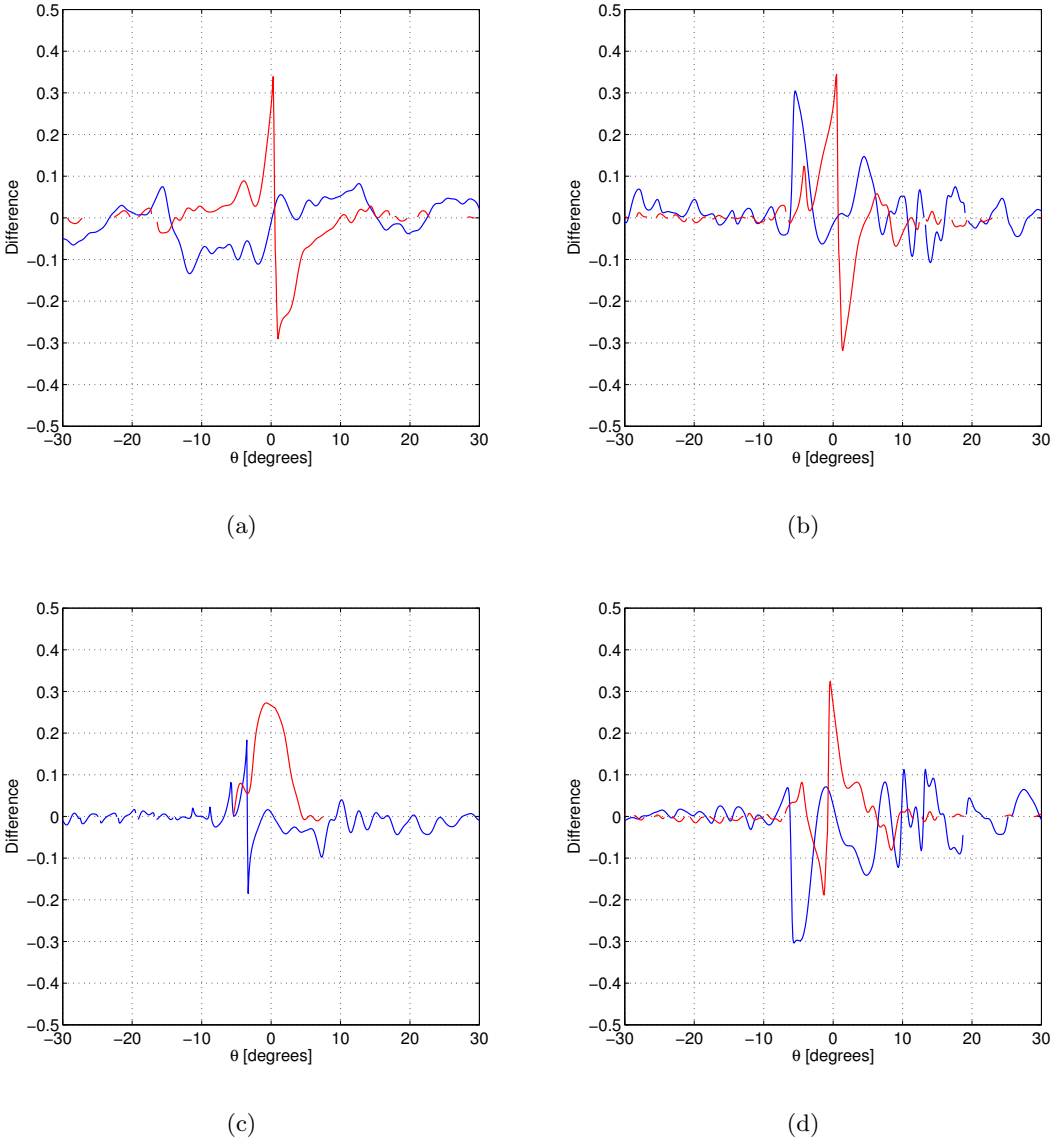

Figure 6.43 The Weighted logarithmic difference for the REF1 and UPM1 patterns. In (a), (b), (c), and (d) the difference in the $\phi = 0°$, $\phi = 45°$, $\phi = 90°$, and $\phi = 135°$ cuts are shown, respectively. The blue graph shows the difference for the co-polar component and the red graph shows the difference for the cross-polar component.

The information contained in this document should be used only for the scope of the contract for which this document is prepared.

	Mean	STD
co-polar ($\theta \leq 30°$)	-0.004	0.058
cross-polar ($\theta \leq 30°$)	0.012	0.085
co-polar ($\theta \leq 180°$)	-0.005	0.034
cross-polar ($\theta \leq 180°$)	0.001	0.049

Table 6.10 Statistical data for the Weighted logarithmic difference between REF1 and UPM1.

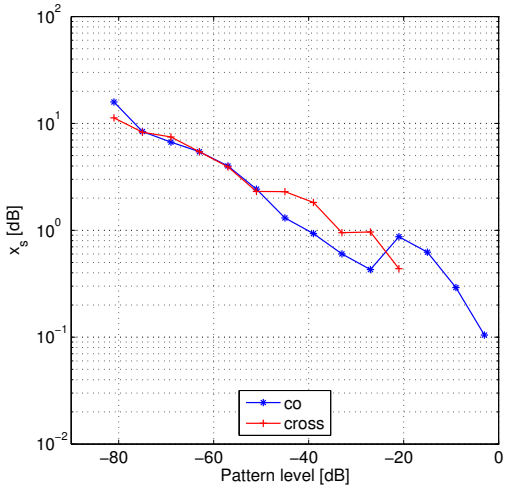

Figure 6.44 Limit value x_s of the Logarithmic difference for the CDF $F(\Delta_i \leq x_s) = 0.9$ in each ±3 dB interval.

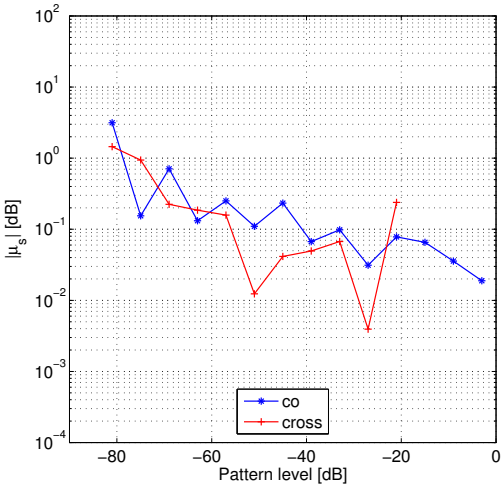

Figure 6.45 Absolute value of the mean $|\mu_s|$ of the Logarithmic difference in each ±3 dB interval.

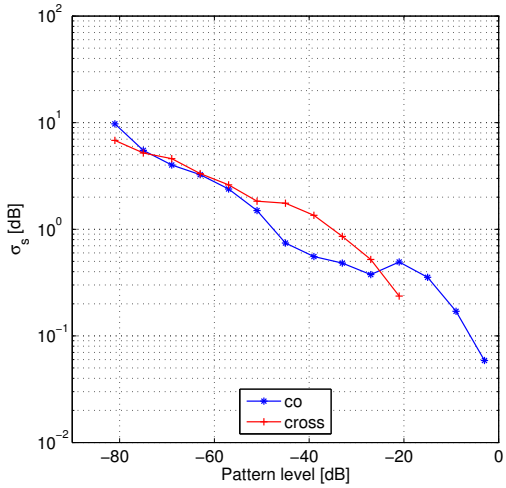

Figure 6.46 Standard deviation σ_s of the Logarithmic difference in each ±3 dB interval.

The information contained in this document should be used only for the scope of the contract for which this document is prepared.

6.3.5.4 Comparison of UPM2 Measurement to Reference Pattern 1

The results from a comparison of the UPM2 planar near-field measurement and Reference Pattern 1 are presented here. The results are presented without comments and observations. However, the results of all comparisons with Reference pattern 1 are summarized in Section 6.3.5.7.

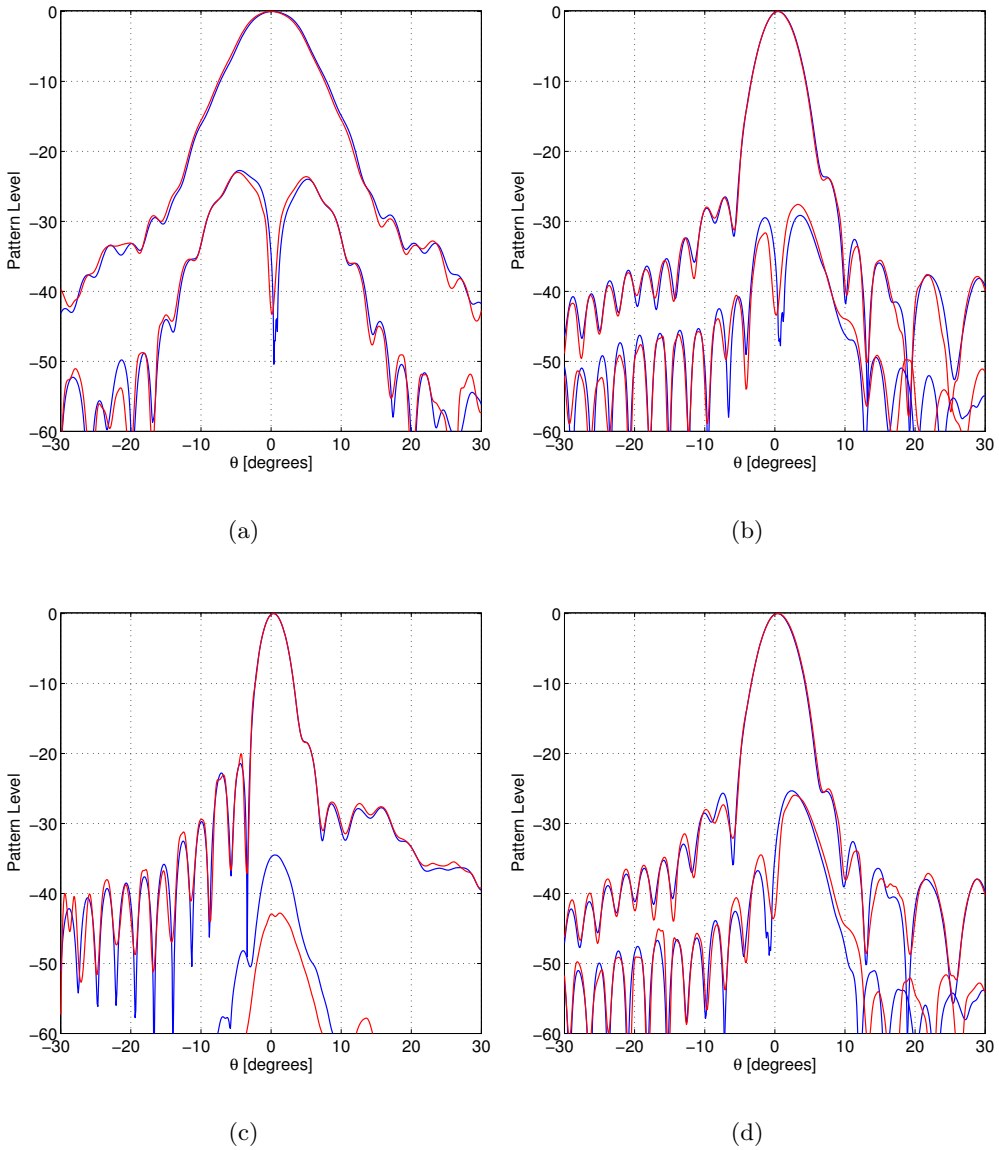

(a) (b)

(c) (d)

Figure 6.47 The co- and cross-polar patterns for the REF1 and UPM2 patterns. In (a), (b), (c), and (d) the $\phi = 0°$, $\phi = 45°$, $\phi = 90°$, and $\phi = 135°$ cuts are shown, respectively. The blue graph shows the REF1 pattern and the red graph shows the UPM2 pattern.

The information contained in this document should be used only for the scope of the contract for which this document is prepared.

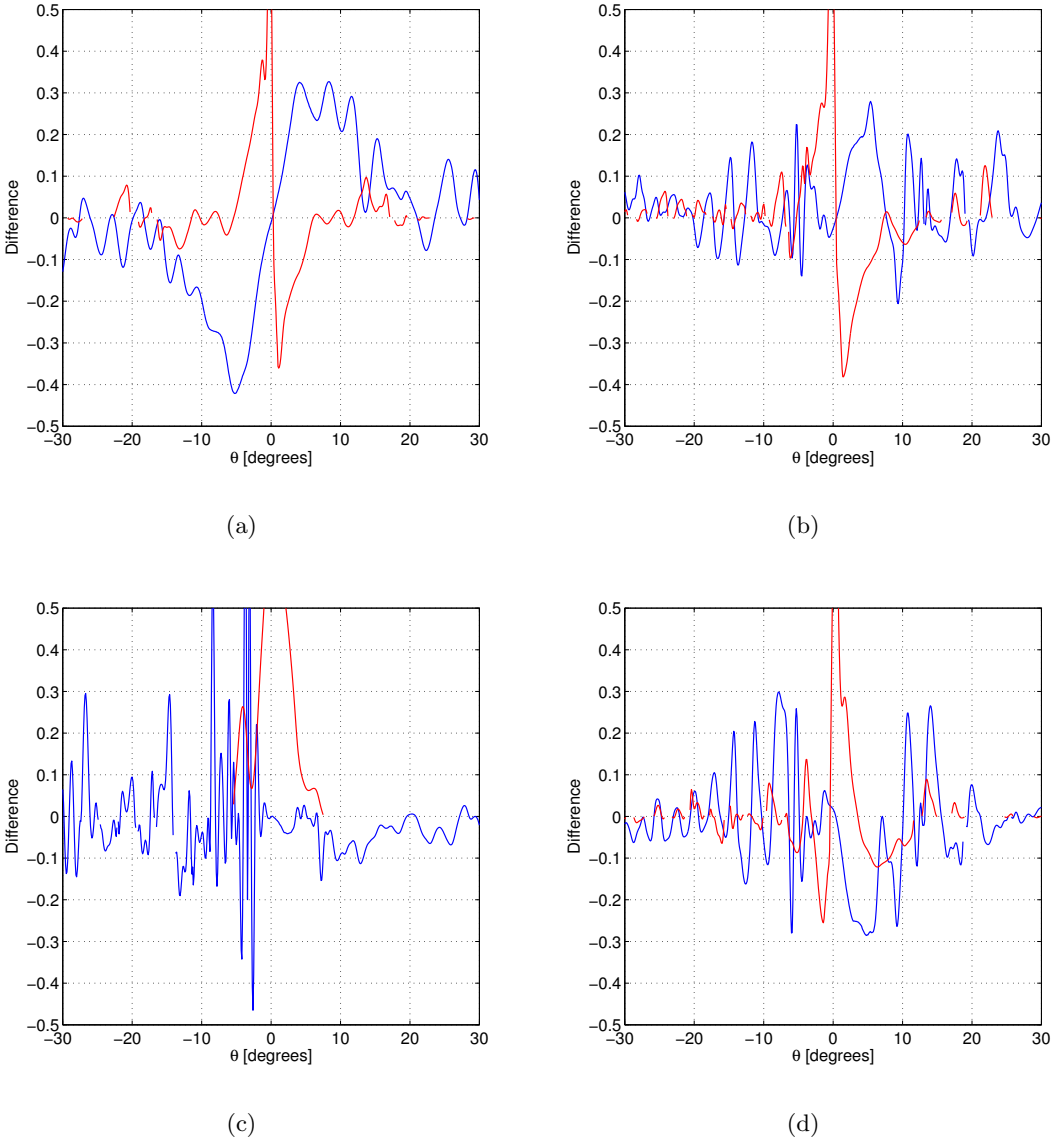

Figure 6.48 The Weighted logarithmic difference for the REF1 and UPM2 patterns. In (a), (b), (c), and (d) the difference in the $\phi = 0°$, $\phi = 45°$, $\phi = 90°$, and $\phi = 135°$ cuts are shown, respectively. The blue graph shows the difference for the co-polar component and the red graph shows the difference for the cross-polar component.

The information contained in this document should be used only for the scope of the contract for which this document is prepared.

	Mean	STD
co-polar ($\theta \leq 30°$)	0.000	0.131
cross-polar ($\theta \leq 30°$)	0.035	0.169

Table 6.11 Statistical data for the Weighted logarithmic difference between REF1 and UPM2.

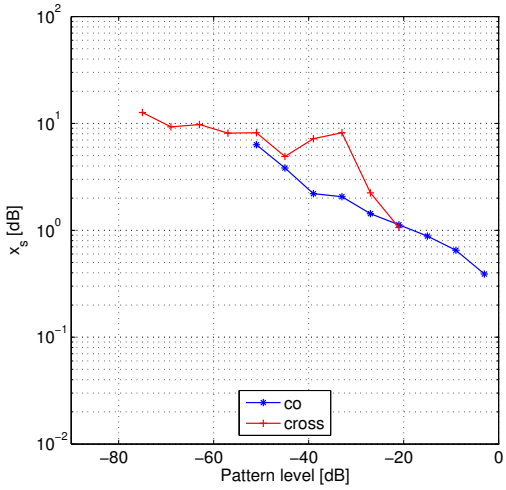

Figure 6.49 Limit value x_s of the Logarithmic difference for the CDF $F(\Delta_i \leq x_s) = 0.9$ in each ±3 dB interval.

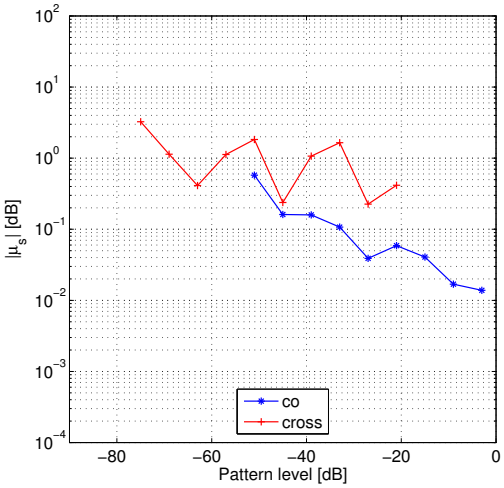

Figure 6.50 Absolute value of the mean $|\mu_s|$ of the Logarithmic difference in each ±3 dB interval.

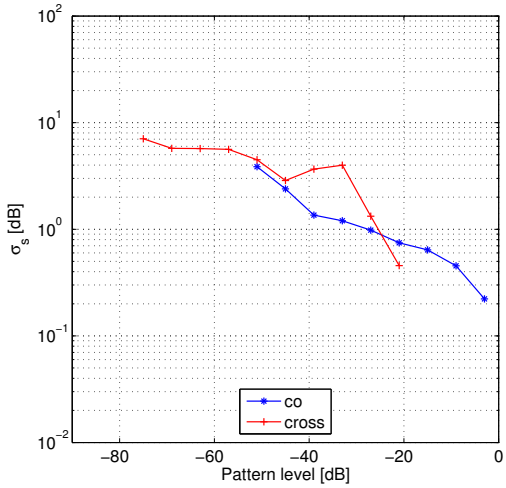

Figure 6.51 Standard deviation σ_s of the Logarithmic difference in each ±3 dB interval.

The information contained in this document should be used only for the scope of the contract for which this document is prepared.

6.3.5.5 Comparison of SES Measurement to Reference Pattern 1

The results from a comparison of the SES spherical near-field measurement and Reference Pattern 1 are presented here. SES is one of the patterns that were used in the definition of Reference Pattern 1. The results are presented without comments and observations. However, the results of all comparisons with Reference pattern 1 are summarized in Section 6.3.5.7.

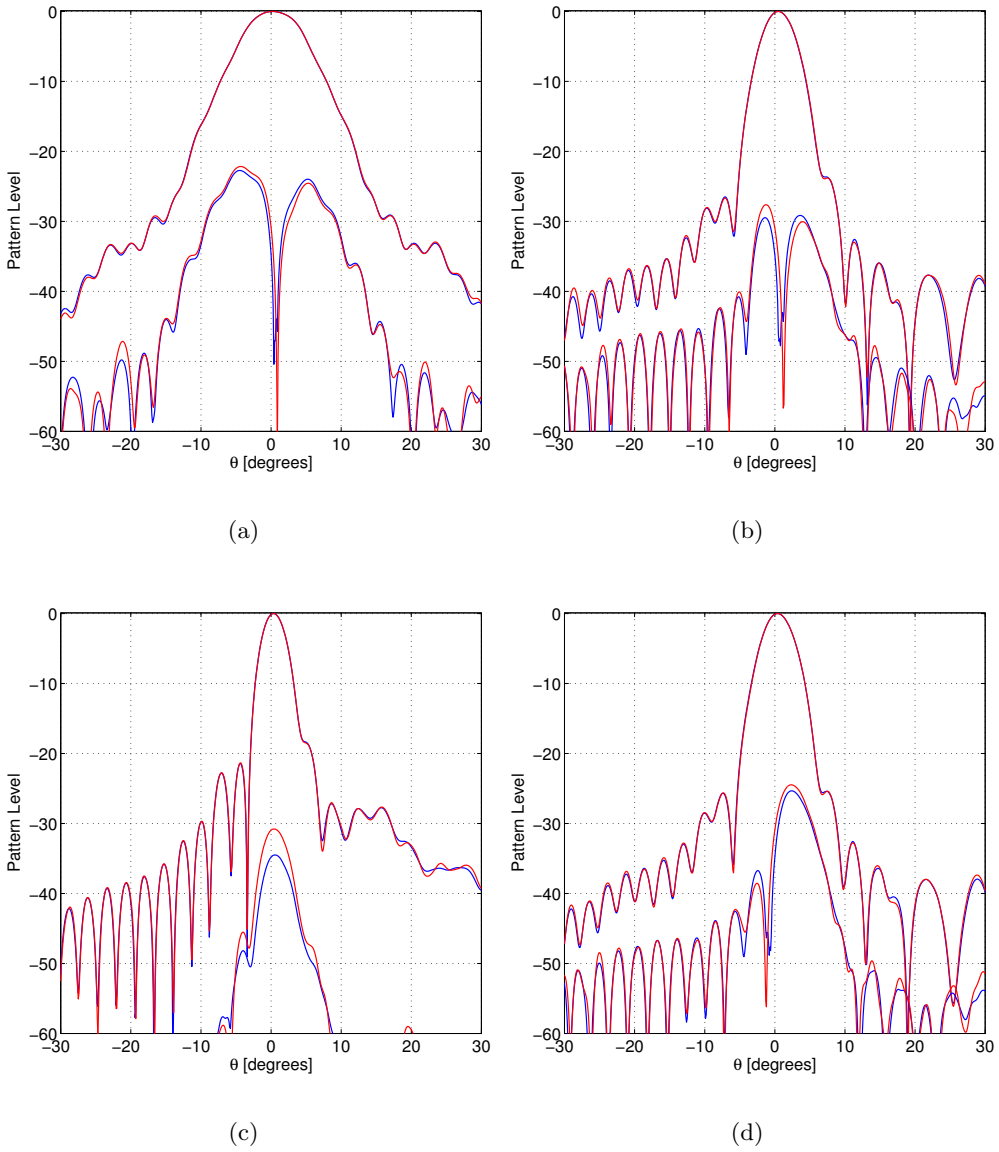

(a) (b)

(c) (d)

Figure 6.52 The co- and cross-polar patterns for the REF1 and SES patterns. In (a), (b), (c), and (d) the $\phi = 0°$, $\phi = 45°$, $\phi = 90°$, and $\phi = 135°$ cuts are shown, respectively. The blue graph shows the REF1 pattern and the red graph shows the SES pattern.

The information contained in this document should be used only for the scope of the contract for which this document is prepared.

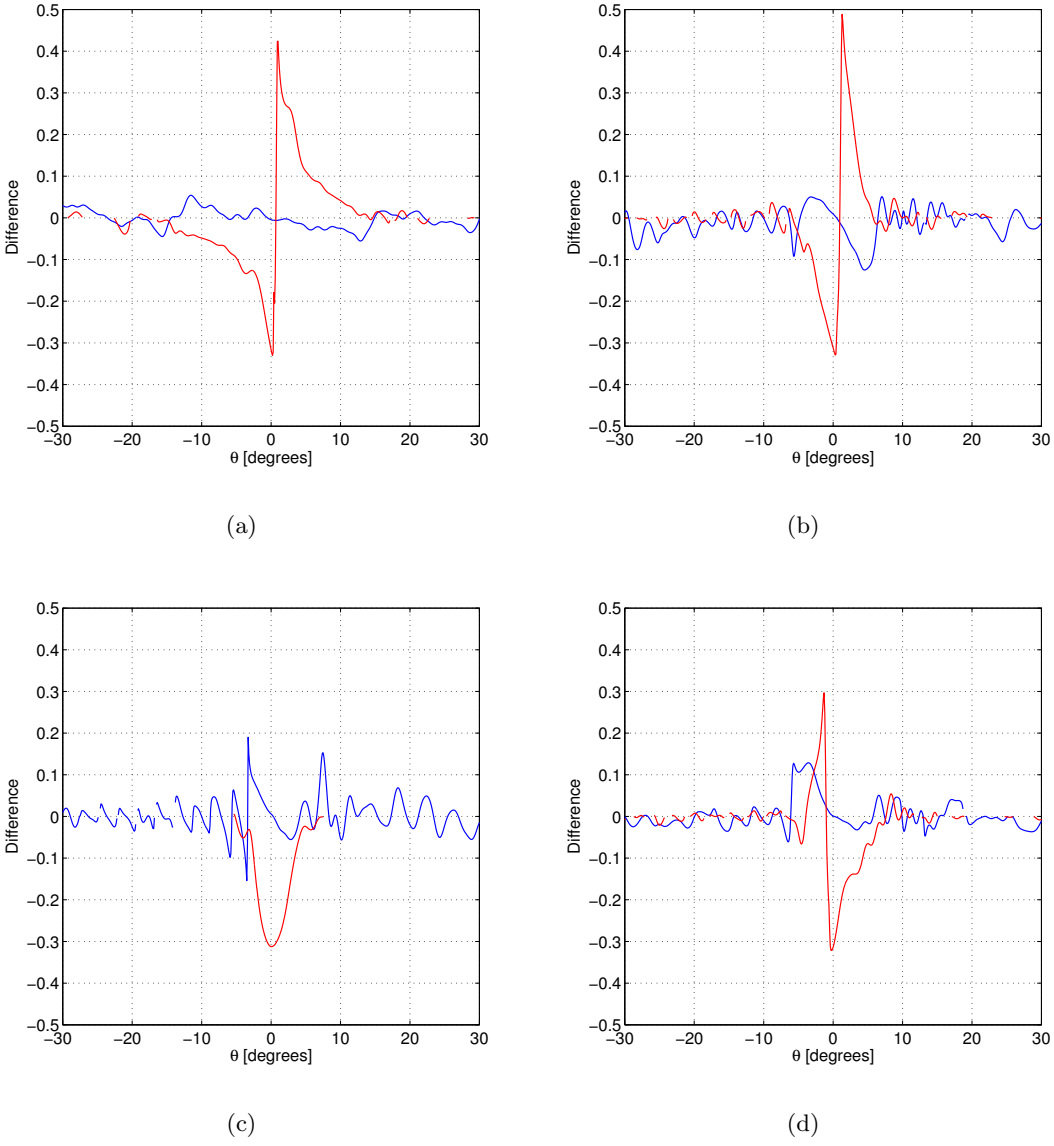

Figure 6.53 The Weighted logarithmic difference for the REF1 and SES patterns. In (a), (b), (c), and (d) the difference in the $\phi = 0°$, $\phi = 45°$, $\phi = 90°$, and $\phi = 135°$ cuts are shown, respectively. The blue graph shows the difference for the co-polar component and the red graph shows the difference for the cross-polar component.

The information contained in this document should be used only for the scope of the contract for which this document is prepared.

	Mean	STD
co-polar ($\theta \leq 30°$)	-0.003	0.034
cross-polar ($\theta \leq 30°$)	-0.019	0.108
co-polar ($\theta \leq 180°$)	0.001	0.023
cross-polar ($\theta \leq 180°$)	-0.004	0.057

Table 6.12 Statistical data for the Weighted logarithmic difference between REF1 and SES.

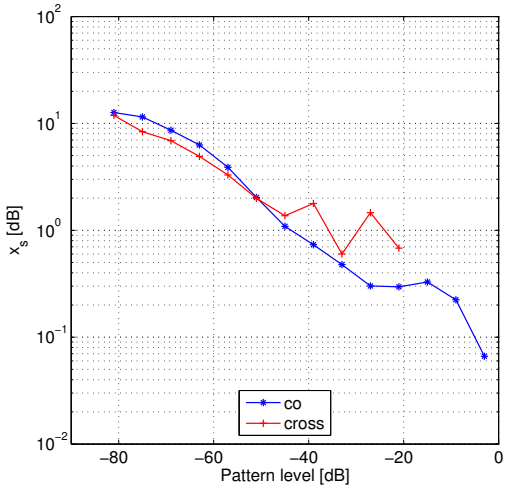

Figure 6.54 Limit value x_s of the Logarithmic difference for the CDF $F(\Delta_i \leq x_s) = 0.9$ in each ±3 dB interval.

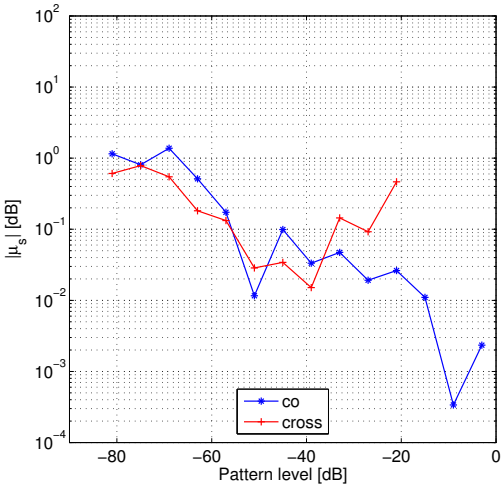

Figure 6.55 Absolute value of the mean $|\mu_s|$ of the Logarithmic difference in each ±3 dB interval.

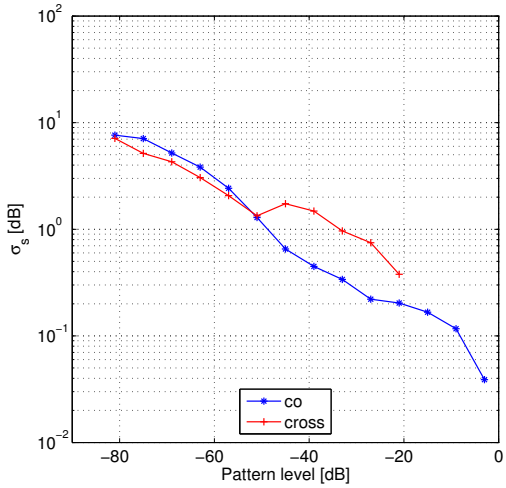

Figure 6.56 Standard deviation σ_s of the Logarithmic difference in each ±3 dB interval.

The information contained in this document should be used only for the scope of the contract for which this document is prepared.

6.3.5.6 Comparison of UPC Measurement to Reference Pattern 1

The results from a comparison of the UPC spherical near-field measurement and Reference Pattern 1 are presented here. The results are presented without comments and observations. However, the results of all comparisons with Reference pattern 1 are summarized in Section 6.3.5.7.

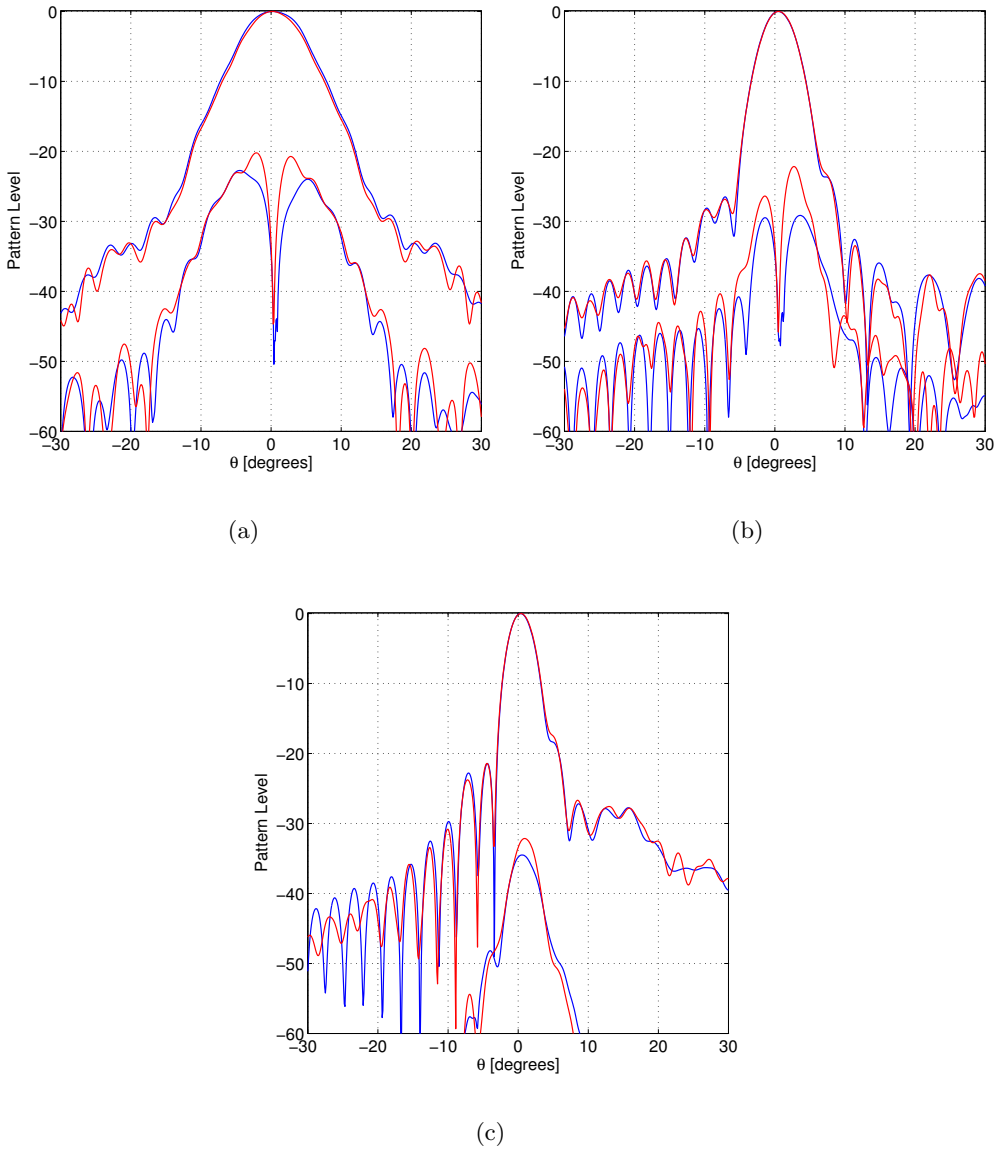

(a) (b)

(c)

Figure 6.57 The co- and cross-polar patterns for the REF1 and UPC patterns. In (a), (b), and (c) the $\phi = 0°$, $\phi = 45°$, and $\phi = 90°$ cuts are shown, respectively. The blue graph shows the REF1 pattern and the red graph shows the UPC pattern.

The information contained in this document should be used only for the scope of the contract for which this document is prepared.

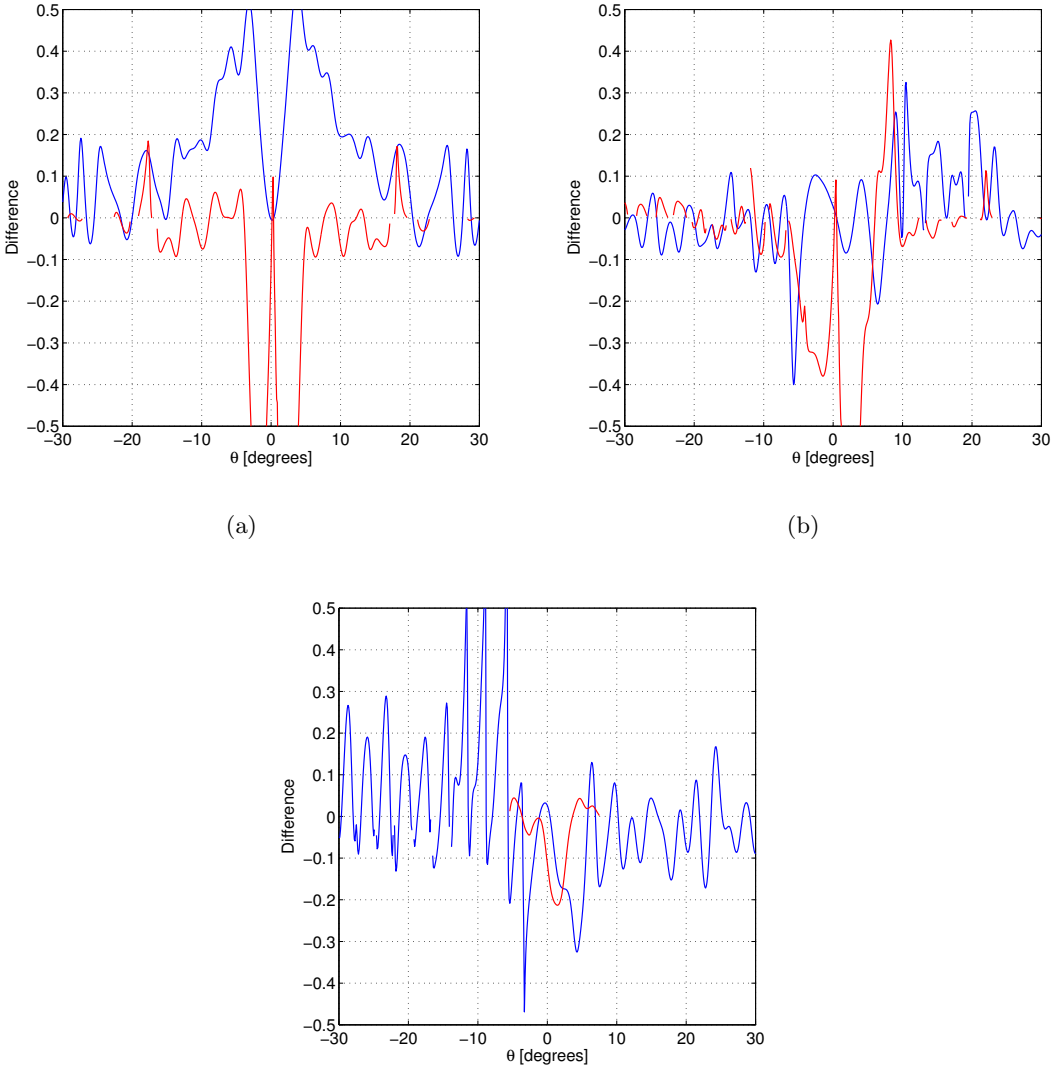

(a) (b)

(c)

Figure 6.58 The Weighted logarithmic difference for the REF1 and UPC patterns. In (a), (b), and (c) the difference in the $\phi = 0°$, $\phi = 45°$, and $\phi = 90°$ cuts are shown, respectively. The blue graph shows the difference for the co-polar component and the red graph shows the difference for the cross-polar component.

The information contained in this document should be used only for the scope of the contract for which this document is prepared.

	Mean	STD
co-polar ($\theta \leq 30°$)	0.058	0.155
cross-polar ($\theta \leq 30°$)	-0.097	0.232

Table 6.13 Statistical data for the Weighted logarithmic difference between REF1 and UPC.

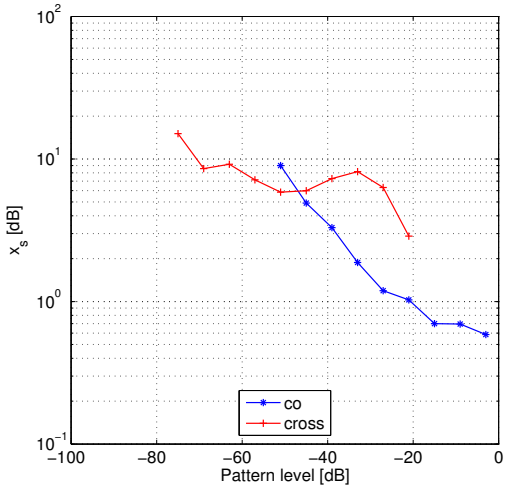

Figure 6.59 Limit value x_s of the Logarithmic difference for the CDF $F(\Delta_i \leq x_s) = 0.9$ in each ±3 dB interval.

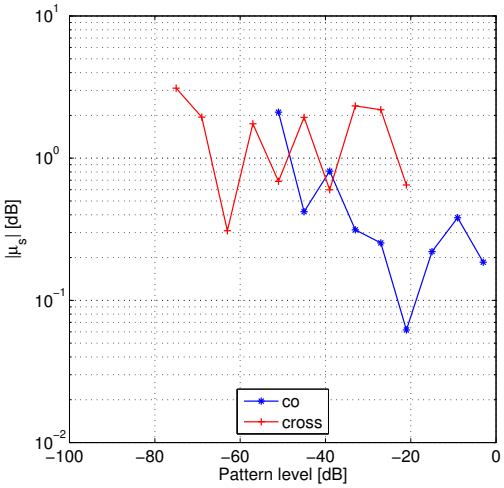

Figure 6.60 Absolute value of the mean $|\mu_s|$ of the Logarithmic difference in each ±3 dB interval.

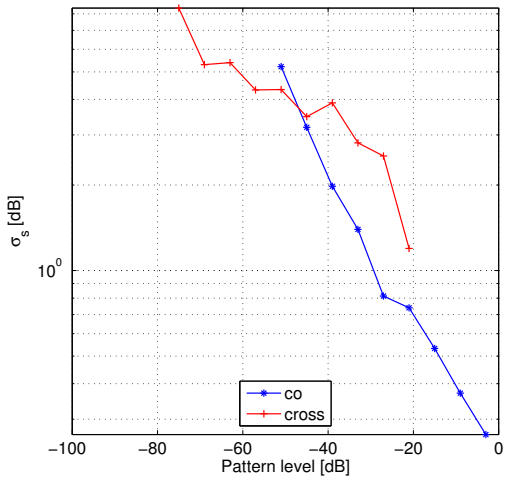

Figure 6.61 Standard deviation σ_s of the Logarithmic difference in each ±3 dB interval.

The information contained in this document should be used only for the scope of the contract for which this document is prepared.

6.3.5.7 Results of Comparisons to Reference Pattern 1

The result of the comparisons to Reference Pattern 1 can be characterized by the mean and standard deviation which has been calculated for the Weighted logarithmic difference in each of the comparisons. For each comparison the values of these which was found for the co-polar component are listed in Table 6.14. These values can be used to perform a benchmarking of the participating facilities based on Reference Pattern 1.

	DTU1	DTU2	UPM1	UPM2	SES	UPC
Mean	0.011	0.007	-0.004	0.000	-0.003	0.058
STD	0.037	0.045	0.058	0.131	0.034	0.155

Table 6.14 The calculated mean and standard deviation for the Weighted logarithmic difference of the co-polar component in the $\theta \leq 30^\circ$ interval.

The mean of the difference, which is found for the individual facilities is noted to be generally very low when considering the values presented in Table 6.14, where only the mean difference found for UPC stands out by being relatively large. This noticeable difference of the UPC measurement is also present in the standard deviation and can be attributed to the fact that the UPC measurement data has not been probe corrected. The spherical near-field facilities DTU1, DTU2, UPM1, and SES all perform very well in this comparison, while it is seen that the planar near-field measurement has a high standard deviation. While the spherical near-field facilities could be expected to perform well, when compared to a planar near-field measurement, the observed result could also be due to the fact that Reference Pattern 1 was constructed from the spherical near-field patterns DTU2, UPM1, and SES.

The information contained in this document should be used only for the scope of the contract for which this document is prepared.

6.3.6 Comparison of Measurements to Common Reference Pattern 2

In order to evaluate the performance of the participating facilities the measured patterns from these are compared to a reference pattern. Reference pattern 2 (REF2), which was defined in Section 6.2.1, is constructed in the electrical coordinate system from the DTU2, UPM1, UPM2, and FTRD patterns.

In this investigation the reference pattern is compared to: DTU1, DTU2, UPM1, UPM2, and FTRD.

The information contained in this document should be used only for the scope of the contract for which this document is prepared.

6.3.6.1 Comparison of DTU1 Measurement to Reference Pattern 2

The results from a comparison of the DTU1 spherical near-field measurement and Reference Pattern 2 are presented here. The results are presented without comments and observations. However, the results of all comparisons with Reference pattern 2 are summarized in Section 6.3.6.6.

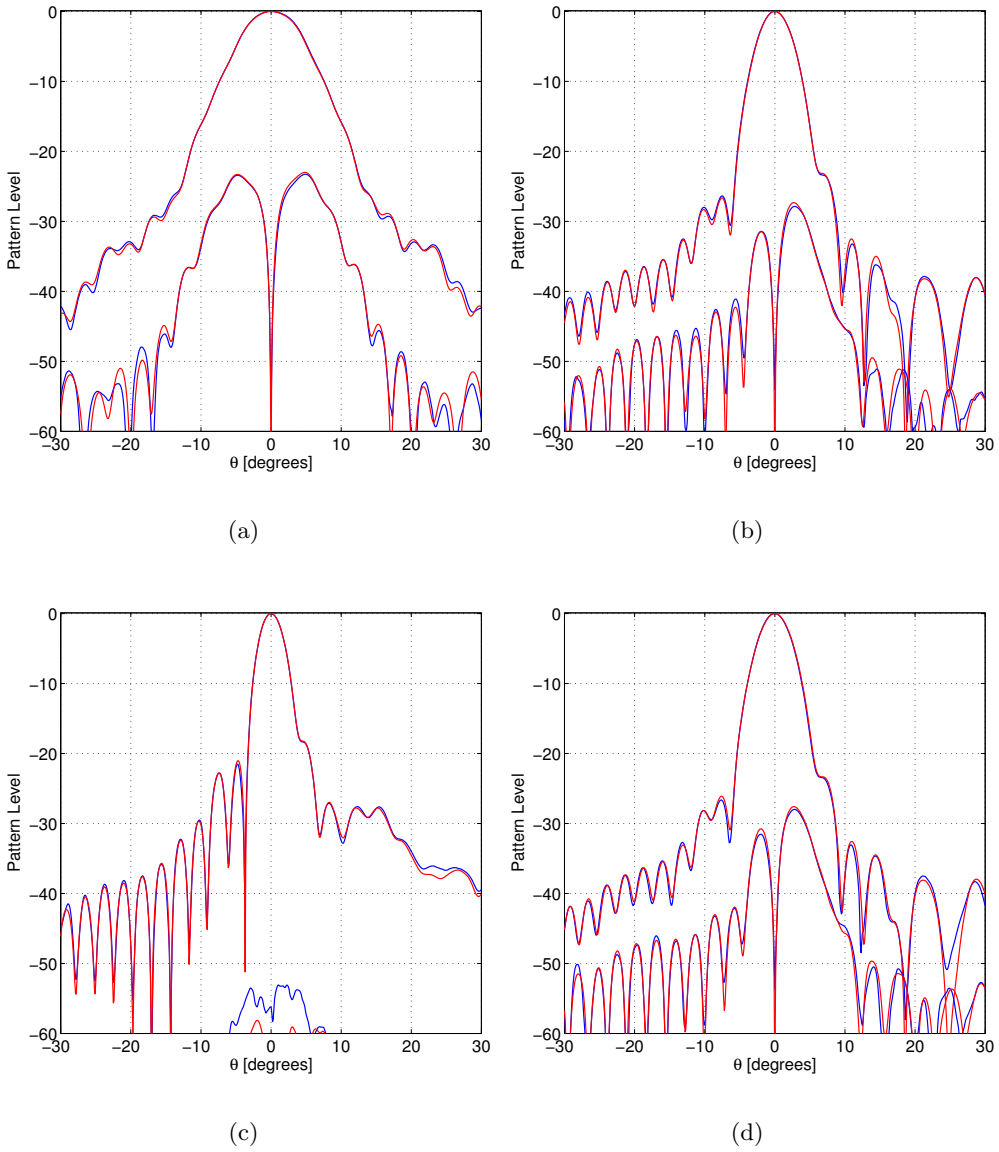

(a) (b)

(c) (d)

Figure 6.62 The co- and cross-polar patterns for the REF2 and DTU1 patterns. In (a), (b), (c), and (d) the $\phi = 0°$, $\phi = 45°$, $\phi = 90°$, and $\phi = 135°$ cuts are shown, respectively. The blue graph shows the REF2 pattern and the red graph shows the DTU1 pattern.

The information contained in this document should be used only for the scope of the contract for which this document is prepared.

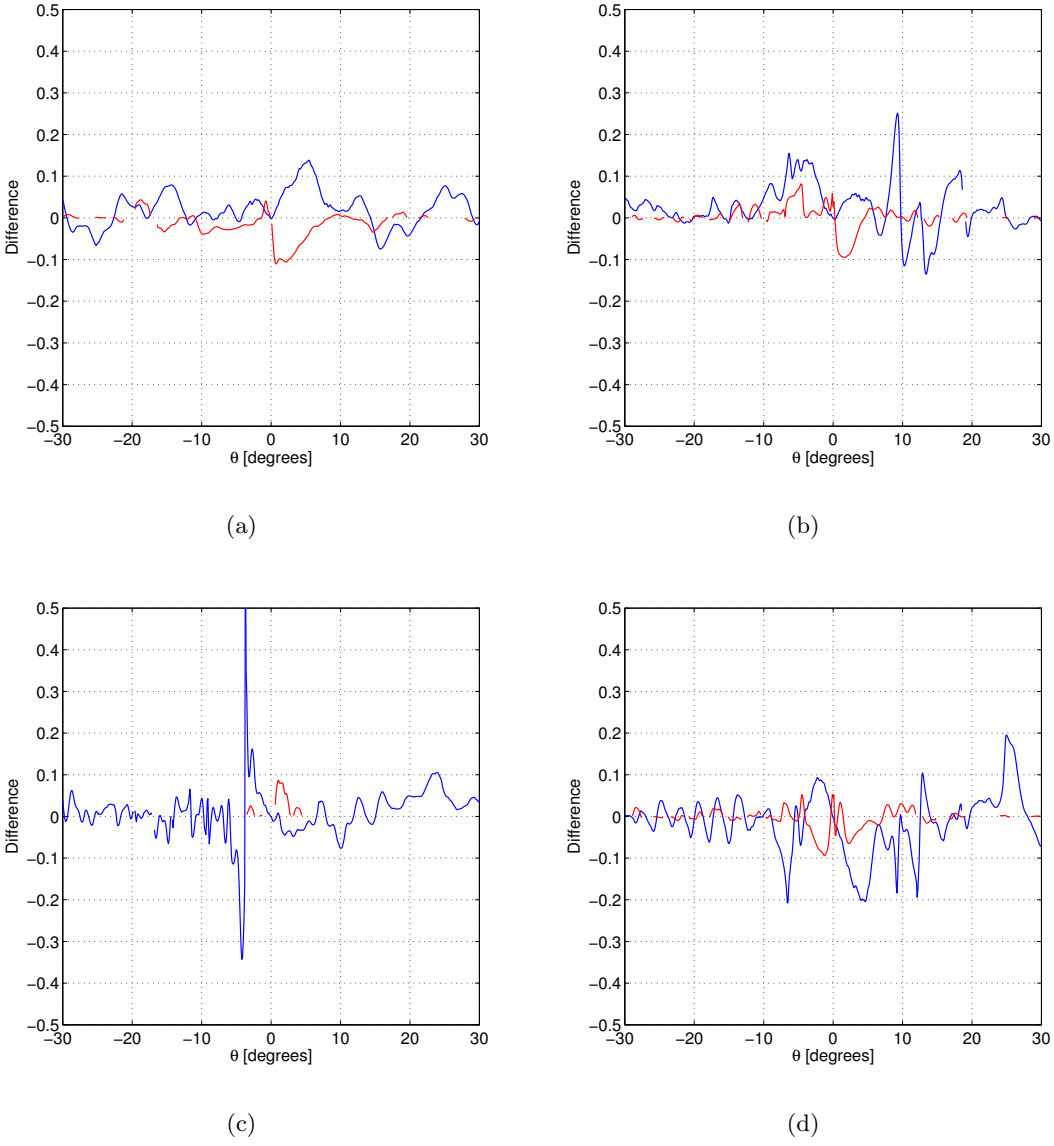

Figure 6.63 The Weighted logarithmic difference for the REF2 and DTU1 patterns. In (a), (b), (c), and (d) the difference in the $\phi = 0°$, $\phi = 45°$, $\phi = 90°$, and $\phi = 135°$ cuts are shown, respectively. The blue graph shows the difference for the co-polar component and the red graph shows the difference for the cross-polar component.

The information contained in this document should be used only for the scope of the contract for which this document is prepared.

	Mean	STD
co-polar ($\theta \leq 30°$)	0.010	0.061
cross-polar ($\theta \leq 30°$)	-0.005	0.030

Table 6.15 Statistical data for the Weighted logarithmic difference between REF2 and DTU1.

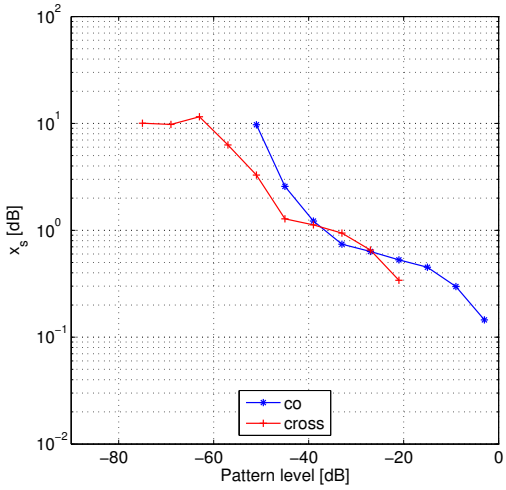

Figure 6.64 Limit value x_s of the Logarithmic difference for the CDF $F(\Delta_i \leq x_s) = 0.9$ in each ±3 dB interval.

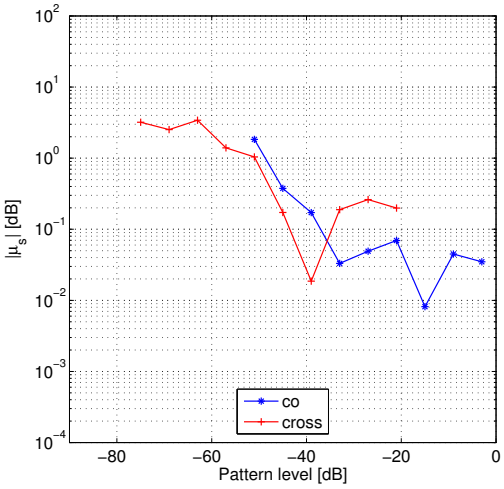

Figure 6.65 Absolute value of the mean $|\mu_s|$ of the Logarithmic difference in each ±3 dB interval.

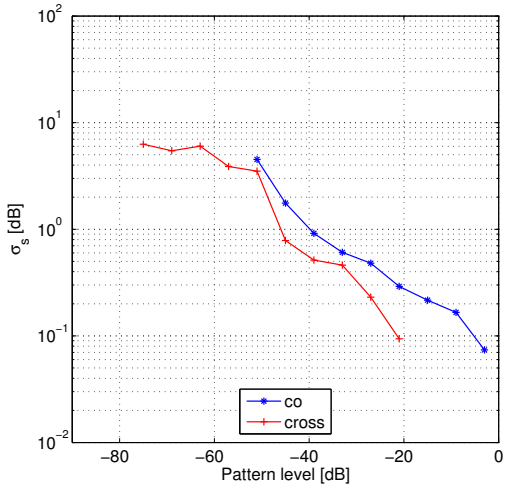

Figure 6.66 Standard deviation σ_s of the Logarithmic difference in each ±3 dB interval.

The information contained in this document should be used only for the scope of the contract for which this document is prepared.

6.3.6.2 Comparison of DTU2 Measurement to Reference Pattern 2

The results from a comparison of the DTU2 spherical near-field measurement and Reference Pattern 2 are presented here. DTU2 is one of the patterns that were used in the definition of Reference Pattern 2. The results are presented without comments and observations. However, the results of all comparisons with Reference pattern 2 are summarized in Section 6.3.6.6.

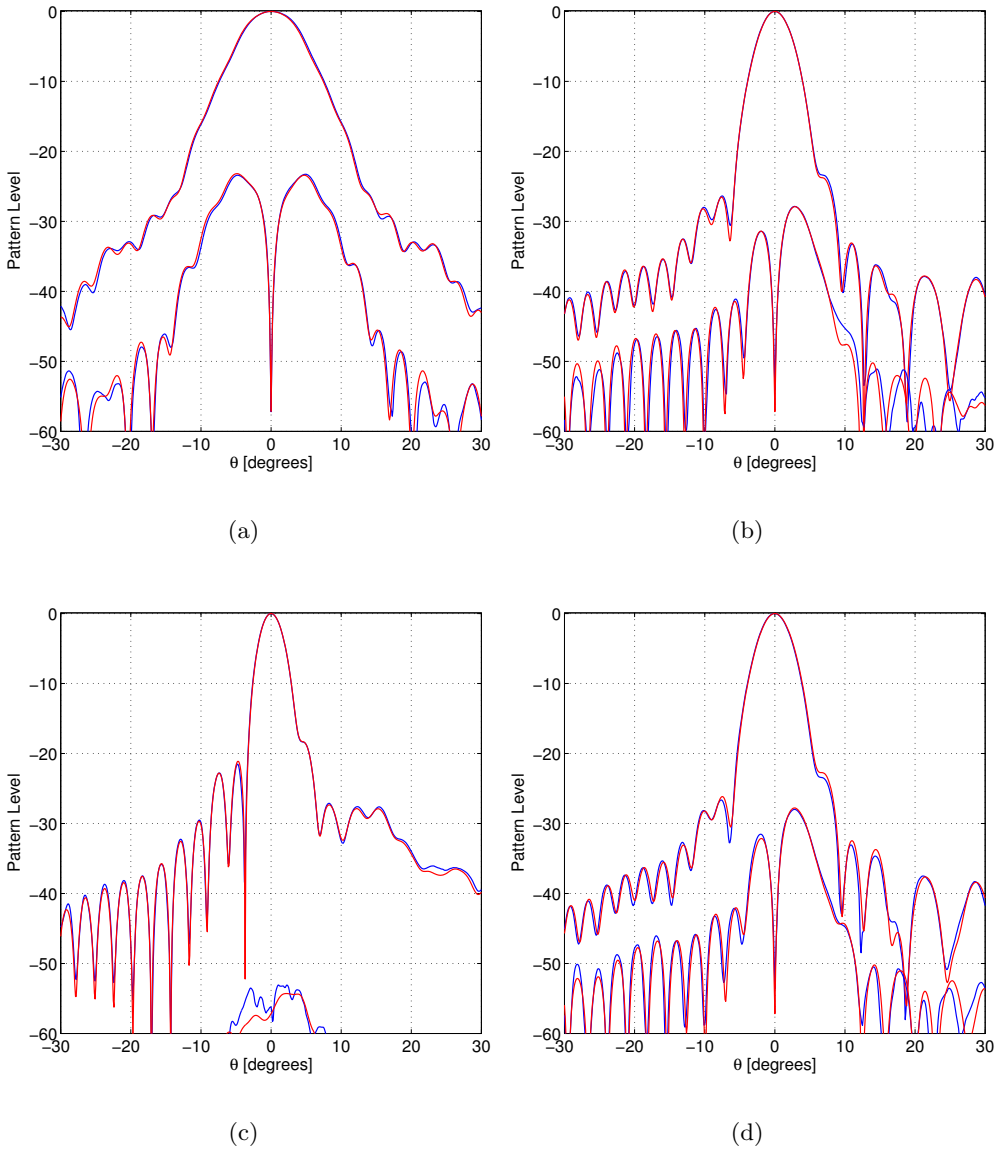

(a) (b)

(c) (d)

Figure 6.67 The co- and cross-polar patterns for the REF2 and DTU2 patterns. In (a), (b), (c), and (d) the $\phi = 0°$, $\phi = 45°$, $\phi = 90°$, and $\phi = 135°$ cuts are shown, respectively. The blue graph shows the REF2 pattern and the red graph shows the DTU2 pattern.

The information contained in this document should be used only for the scope of the contract for which this document is prepared.

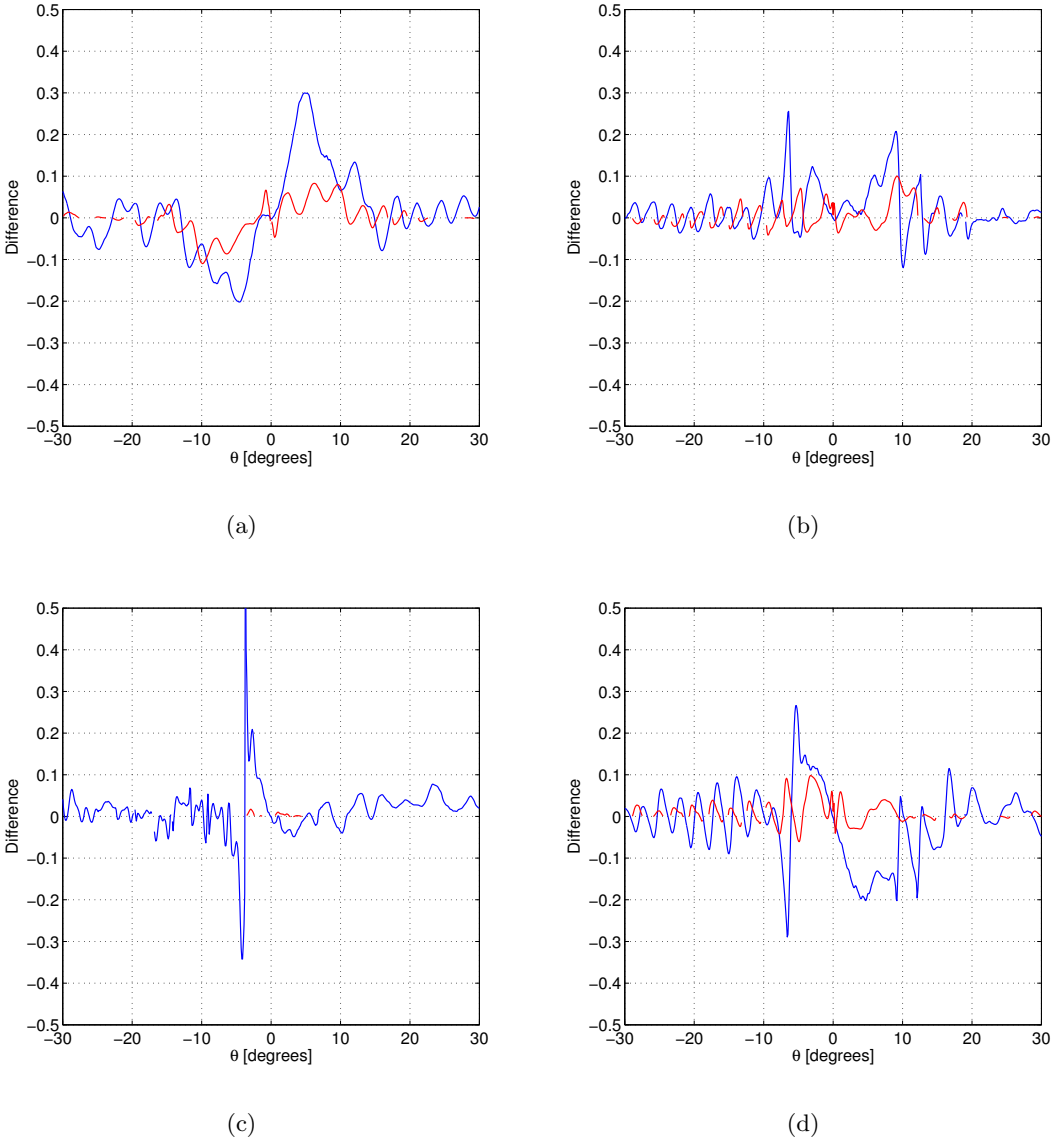

Figure 6.68 The Weighted logarithmic difference for the REF2 and DTU2 patterns. In (a), (b), (c), and (d) the difference in the $\phi = 0°$, $\phi = 45°$, $\phi = 90°$, and $\phi = 135°$ cuts are shown, respectively. The blue graph shows the difference for the co-polar component and the red graph shows the difference for the cross-polar component.

The information contained in this document should be used only for the scope of the contract for which this document is prepared.

	Mean	STD
co-polar ($\theta \leq 30°$)	0.007	0.079
cross-polar ($\theta \leq 30°$)	0.006	0.033

Table 6.16 Statistical data for the Weighted logarithmic difference between REF2 and DTU2.

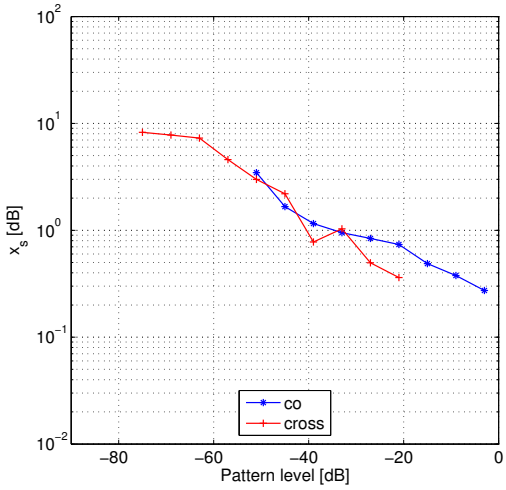

Figure 6.69 Limit value x_s of the Logarithmic difference for the CDF $F(\Delta_i \leq x_s) = 0.9$ in each ±3 dB interval.

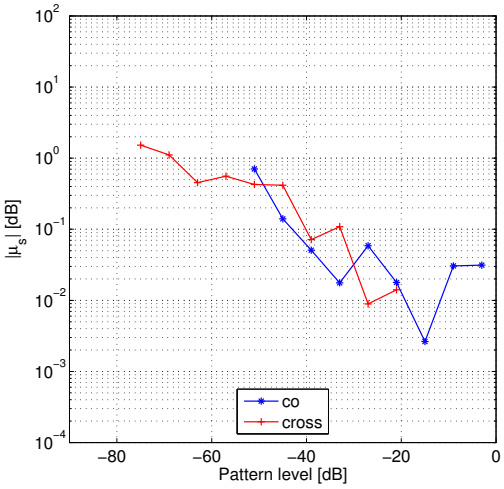

Figure 6.70 Absolute value of the mean $|\mu_s|$ of the Logarithmic difference in each ±3 dB interval.

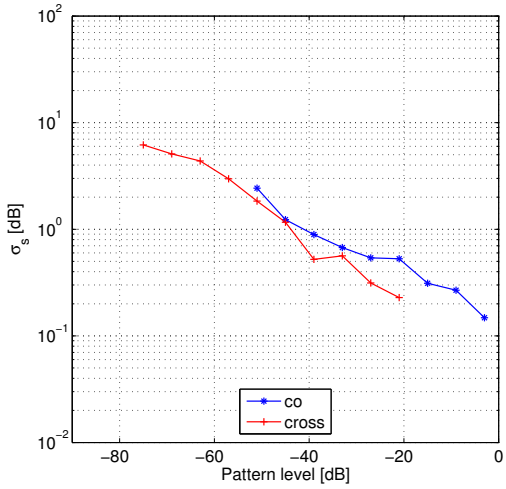

Figure 6.71 Standard deviation σ_s of the Logarithmic difference in each ±3 dB interval.

The information contained in this document should be used only for the scope of the contract for which this document is prepared.

6.3.6.3 Comparison of UPM1 Measurement to Reference Pattern 2

The results from a comparison of the UPM1 spherical near-field measurement and Reference Pattern 2 are presented here. UPM1 is one of the patterns that were used in the definition of Reference Pattern 2. The results are presented without comments and observations. However, the results of all comparisons with Reference pattern 2 are summarized in Section 6.3.6.6.

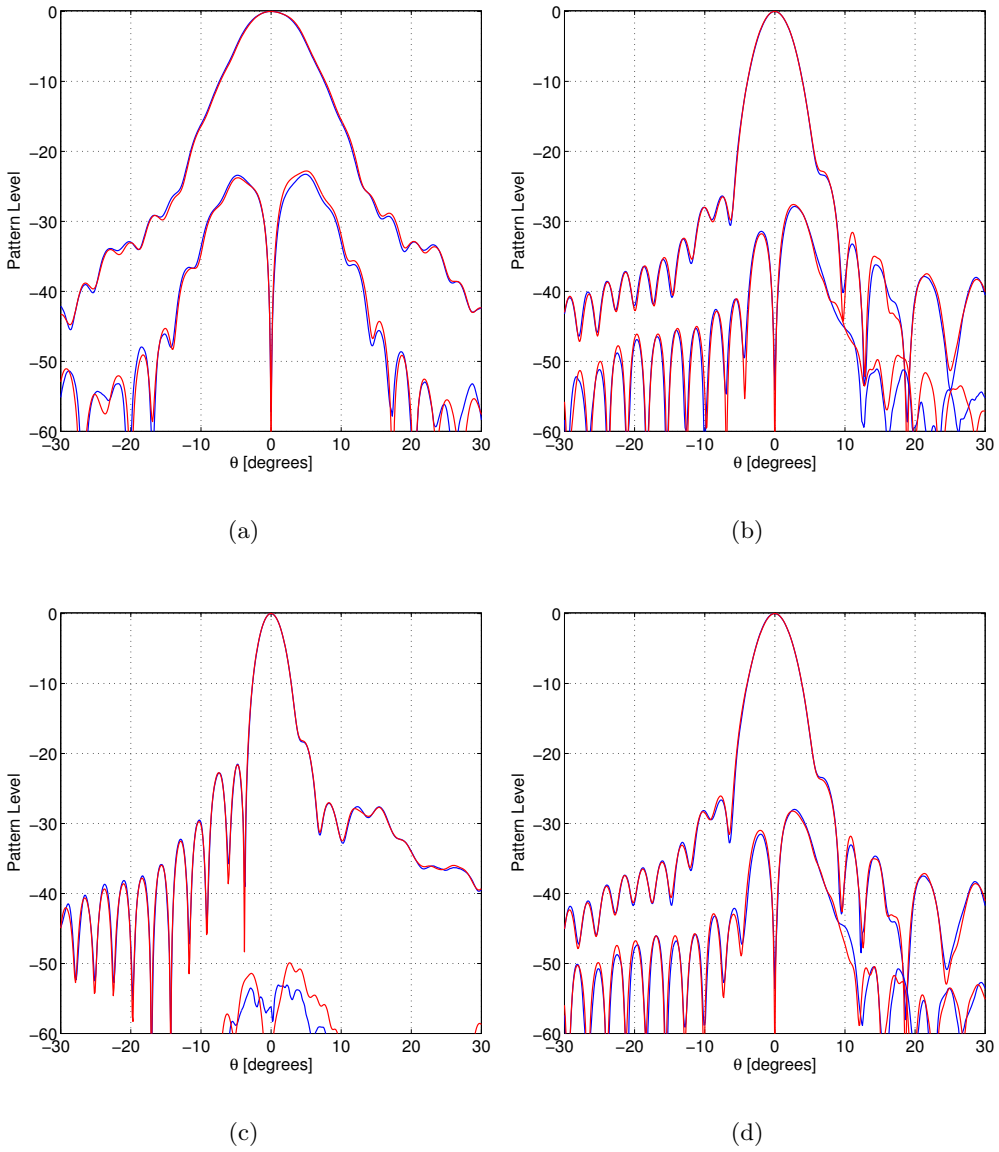

(a) (b)

(c) (d)

Figure 6.72 The co- and cross-polar patterns for the REF2 and UPM1 patterns. In (a), (b), (c), and (d) the $\phi = 0°$, $\phi = 45°$, $\phi = 90°$, and $\phi = 135°$ cuts are shown, respectively. The blue graph shows the REF2 pattern and the red graph shows the UPM1 pattern.

The information contained in this document should be used only for the scope of the contract for which this document is prepared.

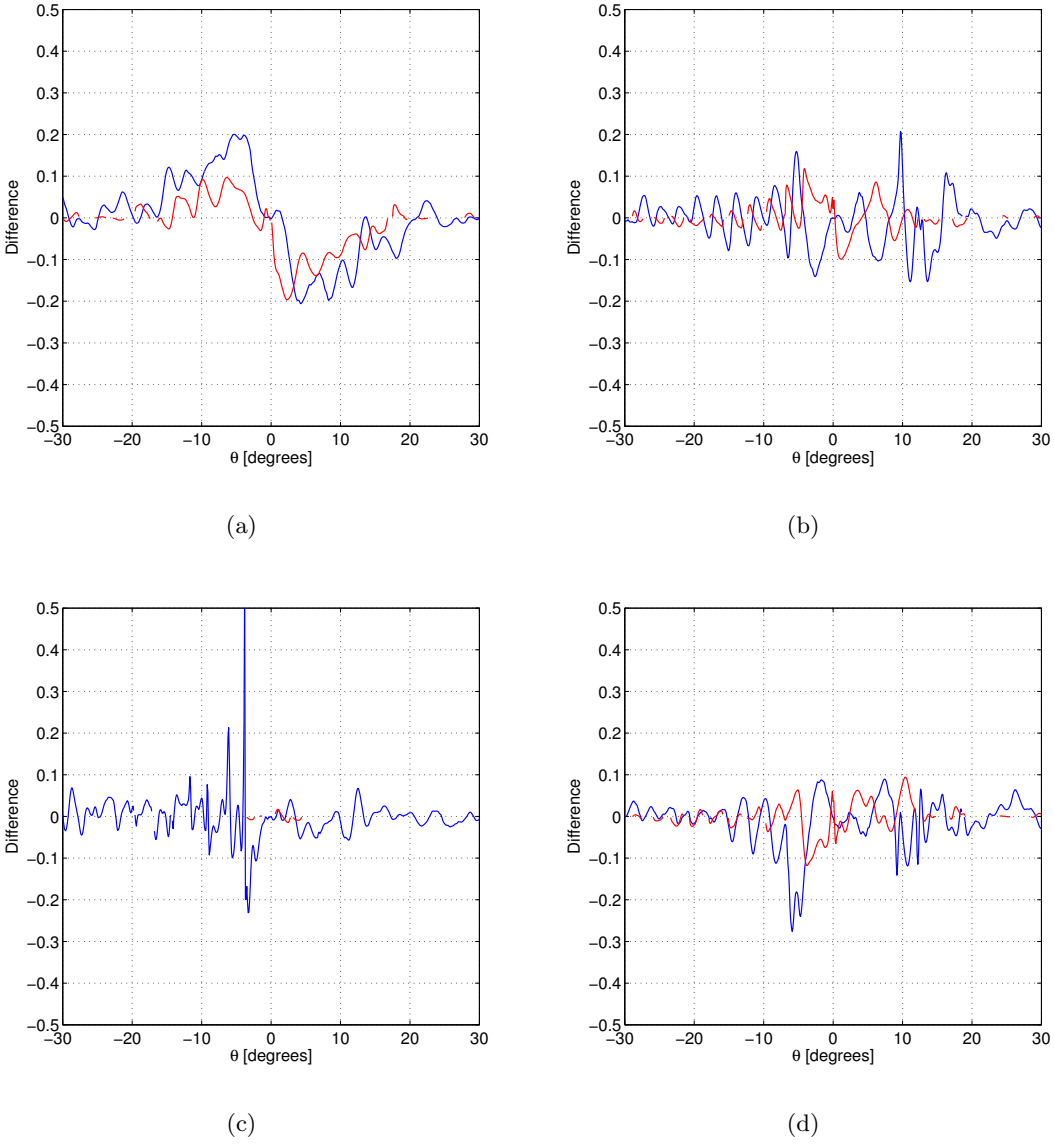

Figure 6.73 The Weighted logarithmic difference for the REF2 and UPM1 patterns. In (a), (b), (c), and (d) the difference in the $\phi = 0°$, $\phi = 45°$, $\phi = 90°$, and $\phi = 135°$ cuts are shown, respectively. The blue graph shows the difference for the co-polar component and the red graph shows the difference for the cross-polar component.

The information contained in this document should be used only for the scope of the contract for which this document is prepared.

	Mean	STD
co-polar ($\theta \leq 30°$)	-0.005	0.067
cross-polar ($\theta \leq 30°$)	-0.006	0.049

Table 6.17 Statistical data for the Weighted logarithmic difference between REF2 and UPM1.

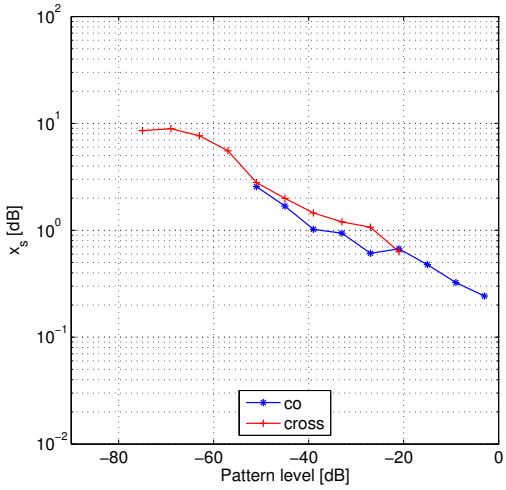

Figure 6.74 Limit value x_s of the Logarithmic difference for the CDF $F(\Delta_i \leq x_s) = 0.9$ in each ±3 dB interval.

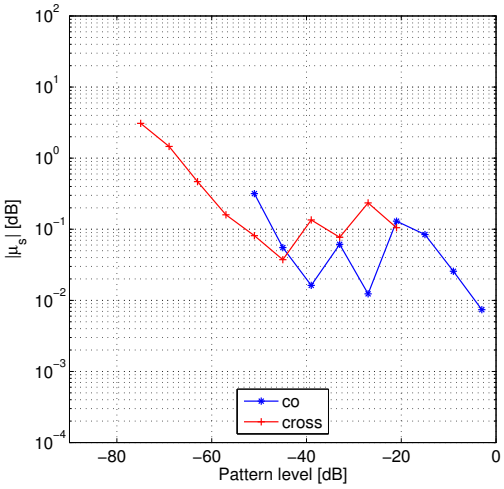

Figure 6.75 Absolute value of the mean $|\mu_s|$ of the Logarithmic difference in each ±3 dB interval.

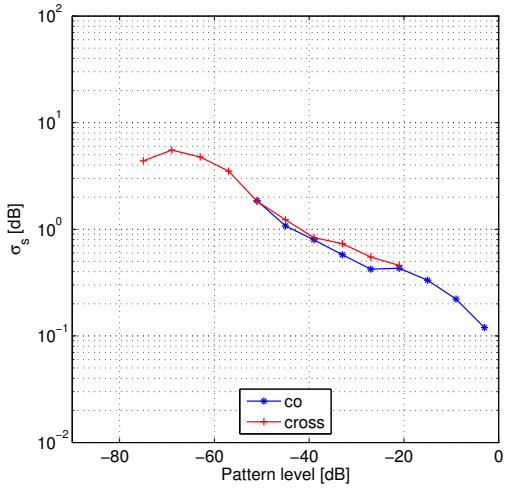

Figure 6.76 Standard deviation σ_s of the Logarithmic difference in each ±3 dB interval.

The information contained in this document should be used only for the scope of the contract for which this document is prepared.

6.3.6.4 Comparison of UPM2 Measurement to Reference Pattern 2

The results from a comparison of the UPM2 planar near-field measurement and Reference Pattern 2 are presented here. UPM2 is one of the patterns that were used in the definition of Reference Pattern 2. The results are presented without comments and observations. However, the results of all comparisons with Reference pattern 2 are summarized in Section 6.3.6.6.

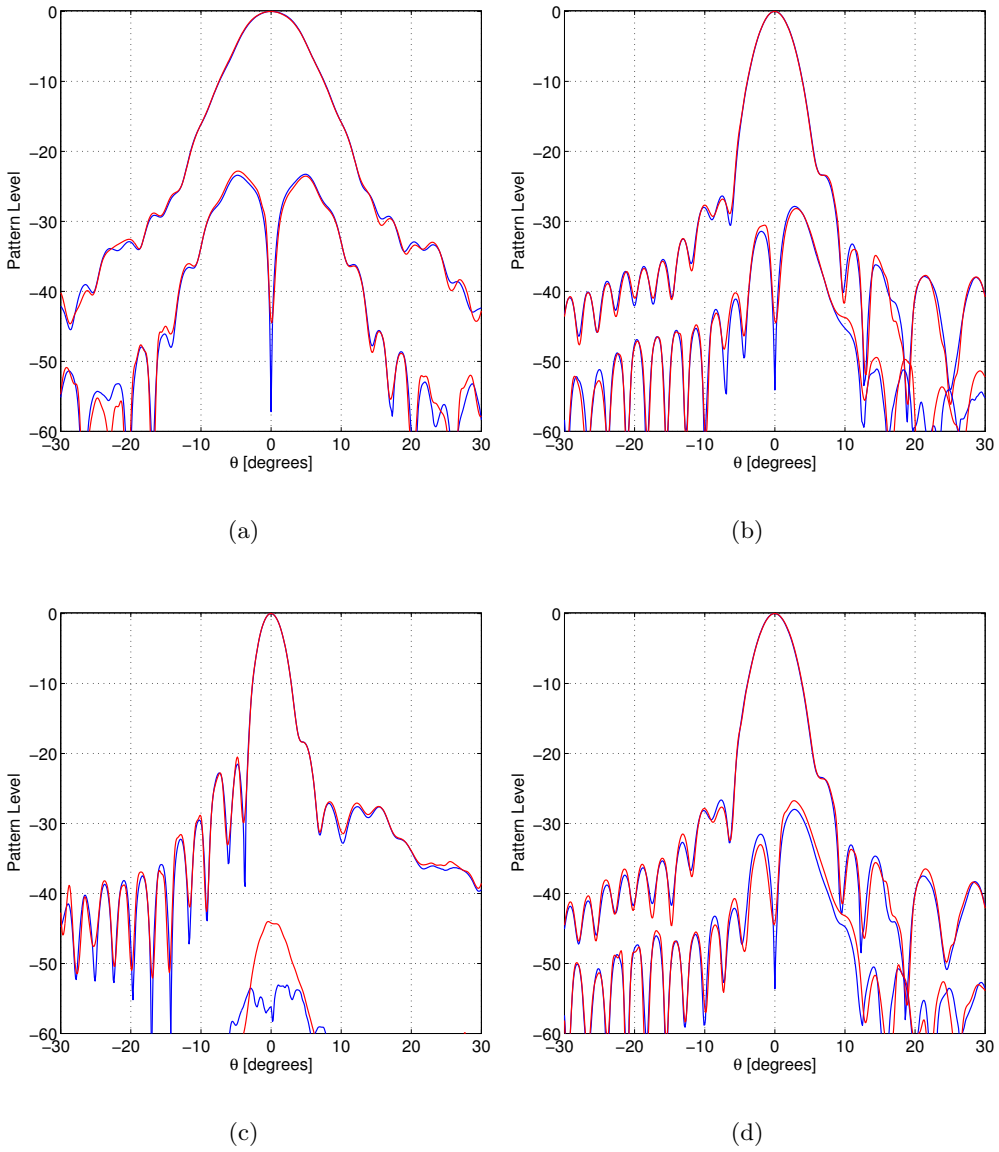

Figure 6.77 The co- and cross-polar patterns for the REF2 and UPM2 patterns. In (a), (b), (c), and (d) the $\phi = 0°$, $\phi = 45°$, $\phi = 90°$, and $\phi = 135°$ cuts are shown, respectively. The blue graph shows the REF2 pattern and the red graph shows the UPM2 pattern.

The information contained in this document should be used only for the scope of the contract for which this document is prepared.

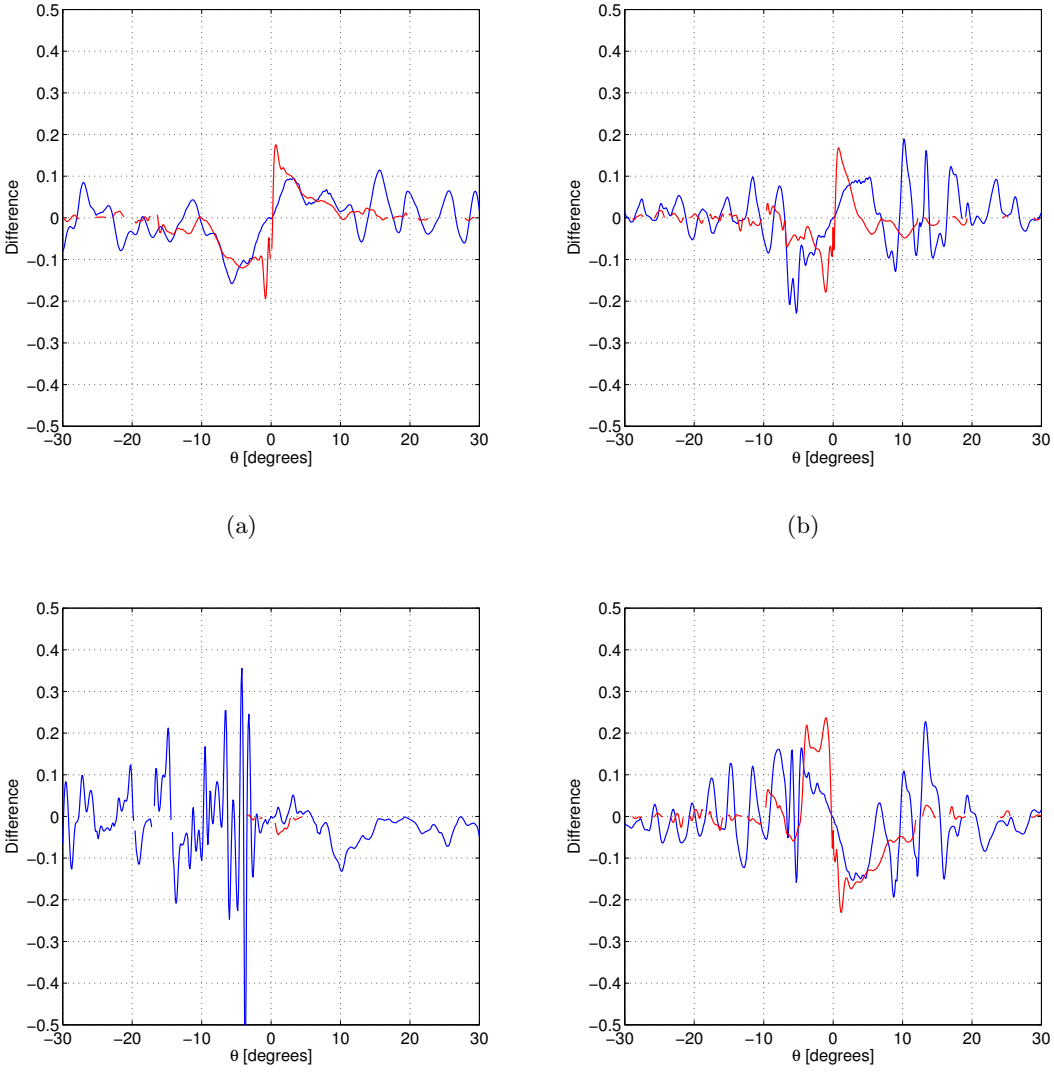

Figure 6.78 The Weighted logarithmic difference for the REF2 and UPM2 patterns. In (a), (b), (c), and (d) the difference in the $\phi = 0°$, $\phi = 45°$, $\phi = 90°$, and $\phi = 135°$ cuts are shown, respectively. The blue graph shows the difference for the co-polar component and the red graph shows the difference for the cross-polar component.

The information contained in this document should be used only for the scope of the contract for which this document is prepared.

	Mean	STD
co-polar ($\theta \leq 30°$)	-0.006	0.069
cross-polar ($\theta \leq 30°$)	-0.010	0.064

Table 6.18 Statistical data for the Weighted logarithmic difference between REF2 and UPM2.

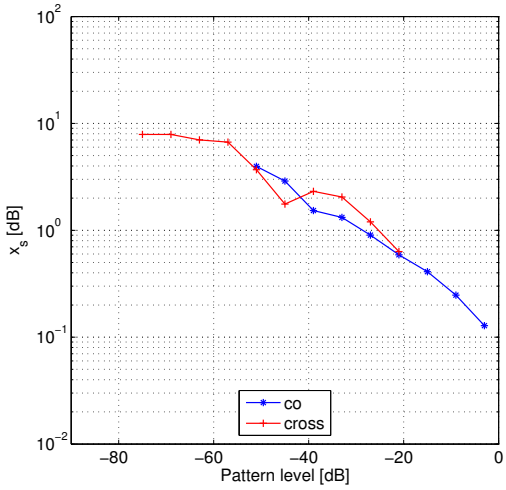

Figure 6.79 Limit value x_s of the Logarithmic difference for the CDF $F(\Delta_i \leq x_s) = 0.9$ in each ±3 dB interval.

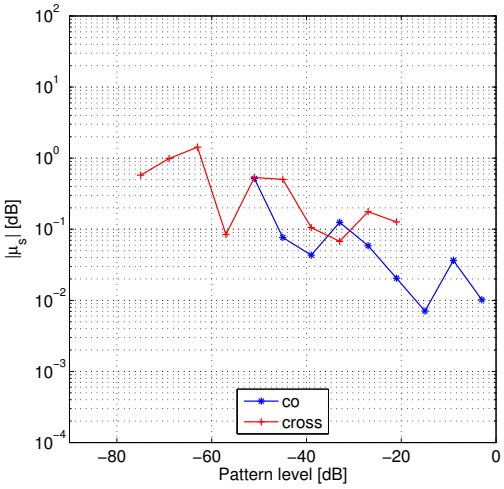

Figure 6.80 Absolute value of the mean $|\mu_s|$ of the Logarithmic difference in each ±3 dB interval.

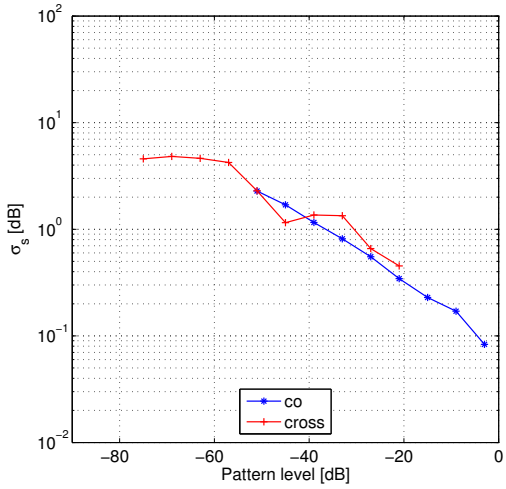

Figure 6.81 Standard deviation σ_s of the Logarithmic difference in each ±3 dB interval.

The information contained in this document should be used only for the scope of the contract for which this document is prepared.

6.3.6.5 Comparison of FTRD Measurement to Reference Pattern 2

The results from a comparison of the FTRD far-field measurement and Reference Pattern 2 are presented here. FTRD is one of the patterns that were used in the definition of Reference Pattern 2. The results are presented without comments and observations. However, the results of all comparisons with Reference pattern 2 are summarized in Section 6.3.6.6.

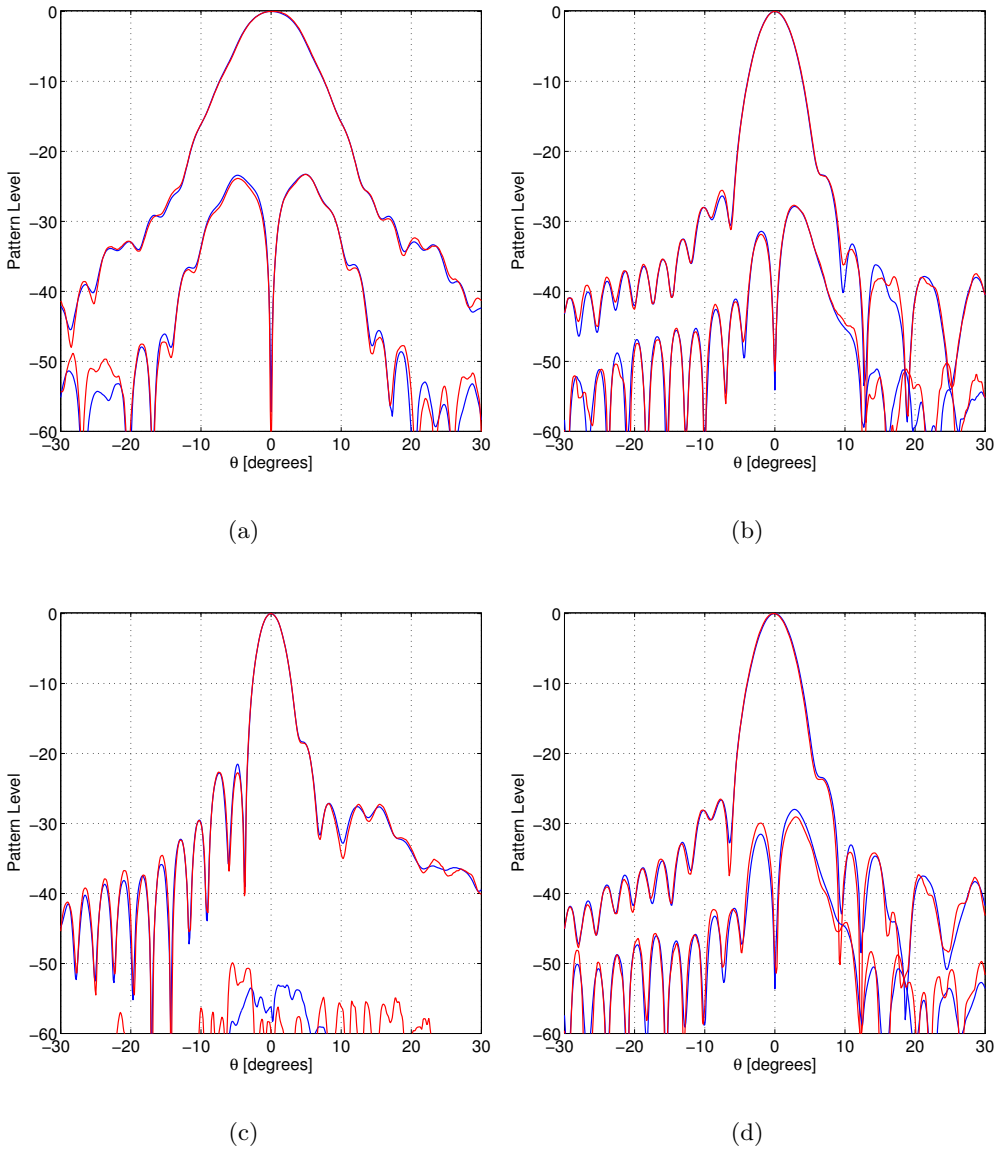

Figure 6.82 The co- and cross-polar patterns for the REF2 and FTRD patterns. In (a), (b), (c), and (d) the $\phi = 0°$, $\phi = 45°$, $\phi = 90°$, and $\phi = 135°$ cuts are shown, respectively. The blue graph shows the REF2 pattern and the red graph shows the FTRD pattern.

The information contained in this document should be used only for the scope of the contract for which this document is prepared.

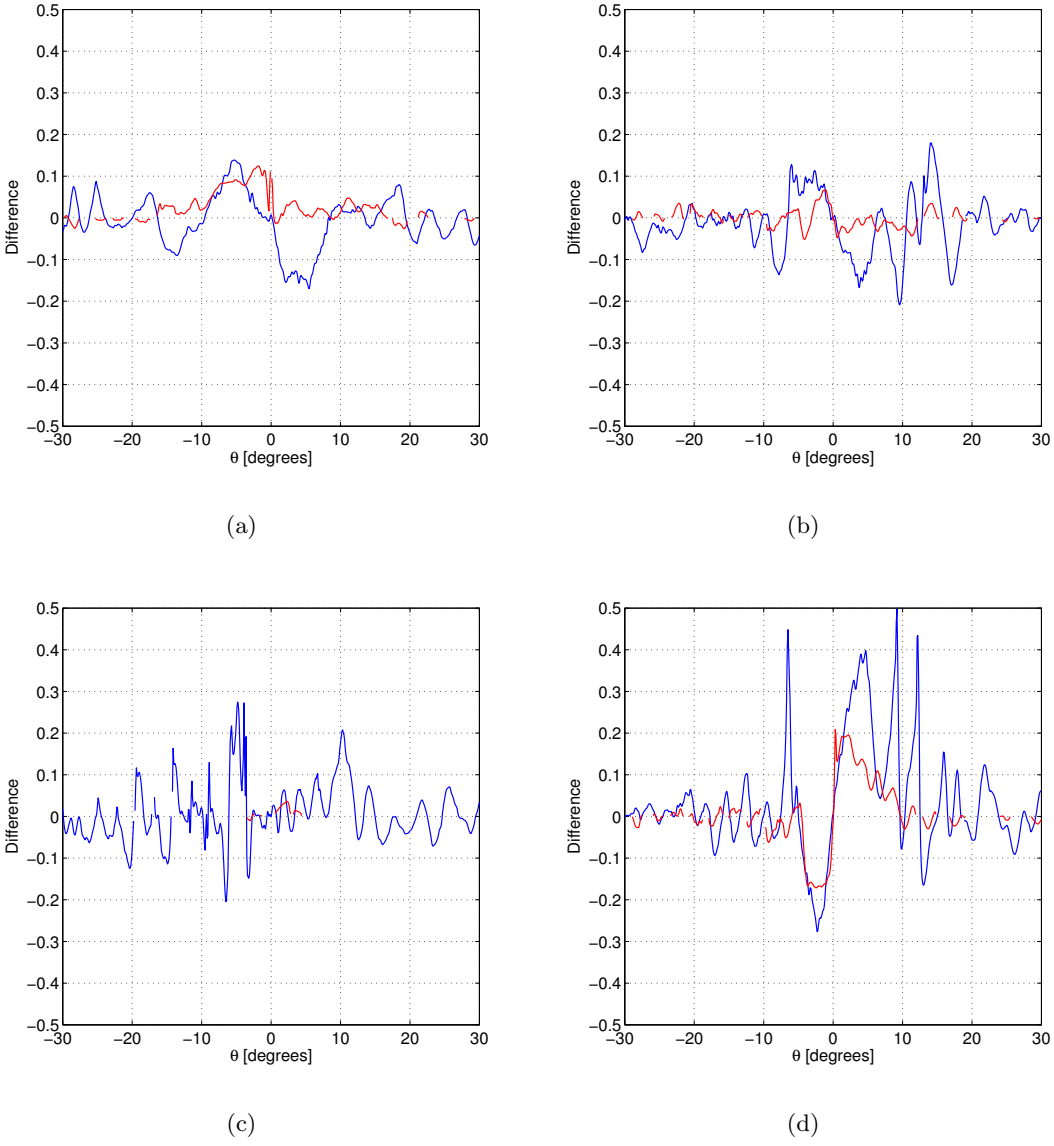

Figure 6.83 The Weighted logarithmic difference for the REF2 and FTRD patterns. In (a), (b), (c), and (d) the difference in the $\phi = 0°$, $\phi = 45°$, $\phi = 90°$, and $\phi = 135°$ cuts are shown, respectively. The blue graph shows the difference for the co-polar component and the red graph shows the difference for the cross-polar component.

The information contained in this document should be used only for the scope of the contract for which this document is prepared.

	Mean	STD
co-polar ($\theta \leq 30°$)	0.004	0.088
cross-polar ($\theta \leq 30°$)	0.011	0.051

Table 6.19 Statistical data for the Weighted logarithmic difference between REF2 and FTRD.

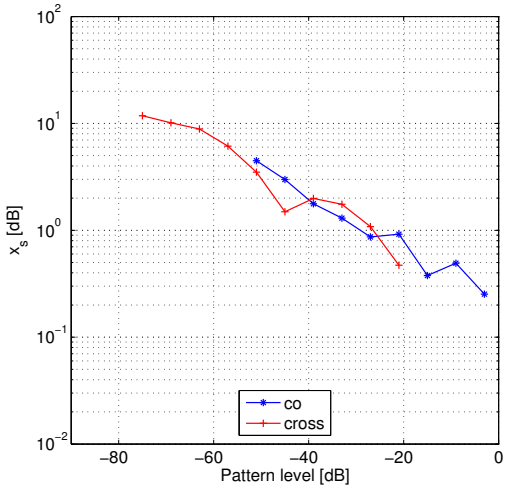

Figure 6.84 Limit value x_s of the Logarithmic difference for the CDF $F(\Delta_i \leq x_s) = 0.9$ in each ±3 dB interval.

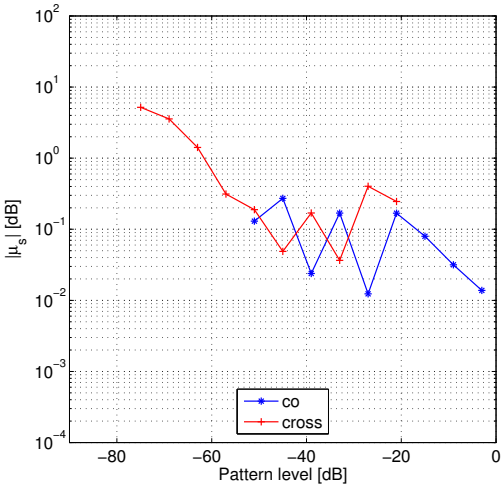

Figure 6.85 Absolute value of the mean $|\mu_s|$ of the Logarithmic difference in each ±3 dB interval.

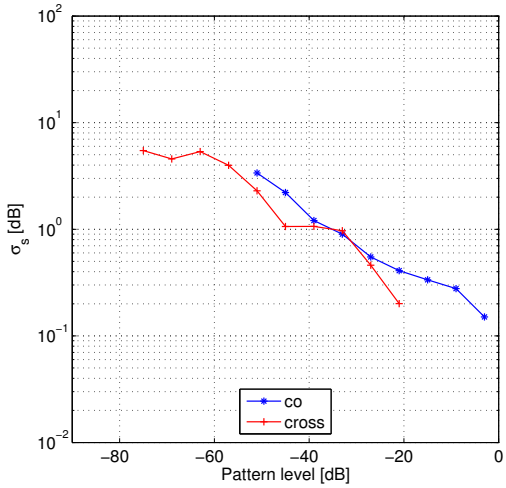

Figure 6.86 Standard deviation σ_s of the Logarithmic difference in each ±3 dB interval.

The information contained in this document should be used only for the scope of the contract for which this document is prepared.

6.3.6.6 Results of Comparisons to Reference Pattern 2

As was done for Reference Pattern 1, the results of the comparisons to Reference Pattern 2 are characterized by the mean and standard deviation, which has been calculated for the Weighted logarithmic difference. For each comparison the values of these, which were found for the co-polar component, are listed in Table 6.20. These values can be used to perform a benchmarking of the participating facilities based on Reference Pattern 2.

	DTU1	DTU2	UPM1	UPM2	FTRD
Mean	0.010	0.007	-0.005	-0.006	0.004
STD	0.061	0.079	0.067	0.069	0.088

Table 6.20 The calculated mean and standard deviation for the Weighted logarithmic difference of the co-polar component in the $\theta \leq 30^\circ$ interval.

Similar to what was found in the comparison with Reference Pattern 1, the mean of the difference for the individual facilities, when using Reference Pattern 2, is found to be very low as well. It is observed that the standard deviations that have been determined for each of the facilities are very similar. This behavior is opposite to what was observed in the comparisons with Reference Pattern 1, where large variations in the obtained standard deviations were observed. In particular it can be noted that the STD for the UPM2 measurement was observed to be high in the comparison with Reference Pattern 1, whereas in the comparison with Reference Pattern 2 it is low.

From a comparison of the results of the comparisons with Reference Pattern 1 and with Reference Pattern 2 it is clear that the results from comparisons with a Reference Pattern are very dependent on the definition of the reference pattern.

The information contained in this document should be used only for the scope of the contract for which this document is prepared.

6.4 Directivity and Gain Comparisons

As a part of the measurements of the VAST12 antenna some of the participating facilities have determined the directivity and the gain. Furthermore, the exact location of the peak of the co-polar pattern has been determined. The results from each facility are listed in Table 6.21.

It is seen that a very good agreement in the determined peak directivities can be observed if the FTRD value is omitted from the comparison. The FTRD directivity has been determined on the basis of only few pattern cuts, and should thus be expected to be relatively inaccurate.

The peak gains that have been determined by the participating facilities are seen to correspond very well. Here only the DTU2 measurement stands out with a value that is slightly above the rest.

As a part of the measurements some facilities have determined the location of the peak. The locations that have been determined are listed in Table 6.21, using the optical coordinate system. The main beam of the VAST12 antenna is quite narrow in one direction and wide in the other. For this reason the peak location is relatively difficult to determine accurately. This is reflected in the locations found by the participants where the agreement in the θ value is quite good, but the ϕ value varies some.

Facility	Peak Directivity [dBi]	Peak Gain [dBi]	Loss [dB]	Peak Location (θ, ϕ) [degrees]
DTU1	30.71	30.35	0.36	(0.44, 49.0)
DTU2	30.72	30.59	0.13	(0.54, 37.0)
SES	30.67	30.41	0.26	(0.50, 42.3)
FTRD	31.1	30.4	0.7	–
UPM1	30.65	30.39	0.26	(0.4, 82.8)
UPM2	–	30.38	–	(0.57, 90)
UPM3	–	–	–	–
UPC	30.87	–	–	(0.45, 78)
EMW	30.72	30.43	0.29	–

Table 6.21 The directivity, gain, and loss values measured by the participating facilities.

The information contained in this document should be used only for the scope of the contract for which this document is prepared.

6.5 Comparisons of Polarization Characteristics

As a part of the measurements of the VAST12 antenna some of the participating facilities have determined the polarization characteristics for the antenna in the on-axis direction of the optical coordinate system. In this direction the facilities have determined the Axial Ratio and the Tilt Angle as presented in Table 6.22.

Facility	Tilt Angle [degrees]	Axial Ratio [dB]
DTU1	-88.99	54.63
DTU2	-89.02	52.0
SES	-88.36	53.3
FTRD	–	–
UPM1	-89.28	66.51
UPM2	–	–
UPM3	–	–
UPC	89.7	42
EMW	–	–

Table 6.22 The polarization characteristics measured by the participating facilities. The presented values are related to the optical coordinate system.

It can be noted that the found values agree well except for the UPC results, which can also be attributed to the fact that these results are not probe corrected.

The information contained in this document should be used only for the scope of the contract for which this document is prepared.

Chapter 7

Conclusion

This report documents the work carried out within the Work Package WP1.2-2 *First Facility Comparison Campaign* of Activity A1.2 *Antenna Measurement Techniques and Facilities sharing* in the Antenna Centre of Excellence, ACE.

With the large number of participating measurement facilities, which have provided measurement data, it has been possible to perform an extensive amount of comparisons and investigations. A number of different ways of comparing the measured patterns have been proposed and investigated by use of the available measurement data from the participating facilities.

The measurement campaign has been carried out using the DTU-ESA 12 GHz Validation Standard Antenna. This antenna and the associated coordinate systems have been described in Chapter 2.

A total number of 9 measurement facilities participated in the measurement campaign. These included: The DTU-ESA Spherical Near-Field Test Facility at the Technical University of Denmark (DTU), three different facilities at the Technical University of Madrid - a spherical near-field facility (UPM1), a planar near-field facility (UPM2), and a compact range facility (UPM3), the France Telecom Research & Development far-field range facility at La Turbie (FTRD), the Saab Ericsson Space A6 test range - a spherical near-field facility (SES), the spherical near-field facility at the Technical University of Catalonia (UPC), the Ericsson Microwave Systems A15 Compact Antenna Test Range (EMW). Finally, it was measured at the University of Liverpool (LIVUNI), but unfortunately, it was not possible to include this facility in the comparisons. A presentation of each of the participating facilities has been given in Chapter 3

A detailed account of the development of the measurement campaign has been given in Chapter 4. A "Verification Test Plan" and a time schedule were agreed upon by the participants. The schedule of the campaign allowed for 2 weeks for measurements at each facility and 1 week for shipment of the VAST12 antenna between facilities. This has shown to be appropriate and sufficient during the execution of the campaign. The campaign was carried out with great success, and as a result, a large amount of measurement results were communicated to DTU for comparisons.

The information contained in this document should be used only for the scope of the contract for which this document is prepared.

In Chapter 5 a thorough discussion has been given on the different ways to compare the measured data. In particular, special attention has been given to the comparison of the radiation patterns and analysis of the difference between patterns. Several definitions of the difference of two patterns have been discussed and their characteristics investigated by use of patterns measured in this campaign. These differences also included weighted differences for which particular weighting functions were suggested and illustrated. Based upon the differences some measures of merit were presented and discussed in order to facilitate a quantification of the similarity of two patterns. As a separate way of investigating the difference between the patterns it was suggested to perform a comparison at discrete pattern levels. This comparison was investigated using the Logarithmic difference and then at each pattern level computing a particular measure of merit. Following the extensive discussions of how to compare the patterns a note was given on comparisons of gain and polarization characteristics.

A specific strategy was chosen in Chapter 6, and used to perform a number of specific comparisons of the measurements from the participating facilities. These comparisons include:

1) A repeatability comparison based on the two measurements at the DTU facility. In this comparison it was found that the DTU-ESA facility is capable of producing measurements with good repeatability. However, the comparisons did uncover a small but noticeable difference in a narrow region of the pattern.

2) An inter-comparison of measurements from a spherical near-field range, a planar near-field range, and a compact range. This comparison was based on the measurements from the three UPM facilities and showed that some noticeable differences are visible when comparing the patterns.

3) A comparison of spherical near-field measurements at two different facilities based on measurements from the SES and DTU facilities. From this comparison it was found that a very good agreement in the patterns could be observed, but that a noticeable difference in the patterns in narrow regions of the pattern.

4) A comparison of measurements obtained at a far-field range and at a spherical near-field range. This comparison is based on measurements at the FTRD far-field range and a measurement from the DTU spherical near-field range. In this comparison a generally good agreement between the patterns was found, but some noticeable differences could be observed in particular for the main lobe region.

5) Comparisons against reference patterns. In these investigations two reference patterns were constructed in different ways and such that one was defined in the optical and one in the electrical coordinate system. Comparisons of the available measurements against these reference patterns were shown to allow, in particular, a benchmarking of the accuracy of the participating facilities. However, the large differences in the results that are found with the two reference patterns indicate that the definitions used for these are not good.

The comparison campaign has proven to be both useful and successful in several aspects.

The information contained in this document should be used only for the scope of the contract for which this document is prepared.

- It was possible to attract many participants for the campaign, and in the end a total number of 7 participants with 9 facilities were included in the campaign.
- The comparison campaign has provided a possibility for each facility to assess its performance in comparison to other facilities and to validate, benchmark, and analyze its own measurement capabilities.
- The comparison campaign has provided each facility with an opportunity for testing and improving its procedures for carrying out a measurement for an external partner.
- The comparison campaign has in several cases lead to improvements of procedures for measurements and/or processing of measured data at participating facilities.

Furthermore, several good lessons have been learned about carrying out such a comparison campaign.

- The execution of the measurement campaign was a success and it was found that the scheduled 2 weeks for measurements and 1 week for shipment of the VAST12 antenna between participants was appropriate and sufficient. An additional 1 week for measurements at each additional facility of the same participant was also found to be appropriate and sufficient.
- The well defined Verification Test Plan has ensured that the measurement data, which were supplied by the participating facilities, formed a good basis for the comparisons. However, experience has been gained regarding the importance of an even more precisely defined VTP. As an example, the fact that data from the different coordinate systems, which have been used, cannot be compared directly has limited the number of pattern comparisons to 6 rather than the possible 8.
- It has been found that the handling instructions and mounting requirements for the reference antenna should be made available for, and reviewed by, the participating facilities before the start of the campaign, in order to ensure that all facilities fulfill the requirements for performing measurements on the antenna.

With the large amount of data for patterns combined with the large number of facilities, it has been necessary to determine the most efficient and effective ways to perform comparisons. Different methods for carrying out these comparisons have been analyzed, and advantages and disadvantages of the methods have been clarified. The possible definitions of a reference pattern have been discussed and clarified, and some specific definitions have been investigated by use of the available data.

Based on the experience gathered through this comparison campaign the following recommendations can be made:

- In the planning phase of the campaign the participants should agree, not only on the VTP, but also on the type of processing and analysis that should be performed for the collected data.

The information contained in this document should be used only for the scope of the contract for which this document is prepared.

- A great effort should be made to define the VTP such that as much of the measured data as possible is comparable between the facilities, and that the data is suitable for the processing and analysis that has been agreed on.
- It is important that each facility provide an accuracy estimate or error budget. In particular, these can be used for establishing a good reference pattern. The accuracy estimates and error budgets from the individual facilities must be comparable.
- If a benchmarking of the participating facilities is an objective, a good definition for the reference pattern should be determined as the definitions investigated in this work were not found to provide reliable results.

Generally it can be concluded that all participating facilities are capable of providing measurements of high to very high accuracy.

The information contained in this document should be used only for the scope of the contract for which this document is prepared.

Appendix A

Euler angles

Two right-handed rectangular coordinate systems with a common origin and arbitrarily oriented with respect to each other can be related through three Euler angles as illustrated in Figure A.1, (see Appendix 2 in [13]).

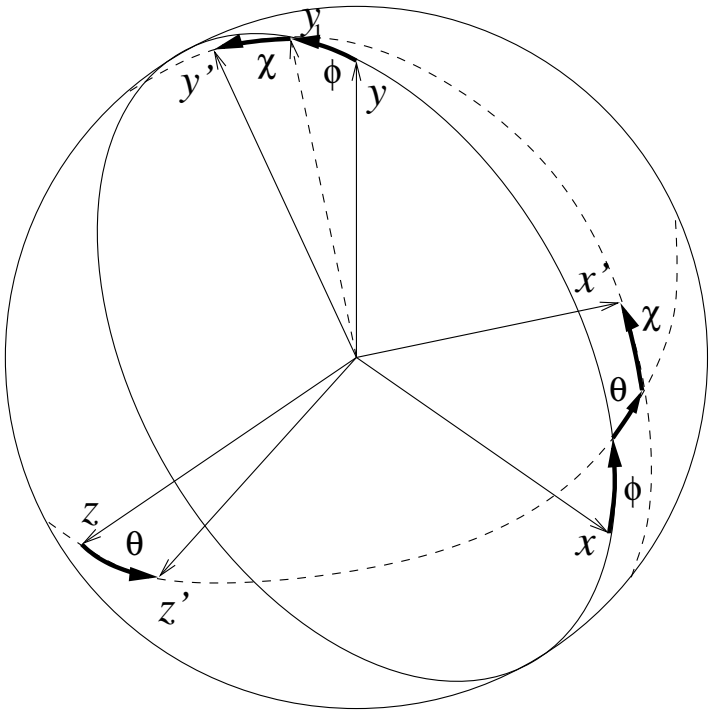

Figure A.1 Euler angles.

The unprimed coordinate system (x, y, z) can be transformed to the primed coordinate system (x', y', z') through three successive rotations about its own axes. The three rotations are:

1. A rotation about the z-axis through an angle ϕ.
2. A rotation about the y_1-axis through an angle θ.
3. A rotation about the z'-axis through an angle χ.

The information contained in this document should be used only for the scope of the contract for which this document is prepared.

Appendix B

Measurement Report from Ericsson Microwave Systems

The information contained in this document should be used only for the scope of the contract for which this document is prepared.

ERICSSON

Open
REPORT 1 (21)

Prepared (also subject responsible if other)	No.		
EMW/DD/UHNT Håkan Eriksson +46317472779	2/1597-LPA 201 186 Uen		
Approved / Checked	Date	Rev	Reference
EMW/DD/UHNC	2005-11-23	A	

A15. VAST12 Measurement report

Contents

Applicable documents

[1] 1/171 32-LPA 201 186 Uen Rev A. A15. Alignment of room reference - record

1 Introduction

The measurement of the VAST12 antenna was performed for the ACE facility comparison campaign.

The information contained in this document should be used only for the scope of the contract for which this document is prepared.

2 Summary

2.1 Quality assurance

The accuracies of the A15 Compact Antenna Test Range are verified during installation according to general standards for accuracies within measurements and qualified according to current quality assurance (ISO9001) at Ericsson Microwave Systems AB. Range documentation, procedures and calibration are also prepared for accreditation to EN ISO 17025 (spring 2006).

2.2 Alignment

The alignment capabilities in A15 are extreme because of the pre-aligned positioner that is very stable, accurate encoders and optimum conditions for theodolite measurements. The uncertainty budget for A15 is double-checked with a RCS-plate and triple-checked by measuring the beampointing with two separable methods. All with an agreement within 0.005°.

2.3 Gain and Directivity

The directivity uncertainty is 0.08 dB and the gain uncertainty 0.16 dB.

2.4 Sidelobe level

The relative small VAST12 antenna opens for possibilities for the feed to pick up differences in the mounting arrangements at the different ranges. The azimuth cuts are probably less sensitive for this type of test setup differences.

The limiting uncertainty is in the angular region around the serrations of the compact range reflector (8 –12 deg) and the disturbance level of –55 dB. Elsewhere in the room the disturbance level is better than –70 dB.

2.5 Cross-polarization

Better than –50 dB for a small antenna like VAST12.

3 The A15 Compact Antenna Measurement Range

The information contained in this document should be used only for the scope of the contract for which this document is prepared.

ERICSSON

Open
REPORT 3 (21)

Prepared (also subject responsible if other)	No.		
EMW/DD/UHNT Håkan Eriksson +46317472779	2/1597-LPA 201 186 Uen		
Approved / Checked	Date	Rev	Reference
EMW/DD/UHNC	2005-11-23	A	

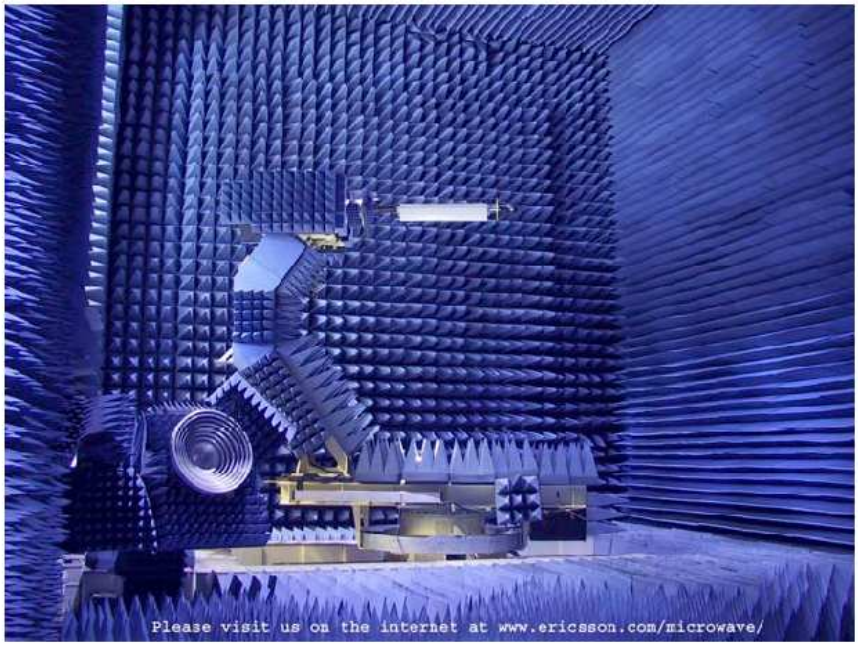

General		
	Frequency	800 MHz to 75 GHz
	Weight (with fixture)	700 Kg
	Antenna Dimensions	Width: 4m Height: 4m Depth: 3m
	Cuts	Conical Cuts, Great Circle Cuts or Theta/Phi Cuts
	Polarization	Dual Linear, Circular, All Ludwig
	Control of steer able antenna parameters	Yes (method dependent of timing requirement)

Quality, classification and additional services		
	Quality Assurances	ISO 9001
	Accreditation	EN ISO 17025 (2005)
	Qualified Against Reference range	Yes
	Defense class	Range prepared to handle National and International defense products according to the highest security level in Sweden
	Independency	Independent measurements can be performed by SP personnel
	Environment	Temperature: 21 ±0,5 °C Humidity: Proposal upon request Particles: Proposal upon request
	Analysis	Proposal upon request
	Environmental testing and EMC	Proposal upon request

Measurements
Diagram
Gain
Directivity
Efficiency
Insertion phase
EIRP
Axial Ratio
Phase center

Special Measurements
Antenna noise temperature
S-parameters
PIM
Alignment
RCS

Antennas		Compliancy	SLL noise level (without Time domain or AAPC) (dB)	Gain accuracy (+/-dB)	Alignment (+/- deg)	Experience
	Omni directional	Yes	-30	0,5	0,1	
	Base station	Yes	-32 (800 MHz) -40 (2 GHz)	0,2	0,1	Recurrent
	Link	Yes	-50	0,2	0,005	Recurrent
	Space	Yes	-50	0,2	0,005	Recurrent
	Defense	Yes	-50	0,2	0,005	Recurrent

The information contained in this document should be used only for the scope of the contract for which this document is prepared.

4 Conditions

The qualification is performed for 12 GHz and is directly valid for the 12-18 GHz band since the same feed is used and the complete band has been verified for quiet zone performance which includes influence on co-polar sidelobe level crosspol level and beampointing for instance. The quiet zone performance verification for other bands shows that the data in this report is valid at least down to C-band where reflector edge diffractions starts to influence the performance. For the bands above 18 GHz the quiet zone performance is linearly scaled from the verification done at 18 GHz.

The information contained in this document should be used only for the scope of the contract for which this document is prepared.

5 Range alignment reference determination

The electrical direction or Angle of Attack (AoA) of the test range has been calibrated to coincide with gravity in elevation and to a mechanical reference in azimuth. An optical reference is also calibrated to this direction (appl doc [1]). The initial calibration was performed during installation and is proven to be very stable over time. Recurring calibration checks that the positioner encoders have not drifted. The alignment procedure for optical alignment of an antenna to this coordinate system is however independent of the positioner encoders absolute angle and only dependent of the optical alignment of the room reference (appl doc [1]).

Below is a comparison between the installation calibration (linear scanner) and the recurring calibration with a RCS plate.

The calibration with the linear scanner was performed during 2003 at 12-18 GHz. A theodolite has been aligned to the gravity vector. By following the path of the scanner probe with the theodolite, the scanner is aligned to be vertical. A similar procedure is used for the horizontal dimension. The picture below shows the linear scanner on the test range.

Figure 3.1 The linear scanner.

The angle of attack, both in azimuth and elevation, is determined by making a best-fit optimization of the measured phase front to a straight line.

The second calibration, the RCS measurement on a flat plate, was performed in September 2004. In this test, the radar cross section of a large flat plate is measured. When the plate is perpendicular to the incoming field, the RCS has its maximum. The picture below shows the large flat plate mounted on the positioner.

The information contained in this document should be used only for the scope of the contract for which this document is prepared.

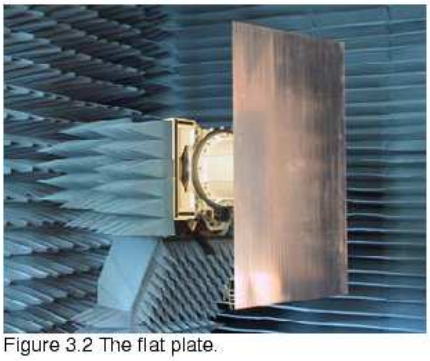

Figure 3.2 The flat plate.

The differences between the two measurements were 0.0047° in azimuth and an incredible 0.0002° in elevation. This is a very good result, considering that the two measurements were performed 18 months apart and that the first one was done during winter and the second one during one of the hottest summer days.

During the VAST antenna tests, the antenna AoA was determined with the same alignment method as the RCS-plate were used. Since these results agree extremely well with the results of the first test, they are considered as very reliable.

The information contained in this document should be used only for the scope of the contract for which this document is prepared.

6 Measurement Coordinate System

The figure below shows the measurement coordinate system with the different angles used during the tests.

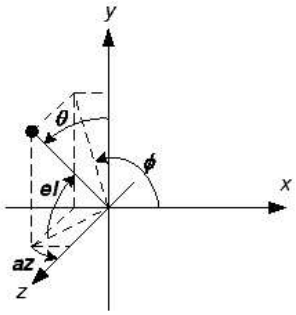

Figure 4.1 Coordinate system and angles.

7 Alignment

After mounting the antenna on the test range, alignment of the roll axis was done with a precision water level mounted on the CFRP tower structure of the antenna, as recommended in the DTU report. Then, the pointing of the *+y* and *–x* surfaces of the mirror cube was registered using a theodolite in auto collimation (calibrated to coincide with the range AoA) mode while also noting the turn table position for each reading.

The data from reading the y and -x surfaces above was used to calculate the normal of the z surface. From these three normals, a transformation matrix between the mirror cube and the measurement coordinate system was constructed.

The information contained in this document should be used only for the scope of the contract for which this document is prepared.

8 Antenna Measurements

The following measurements were performed:

Polar scans with the roll axis as scan axis and azimuth as step axis. A full sphere with a grid step of 0.5° in both azimuth and elevation (θ=0, 0.5,... 180°; ϕ=0, 0.5,... 359.5°). AUT placed at the centre of the quiet zone. This measurement is directly comparable to the data from DTU.

A gain measurement using a calibrated standard gain horn.

9 Antenna Pattern Comparison to DTU Results

9.1 Repointing the Antenna

In order for the coordinate axes to move correctly during the polar scans, the measurement shall be done in the test range system, with the roll axis parallel to the direction of the incoming field. Therefore, the data has been repointed to the mirror cube coordinate system before comparing to the results from DTU. The coordinate transformations for this repointing were found from the pointing directions of the mirror cube surfaces, as measured during the antenna alignment.

The information contained in this document should be used only for the scope of the contract for which this document is prepared.

9.2 Comparison table

The table below summarizes the comparison between the data measured at A15 and the data measured at DTU. Since each range has its own set of errors, it can not be determined which value that is the most correct. Therefore we have chosen not to use terms like "error" for any data. Instead, the table points out the major differences between the two measurements.

Parameter	Comparison
Peak Gain	30.43 dBi (A15), 30.35 dBi (DTU)
Peak Directivity	30.72 dBi (A15), 30.71 dBi (DTU)
Max azimuth side lobe difference level	-64 dB
Max elevation side lobe difference level	-47 dB at 6°, -57 dB at 25°
Max cross polarization difference level in main beam	-52 dB
* Difference relative to the DTU data	

Table 9.2.1 Comparison between A15 and DTU data.

9.3 Antenna Patterns in Polar Cuts

The data provided for comparison by DTU are given as polar cuts with azimuth (θ) as scan axis and roll (ϕ) as step axis. Four cuts have been provided: $\phi = 0$, 45, 90 and 135°. The figures below compare the data from A15 with the data from DTU in these four cuts.

The information contained in this document should be used only for the scope of the contract for which this document is prepared.

ERICSSON

Open
REPORT 10 (21)

Prepared (also subject responsible if other)	No.		
EMW/DD/UHNT Håkan Eriksson +46317472779	2/1597-LPA 201 186 Uen		
Approved / Checked	Date	Rev	Reference
EMW/DD/UHNC	2005-11-23	A	

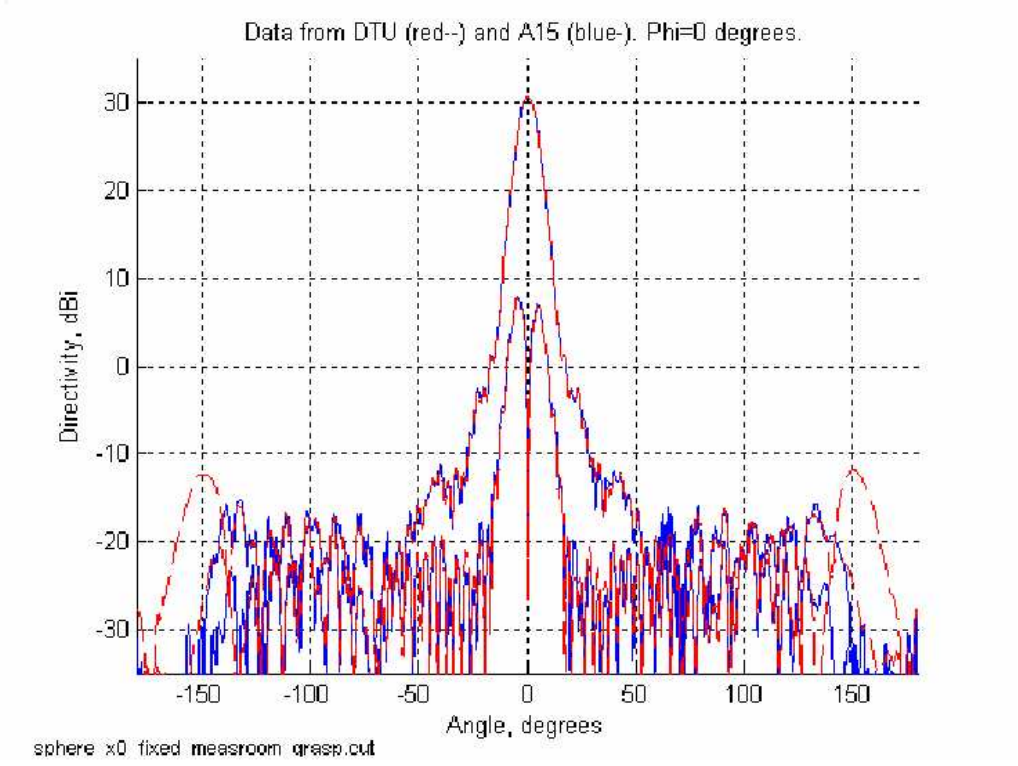

Figure 9.3.1 $\phi = 0°$. Large view.

The information contained in this document should be used only for the scope of the contract for which this document is prepared.

ERICSSON

Open
REPORT 11 (21)

Prepared (also subject responsible if other)	No.		
EMW/DD/UHNT Håkan Eriksson +46317472779	2/1597-LPA 201 186 Uen		
Approved / Checked	Date	Rev	Reference
EMW/DD/UHNC	2005-11-23	A	

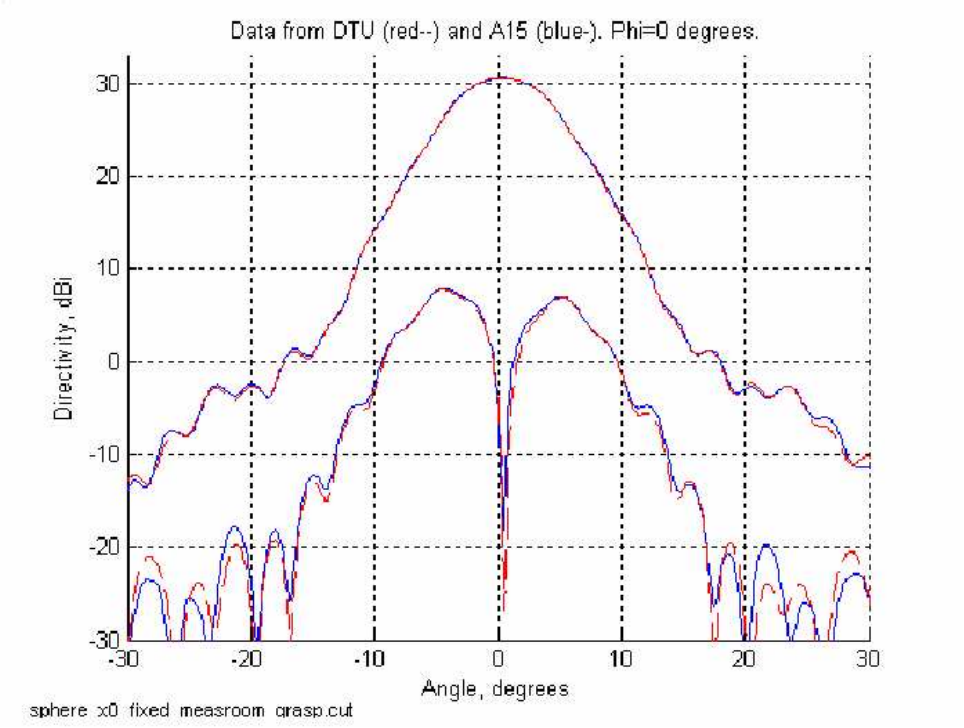

Figure 9.3.2 $\phi = 0°$. Central part only.

The information contained in this document should be used only for the scope of the contract for which this document is prepared.

ERICSSON

Open
REPORT 12 (21)

Prepared (also subject responsible if other)	No.		
EMW/DD/UHNT Håkan Eriksson +46317472779	2/1597-LPA 201 186 Uen		
Approved / Checked	Date	Rev	Reference
EMW/DD/UHNC	2005-11-23	A	

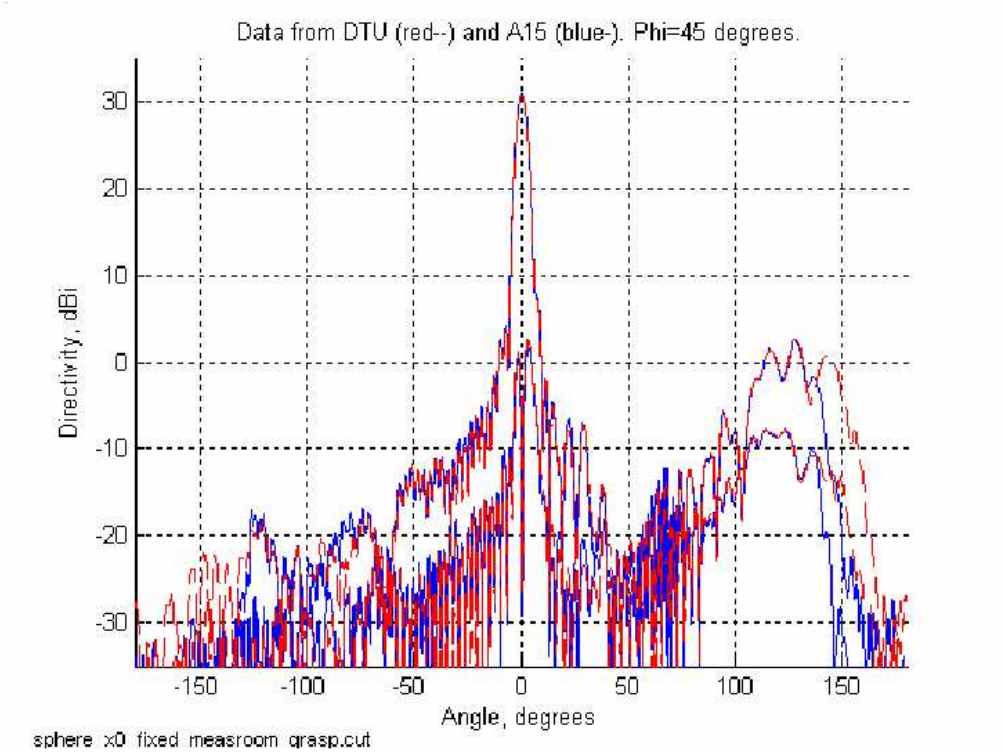

Figure 9.3.3 $\phi = 45°$. Large view.

The information contained in this document should be used only for the scope of the contract for which this document is prepared.

ERICSSON

Open
REPORT 13 (21)

Prepared (also subject responsible if other)	No.		
EMW/DD/UHNT Håkan Eriksson +46317472779	2/1597-LPA 201 186 Uen		
Approved / Checked	Date	Rev	Reference
EMW/DD/UHNC	2005-11-23	A	

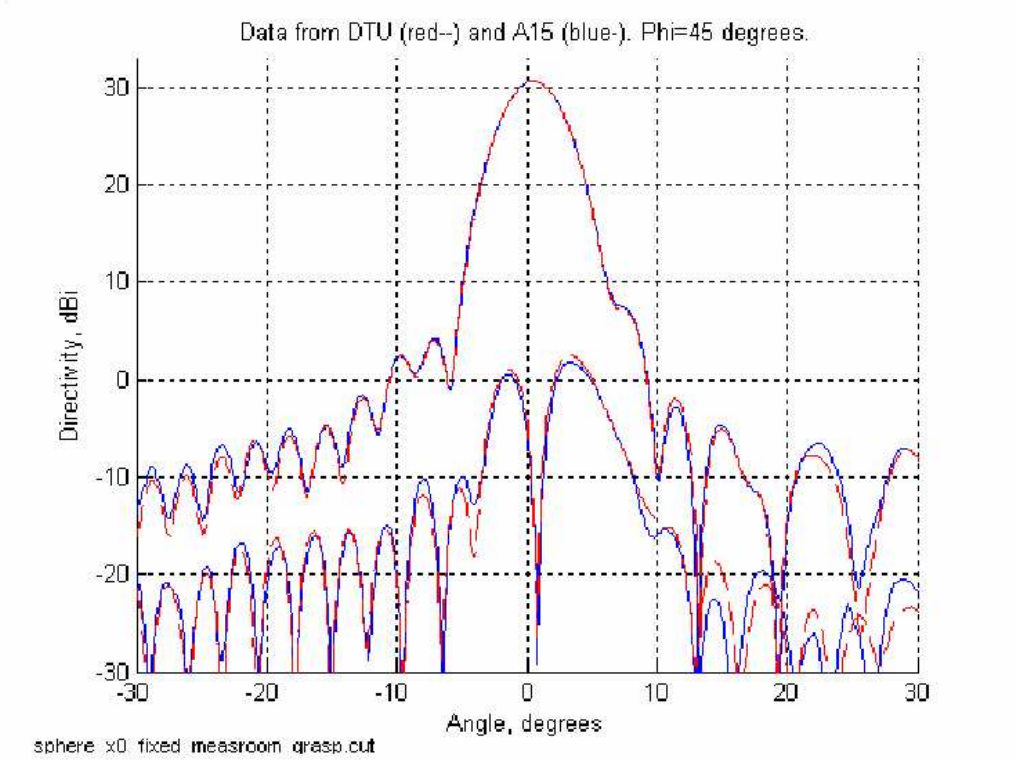

Figure 9.3.4 $\phi = 45°$. Central part only.

The information contained in this document should be used only for the scope of the contract for which this document is prepared.

ERICSSON

Open
REPORT 14 (21)

Prepared (also subject responsible if other)	No.		
EMW/DD/UHNT Håkan Eriksson +46317472779	2/1597-LPA 201 186 Uen		
Approved / Checked	Date	Rev	Reference
EMW/DD/UHNC	2005-11-23	A	

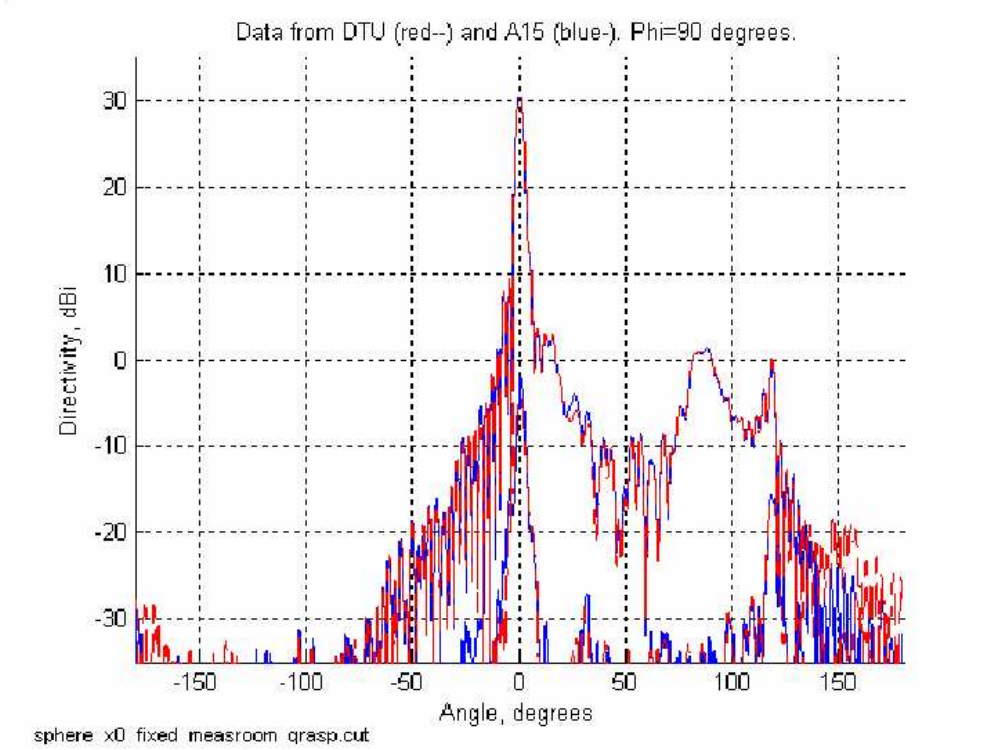

Figure 9.3.5 $\phi = 90°$. Large view.

The information contained in this document should be used only for the scope of the contract for which this document is prepared.

ERICSSON

Open
REPORT 15 (21)

Prepared (also subject responsible if other)	No.		
EMW/DD/UHNT Håkan Eriksson +46317472779	2/1597-LPA 201 186 Uen		
Approved / Checked	Date	Rev	Reference
EMW/DD/UHNC	2005-11-23	A	

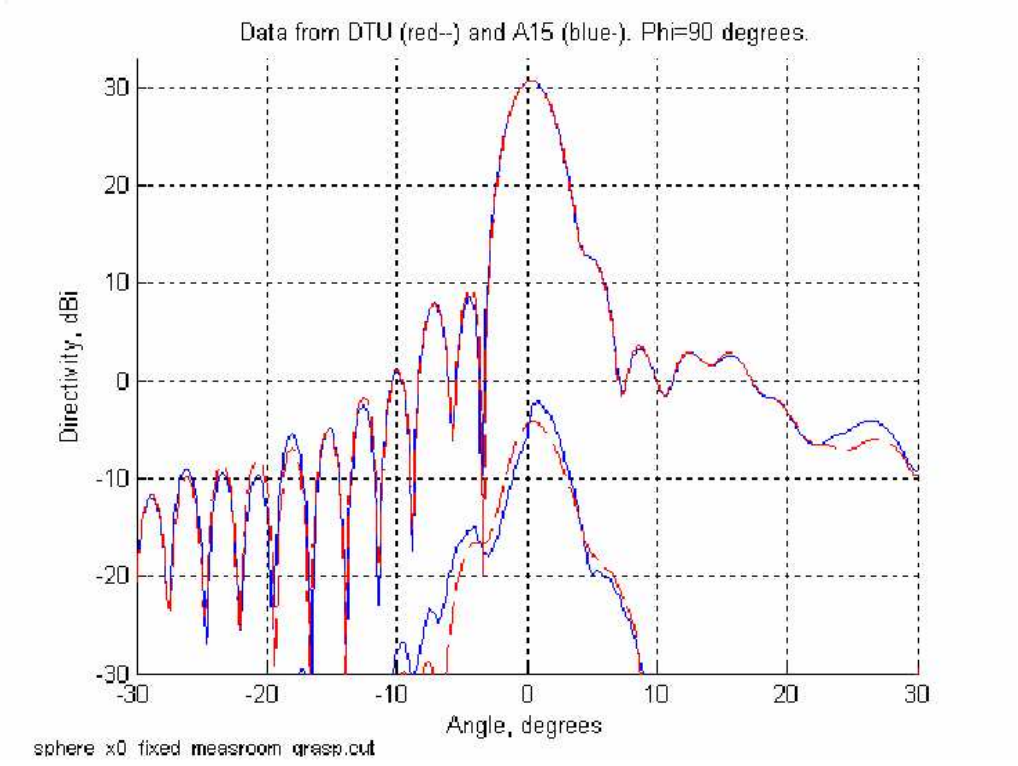

Figure 9.3.6 $\phi = 90°$. Central part only.

The information contained in this document should be used only for the scope of the contract for which this document is prepared.

ERICSSON

Open
REPORT 16 (21)

Prepared (also subject responsible if other)	No.		
EMW/DD/UHNT Håkan Eriksson +46317472779	2/1597-LPA 201 186 Uen		
Approved / Checked	Date	Rev	Reference
EMW/DD/UHNC	2005-11-23	A	

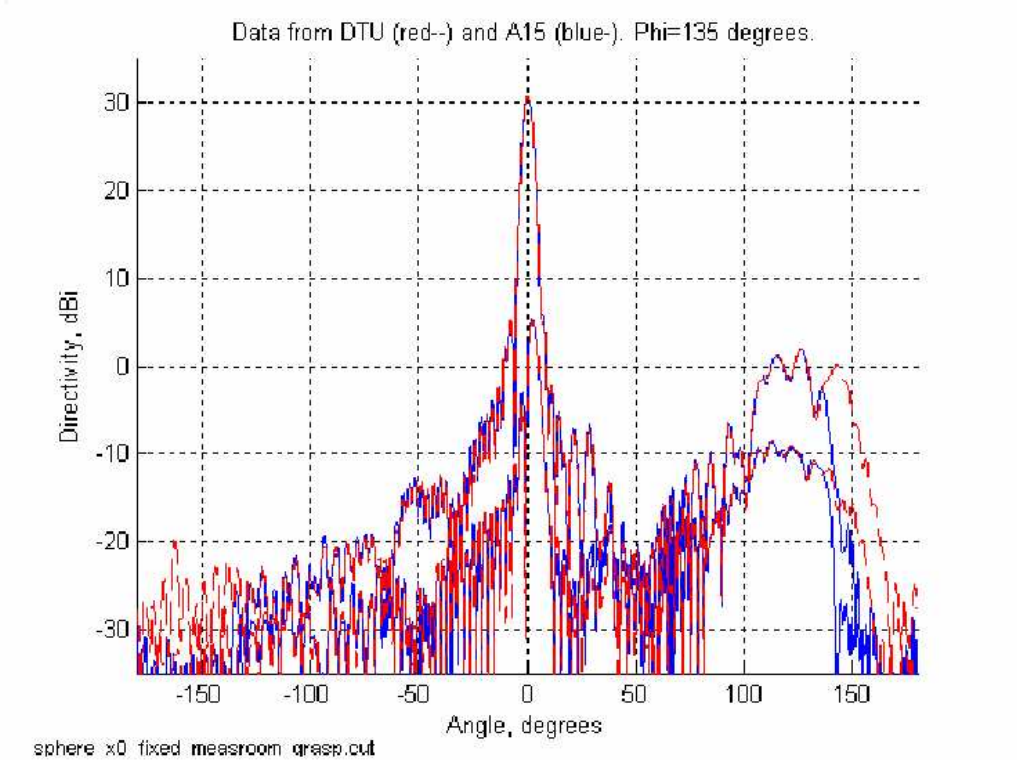

Figure 9.3.7 $\phi = 135°$. Large view.

The information contained in this document should be used only for the scope of the contract for which this document is prepared.

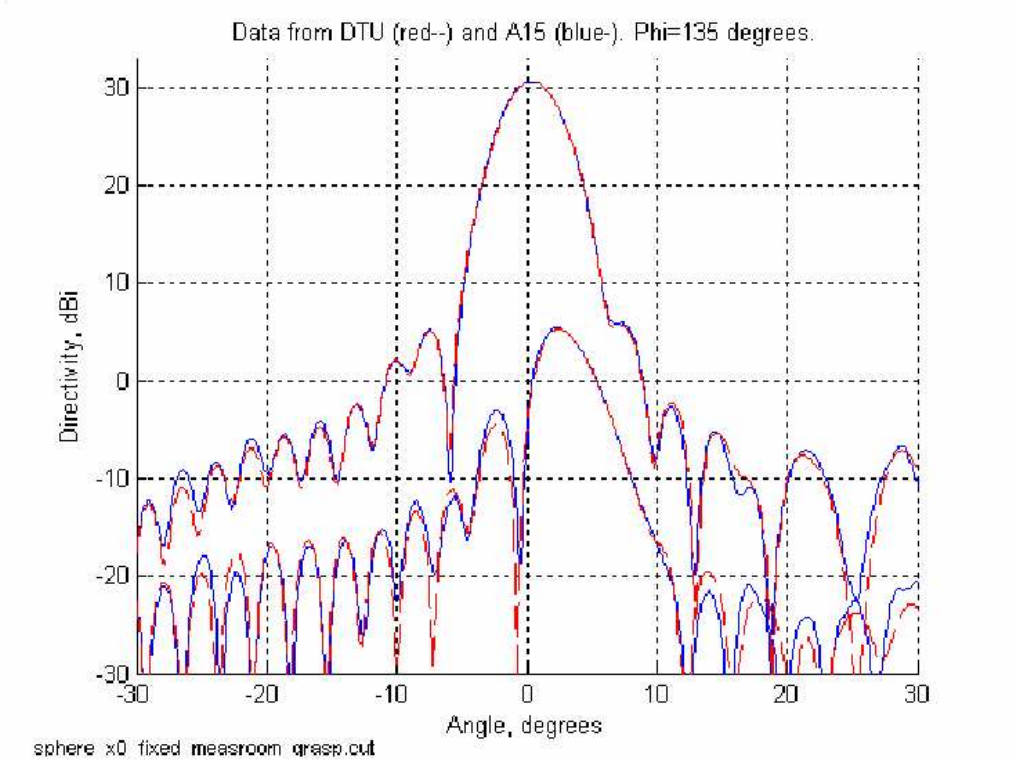

Figure 9.3.8 $\phi = 135°$. Central part only.

9.4 Antenna Patterns – the Raster Scan

For the raster scan measurement, there is no comparison data from DTU.

The raster scan data is measured with a 0.2 degree step in azimuth and elevation and the repointing to the mirror cube system was done by applying an offset directly on each axis. The polar cuts were measured with a step of 0.5 degrees in θ and ϕ. Then the measured pattern was read into Grasp 8 for repointing to the mirror cube system before writing the directivity normalized files.

The information contained in this document should be used only for the scope of the contract for which this document is prepared.

ERICSSON

Open
REPORT 18 (21)

Prepared (also subject responsible if other)	No.		
EMW/DD/UHNT Håkan Eriksson +46317472779	2/1597-LPA 201 186 Uen		
Approved / Checked	Date	Rev	Reference
EMW/DD/UHNC	2005-11-23	A	

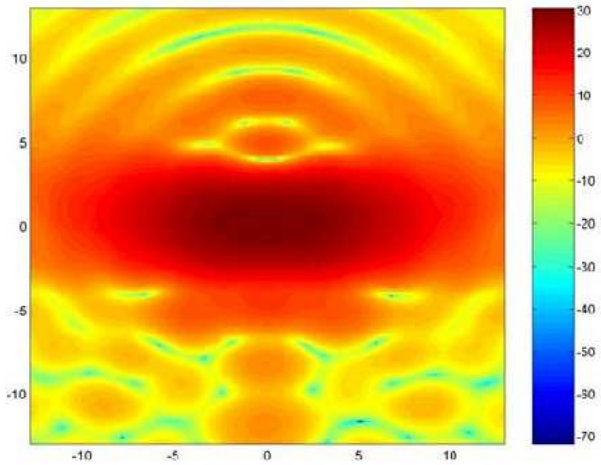

Figure 9.4.3 Raster scan co-polar.

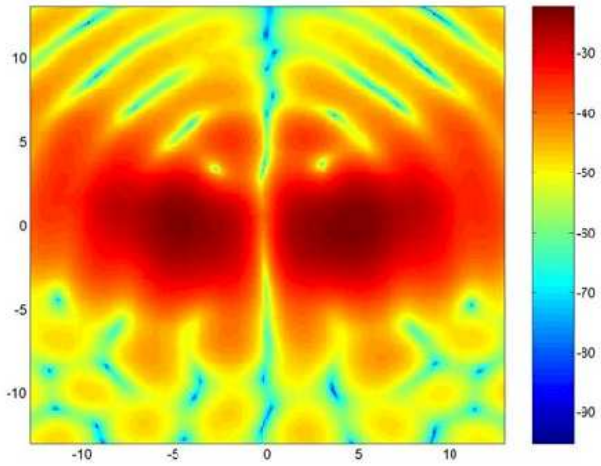

Figure 9.4.4 Raster scan cross-polar.

The information contained in this document should be used only for the scope of the contract for which this document is prepared.

10 Uncertainty

10.1 Alignment

Angle Of Arrival		Standard Uncertainty (+/- deg)
Appl. Doc. [1]	A15. Alignment of room reference - record	0,001
Typical	A15. ALIGNMENT. Alignment of theodolite to room reference and transfer of reference to a second theodolite.	0,0014
Typical	A15. Alignment of antennn to room reference	0,0016
Typical	Drift from calibration	0,002
Combined Standard Uncertainty		**0,0031**

The information contained in this document should be used only for the scope of the contract for which this document is prepared.

10.2 Sidelobe level and gain

	Side-lobe level	Gain	
	Noise level (dB)	Uncert (±dB)	Source
Dynamic range (BWIF=10KHz)	-100	0	RF-Test:
AUT directivity		0,08	
SGH		0,1	Measured directivity and estimated loss
Impedance mismatch error		0,05	Gain only
Multiple reflections (Feeder/AUT)		0,02	1/4 wave test (Gain only)
Receiver amplitude nonlinearity		0,05	RF Test:
Receiver phase errors	0	0	
Flexing cables/rotary joints 0,2º			0.2º @ 5.6GHz
Temperature effects 0,05/ 0,5º		0,05	RF Test: 0.05 dB and 0.5º over 1 hour
Scattering and feeder leakage	-75	0	
Leakage and cross-talk	-80	0	RF Loaded port test
Random errors in amplitude/phase	-80	0	RF Repeatability Test
Edge diffraction without AAPC	-55	0	AUT Comp.Test
Edge diffraction with AAPC	-65	0	AUT Comp.Test
QZ amplit. Taper/Ripple 0,1/ ±0,1	-70	0	Field Probing Test
QZ phase Taper/Ripple <0,5º/ <1º	-70		
TOTAL=	-55 around ±10º and -70 elsewhere	0,16	RSS

The information contained in this document should be used only for the scope of the contract for which this document is prepared.

10.3 Cross-polarization

The cross-polarization uncertainty consists of 3 components:

1. Uncertainty according to previous chapter (-55 around ±10º and -70 elsewhere).
2. Range feed cross-polarization. The comparison in this report shows that for this small (D=1m) antenna the agreement with spherical nearfield is –52 dB, which is better than expected.
3. Geometry error from range feed offset mount: A measurement where the antenna is positioned 0.8m at the side of the center of the quiet zone (antenna edge 1.3m from quiet zone center) shows how this effect affects the cross performance from the – 52 dB difference level to -40dB difference level. For a larger antenna the different cross-polarization level in the quiet zone will be integrated over the surface and antenna taper will for instance compensate for this effect.

The information contained in this document should be used only for the scope of the contract for which this document is prepared.

Appendix C

Verification Test Plans from the Participating Facilities

The information contained in this document should be used only for the scope of the contract for which this document is prepared.

C.1 Verification Test Plan for DTU

Verification Test Plan
(questionnaire)

Please, fill in all applicable fields. Filled example text in red must be removed
Note! VAST12 is linearly vertically (y) polarized antenna (see description of the coordinate system)

1. Project description: Measurement of the 12 GHz Validation Standard (VAST12) antenna followed by comparison with the reference results provided by the DTU-ESA Spherical Near-Field Antenna Test Facility.

2. Participating institution/organization:	Technical University of Denmark
Address	Oersted-DTU, bldg. 348, 2800. Kgs.Lyngby, Denmark
Contact person	Sergey Pivnenko
Telephone	45-4525-3860
Fax	45-4593-1634
E-mail	sp@oersted.dtu.dk

3. Technical details:					
Measurement technique	spherical near-field				
Positioner type	roll-over-azimuth				
Gain determination technique	substitution technique with standard gain horn				
Angular window:	theta, degrees	-180..180			
	phi, degrees	0..360			
Coordinate system definition:	mirror cube coordinate system	yes	x	no	
	mechanical coordinate system	yes	x	no	
	electrical coordinate system	yes	x	no	

4.Parameters to be measured/presented:					
	peak directivity [dBi]	yes	x	no	
	boresight directivity [dBi]	yes	x	no	
	peak gain [dBi]*	yes		no	x
	boresight gain [dBi]*	yes	x	no	
	polarization (axial ratio, tilt, sense)	yes	x	no	
	pointing (peak directivity direction)	yes	x	no	
	pattern (phi=0deg and phi=90deg)	yes	x	no	
	pattern (phi=45deg and phi=135deg)	yes	x	no	
	contour plots (theta=+/-90deg)	yes	x	no	
	error budget/accuracy	yes	x	no	

* gain according to IEEE definition

5. Data transfer:					
	medium: CD	yes	x	no	
	e-mail	yes	x	no	
	diskette	yes	x	no	

Regarding the data format, we suggest amplitude (phase is not necessary) of co-polar and cross-polar components (according to Ludwig 3rd definition with phi0=90deg.) for specified cuts of the pattern, e.g. for phi=0deg and theta=[-180,180]deg — yes x no

Other, specify here:

Comments:

Figure C.1 Verification Test Plan for DTU.

The information contained in this document should be used only for the scope of the contract for which this document is prepared.

C.2 Verification Test Plan for SES

Verification Test Plan
(questionnaire)

Please, fill in all applicable fields. Filled example text in red must be removed
Note! VAST12 is linearly vertically (y) polarized antenna (see description of the coordinate system)

1. Project description: Measurement of the 12 GHz Validation Standard (VAST12) antenna followed by comparison with the reference results provided by the DTU-ESA Spherical Near-Field Antenna Test Facility.

2. Participating institution/organization:	
Address	SE-405 15 Göteborg, Sweden
Contact person	Jan Zackrisson
Telephone	+46 31 735 4004
Fax	+46 31 735 4000
E-mail	jan.zackrisson@space.se

3. Technical details:					
Measurement technique	spherical near-field				
Positioner type	roll-over-slide-over-azimuth				
Gain determination technique	substitution technique with standard gain horn				
Angular window:	theta, degrees	-180..180			
	phi, degrees	0..360			
Coordinate system definition:	mirror cube coordinate system	yes	x	no	
	mechanical coordinate system	yes		no	x
	electrical coordinate system	yes		no	x

4.Parameters to be measured/presented:

peak directivity [dBi]	yes	x	no	
boresight directivity [dBi]	yes	x	no	
peak gain [dBi]*	yes	x	no	
boresight gain [dBi]*	yes	x	no	
polarization (axial ratio, tilt, sense)	yes		no	x
pointing (peak directivity direction)	yes	x	no	
pattern (phi=0deg and phi=90deg)	yes	x	no	
pattern (phi=45deg and phi=135deg)	yes	x	no	
contour plots (theta=+/-90deg)	yes		no	x
error budget/accuracy	yes	x	no	

* gain according to IEEE definition

5. Data transfer:

medium:	CD	yes		no	x
	e-mail	yes	x	no	
	diskette	yes		no	x

Regarding the data format, we suggest amplitude (phase is not necessary) of co-polar and cross-polar components (according to Ludwig 3rd definition with phi0=90deg.) for specified cuts of the pattern, e.g. for phi=0deg and theta=[-180,180]deg — yes ☐ no ☐

Other, specify here:

Comments:

Figure C.2 Verification Test Plan for SES.

The information contained in this document should be used only for the scope of the contract for which this document is prepared.

C.3 Verification Test Plan for FTRD

Verification Test Plan
(questionnaire)

Please, fill in all applicable fields. Filled example text in red must be removed
Note! VAST12 is linearly vertically (y) polarized antenna (see description of the coordinate system)

1. Project description: Measurement of the 12 GHz Validation Standard (VAST12) antenna followed by comparison with the reference results provided by the DTU-ESA Spherical Near-Field Antenna Test Facility.

2. Participating institution/organization:	France Telecom R&D La Turbie					
Address	1581 Fort de la Tête de Chien 06320 La Turbie France					
Contact person	Christian Sabatier					
Telephone	33492106526					
Fax	33492106619					
E-mail	Chris.sabatier@francetelecom.com					
3. Technical details:						
Measurement technique	far-field (Radôme)					
Positioner type	elevation-over-azimuth					
Gain determination technique	substitution technique with standard gain horn					
Angular window:	theta, degrees	75;105				elevation angle (equatorial mount)
	phi, degrees	-180, 180				azimut angle
Coordinate system definition:	mirror cube coordinate system	yes		no	x	
	mechanical coordinate system	yes		no	x	
	electrical coordinate system	yes	x	no		
4.Parameters to be measured/presented:						
	peak directivity [dBi]	yes	x	no		
	boresight directivity [dBi]	yes	x	no		
	peak gain [dBi]*	yes	x	no		
	boresight gain [dBi]*	yes	x	no		
	polarization (axial ratio, tilt, sense)	yes	x	no		
	pointing (peak directivity direction)	yes	x	no		
	pattern (phi=0deg and phi=90deg)	yes	x	no		
	pattern (phi=45deg and phi=135deg)	yes	x	no		
	contour plots (theta=+/-90deg)	yes	x	no		limitation (+/- 15deg)
	error budget/accuracy	yes	x	no		
	* gain according to IEEE definition					
5. Data transfer:						
	medium: CD	yes	x	no		
	e-mail	yes	x	no		
	diskette	yes	x	no		

Regarding the data format, we suggest amplitude (phase is not necessary) of co-polar and cross-polar components (according to Ludwig 3rd definition with phi0=90deg.) for specified cuts of the pattern, e.g. for phi=0deg and theta=[-180,180]deg — yes x no

Other, specify here:

Comments:

Figure C.3 Verification Test Plan for FTRD.

The information contained in this document should be used only for the scope of the contract for which this document is prepared.

C.4 Verification Test Plan for UPM1

Verification Test Plan
(questionnaire)

Please, fill in all applicable fields. Filled example text in red must be removed
Notel VAST12 is linearly vertically (y) polarized antenna (see description of the coordinate system)

1. Project description: Measurement of the 12 GHz Validation Standard (VAST12) antenna followed by comparison with the reference results provided by the DTU-ESA Spherical Near-Field Antenna Test Facility.

2. Participating institution/organization:	Universidad Politécnica de Madrid				
Address	ETSITelecomunicación. C. Universitaria. 28040 Madrid				
Contact person	Manuel Sierra Castañer				
Telephone	34-913367360				
Fax	34-915432002				
E-mail	m.sierra.castaner@gr.ssr.upm.es				
3. Technical details:					
Measurement technique	spherical near-field				
Positioner type	roll-over-azimuth				
Gain determination technique	substitution technique with standard gain horn				
Angular window:	theta, degrees	-180..180			
	phi, degrees	0..360			
Coordinate system definition:	mirror cube coordinate system	yes	x	no	
	mechanical coordinate system	yes	x	no	
	electrical coordinate system	yes	x	no	
4.Parameters to be measured/presented:					
	peak directivity [dBi]	yes	x	no	
	boresight directivity [dBi]	yes	x	no	
	peak gain [dBi]*	yes	x	no	
	boresight gain [dBi]*	yes	x	no	
	polarization (axial ratio, tilt, sense)	yes	x	no	
	pointing (peak directivity direction)	yes	x	no	
	pattern (phi=0deg and phi=90deg)	yes	x	no	
	pattern (phi=45deg and phi=135deg)	yes	x	no	
	contour plots (theta=+/-90deg)	yes	x	no	
	error budget/accuracy	yes	x	no	
	* gain according to IEEE definition				
5. Data transfer:					
	medium: CD	yes	x	no	
	e-mail	yes	x	no	
	diskette	yes	x	no	

Regarding the data format, we suggest amplitude (phase is not necessary) of co-polar and cross-polar components (according to Ludwig 3rd definition with phi0=90deg.) for specified cuts of the pattern, e.g. for phi=0deg and theta=[-180,180]deg — yes x no

Other, specify here:

Comments:

Figure C.4 Verification Test Plan for UPM1.

The information contained in this document should be used only for the scope of the contract for which this document is prepared.

C.5 Verification Test Plan for UPM2

Verification Test Plan
(questionnaire)

Please, fill in all applicable fields. Filled example text in red must be removed
Notel VAST12 is linearly vertically (y) polarized antenna (see description of the coordinate system)

1. Project description: Measurement of the 12 GHz Validation Standard (VAST12) antenna followed by comparison with the reference results provided by the DTU-ESA Spherical Near-Field Antenna Test Facility.

2. Participating institution/organization:	Universidad Politécnica de Madrid				
Address	ETSITelecomunicación. C. Universitaria. 28040 Madrid				
Contact person	Manuel Sierra Castañer				
Telephone	34-913367360				
Fax	34-915432002				
E-mail	m.sierra.castaner@gr.ssr.upm.es				
3. Technical details:					
Measurement technique	planar near field				
Positioner type	rectangular xy				
Gain determination technique	direct gain measurement				
Angular window:	theta, degrees	-50..50			
	phi, degrees	0..360			
Coordinate system definition:	mirror cube coordinate system	yes		no	x
	mechanical coordinate system	yes	x	no	
	electrical coordinate system	yes	x	no	
4.Parameters to be measured/presented:					
	peak directivity [dBi]	yes	x	no	
	boresight directivity [dBi]	yes	x	no	
	peak gain [dBi]*	yes	x	no	
	boresight gain [dBi]*	yes	x	no	
	polarization (axial ratio, tilt, sense)	yes	x	no	
	pointing (peak directivity direction)	yes	x	no	
	pattern (phi=0deg and phi=90deg)	yes	x	no	
	pattern (phi=45deg and phi=135deg)	yes	x	no	
	contour plots (theta=+/-50deg)	yes	x	no	
	error budget/accuracy	yes	x	no	
	* gain according to IEEE definition				
5. Data transfer:					
	medium: CD	yes	x	no	
	e-mail	yes	x	no	
	diskette	yes	x	no	

Regarding the data format, we suggest amplitude (phase is not necessary) of co-polar and cross-polar components (according to Ludwig 3rd definition with phi0=90deg.) for specified cuts of the pattern, e.g. for phi=0deg and theta=[-180,180]deg — yes [x] no [ ]

Other, specify here:

Comments:
Contour plot for theta +/-50 deg

Figure C.5 Verification Test Plan for UPM2.

The information contained in this document should be used only for the scope of the contract for which this document is prepared.

C.6 Verification Test Plan for UPC

Verification Test Plan
(questionnaire)

Please, fill in all applicable fields. Filled example text in red must be removed
Note! VAST12 is linearly vertically (y) polarized antenna (see description of the coordinate system)

1. Project description: Measurement of the 12 GHz Validation Standard (VAST12) antenna followed by comparison with the reference results provided by the DTU-ESA Spherical Near-Field Antenna Test Facility.

2. Participating institution/organization:	Polytechnical University of Catalonia
Address	Jordi Girona 1-3, Campus Nord, Mod. D3 08034 Barcelo
Contact person	Sebastián Blanch
Telephone	34-934016811
Fax	34-934017232
E-mail	blanch@tsc.upc.es

3. Technical details:					
Measurement technique	spherical near-field				
Positioner type	roll-over-azimuth				
Gain determination technique	substitution technique with standard gain horn				
Angular window:	theta, degrees	-180..180			
	phi, degrees	0..360			
Coordinate system definition:	mirror cube coordinate system	yes	x	no	
	mechanical coordinate system	yes	x	no	
	electrical coordinate system	yes	x	no	

4.Parameters to be measured/presented:					
	peak directivity [dBi]	yes	x	no	
	boresight directivity [dBi]	yes	x	no	
	peak gain [dBi]*	yes	x	no	
	boresight gain [dBi]*	yes	x	no	
	polarization (axial ratio, tilt, sense)	yes	x	no	
	pointing (peak directivity direction)	yes	x	no	
	pattern (phi=0deg and phi=90deg)	yes	x	no	
	pattern (phi=45deg and phi=135deg)	yes	x	no	
	contour plots (theta=+/-90deg)	yes	x	no	
	error budget/accuracy	yes		no	x

* gain according to IEEE definition

5. Data transfer:					
	medium: CD	yes	x	no	
	e-mail	yes	x	no	
	diskette	yes	x	no	

Regarding the data format, we suggest amplitude (phase is not necessary) of co-polar and cross-polar components (according to Ludwig 3rd definition with phi0=90deg.) for specified cuts of the pattern, e.g. for phi=0deg and theta=[-180,180]deg — yes [x] no [ ]

Other, specify here:

Comments:

Figure C.6 Verification Test Plan for UPC.

The information contained in this document should be used only for the scope of the contract for which this document is prepared.

Bibliography

[1] J. Lemanczyk and F. Holm Larsen. Experimental Spherical Near Field Antenna Test Facility, Phase 3, Final Report Vol. III: An intercomparison of antenna measurements made at a spherical near field range (TUD), a cylindrical near field range (MBB) and a compact test range (THE). Technical Report R282, Technical University of Denmark, Lyngby, Denmark, December 1983.

[2] J. Lemanczyk. An Intercomparison of Near Field Antenna Measurements Carried out at TUD, MSS and BAe. Technical Report R323, Technical University of Denmark, Lyngby, Denmark, January 1986. ESTEC contract No. 52276.

[3] Jerzy Lemanczyk and F. Holm Larsen. "Comparison of Near-Field Range Results". *IEEE Transactions on Antennas and Propagation*, vol. AP-36:845–851, June 1988.

[4] J. Lemanczyk. Technical Assistance for the Design and Development of Antenna Test Range Validation Standardization. ESTEC CATR Intercomparison with the TUD-ESA Spherical Near Field Antenna Test Facility. Technical Report R557, Technical University of Denmark, Lyngby, Denmark, September 1993. ESTEC contract No. 7407/87/NL/PB.

[5] J. Lemanczyk. An Intercomparison of Measurements Carried Out on The ERS-1 SAR Breadboard Antenna Panel at The Technical University of Denmark and CASA, Spain. Technical Report R612, Technical University of Denmark, Lyngby, Denmark, April 1995.

[6] Michael Dich and Hans Erik Gram. An Intercomparison of Measurements Carried Out on The ERS-1 SAR Breadboard Antenna Panel at The Technical University of Denmark and Alcatel Espace, France. Technical Report R667, Technical University of Denmark, Lyngby, Denmark, September 1997.

[7] Carl F. Stubenrauch, Allen C. Newell, Andrew G. Repjar, Katie MacReynolds, Douglas T. Tamura, Flemming Holm Larsen, J. Lemanczyk, R. Behe, G. Portier, J. C. Zehren, Heinrich Hollmann, John D. Hunter, David G. Gentle, and Jan P. M. de Vreede. "International Intercomparison of Horn Gain at X-Band". *IEEE Transactions on Antennas and Propagation*, vol. AP-44:1367–1374, October 1996.

[8] Jeffrey Fordham and Mike Scott. "Antenna Pattern Comparison Between an Outdoor Cylindrical Near-Field Test Facility and an Indoor Spherical Near-Field Test Facility". *IEEE Antennas and Propagation Magazine*, vol. 46(3):146–151, June 2004.

[9] Annex I - "Description of Work", November 2003. Antenna Centre of Excellence - ACE.

The information contained in this document should be used only for the scope of the contract for which this document is prepared.

[10] J. E. Hansen. Definition, design, manufacture, test and use of a 12GHz Validation Standard Antenna. Executive Summary. Technical Report R672, Technical University of Denmark, Copenhagen, Denmark, October 1997. ESTEC contract No. 7407/87/NL/PB.

[11] J. Lemanczyk. Measurements on a 12GHz Validation Standard Antenna. Technical Report R670, Technical University of Denmark, Lyngby, Denmark, October 1997. ESTEC contract No. 7407/87/NL/PB.

[12] Sergey Pivnenko and Olav Breinbjerg. EU Antenna Centre of Excellence WP 1.2-2: First Facility Comparison Campaign May 2004 Reference Measurement of the VAST12 Antenna. Technical Report R716, Technical University of Denmark, Lyngby, Denmark, 2004.

[13] J. E. Hansen (ed.). *Spherical Near-Field Measurements*. Peter Peregrinus Ltd., on behalf of IEE, London, 1988. ISBN 0-86341-110-X.

[14] S. Ramo, J. R. Whinnery, and T. Van Duser. *Fields and Waves in Communication Electronics*. John Wiley & Sons, Inc., New York, third edition, 1993.

[15] A. Frandsen (ed.). *Spherical near-field transformation program with probe correction. Manual for computer program SNIFTD*. TICRA, Copenhagen, Denmark, 1995.

[16] F. Mendoza. Test report for an anechoic chamber. Technical Report Document No. 15291-ATR, RANTEC Microwave and Electronics Inc., May 1993.

[17] Manuel Sierra Castañer. Measurement of the VAST12 Antenna at UPM. Technical Report UPM/LEHA/3/2005, Polytechnical University of Madrid, Madrid, Spain, 2005.

[18] A. C. Newell. "Improved Polarization Measurements Using a Three-Antenna Technique". *IEEE Transactions on Antennas and Propagation*, vol. AP-36:852–854, June 1988.

[19] A. López Alonso and J. L. Besada Sanmartín. Software for the planar near field to far field transformation, including probe correction: PNIFT. Technical Report UPM/ETSIT/DSSR/GR/26/92, Gruppo Radiación de la UPM, Madrid, Spain, october 1992. (in Spanish).

[20] A. C. Newell, R. D. Ward, and E. J. McFarlane. "Gain and Power Parameter Measurements Using Planar Near Field Techniques". *IEEE Transactions on Antennas and Propagation*, vol. AP-36:792–803, June 1988.

[21] A. Calderone and C. Sabatier. Measurements of the VAST12 Antenna for the Inter-comparison Campaign ACE - WP1.2-2. Technical Report FT/RD/RESA/FACE/04.89/CS, France Telecom Research & Development, La Turbie, France, 2004.

[22] Jan Zackrisson. Measurement of the VAST12 Antenna at Saab Ericsson Space Test Range A6. Technical Report U-ANTV-REP-00001-SE, Saab Ericsson Space AB, Göteborg, Sweden, 2004.

[23] J. Lemanczyk. Technical Assistance for the Design and Development of Antenna Test Range Validation Standardization. The Verification Test Plan. Technical Report R595,

The information contained in this document should be used only for the scope of the contract for which this document is prepared.

Technical University of Denmark, Lyngby, Denmark, August 1994. ESTEC contract No. 7407/87/NL/PB.

[24] A. Martin. *Quantitative Data Validation (Automated Visual Evaluations).* PhD thesis, De Montfort University, Leicester, UK, 1999.

[25] A. Duffy, A. Martin, G. Antonini, and A. Ciccomancini. "Issues in Validation of Complex-Valued Simulations for Signal Integrity Analysis". In *2004 IEEE International Symposium on Electromagnetic Compatibility.*, volume 3, pages 1011–1016, August 2004.

[26] Juan M. Ruis, María C. Santos, and Josep Parrón. "Figure of Merit for Multiband Antennas". *IEEE Transactions on Antennas and Propagation*, vol. AP-51:3177–3180, November 2003.

[27] IEEE Standard Definitions of Terms for Antennas, March 1993. IEEE STD 145-1993.

[28] IEEE Standard Test Procedures for Antennas, August 1980. IEEE STD 149-1979.

The information contained in this document should be used only for the scope of the contract for which this document is prepared.